# AB-INITIO INVESTIGATION OF STRUCTURAL, ELECTRONIC AND ELASTIC PROPERTIES OF SOME II-$V_2$ SEMICONDUCTING COMPOUNDS

A
Thesis

Submitted to the
**UNIVERSITY OF KOTA**

in the Partial Fulfillment of the Requirements for the
Award of the Degree of
**DOCTOR OF PHILOSOPHY**

in
**Physics**
Under the
**Faculty of Science**

*Submitted by*
**Sushil Rajpurohit**
Registration No.: RS/2072/18

*Under the Supervision of*
**Dr. Ghanshyam Sharma**
Associate Professor

Department of Pure & Applied Physics

**UNIVERSITY OF KOTA**
**KOTA (RAJASTHAN)-324005**
**INDIA**

**August, 2024**

**DEPARTMENT OF PURE & APPLIED PHYSICS**
**UNIVERSITY OF KOTA, KOTA**
**M.B.S. MARG, KABIR CIRCLE, KOTA**

**Dr. Ghanshyam Sharma**
**Email Id: gsharma@uok.ac.in** **Associate Professor**

# *CERTIFICATE*

I feel great pleasure in certifying that the Ph.D. thesis entitled ***"Ab-Initio Investigation of Structural, Electronic and Elastic Properties of Some II-$V_2$ Semiconducting Compounds"*** submitted by **Sushil Rajpurohit** to the University of Kota in the partial fulfillment of the requirements for the award of the degree of Doctor of Philosophy is based on the research work carried out under my guidance.

He has completed the following requirements as per UGC Regulations and research ordinance of the University:

(a) Satisfactory Completion of the Ph.D. Course Work.
(b) Submission of Half Yearly Progress Reports.
(c) Fulfillment of residential requirement of the Research Centre (Minimum 200 Days).
(d) Presentation of research work before the Departmental Committee.
(e) Publication of at least one research paper in the referred research journal of national and international repute.
(f) Two paper presentations in the Conferences/ Seminars.

I recommend the submission of the Ph.D. thesis and certify that it is fit to be evaluated by the examiners.

Date: **Dr. Ghanshyam Sharma**
Place: (Research Supervisor)

शोध निदेशालय
कोटा विश्वविद्यालय
एम.बी.एस. मार्ग, कोटा (राजस्थान)-324005
फोन न. 0744-2471037

Directorate of Research
University of Kota
MBS Marg, KOTA (Rajasthan)-324005
Phone No.: 0744-2471037

# *DECLARATION*

I, **Sushil Rajpurohit**, hereby certify that the research work presented in my Ph.D. thesis entitled ***"Ab-Initio Investigation of Structural, Electronic and Elastic Properties of Some II-$V_2$ Semiconducting Compounds"*** which is carried out by me under the supervision of **Dr. Ghanshyam Sharma** and submitted in the partial fulfillment of the requirement for the award of the degree of Doctor of Philosophy of the University of Kota, represents my ideas in my own words and where others' ideas or words have been included in this thesis, I have adequately cited and referenced the original sources.

The work presented in this thesis has not been submitted elsewhere for the award of any degree or diploma from any other institution or university in India or abroad. I declare that I have adhered to all the principles of academic honesty and integrity and have not misrepresented or fabricated or falsified any idea / data / fact / source in my submission.

I understand that any violation of the above will cause for disciplinary action by the University and can also evoke penal action from the sources which have thus not been properly cited or from whom proper permission has not been taken when needed.

Date: **Sushil Rajpurohit**
Place: (Research Scholar)

This is to certify that the above statement made by **Sushil Rajpurohit** (Registration Number: RS/2072/18) is correct to the best of my knowledge.

Date: **Dr. Ghanshyam Sharma**
Place: (Research Supervisor)
Associate Professor
Department of Pure & Applied Physics
University of Kota, Kota

शोध निदेशालय
कोटा विश्वविद्यालय
एम.बी.एस. मार्ग, कोटा (राजस्थान)-324005
फोन न. 0744-2471037

**Directorate of Research**
**University of Kota**
**MBS Marg, KOTA (Rajasthan)-324005**
**Phone No.: 0744-2471037**

# *ANTI-PLAGIARISM CERTIFICATE*

It is certified that the Ph.D. thesis entitled ***"Ab-Initio Investigation of Structural, Electronic and Elastic Properties of Some II-$V_2$ Semiconducting Compounds"*** submitted by Mr. **Sushil Rajpurhit** has been examined with the anti-plagiarism tool.

We undertake that:

a. The thesis has significant new work/knowledge as compared already published or are under consideration to be published elsewhere. No sentence, equation, diagram, table, paragraph or section has been copied verbatim from previous work unless it is placed under quotation mark and duly referenced.
b. The work presented is original and own work of the author i.e. there is no plagiarism. No ideas, processes, results or words of others have been presented as the author's own work
c. There is no fabrication of data or results which have been compiled and analyzed.
d. There is no falsification by manipulating research materials, equipment or processes, or changing or omitting data or results such that the research is not accurately represented in the research record.
e. The thesis has been checked by using *DrillBit Extreme Software* and found within the limits as per UGC plagiarism policy and instructions issued from time to time.

Report is also enclosed along with this Ph.D. thesis.

Date:
Place:

**Sushil Rajpurohit**
(Research Scholar)

**Dr. Ghanshyam Sharma**
(Research Supervisor)
Associate Professor
Department of Pure & Applied Physics
University of Kota, Kota

The Report is Generated by DrillBit Plagiarism Detection Software

### *Submission Information*

| | |
|---|---|
| Author Name | SUSHIL RAJPUROHIT |
| Title | AB-INITIO INVESTIGATION OF STRUCTURAL, ELECTRONIC AND ELASTIC PROPERTIES OF SOME II-V2 SEMICONDUCTING COMPOUNDS |
| Paper/Submission ID | 2211556 |
| Submitted by | gsharma@uok.ac.in |
| Submission Date | 2024-08-07 18:46:32 |
| Total Pages, Total Words | 169, 35996 |
| Document type | Thesis |

### *Result Information*

Similarity **3 %**

1 10 20 30 40 50 60 70 80 90

Sources Type

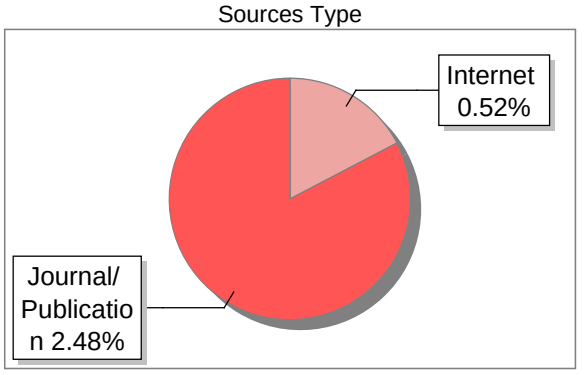


Report Content

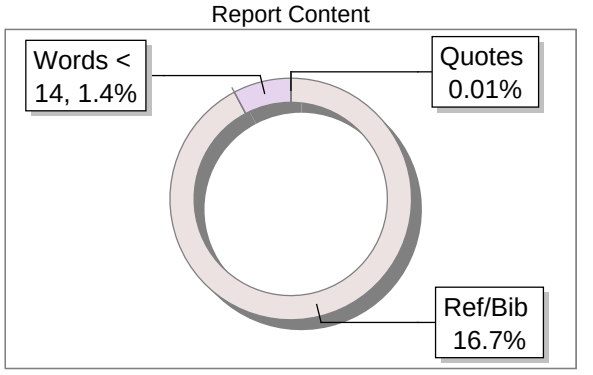


### *Exclude Information*

| | | | |
|---|---|---|---|
| Quotes | Not Excluded | Language | English |
| References/Bibliography | Excluded | Student Papers | Yes |
| Source: Excluded < 14 Words | Not Excluded | Journals & publishers | Yes |
| Excluded Source | **0 %** | Internet or Web | Yes |
| Excluded Phrases | Excluded | Institution Repository | Yes |

### *Database Selection*

A Unique QR Code use to View/Download/Share Pdf File

# *ACKNOWLEDGEMENT*

I would like to extend my deepest gratitude to God Almighty for giving me the strength and courage to reach this point. No words can express my always indebtedness to my parents, who are my first teachers. I would like to express my sincerest heartfelt regard and gratitude to my research supervisor, **Dr. Ghanshyam Sharma**, who encouraged me constantly and provided me with valuable support, attention and guidance throughout the period of my research journey. I sincerely acknowledge his timely advice. I am incredibly grateful to him for his continuous mentorship.

I would like to express my sincere gratitude to the faculty members of the Department of Pure and Applied Physics, University of Kota; **Prof. N. K. Jaiman (Retd.), Dr. Saurabh Dalela, Dr. N. L. Heda, Dr. Namrata Sengar**, for their support during the course of my research work. I wish to extend my gratitude to all my teachers since the start of my school education. I am thankful to the University of Kota for providing research facilities.

I am also thankful to staff members of the Department of Pure & Applied Physics and the Directorate of Research, University of Kota. I am incredibly grateful to my parent organization ,Vardhman Mahaveer Open University, Kota. I am grateful to my family members for being my continuous source of strength. Their consistent support and encouragement have been the most important in this journey. I am thankful to my colleagues at Vardhman Mahaveer Open University, Kota.

I am thankful to my research fellows **Dr. Kuntal Kabra** and **Dr. Maya Kaur** for their help in carrying out my research work. I also extend my acknowledgement to my research colleagues **Dr. Shweta Arora, Dr. Swati Soni, Mr. Mangal Chand Rolania, Dr. Hukma Ram Khakhal, Mrs. Indu Hasnani, Mrs. Mridula, Mr. Pinkesh Meena, Mr. Narendra Singh Leel and Mrs. Kiran Mahavar** for having fruitful discussions. I would also like to thank each and every person who has supported and provided motivation directly or indirectly to carry out this work.

**Sushil Rajpurohit**
(Research Scholar)

# *PREFACE*

This thesis provides an *Ab-Initio* investigation of the structural, electronic and elastic properties of some II-$V_2$ semiconducting compounds. The chapters are arranged into six parts. The properties mentioned in these chapters (3 to 5) are kept as independent as possible. The thesis addresses mostly DFT studies of α-$CdP_2$, α-$ZnP_2$ and $ZnAs_2$. The data in the tables provide an idea of the typical estimated values of the various physical quantities in this thesis. For concreteness and completeness, captions in the tables and figures are included.

This thesis also addresses computational tools relevant to the investigation. The area of computational materials science has seen revolutionary developments in the past few decades. The driving force in computational materials science is the rapid growth of cost-effective computational technology. Computational materials science invites visualization and independent discovery through modern software. Some results in this thesis have been mentioned from published research papers in scientific journals. In the thesis, a list of figures and a list of tables are provided before the start of Chapter 1. The abbreviations used in the thesis are also listed. Tables are presented in conventional units. The symbol *e* represents the charge of a proton. It is taken as a positive.

The first chapter deals with an introduction and review of the literature. Moreover, component elements of II-$V_2$ semiconductors are also introduced in the first chapter. A review survey of II-$V_2$ semiconducting compounds has been introduced in the first chapter. Semiconductors have many technological applications. Chapter 1 illustrates that the usefulness of semiconductors in device applications has become an important area of research. The motivation for the work and outline of the thesis have been incorporated in Chapter 1.

The purpose of the second chapter is to give a glimpse of the basic research methods that are applied in this study. Chapter 2 includes the theoretical framework for this investigation. Chapter 2 addresses useful software/tools such as CRYSTAL Code, DL Visualize, CRYSPLOT and ELATE. In this thesis, a brief description of computational tools is also illustrated in Chapter 2. The second chapter deals with the computational procedure adopted in the thesis.

Chapter 3 is devoted to the structural properties of the compounds. Chapter 3 incorporates optimized lattice parameters for compounds. The third chapter also deals with the equation of states.

Chapter 4 addresses the electronic properties of II-$V_2$ semiconducting compounds. Various descriptions of electronic properties have been included to make it possible to explore the electronic characteristics of the compounds. The description of electron transfer is part of the Mulliken population discussion for II-$V_2$ semiconducting compounds. Electronic band structure calculations are carried out along high symmetry directions for special points in the Brillouin zone. Figures for the density of states illustrate the contribution of nonequivalent atoms and atomic shells to the density of states. The density of state interpretation enhances the understanding of the contribution of electronic shells to conduction properties.

The fifth chapter deals with the elastic properties of the materials. Mathematical expressions are an intrinsic part of elasticity. Essential mathematical equations have been incorporated in Chapter 5 to describe the polycrystalline properties, anisotropy, etc. The anisotropy of compounds is elaborated through two-dimensional and three-dimensional view diagrams. Attention has also been paid to describing anisotropic parameters in the elasticity section. In Chapter 6, attention is turned to important conclusions and future scope. Standard notations and symbols are used in the thesis. A consistent reference style is followed in references. The bibliography section includes the DOI of sources as much as possible. Efforts have been made to form this thesis systematically.

# *CONTENTS*

# *ABBREVIATIONS*

| | |
|---|---|
| **BF** | Bloch Function |
| **BM** | Birch-Murnaghan |
| **BS** | Basis Set |
| **BZ** | Brillouin Zone |
| **CP** | Compton Profile |
| **CPHF** | Coupled Perturbed Hartree-Fock |
| **DFT** | Density Functional Theory |
| **DLV** | Daresbury Laboratory Visualize |
| **DOS** | Density of States |
| **DZ** | Double Zeta |
| **ECD** | Electron Charge Density |
| **EM** | Electromagnetic |
| **EMD** | Electron Momentum Density |
| **FIR** | Far-Infrared |
| **GGA** | Generalized Gradient Approximation |
| **GUI** | Graphical User Interface |
| **HF** | Hartree-Fock |
| **HK** | Hohenberg-Kohn |
| **IBZ** | Irreducible Brillouin Zone |
| **IE** | Ionization Energy |
| **IR** | Infrared |
| **KS** | Kohn-Sham |
| **LCAO** | Linear Combination of Atomic Orbitals |
| **LDA** | Local Density Approximation |
| **LED** | Light Emitting Diode |
| **LSDA** | Local-Spin-Density Approximation |
| **PDOS** | Partial Density of States |
| **PBE** | Perdew-Burke-Ernzerhof |
| **PT** | Poirier-Tarantola |
| **PV** | Photovoltaic |
| **PVT** | Pressure-Volume-Temperature |

| | |
|---|---|
| **PWGGA** | Perdew-Wang Generalized Gradient Approximation |
| **PZ** | Perdew-Zunger |
| **QNA** | Quasi-Newton Algorithm |
| **RMS** | Root Mean Square |
| **SHG** | Second Harmonic Generation |
| **SG** | Space Group |
| **TF** | Thomas-Fermi |
| **TZ** | Triple Zeta |
| **VBH** | von Barth-Hedin |
| **VWN** | Vosko-Wilk-Nusair |
| **WF** | Wannier Function |
| **XC** | Exchange-Correlation |

# *LIST OF TABLES*

# *LIST OF FIGURES*

# CHAPTER 1

# INTRODUCTION

## 1.1 Introduction

The choice, formation and use of materials have been part of civilization**.** There is the continuous advancement of material classes and properties [1]. Materials are represented through their properties, such as electronic band gap, density, thermal conductivity, coefficient of thermal expansion, Young's modulus, Poisson's ratio, etc. The productive application of materials requires that they fulfill specific properties. Exposure to material properties provides upgraded technology with improved performance [1]. The usefulness of semiconductors in devices has encouraged accelerated research endeavors to characterize their properties better [2]. A quantum mechanical *ab-initio* computer program provides the computation scheme to investigate many properties of crystalline systems [3].

Many solids have the crystalline nature. In crystals, the atoms follow a three-dimensional periodic structure. This regularity helps to develop methods to investigate the properties of crystalline solids. In actual situations, solids do not extend to infinity [4]. Real solids terminate on surfaces, which make up defects in the three-dimensional periodic crystalline structure [4]. The typical ratio of atoms in the bulk to atoms on the surface of a real solid is $10^8$: 1 [4]. Therefore, despite the surface defect, it is reasonable to assume that a real solid behaves nearly like an infinite periodic solid [4]. To characterize the crystal, the positions of the atoms of the basis in the conventional cell are to be identified [5]. The crystal structures have significance for technologically advanced materials.

The main method for examining the arrangement of atoms in crystalline solids is X-ray diffraction [6]. The type of lattice and separation between lattice planes can be identified with the X-ray diffraction technique. In X-ray diffraction, the wavelength of an electromagnetic wave is of the order of the distance between atoms. X-ray reflection follows Bragg's law.

The quest for appropriate materials for photovoltaic (PV) applications has broadened over the past several years [7]. Semiconductors have many technological applications, such as solar cells, transistors, light-emitting diodes (LEDs), photoconductors, charge-coupled devices, strain gauges, lasers, etc. [8]. Generally, semiconductor devices are relatively economical and have reliability [8]. Applications of the optical properties of solids are commercially valuable [9]. Photonic crystals for optical integrated circuits have become an important area of research [9]. With

concern about the increasing energy requirements of society, researchers are paying attention to further investigation of renewable energy sources, like solar devices, etc. [10].

Crystal orbitals (solid wave functions) extend throughout the solid, so these may be referred to as delocalized orbitals [11]. For accuracy in electronic structure treatment, the inclusion of electron-electron interactions is very essential [12]. The electronic properties of solids are influenced by crystal potential. Generally, an unfilled band of orbitals is known as a conduction band [6], whereas a filled band is known as a valence band [6]. The band gap depends on the temperature [8]. The band structure can illustrate the manner in which electrons in the solids will react to external disturbances [4]. Here, external disturbances mean the emission or absorption of light [4]. This response of electrons may be correlated with the electrical and optical properties of solids [4]. The electronic band structure of solids has utility in determining the reflectivity and dielectric properties [4].

The plot between the energy *E* and the wave vector *k* is known as the *E*-*k* diagram. The *E*-*k* plot is also known as the dispersion relation or band structure for electronic states [13]. The energy eigenvalue $E_n(\vec{k})$ is associated with band index *n* [11]. Each band has a specific energy range [11]. In crystals, the number of bands is large [11]. If the lowest of the conduction band and the highest of the valence band are at the same wave vector in the *E*-*k* diagram, it is called a direct band gap semiconductor [8]. In the indirect band gap semiconductor, the lowest of the conduction band and the highest of the valence band are not at the same wave vector in the *E*-*k* diagram [8]. The *E*-*k* diagram has utility in the determination of the band gaps (namely, direct and indirect) of semiconductors. To illustrate specific physical phenomena, the Brillouin zone (BZ) scheme in reciprocal space is utilized. There are special $\vec{k}$ points, which are high symmetry points in three-dimensional Brillouin zones. Electronic band structure calculations are generally carried out along high symmetry directions for these special points (namely $X, Z, M, \Delta, \sum, \Gamma,$ etc.) in the Brillouin zone and dispersion *E*-*k* curves are plotted [4]. The characteristics of electronic energy bands along the high-symmetry directions (joining special points) of the Brillouin zones are significantly useful [4].

As a function of energy, the density of electronic states is a useful concept for analyzing the electronic band structure of solids. The density of states is given by $\frac{dN}{dE}$

where $dN$ represents the number of states existing between energy levels $E$ and $E + dE$. Position of Fermi energy in the density of states versus energy plot plays a key role in determining transport properties of solids [13]. The highest occupied energy surface in a wave vector $\vec{k}$ is the Fermi surface for solids at zero Kelvin temperature [8] and energy is constant throughout this Fermi surface [14]. The electrons near the Fermi surface are responsible for many electrical properties [8]. Both extended zone and reduced zone methods are implemented to visualize the Fermi surface [14]. The Fermi surface that is experimentally measured gives a goal at which the first principle electronic band structure computation can target [15]. For the deduction of the geometry of the Fermi surface, one of the powerful techniques is the de Haas-van Alphen effect [15].

Many properties are represented by tensors. Tensors are categorized based on their rank [16]. Different physical properties may be explained by different order tensors, even for the same material. For construction objectives, the applicability of a given solid is also determined by its mechanical properties [2]. Properties that depend on crystal structure are known as structure-sensitive properties [2]. Some specific predictions about the properties of crystals may be made for known crystal structures [2].

There is a change in the shape of the crystal when a stress is applied to it [16]. Strain is recoverable under a certain limit of stress, i.e., under elastic limit [16]. Hooke's law applies only to small strains [17]. For large strains, stress-strain curves enter into the nonlinear region [17]. Elasticity is a centrosymmetric type of property [16]. Elasticity may be dealt with tensors. Elasticity theory forms a mathematical model of the deformation of matter [18]. This mathematical model of elasticity has been commonly formulated using tensor language and calculus. The solid body is assumed to be a continuous medium [19].

The characterization of the mechanical properties of solids is generally carried out with constitutive stress-strain relations [18]. Directional stress-strain responses typically arise from microstructural peculiarities within the anisotropic solid [18]. The deformation response of many solid samples depends upon the orientation [18]. Property that changes with direction is called an anisotropic phenomenon [20]. In general, crystals are said to be anisotropic because of their direction-dependent properties. Such properties of crystals vary with direction. Anisotropy concerns the

type of symmetry of the crystal. As crystals have some direction-dependent properties, all crystals are anisotropic [16]. Anisotropy is an intrinsic quality of a continuum [20]. For anisotropic crystals, applying any stress component results in other strain components. The elastic anisotropy of materials has a significant role in their functions [21]. The elastic anisotropy may affect certain material properties, such as, phase transformations [22] and fracture toughness [23].

Young's modulus and linear compressibility are direction-dependent quantities. For all classes of crystals, Young's modulus is anisotropic, even for cubic crystals [16]. The theory of elasticity elaborates on the utility of crystals for the analysis and design of advanced materials [24]. The elastic perspective is valuable as it provides structural performance. Now, new computational methods have emerged as research tools to examine the elastic properties of materials. In computational materials science, it is expected that computationally predicted results for materials may be experimentally validated in the future. Differences in the performance of the materials may be attributed to specific internal structures of the materials. Complex variable theory also acts as a very useful technique for solving elasticity problems [18]. From the point of view of technological applications, the determination of ductile and brittle materials by means of the theory of elasticity is also important.

II-$V_2$ semiconductor compounds are made from the $12^{th}$ and $15^{th}$ column elements of the periodic table. These compounds have utility in the fabrication of optoelectronic devices [25, 26, 27]. From the thermal point of view of ternary phase diagrams, compounds of As and P with Cd and Zn are of importance [28].

### 1.1.1 Group II and Group V Elements for II-$V_2$ Semiconducting Compounds

Zn, Cd and Hg are elements of Group $II_B$. Group 12 is also known as Group $II_B$. Zn, Cd and Hg each have an electronic ground state $^1S_0$ [29, 30]. The electron configurations of zinc (30), cadmium (48) and mercury (80) are $[\mathrm{Ar}]3d^{10}4s^2$, $[\mathrm{Kr}]4d^{10}5s^2$ and $[\mathrm{Xe}]4f^{14}5d^{10}6s^2$, respectively [29, 30]. The first ionization energies of Zn, Cd and Hg are 9.394197 eV, 8.993820 eV and 10.437504 eV, respectively [30]. The second ionization energy (IE) of Zn is 17.96440 eV [29]. The second ionization energies of Cd and Hg are 16.90832 eV and 18.756 eV, respectively

[29]. The crystal structure of Zn and Cd is hexagonal [29]. At a temperature of 293 K, the shortest interatomic distances in solids for Zn and Cd crystals are 2.66 Å and 2.97 Å, respectively [29]. Young's modulus *E*, shear modulus (modulus of rigidity) *G* and Poisson's ratio *v* of zinc are 92.7 GPa, 34.3 GPa and 0.29, respectively [29]. Young's modulus *E*, modulus of rigidity *G* and Poisson's ratio *v* of cadmium are 62.3 GPa, 24.5 GPa and 0.30, respectively [29]. Zinc is a ductile metal, whereas cadmium is a soft metal [29]. Zn and Cd metals are bluish-white [31]. At temperature 293 K, the electrical resistivities of zinc and cadmium are $5.43 \times 10^{-8}\ \Omega\ \mathrm{m}$ and $6.8 \times 10^{-8}\ \Omega\ \mathrm{m}$, respectively [29]. Cadmium has utility in Ni-Cd rechargeable batteries [31, 32]. Zn has utility in galvanizing the other metals [32]. Zinc is used to form alloys [31, 33]. Hg is a virulent poison [31]. Group 15 is also known as Group $V_A$ [29]. Nitrogen, phosphorus, arsenic, antimony and bismuth are elements of Group $V_A$. The electron configurations of N, P, As and Sb are $[\mathrm{He}]2s^2 2p^3$, $[\mathrm{Ne}]3s^2 3p^3$, $[\mathrm{Ar}]3d^{10}4s^2 4p^3$ and $[\mathrm{Kr}]4d^{10}5s^2 5p^3$, respectively [29, 30]. Elements N, P, As, Sb and Bi each have an electronic ground state ${}^4S_{3/2}$ [29]. The first ionization energies of N, P, As, Sb and Bi are 14.53413 eV, 10.486686 eV, 9.78855 eV, 8.608389 eV and 7.285516 eV, respectively [30]. The crystal structure of P is orthorhombic (C) [29]. As, Sb and Bi have a trigonal (R) crystal structure [29]. N has characteristics of gases, whereas P and As have characteristics of semiconductors [29]. Sb and Bi have semimetal and brittle metal characteristics, respectively [29]. At room temperature, the electrical resistivities $\rho_s$ of As, Sb and Bi are nearly $2.60 \times 10^{-7}\ \Omega\ \mathrm{m}$, $3.70 \times 10^{-7}\ \Omega\ \mathrm{m}$ and $1.068 \times 10^{-6}\ \Omega\ \mathrm{m}$, respectively, in the solid state [29].

## 1.2 An Overview of Some II-$V_2$ Semiconducting Compounds

### 1.2.1 II-$V_2$ Phosphides

Two different crystalline phases of $ZnP_2$ are designated as α-$ZnP_2$ and β-$ZnP_2$ [28, 34]. The α-$ZnP_2$ and β-$ZnP_2$ have tetragonal and monoclinic structures, respectively [28, 34]. A tetragonal crystal structure of the alpha phase of $ZnP_2$ was reported by Stackelberg *et al.* [35] and White [36]. At temperature 293 K, an indirect energy band gap of 1.65 eV (polarization $E \perp c$) is found in α-$ZnP_2$ [37]. The space group of β-$ZnP_2$ is $C_{2h}^5$ [38]. Monoclinic $ZnP_2$ has lattice parameters nearly

$a = 8.85\,\text{Å}$, $b = 7.29\,\text{Å}$, $c = 7.56\,\text{Å}$ and angle $\beta = 102.3°$ [34]. β-$ZnP_2$ crystal is black-greenish [39]. The resistivity of β-$ZnP_2$ is nearly $10\,\Omega\text{cm}$ [34, 39]. The unit cell of the beta phase of $ZnP_2$ has 08 formula units [39]. Also, the optical energy gap of monoclinic $ZnP_2$ is around 1.33 ~1.37 eV [34, 39]. Two phases of $CdP_2$ are designated as α-$CdP_2$ and β-$CdP_2$ [40, 41]. α-$CdP_2$ and β-$CdP_2$ have Orthorhombic [28, 40] and tetragonal [28] structures, respectively. The band gap of the beta phase of $CdP_2$ for polarizations $E||C$ and $E\perp c$ was studied by Sobolev *et al.* [37]. Cadmium diphosphide finds applications in optoelectronics because of its nonlinear light absorption property [42]. $CdP_2$ may be useful in the fabrication of photoresistors because of its photosensitivity in the visible region [43]. Tetragonal $CdP_2$ and $ZnP_2$ crystals are gyrotropic [44].

### 1.2.2 II-$V_2$ Arsenides

$CdAs_2$ and $ZnAs_2$ have tetragonal [45] and monoclinic [46] structures, respectively. The space group (SG) of monoclinic $ZnAs_2$ is $P2_1/c$ ($C_{2h}^5$) [46, 47]. $CdAs_2$ and $ZnAs_2$ have anisotropic optical and electrical properties [48, 49]. The lattice constants of $CdAs_2$ crystal structure are $a = 7.96\,\text{Å}$, $c = 4.67\,\text{Å}$ [45]. The unit cell of $CdAs_2$ has 04 formula units and a space group $I4_122$ [45]. The mass density of $CdAs_2$ is $5.8\ \text{g/cm}^3$ [45]. At a temperature of 300 K, the indirect energy gap for $CdAs_2$ is 0.995 eV (polarization $E||C$) [48]. $CdAs_2$ has specific molar heat capacities $C_V = 74.46\ \text{J/(mol-K)}$ and $C_P = 74.75\ \text{J/(mol-K)}$ at a temperature of 300 K [50]. The value of birefringence in the infrared region is high for the $CdAs_2$ crystals [51].

## 1.3 Review of Literature

### 1.3.1 $CdP_2$

Berak *et al.* (1968) studied the cadmium-phosphorus system [52]. As per their study [52], $CdP_2$ could exist in 02 phases. The alpha phase of $CdP_2$ is an orthorhombic crystal low-temperature form [40, 52]. As per investigation by the X-Ray powder method, the alpha phase of $CdP_2$ has lattice parameters $a = 9.90\,\text{Å}$, $b = 5.408\,\text{Å}$ & $c = 5.171\,\text{Å}$ [40]. The space group of the alpha phase of $CdP_2$ is

*Pna*$2_1$ [40]. Goodyear *et al.* [40] also investigated the fractional coordinates of non-equivalent atoms of α-$CdP_2$. They [40] also studied the bond length between atoms of α-$CdP_2$. The density of α-$CdP_2$ is nearly 4.18 g/$cm^3$ [40]. Olofsson *et al.* [53] provided further refined data on fractional coordinates and bond lengths for α-$CdP_2$ using the least-squares program. The energy band structure of tetragonal cadmium diphosphide was studied experimentally by Sobolev *et al.* [37]. Tetragonal cadmium diphosphide has a Brillouin zone in a rectangular parallelepiped shape [37]. The energy band gaps (direct and indirect) of tetragonal $CdP_2$ were studied by Sobolev *et al.* [37]. The variation in the optical activity of $CdP_2$ with frequency was studied by Borshch *et al.* [42]. An investigation of the self-induced rotation of polarized electromagnetic waves in tetragonal $CdP_2$ was carried out [54]. The Raman spectrum of β-$CdP_2$ was observed by Gorban *et al.* [55] and Garasevich *et al.* [44]. For the $ZnP_2$-$CdP_2$ system, phase diagram investigation was carried out by Smolyarenko *et al.* [56]. Babonas *et al.* [57] examined the optical activity of tetragonal $CdP_2$ crystals. Manolikas *et al.* investigated different phases of cadmium diphosphide by the electron diffraction method [58]. The thermal expansion coefficient of β-$CdP_2$ as a function of temperature was examined by Sheleg *et al.* [59]. $CdP_2$ crystals have high photosensitivity [43]. Polygalov *et al.* calculated the electron density of the beta phase of $CdP_2$ by means of the pseudo-potential method [60]. The dielectric properties of tetragonal $CdP_2$ were investigated by Aleinikova *et al.* [61] and Kozlov *et al.* [62]. Gnatyuk *et al.* [63] studied the optical dispersion of tetragonal $CdP_2$ crystals. Tetragonal $CdP_2$ crystals have utility in the fabrication of light (electromagnetic wave) filters and temperature sensors [64]. Tetragonal $CdP_2$ crystals are useful in making deflectors of laser beams due to their temperature-dependent refractive index and low heat conduction properties [65]. The variation of the specific heat of β-$CdP_2$ with temperature was studied by Kopytov *et al.* [66]. For the tetragonal $CdP_2$, temperature-dependent elastic stiffness coefficients were examined by Soshnikov *et al.* [67]. Tetragonal $CdP_2$ has a high Verdet constant [68]. Yeshchenko *et al.* [69] fabricated $CdP_2$ nanoclusters and investigated their optical properties. Stamov *et al.* [70] investigated the electrical properties of Schottky barriers made on *n*-type $CdP_2$. Using LDA (Local Density Approximation) and GGA (Generalized Gradient Approximation) functionals, the structural and electronic properties of tetragonal cadmium diphosphide were examined by Feng *et al.* [71]. In the case of $CdP_2$ crystal (symmetry $D_4^8$), 6540 Å is

isotropic wavelength [27]. Feng *et al.* [72] computed the Vickers hardness values for both phases of cadmium diphosphide. Feng *et al.* [72] studied the phonon properties of α-$CdP_2$ and β-$CdP_2$. Shportko [73] examined the impact of P and Cd vacancies on the characteristics of β-$CdP_2$. Popov *et al.* [74] studied the variation of the thermal conductivity of β-$CdP_2$ with temperature. The variation of the resistivity of $CdP_2$ with electron fluence (14-MeV) was studied by Zavada *et al.* [75]. The beta phase of $CdP_2$ has a band gap of about 2.02 eV [54, 68, 73]. The alpha phase of cadmium diphosphide has a band gap of 2.01 eV [76]. The α-$CdP_2$ was prepared by a chemical transport reaction [76]. The alpha phase of cadmium diphosphide shows a strong SHG effect and high laser-induced damage thresholds [76]. The α-$CdP_2$ has a large birefringence and a broad infrared transparent range [76]. These optical properties indicate that the alpha phase of $CdP_2$ is an attractive infrared (IR) nonlinear optical material [76]. The alpha phase of cadmium diphosphide has a second-order nonlinear optical susceptibility [76].

### 1.3.2 $ZnP_2$

The resistivity of α-$ZnP_2$ is of the order of $10^8\,\Omega\text{cm}$ [34]. A study of the photoluminescence of α-$ZnP_2$ with ultraviolet light was carried out by Hegyi *et al.* [34]. The resistivity of β-$ZnP_2$ is of the order of $10\,\Omega\text{cm}$ [34]. Hegyi *et al.* [34] reported fractional coordinates of non-equivalent atoms in the unit cells of α-$ZnP_2$ and β-$ZnP_2$ crystals. The crystal structure of tetragonal $ZnP_2$ was investigated experimentally by White [36]. The pressure-induced transition in $ZnP_2$ was examined by Tanaka [39]. Rubenstein *et al.* [77] prepared single crystals of α-$ZnP_2$ and β-$ZnP_2$. Rubenstein *et al.* [78] studied the electroluminescence emission spectra of tetragonal $ZnP_2$. The thermodynamic properties of $ZnP_2$ were studied by Jordan [79]. The energy band structure of tetragonal zinc diphosphide was studied experimentally by Sobolev *et al.* [37]. As stated by Sobolev *et al.* [37], tetragonal zinc diphosphide has a Brillouin zone in a rectangular parallelepiped shape. Sobolev and Syrbu experimentally investigated the energy band structure of monoclinic zinc diphosphide [38]. The energy band gap $E_g$ of monoclinic $ZnP_2$ was studied through photoconductivity and edge reflectivity [38]. Wardzynski *et al.* illustrated the photoluminescence spectra of tetragonal zinc diphosphide [80]. The alpha phase of zinc diphosphide may have utility in the field of optoelectronics [28]. Self-induced

rotation of polarized electromagnetic waves in tetragonal $ZnP_2$ was analyzed by Borshch [54]. The study of the Raman spectrum of α-$ZnP_2$ was carried out by Gorban *et al.* [55]. The variation of thermal expansion coefficients of α-$ZnP_2$ with temperature is examined by Sheleg *et al.* [81]. The nature of the acceptor levels in α-$ZnP_2$ was examined by Januskevicius *et al.* [82]. Sobolev *et al.* [83] studied the reflection spectra of monoclinic $ZnP_2$. Jayaraman *et al.* [84] studied the pressure-dependent Raman spectra of the alpha phase of $ZnP_2$. The crystal structure of zinc diphosphide with pressure variation was studied by Rubtsov *et al.* [85]. The elastic properties of α-$ZnP_2$ were investigated on the basis of sound speed measurement by Soshnikov *et al.* [67]. The dielectric properties of α-$ZnP_2$ were investigated by Aleinikova *et al.* [61]. Structural investigation of β-$ZnP_2$ was carried out using the X-ray diffraction method [86]. Ultrasonic shear and longitudinal speeds were determined along the axes of α-$ZnP_2$ crystals [67]. For the tetragonal α-$ZnP_2$, temperature-dependent elastic stiffness coefficients were examined by Soshnikov *et al.* [67]. Modulus of rigidity and bulk modulus of α-$ZnP_2$ were determined by Soshnikov *et al.* [67]. The phase composition of $ZnP_2$ crystals in different temperature regimes was examined by Shportko *et al.* [87]. The computed Debye temperature of the alpha phase of zinc diphosphide is 292 K [88]. The alpha phase of zinc diphosphide has a lower elastic anisotropy than that of the beta phase of zinc diphosphide [88]. As per Stamov *et al.*, $ZnP_2 - C_{2h}^5$ has an isotropic wavelength $9060\,\text{Å}$ [89]. The Raman spectra of tetragonal zinc diphosphide were studied by Shportko *et al.* [90]. The study of phase diagrams for $ZnP_2$ was carried out by Trukhan *et al.* [91]. Stamov *et al.* [92] studied the luminescence spectra of tetragonal $ZnP_2$ doped with Mn, Sb and Cd. The Debye temperature for α-$ZnP_2$ is 280 K [93]. Dorogan [94] studied the optical anisotropy of zinc diphosphide. The gyration property of $ZnP_2 - D_4^8$ is useful for governing photodiode characteristics [95]. Živković *et al.* [96] investigated the structural and elastic properties of the alpha and beta phases of zinc diphosphide through the DFT method. Carbon-modified $ZnP_2$-based composites are useful for better electrochemical performance [97]. $ZnP_2$ is useful in making carbon-modified composites due to its better sodium reactivity [97]. An investigation of phonon dispersion for tetragonal zinc diphosphide was carried out by Litvinchuk *et al.* [7]. S. H. Oh *et al.* [98] synthesized zinc diphosphide nanowires using bismuth catalysts.

### 1.3.3 $ZnAs_2$

$ZnAs_2$ is a monoclinic crystal with 08 formula units in the unit cell, as reported by Senko *et al.* [46]. Sobolev *et al.* [38] studied the optical spectra of the $ZnAs_2$ crystal. Lattice parameters of $ZnAs_2$ were experimentally reported by Fleet [47]. $ZnAs_2$ crystals have anisotropy in optical absorption and electrical resistivity [47]. The resistivity $\rho$ of $ZnAs_2$ along vector $\boldsymbol{a}$ is nearly ten times greater than that along vector $\boldsymbol{c}$ at room temperature [28]. FIR absorption spectra in $ZnAs_2$ were investigated by Weszka *et al.* [99]. Matveeva *et al.* [100] studied the photo-reflectivity properties of monoclinic $ZnAs_2$ by the electro-reflectance method. The variation of the Hall coefficient with pressure was studied for *p*-$ZnAs_2$ by Mollaev *et al.* [101]. Temperature-dependent Hall coefficients of *n*-type and *p*-type $ZnAs_2$ were studied by Morozova *et al.* [102]. Yakushev *et al.* [103] studied the Er-implanted $ZnAs_2$ and its temperature stability. Zinc diarsenide crystals have high optical and electrical anisotropy [64]. $ZnAs_2$ crystals are useful for making sensitive thermoelements [64]. Zinc diarsenide crystals may be useful in making light (electromagnetic wave) filters [64]. Light (EM wave) filters for nearly IR region using $ZnAs_2$ crystals have technical applications [64]. Soshnikov *et al.* [67] studied the elastic properties of $ZnAs_2$ crystals. Ultrasonic shear and longitudinal speeds were determined along the axes of zinc diarsenide crystals [67].

Nikolaev *et al.* [104] carried out an investigation of the polarization photosensitivity of the Schottky barriers on the zinc diarsenide. Marenkin *et al.* [48] investigated the optical and transport properties of $ZnAs_2$ crystals to study their band structure. $ZnAs_2$ may be used for infrared polarizers, as $ZnAs_2$ crystal has inhomogeneities in the refractive index [48, 105]. Zinc diarsenide crystals have a high value of infrared transmissivity in a wide range [48]. Zinc diarsenide crystal has a sharp fundamental absorption edge [48]. $ZnAs_2$ crystal is a promising material for devising infrared cut-off filters [48]. An investigation of the phase diagram for $ZnAs_2$ was carried out by Trukhan *et al.* [91]. A phase diagram study of the $ZnAs_2$–MnAs system was carried out by Marenkin *et al.* [106]. Stamov *et al.* studied the dispersion in $ZnAs_2$ for excitonic transitions [107]. The thermodynamic properties of $ZnAs_2$ were examined by Kidari *et al.* [108]. Excitonic polaritons of zinc diarsenide were studied by Syrbu *et al.* [109]. The photovoltaic characteristics of surface-barrier photosensitive structures based on $ZnAs_2$ were studied by Stamov *et al.* [110].

## 1.4 Motivation for Work and Outline of the Thesis

II-V semiconductor compounds are promising materials for photovoltaic applications, as they are made from relatively cost-effective materials. Alpha phase of $CdP_2$ has not yet been explored much. As far as we know, until present, there has been no extensive analysis of the elastic anisotropy of II-$V_2$ semiconductor compounds. Little attention was paid to the Mulliken population analysis of II-$V_2$ materials by researchers. Therefore, the study of overlap populations between the atoms of these compounds was not well known. There was little experimental information on the elastic quantities of II-$V_2$ compounds. As far as we know, there is no other extensive study of the equation of states and pressure derivatives of these compounds. There is no significant study of the pressure-dependent properties of II-$V_2$ compounds. Our comprehensive theoretical analysis with the DFT method will be useful for experimenters.

Our study is aimed at filling this research gap by investigating the structural, electronic and elastic properties of the alpha phase of cadmium diphosphide, the alpha phase of zinc diphosphide and monoclinic zinc diarsenide. To the best of our knowledge, until the present work, there has been almost no study about the variation of Young's modulus, linear compressibility, shear modulus and Poisson's ratio in different planes. Our elastic anisotropy investigation will be useful for determining the orientation of crystals for optimum performance of the optoelectronic devices made from these compounds. The nonlinear optical properties of these compounds are useful for governing the characteristics of optoelectronic devices. Owing to the dearth of work, such as elastic anisotropy, etc., our investigation will give an outlook on relevant device design for experimental research.

The thesis comprises six chapters. Chapter 1 deals with II-V Group elements, II-$V_2$ semiconductors, a review of the literature, etc. Chapter 2 introduces the theoretical framework and useful software/tools for the present work. In Chapter 3, structural properties, such as structural details, structural diagrams, equation of states, etc., are elaborated. Chapter 4 deals with the band structures and the density of states. It also illustrates the Mulliken population analysis. Chapter 5 introduces elastic properties. It illustrates elastic stiffness constants, Young's modulus, bulk modulus, shear modulus and Poisson's ratio of compounds. Chapters 3 to 5 are relatively independent. The final Chapter 6 of the thesis describes the important conclusions drawn.

# CHAPTER 2

# RESEARCH METHODOLOGY

## 2.1 Introduction

Applications of *ab-initio* calculations are on a large scale in chemistry and materials science. *Ab-initio* computations explore the properties of the many-electron system for atoms, molecules, solids, etc. The computation cost (in terms of the computer run time for computation) of *ab-initio* methods is continuously decreasing because of the advancement of computer technology. In density functional theory (DFT), the properties of a system are predicted with the help of the electron density of the system. As per LDA (Local Density Approximation), only the electron density influences the exchange-correlation energy. The GGA (Generalized Gradient Approximation) also includes the gradient of the charge density term. The estimated results obtained with the *ab-initio* methods may be compared with experimental results for further interpretation.

## 2.2 Theoretical Framework

### 2.2.1 DFT (Density Functional Theory)

Along with the variation principle, the Thomas-Fermi (TF) equations are considered the first endeavor to formulate density functional theory (DFT) [111, 112, 113]. DFT is based on the electron density $\rho(x,y,z)$ [114]. Density functional theory (DFT) describes that the ground-state electronic energy of a molecule or atom can be estimated from the electron density $\rho(x,y,z)$ instead of the wavefunction $\psi(x,y,z)$ [115]. In DFT, electron density distribution $\rho(\vec{r})$ performs a key role in lieu of the many-electron wavefunction [116]. The conventional wave function schemes deal quite successfully with a system of a few atoms [116]. However, in dealing with very many-atom systems, conventional wave function schemes have limitations [116]. The determination of all ground-state electronic energy is uniquely carried out by means of electron density in the Hohenberg-Kohn (HK) formulation [12, 115, 117]. The Hohenberg-Kohn formulation does not reveal the form of functional dependence of ground-state energy on the electron density [12]. Kohn and Sham formulated a practical application of DFT by employing Kohn-Sham (KS) orbitals [118, 119]. Kohn-Sham orbitals are functions that illustrate the electron density in DFT calculations [118, 119]. As per the Kohn-Sham formulation [119, 120]

$$n(\vec{r}) = \sum_{k=1}^{N} \left|\psi_k(\vec{r})\right|^2$$

$$V_{xc}[n](\vec{r}) = \frac{\delta}{\delta n(\vec{r})} E_{xc}[n]$$

$$\left[-\frac{1}{2}\nabla^2 + V_{eff}(\vec{r})\right]\psi_k(\vec{r}) = \varepsilon_k \psi_k(\vec{r})$$

$$V_{eff}(\vec{r}) = V(\vec{r}) + \int \frac{1}{\left|\vec{r} - \vec{r}'\right|} n(\vec{r}')d\vec{r}' + V_{xc}[n](\vec{r})$$

$$E = \sum_{k=1}^{N} \varepsilon_k - \frac{1}{2}\iint n(\vec{r}) \frac{1}{\left|\vec{r} - \vec{r}'\right|} n(\vec{r}')\, d\vec{r}\, d\vec{r}' + E_{xc}[n] - \int V_{xc}[n(\vec{r})]n(\vec{r})d\vec{r}$$

where

$n(\vec{r})$ represents electron density

$N$ represents the number of electrons in the system

$\psi_k(\vec{r})$ represents occupied Kohn-Sham (KS) orbitals

$V_{xc}$ represents exchange-correlation potential

$E_{xc}$ represents exchange-correlation energy

$V_{eff}(\vec{r})$ represents effective potential

$V(\vec{r})$ represents external potential

$E$ represents the total energy of many-electron system

$\varepsilon_k$ represents the eigenvalues of occupied states

As per Kohn-Sham formalism, the kinetic energy functional is split mainly into two parts [115]. Kohn-Sham DFT has many similarities with HF (Hartree-Fock) theory, but in general, results obtained with KS DFT are much better [115]. The Hartree-Fock scheme does not take account of the electron correlation [12]. After Kohn-Sham formalism, material scientists employed Kohn-Sham DFT using the LSDA (Local-Spin-Density Approximation) to investigate the properties of solids [121]. In the mid-1980s, gradient-corrected functionals were introduced; this led to major advancements in DFT [121]. Then, analytic gradients were introduced in DFT, which immensely helped in the calculation of geometries [121]. The facility for density functional

calculations was introduced to the Gaussian program in 1993 [121]. The inclusion of correlation effects in the calculations is an advantageous feature of DFT [119, 121]. The used percentage of Hartree-Fock exchange energy is a major distinguishing feature of the hybrid functionals [114].

## 2.2.2 LCAO (Linear Combination of Atomic Orbitals)

Electrons that reside in the low energy core levels of a free atom obey strong localization [122]. These core electrons are strongly localized when atoms form crystals [122]. Hence, electrons in the crystals may be illustrated using the linear superposition of atomic eigenfunctions [122]. LCAO (Linear Combination of Atomic Orbitals) or tight binding approximation is useful for dealing with solutions of periodic potential crystals [123].

Crystalline orbitals may be expressed as a linear combination of Bloch functions in the following manner [124]:

$$\psi_i(\vec{r};\vec{k}) = \sum_{\mu} a_{\mu,i}(\vec{k})\,\phi_\mu(\vec{r};\vec{k})$$

$$\phi_\mu(\vec{r};\vec{k}) = \sum_{g} \varphi_\mu(\vec{r}-\vec{A}_\mu-\vec{g})\,e^{i\vec{k}.\vec{g}}$$

$\psi_i(\vec{r};\vec{k})$ denotes a crystalline orbital

$\phi_\mu(\vec{r};\vec{k})$ denotes the Bloch function

$\varphi_\mu(\vec{r})$ denotes atomic orbitals (local functions)

$\vec{g}$ denotes a lattice vector

$\vec{A}_\mu$ represents the nucleus position in the zero reference cell, on which $\varphi_\mu(\vec{r})$ is centered

The local functions may be represented as linear combinations of Gaussian type functions [124]:

$$\varphi_\mu(\vec{r}-\vec{A}_\mu-\vec{g}) = \sum_{j}^{n_G} d_j G(\alpha_j;\vec{r}-\vec{A}_\mu-\vec{g})$$

$d_j$ denotes a fixed coefficient

$\alpha_j$ denotes an exponent

### 2.2.3 Basis Set

A set of mathematical functions that constructs the wave function is called the basis set [111]. A complete basis set (BS) is made up of an infinite number of functions [115]. Such a complete basis set is not feasible in actual computations [12, 115]. A finite basis set is implemented in computations [12]. Hence, the implementation of a finite basis set creates an inherent approximation [115]. This incompleteness of the basis set produces an error, known as the basis-set truncation error [12]. In the calculation of electronic structure, two types of basis functions are commonly used, namely, Gaussian type orbitals and Slater type orbitals [115]. The next advancement of the basis sets is the Double Zeta (DZ) basis sets [115]. The next improvement in the basis sets is a Triple Zeta (TZ) basis sets [115]. For the basis sets, higher angular momentum functions concern the polarization functions [115]. In the presence of loosely bound electrons, diffuse functions are required [115]. The plane-wave basis set has the orthonormality property [125]. Larger basis sets may increase accuracy in results, but they may also increase computation time [114].

### 2.2.4 Mulliken Population

Atomic and overlap populations can be determined using the Mulliken population analysis scheme [126]. The computation of LCAO coefficients provides the overlap population, which measures quantitatively the bonding and antibonding strengths [126]. The covalency of the bonds within the crystal and the overlap population of the nearest neighbors have a correlation [127]. The positive value of the overlap population between two atoms is considered a bonding state [126]. Similarly, the negative value of the overlap population between two atoms is considered an antibonding state [126]. Overlap population may be considered as an index of binding [128, 129]. Overlap population values close to zero suggest that the electronic populations of the two atoms do not have considerable interaction [127]. There is a correlation between the overlap population of bonds and the bulk modulus of the crystals [127].

## 2.2.5 Equation of State (EOS)

A PVT (Pressure-Volume-Temperature) relation forms an equation of state [130, 131]. It has utility in investigating solid state theories [130, 131]. The values of various thermodynamic parameters, such as bulk modulus, the first pressure derivative of bulk modulus, etc., may be predicted using the equation of state [130, 131]. Thermal expansions of solids are much less than those of gases [132]. Therefore, the isothermal equation of state is usually used for the study of solids [132].

The equilibrium isothermal bulk modulus ( $B_0$ ) of a crystal may be expressed as

$$B_0 = -V\left(\frac{\partial P}{\partial V}\right)_T$$

The isothermal first pressure derivative $B_0'$ (dimensionless parameter) may be expressed as

$$B_0' = \left(\frac{\partial B_0}{\partial P}\right)_T$$

Various equations of states have been derived by many scientists. Some important equations of state that very much hold for materials are as follows:
The third-order Birch-Murnaghan (BM) equation of state is given as [124, 132, 133, 134, 135]:

$$P = \frac{3B_0}{2}\left[\left(\frac{V_0}{V}\right)^{\frac{7}{3}} - \left(\frac{V_0}{V}\right)^{\frac{5}{3}}\right]\left\{1 + \frac{3}{4}\left(B' - 4\right)\left[\left(\frac{V_0}{V}\right)^{\frac{2}{3}} - 1\right]\right\}$$

where $V_0$ is the equilibrium volume at zero pressure.

The third-order Poirier-Tarantola (PT) logarithmic equation of state is given as [124, 132, 136]:

$$P = \frac{B_0 V_0}{V}\left[\ln\left(\frac{V_0}{V}\right) + \left[\ln\left(\frac{V_0}{V}\right)\right]^2 \frac{\left(B_0' - 2\right)}{2}\right]$$

Vinet's equation of state is given by [124, 130, 131, 132]:

$$P = 3B_0\left(\frac{V}{V_0}\right)^{-\frac{2}{3}}\left[1-\left(\frac{V}{V_0}\right)^{\frac{1}{3}}\right]\exp\left[-\frac{3}{2}\left\{\left(\frac{V}{V_0}\right)^{\frac{1}{3}}-1\right\}\left(B_0'-1\right)\right]$$

## 2.2.6 Elastic Stiffness and Compliance Constants

Crystal is assumed to be a homogeneous continuous medium for elastic properties [17]. Homogeneity of the body means that mechanical properties are the same throughout the body [19]. Homogeneous and isotropic terms are not the same [19]. Hooke's law is the basic principle for studying elastic properties [16, 17]. As per this law, strains are considered infinitesimally small [16, 17].

Elastic energy density may be expressed as [17]

$$U = \frac{1}{2}\sum_{u=1}^{6}\sum_{v=1}^{6}\tilde{C}_{uv}e_u e_v$$

Indices are designated as

$1 \equiv xx$, $2 \equiv yy$, $3 \equiv zz$, $4 \equiv yz$, $5 \equiv zx$, $6 \equiv xy$

The generalized Hooke's law forms the basis of the mathematical formulation of elasticity [137]. For small deformations, relationships between strain and stress components are given below [17].

$$X_x = C_{11}e_{xx} + C_{12}e_{yy} + C_{13}e_{zz} + C_{14}e_{yz} + C_{15}e_{zx} + C_{16}e_{xy}$$
$$Y_y = C_{21}e_{xx} + C_{22}e_{yy} + C_{23}e_{zz} + C_{24}e_{yz} + C_{25}e_{zx} + C_{26}e_{xy}$$
$$Z_z = C_{31}e_{xx} + C_{32}e_{yy} + C_{33}e_{zz} + C_{34}e_{yz} + C_{35}e_{zx} + C_{36}e_{xy}$$
$$Y_z = C_{41}e_{xx} + C_{42}e_{yy} + C_{43}e_{zz} + C_{44}e_{yz} + C_{45}e_{zx} + C_{46}e_{xy}$$
$$Z_x = C_{51}e_{xx} + C_{52}e_{yy} + C_{53}e_{zz} + C_{54}e_{yz} + C_{55}e_{zx} + C_{56}e_{xy}$$
$$X_y = C_{61}e_{xx} + C_{62}e_{yy} + C_{63}e_{zz} + C_{64}e_{yz} + C_{65}e_{zx} + C_{66}e_{xy}$$

where $C_{11}$, $C_{12}$, $C_{13}$,... are elastic stiffness constants

$X_x$, $Y_y$, $Z_z$, $Y_z$, $Z_x$ and $X_y$ are stress components

$e_{xx}$, $e_{yy}$, $e_{zz}$, $e_{yz}$, $e_{zx}$ and $e_{xy}$ are strain components

Elastic stiffness constants $C_{uv}$ are material parameters.

The matrix form of the above relations is given as

$$\begin{bmatrix} X_x \\ Y_y \\ Z_z \\ Y_z \\ Z_x \\ X_y \end{bmatrix} = \begin{bmatrix} C_{11} & C_{12} & C_{13} & C_{14} & C_{15} & C_{16} \\ C_{21} & C_{22} & C_{23} & C_{24} & C_{25} & C_{26} \\ C_{31} & C_{32} & C_{33} & C_{34} & C_{35} & C_{36} \\ C_{41} & C_{42} & C_{43} & C_{44} & C_{45} & C_{46} \\ C_{51} & C_{52} & C_{53} & C_{54} & C_{55} & C_{56} \\ C_{61} & C_{62} & C_{63} & C_{64} & C_{65} & C_{66} \end{bmatrix} \begin{bmatrix} e_{xx} \\ e_{yy} \\ e_{zz} \\ e_{yz} \\ e_{zx} \\ e_{xy} \end{bmatrix}$$

Here, the relation $C_{uv} = C_{vu}$ holds [16, 17].

Therefore, the elastic stiffness matrix $C$ is a $6 \times 6$ symmetric matrix [138]. As the relation $C_{uv} = C_{vu}$ holds, the upper triangular form of matrix $C$ is shown below [138].

$$\begin{bmatrix} C_{11} & C_{12} & C_{13} & C_{14} & C_{15} & C_{16} \\ & C_{22} & C_{23} & C_{24} & C_{25} & C_{26} \\ & & C_{33} & C_{34} & C_{35} & C_{36} \\ & & & C_{44} & C_{45} & C_{46} \\ & & & & C_{55} & C_{56} \\ & & & & & C_{66} \end{bmatrix}$$

This leads to 21 independent elastic stiffness constants instead of 36 elastic stiffness constants for fully anisotropic material [17]. The highest number of independent elastic stiffness constants is 21, which can be associated with an elastic material [20]. Depending on the specific symmetry of the crystal, the number of independent stiffness constants is further reduced [17].

For the elastic compliance constants $S_{ij}$ [17]

$$\begin{aligned} e_{xx} &= S_{11}X_x + S_{12}Y_y + S_{13}Z_z + S_{14}Y_z + S_{15}Z_x + S_{16}X_y \\ e_{yy} &= S_{21}X_x + S_{22}Y_y + S_{23}Z_z + S_{24}Y_z + S_{25}Z_x + S_{26}X_y \\ e_{zz} &= S_{31}X_x + S_{32}Y_y + S_{33}Z_z + S_{34}Y_z + S_{35}Z_x + S_{36}X_y \\ e_{yz} &= S_{41}X_x + S_{42}Y_y + S_{43}Z_z + S_{44}Y_z + S_{45}Z_x + S_{46}X_y \\ e_{zx} &= S_{51}X_x + S_{52}Y_y + S_{53}Z_z + S_{54}Y_z + S_{55}Z_x + S_{56}X_y \\ e_{xy} &= S_{61}X_x + S_{62}Y_y + S_{63}Z_z + S_{64}Y_z + S_{65}Z_x + S_{66}X_y \end{aligned}$$

where $S_{11}$, $S_{12}$, $S_{13}$,... are elastic compliance constants.

The matrix form of the above relations is given as

$$\begin{bmatrix} e_{xx} \\ e_{yy} \\ e_{zz} \\ e_{yz} \\ e_{zx} \\ e_{xy} \end{bmatrix} = \begin{bmatrix} S_{11} & S_{12} & S_{13} & S_{14} & S_{15} & S_{16} \\ S_{21} & S_{22} & S_{23} & S_{24} & S_{25} & S_{26} \\ S_{31} & S_{32} & S_{33} & S_{34} & S_{35} & S_{36} \\ S_{41} & S_{42} & S_{43} & S_{44} & S_{45} & S_{46} \\ S_{51} & S_{52} & S_{53} & S_{54} & S_{55} & S_{56} \\ S_{61} & S_{62} & S_{63} & S_{64} & S_{65} & S_{66} \end{bmatrix} \begin{bmatrix} X_x \\ Y_y \\ Z_z \\ Y_z \\ Z_x \\ X_y \end{bmatrix}$$

Here, the relation $S_{uv} = S_{vu}$ holds [16].

Hence, the elastic compliance matrix *S* is the $6 \times 6$ symmetric matrix [138]. As the relation $S_{uv} = S_{vu}$, the upper triangular form of Matrix *S* is shown below [138]

$$\begin{bmatrix} S_{11} & S_{12} & S_{13} & S_{14} & S_{15} & S_{16} \\ & S_{22} & S_{23} & S_{24} & S_{25} & S_{26} \\ & & S_{33} & S_{34} & S_{35} & S_{36} \\ & & & S_{44} & S_{45} & S_{46} \\ & & & & S_{55} & S_{56} \\ & & & & & S_{66} \end{bmatrix}$$

Hooke's law states a linear relation between strain and stress [17]. It holds well enough for many physical phenomena.

## 2.3 Computation Cost

Computational materials science employs computers to investigate and analyze the properties of materials. Computational tools, such as specific software, are utilized to perform computations in materials science. Workstations are computers that are technically configured with hardware and software to perform specific intensive computations with high performance. Efficient and fast computations are important aspects of using workstations regarding their cost-effectiveness. The computation cost is related to the execution time for specific application processing. In *ab-initio* computations for periodic systems, integration in the reciprocal space is a major consideration [124]. Increasing the number of contracted primitives in the basis set significantly lengthens the calculation time for the integrals [124]. Monkhorst and Pack described special *k* points for Brillouin-zone numerical integrations [139]. These symmetry-dependent points concern lattice point-group symmetry [139]. This

Monkhorst-Pack scheme deals in an efficient way for integrating periodic functions in reciprocal space in solid state calculations [139].

## 2.4. Useful Software/Tools

Useful software/tools for the present work are as follows:

### 2.4.1 CRYSTAL Program

The CRYSTAL code [124, 140] can carry out *ab-initio* computations of the electronic wave function of periodic systems. It is an *ab-initio* Hartree-Fock LCAO (Linear Combination of Atomic Orbitals) program for studying of periodic systems.

The initial version of the software was CRYSTAL88, which was released in 1988 [141, 142]. After that, a modified version CRYSTAL92 was released in 1992 [143]. Then after program versions CRYSTAL95 [144], CRYSTAL98 [145], CRYSTAL03 [146], CRYSTAL06 [147], CRYSTAL09 [148, 149] and CRYSTAL14 [150, 151] were developed. In 2017, program version CRYSTAL17 [124, 140] was introduced. Recently, CRYSTAL23 [152, 153] has been released in 2023. Kohn-Sham or Hartree-Fock Hamiltonians may be implemented [124]. The CRYSTAL program can run for 45 point groups, 99 rod groups, 80 layer groups and 230 space groups [124].

The CRYSTAL program is used for the study of the properties of crystalline materials [124]. In this section, a few important features of the CRYSTAL Program are mentioned. The CRYSTAL code provides information about the electronic structure of periodic systems [124]. Computations are performed within density functional theory (DFT), Hartree-Fock (HF) or, hybrid method [124]. A Fock matrix-mixing scheme may be utilized for single-point energy calculation [124]. Also, a Broyden-Anderson [154, 155] accelerator may be used for convergence [124].

A quasi-Newton algorithm (QNA) [156] is employed for geometry optimizations of the system [124, 157, 158, 159, 160]. Atomic coordinates and unit cell parameters are optimized under the full geometry optimization process [124]. Geometry optimization may be carried out in symmetrized fractional coordinates for atomic locations [124]. By default, there is a relaxation of the lattice parameters and nuclear coordinates for geometry optimization [124].

The typical part of computed result of the output file from CRYSTAL Code for geometry optimization is shown below:

```
NEIGHBORS OF THE NON-EQUIVALENT ATOMS

N = NUMBER OF NEIGHBORS AT DISTANCE R
   ATOM   N      R/ANG       R/AU    NEIGHBORS (ATOM LABELS AND CELL INDICES)
  1 CD    1     2.5303     4.7815     7 P     0 0 0
  1 CD    1     2.5588     4.8354     9 P     0 0 0
  1 CD    1     2.5608     4.8393     5 P     0 0 1
  1 CD    1     2.5811     4.8776    10 P     0 0 0
  1 CD    1     3.7381     7.0639     6 P     0 1 0
  1 CD    1     3.7470     7.0807    10 P     0 1 0

  5 P     1     2.1677     4.0964    10 P     0 1-1
  5 P     1     2.2211     4.1972     9 P     0 0 0
  5 P     1     2.5303     4.7815     3 CD    0 1 0
  5 P     1     2.5608     4.8393     1 CD    0 0-1
  5 P     2     3.5717     6.7495     6 P     0 1 0    6 P    0 1-1
  5 P     1     3.7381     7.0639     2 CD    0 1 0

  9 P     1     2.1677     4.0964     6 P     0 1 0
  9 P     1     2.2211     4.1972     5 P     0 0 0
  9 P     1     2.5588     4.8354     1 CD    0 0 0
  9 P     1     2.5811     4.8776     2 CD    0 0 0
  9 P     2     3.5655     6.7379    10 P     0 1 0   10 P    0 1-1
  9 P     1     3.7470     7.0807     2 CD    0 1 0


FINAL OPTIMIZED GEOMETRY - DIMENSIONALITY OF THE SYSTEM      3
(NON PERIODIC DIRECTION: LATTICE PARAMETER FORMALLY SET TO 500)
**********************************************************************
LATTICE PARAMETERS (ANGSTROMS AND DEGREES) - BOHR = 0.5291772083 ANGSTROM
PRIMITIVE CELL - CENTRING CODE 1/0 VOLUME=   273.312083 - DENSITY  4.274 g/cm^3
         A             B             C          ALPHA       BETA        GAMMA
    9.90943135    5.41747907    5.09111440    90.000000   90.000000   90.000000
**********************************************************************
ATOMS IN THE ASYMMETRIC UNIT    3 - ATOMS IN THE UNIT CELL:   12
   ATOM              X/A                 Y/B                 Z/C
**********************************************************************
     1 T  48 CD    1.510931082204E-01  1.041840904521E-01  2.618673672136E-01
     2 F  48 CD   -1.510931082204E-01 -1.041840904521E-01 -2.381326327864E-01
     3 F  48 CD    3.489068917796E-01 -3.958159095479E-01 -2.381326327864E-01
     4 F  48 CD   -3.489068917796E-01  3.958159095479E-01  2.618673672136E-01
     5 T  15 P     1.226211788989E-01  4.437614399261E-01 -3.926345294005E-01
     6 F  15 P    -1.226211788989E-01 -4.437614399261E-01  1.073654705995E-01
     7 F  15 P     3.773788211011E-01 -5.623856007395E-02  1.073654705995E-01
     8 F  15 P    -3.773788211011E-01  5.623856007395E-02 -3.926345294005E-01
     9 T  15 P    -8.709819258754E-03  2.701297597804E-01 -9.123283781300E-02
    10 F  15 P     8.709819258754E-03 -2.701297597804E-01  4.087671621870E-01
    11 F  15 P    -4.912901807412E-01 -2.298702402196E-01  4.087671621870E-01
    12 F  15 P     4.912901807412E-01  2.298702402196E-01 -9.123283781300E-02

T = ATOM BELONGING TO THE ASYMMETRIC UNIT

INFORMATION **** fort.34 **** GEOMETRY OUTPUT FILE

DIRECT LATTICE VECTORS CARTESIAN COMPONENTS (ANGSTROM)
            X                   Y                   Z
  0.990943135018E+01  0.000000000000E+00  0.000000000000E+00
  0.000000000000E+00  0.541747906930E+01  0.000000000000E+00
  0.000000000000E+00  0.000000000000E+00  0.509111439980E+01


CARTESIAN COORDINATES - PRIMITIVE CELL
**********************************************************************
*      ATOM          X(ANGSTROM)         Y(ANGSTROM)         Z(ANGSTROM)
**********************************************************************
   1     48 CD    1.497246783394E+00  5.644151293782E-01  1.333196724058E+00
   2     48 CD   -1.497246783394E+00 -5.644151293782E-01 -1.212360475841E+00
   3     48 CD    3.457468891694E+00 -2.144324405272E+00 -1.212360475841E+00
   4     48 CD   -3.457468891694E+00  2.144324405272E+00  1.333196724058E+00
   5     15 P     1.215106154377E+00  2.404068312562E+00 -1.998947306489E+00
   6     15 P    -1.215106154377E+00 -2.404068312562E+00  5.466098934100E-01
   7     15 P     3.739609520711E+00 -3.046712220883E-01  5.466098934100E-01
   8     15 P    -3.739609520711E+00  3.046712220883E-01 -1.998947306489E+00
   9     15 P    -8.630935601707E-02  1.463422319606E+00 -4.644768143243E-01
  10     15 P     8.630935601707E-02 -1.463422319606E+00  2.081080385575E+00
  11     15 P    -4.868406319071E+00 -1.245317215045E+00  2.081080385575E+00
  12     15 P     4.868406319071E+00  1.245317215045E+00 -4.644768143243E-01
```

```
****    4 SYMMOPS - TRANSLATORS IN FRACTIONAL UNITS
**** MATRICES AND TRANSLATORS IN THE CRYSTALLOGRAPHIC REFERENCE FRAME
  V INV                    ROTATION MATRICES                    TRANSLATORS
  1   1  1.00  0.00  0.00  0.00  1.00  0.00  0.00  0.00  1.00  0.00  0.00  0.00
  2   2 -1.00  0.00  0.00  0.00 -1.00  0.00  0.00  0.00  1.00  0.00  0.00  0.50
  3   3 -1.00  0.00  0.00  0.00  1.00  0.00  0.00  0.00  1.00  0.50  0.50  0.50
  4   4  1.00  0.00  0.00  0.00 -1.00  0.00  0.00  0.00  1.00  0.50  0.50  0.00
TTTTTTTTTTTTTTTTTTTTTTTTTTTTTTTT END          TELAPSE     8448.47 TCPU     6086.93
```

There are different choices available for optimization, such as ATOMONLY, FULLOPTG, CELLONLY, ITATOCEL and INTREDUN [124, 161]. There is the optimization of only atomic coordinates under ATOMONLY option [124]. Under the CELLONLY option, optimization of only cell parameters is carried out [124]. Under the INTREDUN option, optimization in redundant internal coordinates may be performed [124]. The convergence parameter TOLDEG is used for the RMS (root mean square) of the gradient [124]. The convergence parameter TOLDEX is used for the RMS (root mean square) of the displacement. The CRYSTAL Code can also handle geometry optimization with constraints, such as constant volume optimization, linear constraints between atomic coordinates, fixing lattice deformations, fixing internal coordinates and partial optimization of atomic positions [124]. Geometry optimization under external stress may be performed using the keyword EXTPRESS [124]. Transition state search may be carried out with the CRYSTAL program [124, 162].

Electronic properties, such as the band structures, the density of states (DOS), etc., are examined by means of the CRYSTAL Program [124]. Along a specific route in the BZ, the study of the band structure of a crystal may be carried out [124]. Compton profiles (CPs) may be computed from $B(r)$ function [124, 163]. The CRYSTAL Code can compute electronic charge density gradients and charge density maps [124]. The computation of the EMD (Electron Momentum Density) can be performed from the density matrix by means of the CRYSTAL program [124, 164, 165]. Wannier functions (WFs) are calculated from Bloch functions (BFs) [124]. Mulliken population analysis can be carried out using the keyword PPAN [124].

Closed-shell and spin-polarized computations may be carried out with core pseudo-potentials [124]. Certain chemical and physical features of molecules, surfaces, nanotubes and crystals may be investigated with the CRYSTAL program [124]. It is a powerful tool in physics and solid-state chemistry [124].

The CRYSTAL program can perform computations of vibrational frequency and phonon dispersion [124, 166, 167]. The CRYSTAL code can compute the

polarization in ferroelectric crystals [124].

The CRYSTAL Code can explore the dielectric [168, 169, 170], elastic [171, 172, 173, 174], photoelastic [175, 176] and piezoelectric [174, 177, 178] properties of the materials [124]. Frequency-dependent complex dielectric constants can also be calculated using the sub-keyword DYNAMIC [124]. Hence, the refractive index and reflectivity may be calculated [124]. The CRYSTAL code can compute the polarizability and first hyper-polarizability of the systems as well [124].

Elastic tensor, compliance tensor and seismic velocities may be computed by means of CRYSTAL Code [124]. A computation of the elastic stiffness constants under a given pressure can also be performed [124].

The typical force calculation and elastic constant tensor parts of the output file obtained by means of the CRYSTAL Code are shown below:

```
*******************************************************************************
*                              FORCE CALCULATION                              *
*******************************************************************************

TTTTTTTTTTTTTTTTTTTTTTTTTTTTTTTT NUMDFG      TELAPSE      520.57 TCPU      519.44
INFORMATION **** EXCPOG **** EXCH. BIPO BUFFER LENGTH (WORDS) =           0
INFORMATION **** GENPOG **** BIPO BUFFER LENGTH (WORDS) =      388000
TTTTTTTTTTTTTTTTTTTTTTTTTTTTTTTT SHELXG      TELAPSE      581.25 TCPU      580.11

CARTESIAN FORCES IN HARTREE/BOHR (ANALYTICAL)
  ATOM              X                 Y                 Z
   1  48     -1.397978973650E-05 -2.674733165375E-05  3.915374694319E-05
   2  48      1.397978974538E-05  2.674733165864E-05  3.915374695007E-05
   3  48      1.397978952511E-05 -2.674733159647E-05  3.915374694208E-05
   4  48     -1.397978951090E-05  2.674733158603E-05  3.915374694063E-05
   5  15      6.252876411228E-05  1.140667918871E-04 -3.291913787162E-05
   6  15     -6.252876410517E-05 -1.140667918875E-04 -3.291913789738E-05
   7  15     -6.252876416557E-05  1.140667918671E-04 -3.291913791603E-05
   8  15      6.252876414337E-05 -1.140667918702E-04 -3.291913791159E-05
   9  15      5.407249933831E-05  5.047008294223E-05 -6.234609861266E-06
  10  15     -5.407249933742E-05 -5.047008294223E-05 -6.234609875033E-06
  11  15     -5.407249932965E-05  5.047008301151E-05 -6.234609867928E-06
  12  15      5.407249933120E-05 -5.047008299908E-05 -6.234609861711E-06

RESULTANT FORCE      1.043609643148E-14  3.330669073875E-15 -3.286593219798E-12

 ATOMIC PART

 SYMMETRY ALLOWED FORCES (ANALYTICAL) (DIRECTION, FORCE)

    1 -2.7959579E-05    2 -5.3494663E-05    3  9.5906702E-05    4  1.2505753E-04
    5  2.2813358E-04    6 -3.7737621E-05    7  1.0814500E-04    8  1.0094017E-04

 CELL PART

 GRADIENT WITH RESPECT TO THE CELL PARAMETER IN HARTREE/BOHR
ORDER: -D/DA1X, -D/DA1Y, -D/DA1Z
       -D/DA2X, -D/DA2Y, -D/DA2Z
       -D/DA3X, -D/DA3Y, -D/DA3Z
  0.456109284741E-04 -0.134975691715E-13 -0.293793075442E-14
 -0.294177519421E-13  0.851379822819E-04 -0.106590293335E-13
 -0.246468752313E-13 -0.834305417907E-14  0.431142029527E-04

STRESS TENSOR, IN HARTREE/BOHR^3:
ORDER: 11 12 13
       21 22 23
       31 32 33
 -0.463085386805E-06  0.163286452534E-15  0.128563637849E-15
  0.137040118450E-15 -0.472567690763E-06  0.435192447710E-16
  0.298286582916E-16  0.591641091659E-16 -0.224893367720E-06

PRESSURE FROM THE STRESS TENSOR,
```

```
IN HARTREE/BOHR^3:  0.38685E-06
PRESSURE IN GIGAPASCAL:  0.1138E-01
CONVERSION FACTOR: 1 HARTREE/BOHR^3= 29421 GIGAPASCAL
WHEN USING VALUES FOR BOHR RADIUS AND HARTREE
FROM IUPAC WEBSITE, APRIL 2009
ENTHALPY: -2.4569947983521E+04

 SYMMETRY ALLOWED FORCES (ANALYTICAL) (DIRECTION, FORCE)

    1  1.2358260E-03    2  1.7221240E-04    3  3.2301406E-04
 TTTTTTTTTTTTTTTTTTTTTTTTTTTTTTTT TOTGRA_C    TELAPSE      601.33 TCPU      600.18

 VOLUME OF THE CELL: 273.312083

 DENSITY OF THE CRYSTAL =          4.2736 g/cm^3

 STRAIN MATRIX   1 :

  | 1 0 0 |
  | 0 0 0 |
  | 0 0 0 |


   DISPL         ENERGY              DELTA E

-0.0100   -2.4569948440E+04    2.5659149833E-04
 0.0000   -2.4569948697E+04    0.0000000000E+00
 0.0100   -2.4569948223E+04    4.7396548325E-04
 ELASTIC TENSOR CONSTANTS
c11 =              116.69543768 GPa
c12 =               57.51867582 GPa
c13 =               48.88650323 GPa
c14 =                0.00000000 GPa
c15 =               -0.00000000 GPa
c16 =                0.00000000 GPa

 STRAIN MATRIX   2 :

  | 0 0 0 |
  | 0 1 0 |
  | 0 0 0 |


   DISPL         ENERGY              DELTA E

-0.0100   -2.4569948425E+04    2.7206312370E-04
 0.0000   -2.4569948697E+04    0.0000000000E+00
 0.0100   -2.4569948383E+04    3.1418829167E-04

 ELASTIC TENSOR CONSTANTS
c21 =               57.97871800 GPa
c22 =               92.80185127 GPa
c23 =               46.69850866 GPa
c24 =               -0.00000000 GPa
c25 =               -0.00000000 GPa
c26 =                0.00000000 GPa

 STRAIN MATRIX   3 :

  | 0 0 0 |
  | 0 0 0 |
  | 0 0 1 |


   DISPL         ENERGY              DELTA E

-0.0100   -2.4569948390E+04    3.0692274959E-04
 0.0000   -2.4569948697E+04    0.0000000000E+00
 0.0100   -2.4569948481E+04    2.1597814703E-04
 ELASTIC TENSOR CONSTANTS

c31 =               49.81710353 GPa
c32 =               47.26656882 GPa
c33 =               81.86715036 GPa
c34 =               -0.00000000 GPa
c35 =               -0.00000000 GPa
c36 =               -0.00000000 GPa

 STRAIN MATRIX   4 :

  | 0 0 0 |
  | 0 0 1 |
  | 0 1 0 |
```

```
  DISPL         ENERGY              DELTA E

-0.0100   -2.4569948261E+04    4.3587907567E-04
 0.0000   -2.4569948697E+04    0.0000000000E+00
 0.0100   -2.4569948261E+04    4.3578615805E-04
 ELASTIC TENSOR CONSTANTS

c41 =               0.00005917 GPa
c42 =              -0.00016259 GPa
c43 =               0.00002460 GPa
c44 =              34.70221397 GPa
c45 =              -0.00000000 GPa
c46 =               0.00000000 GPa

STRAIN MATRIX   5 :

 | 0 0 1 |
 | 0 0 0 |
 | 1 0 0 |


  DISPL         ENERGY              DELTA E

-0.0100   -2.4569948379E+04    3.1770384885E-04
 0.0000   -2.4569948697E+04    0.0000000000E+00
 0.0100   -2.4569948379E+04    3.1758791374E-04
 ELASTIC TENSOR CONSTANTS

c51 =               0.00019695 GPa
c52 =               0.00029213 GPa
c53 =               0.00040509 GPa
c54 =               0.00000000 GPa
c55 =              25.44113228 GPa
c56 =              -0.00000000 GPa

STRAIN MATRIX   6 :

 | 0 1 0 |
 | 1 0 0 |
 | 0 0 0 |


  DISPL         ENERGY              DELTA E

-0.0100   -2.4569948334E+04    3.6253633152E-04
 0.0000   -2.4569948697E+04    0.0000000000E+00
 0.0100   -2.4569948334E+04    3.6253876533E-04
 ELASTIC TENSOR CONSTANTS

c61 =              -0.00042912 GPa
c62 =              -0.00088103 GPa
c63 =               0.00014724 GPa
c64 =              -0.00000000 GPa
c65 =              -0.00000000 GPa
c66 =              28.97483700 GPa

*****************************************************************************
*****************************************************************************
                          FINAL RESULTS START
*****************************************************************************
*****************************************************************************


THE CALCULATION HAS BEEN PERFORMED WITH   3 POINTS AND
A STEP OF     0.01000
THIS PERMITS TO PERFORM A FITTING UP TO SECOND   ORDER

DATA FOR MAXIMUM NUMBER OF POINTS AND ORDER OF FIT

SYMMETRIZED ELASTIC CONSTANTS FOR ORTHORHOMBIC CASE, IN GPa

|   116.695   57.749   49.352    0.000    0.000    0.000 |
|             92.802   46.983    0.000    0.000    0.000 |
|                      81.867    0.000    0.000    0.000 |
|                              34.702    0.000    0.000 |
|                                       25.441    0.000 |
|                                                 28.975 |


ELASTIC MODULI (COMPLIANCE TENSOR), IN TPa^-1

|   13.5514  -6.0567  -4.6933   0.0000   0.0000   0.0000 |
|            17.8955  -6.6189   0.0000   0.0000   0.0000 |
|                     18.8427   0.0000   0.0000   0.0000 |
|                              28.8166   0.0000   0.0000 |
|                                       39.3064   0.0000 |
|                                                 34.5127 |
```

```
BULK MODULUS K, SHEAR MODULUS G, YOUNG MODULUS E AND
POISSON RATIO v (ALL IN GPa) ACCORDING TO VOIGT-REUSS-HILL

   K_V     G_V     K_R     G_R     K_H     G_H     E_H      v_H

 66.61   26.98   64.30   25.93   65.46   26.45   69.93   0.322

SEISMIC VELOCITIES BY CHRISTOFFEL EQUATION (km/s)

      WAVE VECTOR                Vp        Vs1       Vs2

[ 0.000  0.000  1.000]          4.377     2.850     2.440
[ 0.000  1.000  0.000]          4.660     2.850     2.604
[ 1.000  0.000  0.000]          5.226     2.604     2.440
[ 1.000  1.000  0.000]          5.088     2.653     2.324
[ 1.000  0.000  1.000]          4.856     2.729     2.368
[ 0.000  1.000  1.000]          4.884     2.523     2.168
[ 1.000  1.000  1.000]          4.992     2.549     2.282

*************************************************************************
*************************************************************************
                        FINAL RESULTS END
*************************************************************************
*************************************************************************
```

The piezoelectric and elastic constants of a crystal can be computed using the keyword ELAPIEZO [124]. The piezoelectric tensor may be computed using the keyword PIEZOCON under the numerical Berry phase scheme [124]. Piezoelectric tensors may also be calculated using the keyword PIEZOCP under the CPHF/KS method [124]. For the computation of elastic constants under pressure, using the sub-keyword PREOPTGEOM, pre-optimization is performed [124].

The elasto-optic constants (Pockels tensor) can be computed with the keyword PHOTOELA by means of CRYSTAL program [124].

Electron transport features, such as the Seebeck coefficient and electron thermal conductivity, may be investigated by means of the CRYSTAL program [124]. The electrical conductivity can also be computed [124]. Using the keyword TRANGE, transport properties are computed at different temperatures [124].

### 2.4.2 DL Visualize (DLV)

It is a graphical user interface (GUI) to visualize the different data sets of materials [179]. It is capable of displaying and editing the structures of molecules, periodic structures of surfaces and crystals [179]. DLV facilitates the graphical user interface (GUI) to the CRYSTAL Program [124, 140, 179]. Visualization is an effective way of interpreting data.

DL Visualize is a powerful tool for modeling [179]. DLV provides many features for displaying and analyzing data and specific editing [179]. It provides the flexibility to display the type of cell (primitive/conventional cell) and the number of cells in

periodic structures [179]. Displayed atom radius may be scaled [179]. The Structure Display Panel of DLV is shown in **Fig. 2.1.**

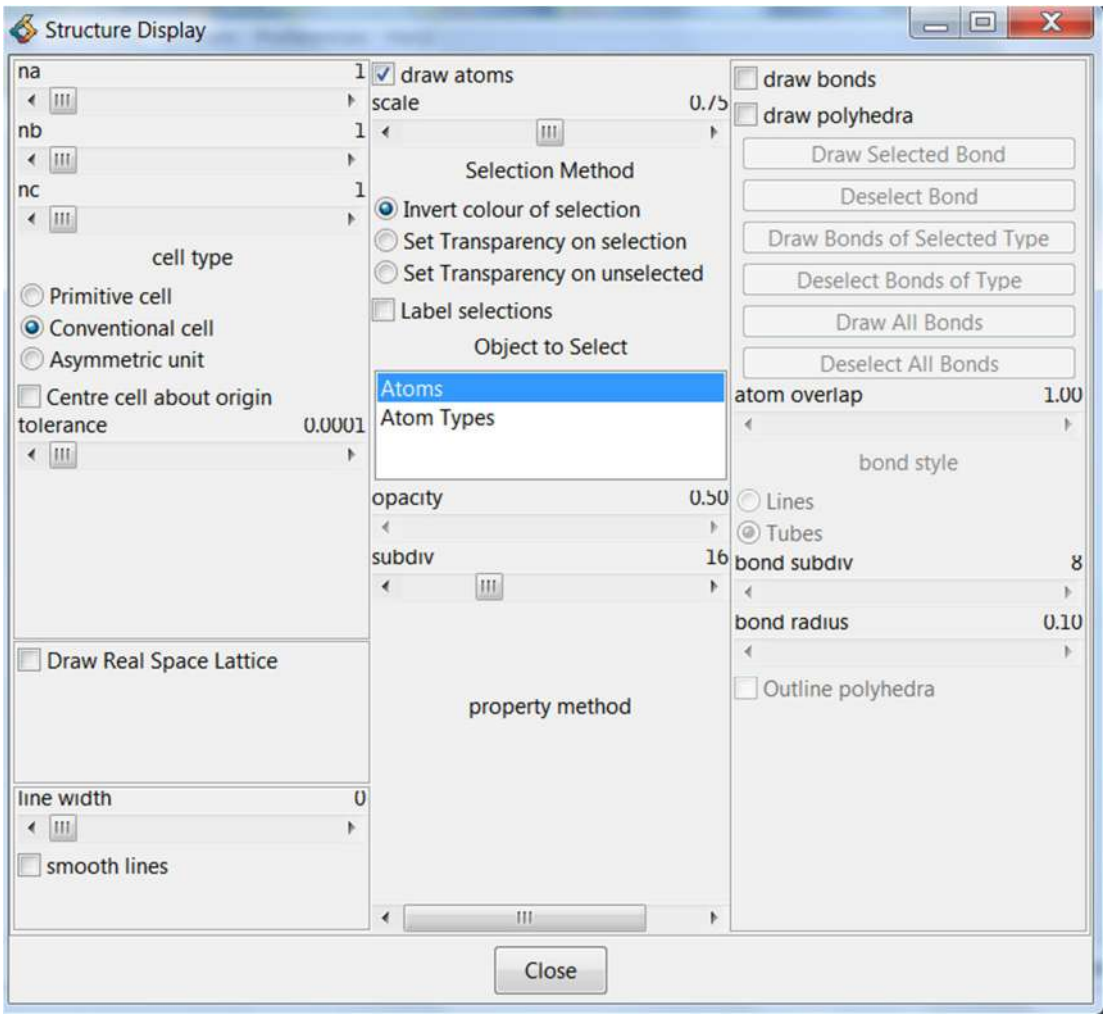


**Figure 2.1:** DL Visualize Structure Display Panel

Properties (radius, color, charge, type, or spin) and positions of atoms can be modified [179]. DLV also provides the facility to delete atoms or introduce a new atom [179]. All the atoms of the same type may also be edited simultaneously [179]. Atoms may also be placed at particular locations [179]. All the atoms of the same type may be highlighted [179].

Displaying specific planes through DLV is possible [179]. DLV also provides a specific animation facility [179]. A slab model may be constructed by entering the Miller indices of particular crystal planes [179]. The lattice may be altered by executing a supercell technique on the primitive unit cell of a periodic system [179].

Specific vectors can be displayed within the structure [179]. DLV is capable of displaying the bonds between atoms in different ways [179]. An option is also available to edit the lattice in certain ways [179]. DLV provides certain facilities for transforming a displayed model into a non-periodic model [179]. DLV is a useful tool for extracting important information by visualizing data sets [179].

### 2.4.3 CRYSPLOT

CRYSPLOT [180] is an online tool for plotting different features of crystals computed with the CRYSTAL Program [124, 140]. The CRYSPLOT is a web-oriented totally free tool and it is a user-friendly program [180]. Certain chemical and physical properties of molecules, surfaces, polymers and crystals may be visualized with the CRYSPLOT [180]. Vibrational spectra, phonon dispersion, density of states, band structure, electron momentum density, electron charge density (ECD), electrostatic potential, topological analysis map, volumetric data, pair correlation function, etc. may be analyzed with the CRYSPLOT [180].

For plotting the band structure, there is a legend option through which a particular band line may be displayed or removed [180]. The CRYSPLOT provides the facility to display the Fermi energy line in the band structure [180]. The *y*-axis unit may be displayed in Hartree or electronvolt in the band structure [180]. Shifting of plot values on the *y*-axis is also possible [180].

It allows plotting the total and projected density of states for all atoms [180]. The DOS and band structure can be plotted in a single combined plot [180]. It is capable of plotting crystal orbital overlap and Hamiltonian populations [180]. The CRYSPLOT is used for the animation of vibrational modes [180]. It is also useful to analyze transport properties, such as electron conductivity, Seebeck coefficient, electron thermal conductivity, etc. [180].

It can also plot the directional Compton profiles and directional autocorrelation function of EMD (electron momentum density) [180]. Raman and infrared spectra may be analyzed [180].

The CRYSPLOT can plot reflectance spectra and complex dielectric function spectra [180]. Energy during the geometrical optimization process and corresponding unit cell structure may be analyzed by means of the CRYSPLOT program [180]. This tool is capable of plotting and analyzing the structure of crystals [180]. The CRYSPLOT can

plot simultaneous multiple datasets of certain properties for comparison [180]. The CRYSPLOT is an advanced tool for customizing graphs and visualizing computed properties [180].

### 2.4.4 ELATE

ELATE [181, 182] is an online tool that is used for the exploration of elastic tensors. Mechanical properties cannot be sufficiently explored fully in the case of the unavailability of experimental data on elastic quantities [181]. *Ab-initio* methods can provide the computed values of elastic constants through computational tools. For plotting Poisson's ratio and shear modulus, representation is used, as described by Marmier [183]. The maximum and minimum values of elastic moduli may be determined through the ELATE tool [181]. The directions in which the maximum and minimum values of elastic moduli exist may be determined [181]. These directions may be different from crystallographic axes. The EALTE Tool also provides the values of the anisotropy parameters (the ratios of maximum to minimum values of elastic quantities) [181]. The computational elastic analysis is important for identifying the materials of requisite usefulness. It is open-source software with a user-friendly interface [181].

A matrix $(6\times6)$ of the elastic stiffness constants is used as input for this application [181]. Directional variations of Poisson's ratio, Young's modulus, linear compressibility and shear modulus are visualized and analyzed through ELATE software [181]. Visualizations of 2D and 3D plots of these elastic quantities are possible by means of this ELATE tool [181]. Thus, it allows visualization of anisotropic elastic properties [181]. The directional-elastic properties may be explored with visualization through ELATE software [181].

It also provides the averaging Voigt-Reuss-Hill scheme [184, 185, 186] values for Young's modulus, bulk modulus, Poisson's ratio and shear modulus [181]. The specific elastic properties are described by elastic tensorial analysis using the ELATE software [181].

For a typical matrix $(6\times6)$ of the elastic stiffness constants, input is processed and part of the resultant output through the ELATE software is shown as [181, 182].

## ELATE: Elastic tensor analysis

Welcome to ELATE, the online tool for analysis of elastic tensors, developed by **Romain Gaillac** and **François-Xavier Coudert** at CNRS / Chimie ParisTech.
If you use the software in published results (paper, conference, etc.), please cite the corresponding paper (*J. Phys. Condens. Matter*, 2016, 28, 275201) and give the website URL.

ELATE is open source software. Any queries or comments are welcome at fx.coudert@chimie-paristech.fr

---

## Summary of the properties (3D material)

### Input: stiffness matrix (coefficients in GPa) of

```
116.69   57.749   49.352       0       0       0
57.749   92.802   46.983       0       0       0
49.352   46.983   81.867       0       0       0
     0        0        0  34.702       0       0
     0        0        0       0  25.441       0
     0        0        0       0       0  28.975
```

### Average properties

| Averaging scheme | Bulk modulus | Young's modulus | Shear modulus | Poisson's ratio |
|---|---|---|---|---|
| Voigt | $K_V$ = 66.615 GPa | $E_V$ = 71.302 GPa | $G_V$ = 26.976 GPa | $\nu_V$ = 0.32161 |
| Reuss | $K_R$ = 64.301 GPa | $E_R$ = 68.566 GPa | $G_R$ = 25.927 GPa | $\nu_R$ = 0.32228 |
| Hill | $K_H$ = 65.458 GPa | $E_H$ = 69.934 GPa | $G_H$ = 26.451 GPa | $\nu_H$ = 0.32194 |

### Eigenvalues of the stiffness matrix

| $\lambda_1$ | $\lambda_2$ | $\lambda_3$ | $\lambda_4$ | $\lambda_5$ | $\lambda_6$ |
|---|---|---|---|---|---|
| 25.441 GPa | 28.975 GPa | 34.702 GPa | 39.885 GPa | 49.331 GPa | 202.15 GPa |

### Variations of the elastic moduli

| | Young's modulus | | Linear compressibility | | Shear modulus | | Poisson's ratio | | |
|---|---|---|---|---|---|---|---|---|---|
| | $E_{min}$ | $E_{max}$ | $\beta_{min}$ | $\beta_{max}$ | $G_{min}$ | $G_{max}$ | $\nu_{min}$ | $\nu_{max}$ | |
| Value | 53.071 GPa | 77.279 GPa | 2.8014 $TPa^{-1}$ | 7.5305 $TPa^{-1}$ | 20.009 GPa | 34.702 GPa | 0.10161 | 0.44694 | Value |
| Anisotropy | 1.456 | | 2.6881 | | 1.734 | | 4.3988 | | Anisotropy |
| Axis | 0.0000<br>0.0000<br>1.0000 | -0.8603<br>0.5098<br>0.0000 | 1.0000<br>0.0000<br>0.0000 | 0.0000<br>0.0000<br>1.0000 | -0.0000<br>0.7071<br>0.7071 | -0.0006<br>-0.0006<br>1.0000 | -0.0001<br>0.7053<br>0.7089 | 1.0000<br>0.0003<br>-0.0001 | Axis |
| | | | | | 0.0001<br>0.7071<br>-0.7071 | -0.0000<br>1.0000<br>0.0006 | 0.0001<br>0.7089<br>-0.7053 | -0.0003<br>1.0000<br>0.0000 | Second axis |

## 2.5 Present Computational Procedure

Properties of the alpha phase of $CdP_2$, the alpha phase of $ZnP_2$ and $ZnAs_2$ are investigated with the CRYSTAL package (periodic *ab-initio* HF and DFT code) [124, 140]. In the present investigation, computations are performed with the DFT exchange-correlation (XC) functionals. In the present study, calculations are carried out with the GGA functionals (PBE [187, 188], PBEsol [189, 190] and PWGGA [191, 192, 193, 194, 195, 196]), LDA functionals (LDA PZ [197, 198], LDA VWN [197, 199]), global hybrid functionals (B3PW [191, 192, 193, 200, 201], B3LYP [199, 200, 202, 203] and PBE0 [204, 205, 206, 207]) and range-separated hybrid functional (HSE06 [187, 188, 208, 209, 210, 211,212, 213, 214, 215]).

The computations of geometrical optimization, equation of state [173], electronic and elastic properties [171, 172, 173] are performed. In this computational work, we have used the basis sets for cadmium, zinc, phosphorus and arsenic atoms from the CRYSTAL-Basis Set Library of the Torino group [124, 140]. The basis set of 31 orbitals for the zinc atom [216] and the basis set of 18 orbitals for the phosphorus atom [217] have been employed. The basis set of 32 orbitals for the arsenic atom is implemented [216]. For the cadmium atom, a basis set of 36 orbitals is implemented. The convergence threshold TOLDEE on energy is adopted $10^{-8}$ Hartree. For carrying out prompt convergence, the BROYDEN accelerator scheme [124, 140, 154, 155] is utilized. The Fock/Kohn-Sham matrix mixing factor (namely, keyword FMIXING) [124, 140] is employed as a convergence tool for the computations. An $8\times8\times8$ Monkhorst-Pack *k*-point mesh [139] is employed for computation. This mesh is associated with 125 *k*-points in the irreducible Brillouin zone (IBZ). For analysis of Mulliken populations [126], the keyword PPAN is used in the CRYSTAL program.

The size of the strain step for the investigation of elastic computations is 0.01. ELATE software [181, 182] is also utilized for the determination of maximum and minimum values of various elastic quantities and for plotting various elastic quantities. The unit cells of α-$CdP_2$, α-$ZnP_2$ and monoclinic $ZnAs_2$ are drawn with the help of DL Visualize (DLV) [179]. The band structures and the DOS are drawn using the CRYSPLOT software [180].

# CHAPTER 3

## STRUCTURAL PROPERTIES OF $CdP_2$, $ZnP_2$ AND $ZnAs_2$ COMPOUNDS

## 3.1 Introduction

Crystal structure characteristics are important for predicting the properties of substances. Theoretical details of crystal structure form the base for experiments. The crystal structure has a correlation with mechanical properties. The crystal system may be illustrated by the relationship between crystal structure and mechanical response. The lattice parameters *a, b, c* and angle between crystallographic axes are important for determining the crystal properties. For the orthorhombic crystal α-$CdP_2$ [40, 41], the unit cell is specified by lattice parameters $a \neq b \neq c$, $\alpha = \beta = \gamma = 90°$. For the tetragonal crystals α-$ZnP_2$ [34, 35, 36] and β-$CdP_2$ [35, 45], the unit cells are specified by lattice parameters $a = b \neq c$, $\alpha = \beta = \gamma = 90°$. Monoclinic crystals $ZnAs_2$ [46, 99] and β-$ZnP_2$ [28, 34] have lattice parameters $a \neq b \neq c$, $\alpha = \gamma = 90°$, $\beta \neq 90°$. In this investigation, the structural properties of the alpha phase of $CdP_2$, the alpha phase of $ZnP_2$ and monoclinic $ZnAs_2$ are studied. In this thesis, the structural properties of II-$V_2$ compounds are studied with classification, such as α-$CdP_2$, α-$ZnP_2$ and $ZnAs_2$, as it enables a logical illustration. A number of aspects of structural properties are described, including the lattice parameters, atomic pair distances and equation of states.

## 3.2 Methodology

The optimized lattice parameters and fractional coordinates of the conventional cells have been investigated using initial geometry data of II-$V_2$ compounds by means of the CRYSTAL Code [124, 140]. The conventional cells of the compounds are plotted using the DLV software [179]. By means of the Birch-Murnaghan [124, 132, 133, 134, 135], Vinet [124, 130, 131] and Poirier-Tarantola [124, 132, 136] equations of states, computations are performed [173]. Also, calculations for the isothermal bulk modulus $B_0$ and its first pressure derivative $B_0'$ are carried out. Atomic pair distances for the first 06 neighbors are obtained using the Mulliken population scheme [126] with the keyword PPAN [124]. For the study of structural properties of II-$V_2$ compounds, computations are carried out with different functionals, such as PBE [187, 188], PBEsol [189, 190], PWGGA [191, 192, 193, 194, 195, 196], LDA PZ [197, 198], LDA VWN [197, 199], B3PW [191, 192, 193, 200, 201], B3LYP [199, 200, 202, 203], PBE0 [204, 205, 206, 207] and HSE06 [187, 188, 208, 209, 210, 211,212, 213, 214, 215].

## 3.3 Results and Discussions

### 3.3.1 Structural Properties of $CdP_2$

#### 3.3.1.1 Structural Details

Two crystalline phases of cadmium diphosphide, namely, alpha and beta, are reported [40, 41, 50]. The alpha phase of cadmium diphosphide has an orthorhombic crystal structure at room temperature [41]. A tetragonal structure is reported for the beta phase of $CdP_2$ [35, 45]. The reported lattice parameters for β-$CdP_2$ are $a$ = 5.28 Å and $c$ = 19.70 Å [35, 45]. The β-$CdP_2$ crystal belongs to 422 class symmetry [42]. The space group of β-$CdP_2$ is $P4_32_12$ and $P4_12_12$ [28].

In this investigation, the structural properties of the alpha phase of $CdP_2$ are studied. The space group of α-$CdP_2$ is $Pna2_1$ [40, 41]. The lattice parameters of α-$CdP_2$ are $a$ = 9.90 Å, $b$ = 5.408 Å and $c$ = 5.171 Å, as reported by Goodyear *et al.* [40]. The α-$CdP_2$ consists of three nonequivalent atoms, namely, Cd, P(I) and P(II) [40]. Four formula units are associated with the unit cell of α-$CdP_2$ [40]. The crystal structure of α-$CdP_2$ is shown in **Fig. 3.1** under the PBE scheme. From **Table 3.1**, it is obvious that the lattice parameters and volume of the cell obtained from LDA functionals are closer to the experimental results. The deviation in unit cell volume is nearly –1.3% with LDA functionals. With HSE06 and B3LYP functionals, deviations in unit cell volume are almost 5.2% and 10.2%, respectively. With LDA VWN functional, deviations in the computed lattice parameters *a*, *b* and *c* with their respective experimental values are about 0.02%, 0.13% and –1.5%, respectively. Deviations in the computed values of the lattice parameters using the B3LYP are the maximum among the functionals mentioned in **Table 3.1**. Using the B3LYP functional, deviations in the computed lattice parameters *a*, *b* and *c* with their respective experimental values are about 2.7%, 3.9% and 3.4%, respectively.

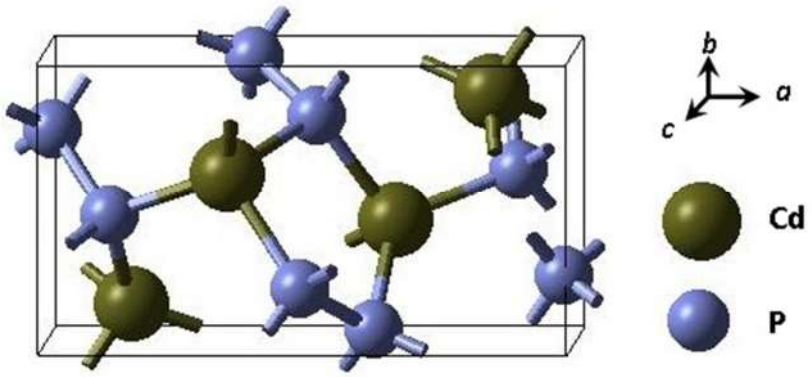


**Figure 3.1:** The crystal structure of an orthorhombic conventional unit cell of α-$CdP_2$. The lengths $a$, $b$ and $c$ are the lattice parameters.

**Table 3.1:** The lattice parameters ($a$, $b$ and $c$ in Å) and volume ($V$ in Å$^3$) of the orthorhombic unit cell of α-$CdP_2$ at zero pressure

| Scheme | *a* | *b* | *c* | *V* |
|---|---|---|---|---|
| PBEsol[3a] | 10.005 | 5.492 | 5.160 | 283.569 |
| PBE | 10.140 | 5.577 | 5.254 | 297.120 |
| PWGGA | 10.124 | 5.572 | 5.253 | 296.331 |
| LDA PZ | 9.909 | 5.417 | 5.091 | 273.312 |
| LDA VWN | 9.902 | 5.415 | 5.095 | 273.178 |
| B3LYP | 10.164 | 5.617 | 5.345 | 305.147 |
| B3PW | 10.105 | 5.550 | 5.230 | 293.332 |
| PBE0 | 10.089 | 5.535 | 5.201 | 290.426 |
| HSE06 | 10.096 | 5.538 | 5.209 | 291.282 |
| Exp[3b]. | 9.90 | 5.408 | 5.171 | 276.9 |
| Other work[3c] | | | | 286.0 |

[3a]Ref. [219].

[3b]Ref. [40].

[3c]Ref. [72].

To enhance the understanding of crystal structure, atomic pair distances for the nearest atoms are described. **Table 3.2** illustrates the atomic pair distances between different atoms in the unit cell of α-$CdP_2$. Under PBE functional, the atomic pair P-P has the nearest distance of about 2.19 Å, whereas the atomic pair Cd-P has the nearest distance of about 2.61Å. The volume of the conventional cell is smaller under the PBEsol scheme than that under the PBE0 scheme, but the atomic pair distance $P_5$-$P_{10}$ is greater under the PBEsol scheme than that under the PBE0 scheme. The same thing is true for atomic pair distances $P_5$-$P_9$. Thus, despite the fact that the computed volume under the PBEsol is less than that under the PBE0 and HSE06, the nearest two P-P pair atoms have a greater atomic distance under the PBEsol functional than under the PBE0 and HSE06 functionals.

**Table 3.2:** Atomic pair distances (in Å) for the first six nearest atoms in α-$CdP_2$

| Atom A | Atom B | Cell | Atomic Pair Distance | | | | | | | | |
|---|---|---|---|---|---|---|---|---|---|---|---|
| | | | PBEsol | PBE | PWGGA | LDA PZ | LDA VWN | B3LYP | B3PW | PBE0 | HSE06 |
| 1Cd | 7P | (0 0 0) | 2.569 | 2.615 | 2.611 | 2.530 | 2.530 | 2.640 | 2.609 | 2.601 | 2.603 |
| | 9P | (0 0 0) | 2.591 | 2.633 | 2.630 | 2.559 | 2.558 | 2.653 | 2.628 | 2.622 | 2.624 |
| | 5P | (0 0 1) | 2.594 | 2.637 | 2.634 | 2.561 | 2.561 | 2.675 | 2.638 | 2.631 | 2.633 |
| | 10P | (0 0 0) | 2.618 | 2.672 | 2.668 | 2.581 | 2.581 | 2.696 | 2.657 | 2.650 | 2.652 |
| | 6P | (0 1 0) | 3.768 | 3.814 | 3.813 | 3.738 | 3.736 | 3.842 | 3.807 | 3.797 | 3.798 |
| | 10P | (0 1 0) | 3.777 | 3.828 | 3.827 | 3.747 | 3.746 | 3.858 | 3.822 | 3.812 | 3.813 |
| 5P | 10P | (0 1–1) | 2.183 | 2.195 | 2.194 | 2.168 | 2.166 | 2.202 | 2.180 | 2.173 | 2.175 |
| | 9P | (0 0 0) | 2.242 | 2.273 | 2.273 | 2.221 | 2.221 | 2.281 | 2.246 | 2.235 | 2.238 |
| | 3Cd | (0 1 0) | 2.569 | 2.615 | 2.611 | 2.530 | 2.530 | 2.640 | 2.609 | 2.601 | 2.603 |
| | 1Cd | (0 0–1) | 2.594 | 2.637 | 2.634 | 2.561 | 2.561 | 2.675 | 2.638 | 2.631 | 2.633 |
| | 6P | (0 1 0) | 3.608 | 3.646 | 3.645 | 3.572 | 3.571 | 3.676 | 3.619 | 3.603 | 3.608 |
| | 2Cd | (0 1 0) | 3.768 | 3.814 | 3.813 | 3.738 | 3.736 | 3.842 | 3.807 | 3.797 | 3.798 |
| 9P | 6P | (0 1 0) | 2.183 | 2.195 | 2.194 | 2.168 | 2.166 | 2.202 | 2.180 | 2.173 | 2.175 |
| | 5P | (0 0 0) | 2.242 | 2.273 | 2.273 | 2.221 | 2.221 | 2.281 | 2.246 | 2.235 | 2.238 |
| | 1Cd | (0 0 0) | 2.591 | 2.633 | 2.630 | 2.559 | 2.558 | 2.653 | 2.628 | 2.622 | 2.624 |
| | 2Cd | (0 0 0) | 2.618 | 2.672 | 2.668 | 2.581 | 2.581 | 2.696 | 2.657 | 2.650 | 2.652 |
| | 10P | (0 1 0) | 3.598 | 3.641 | 3.640 | 3.566 | 3.565 | 3.658 | 3.609 | 3.595 | 3.600 |
| | 2Cd | (0 1 0) | 3.777 | 3.828 | 3.827 | 3.747 | 3.746 | 3.858 | 3.822 | 3.812 | 3.813 |

### 3.3.1.2 Equation of State

An important consideration of pressure derivative in the equation of states is also discussed here. By means of the Birch-Murnaghan [124, 132, 133, 134, 135], Vinet [124, 130, 131] and Poirier-Tarantola [124, 132, 136] equations of states, computations [173] for the isothermal bulk modulus $B_0$, first pressure derivative $B_0'$ and volume of the unit cell of α-$CdP_2$ are performed. The values of bulk modulus, pressure derivative and volume of α-$CdP_2$ are shown in **Table 3.3** under various functionals as computed with the EOS schemes at zero pressure. In most of the cases in **Table 3.3**, bulk modulus has a higher value corresponding to a lower unit cell volume. However, there is no such relationship between volume and pressure derivative in **Table 3.3**.

Here, the value of the pressure derivative $B_0'$ of α-$CdP_2$ under the PBEsol is the lowest, whereas the pressure derivative under the PWGGA is the highest. The typical estimated value of $B_0'$ for the alpha phase of $CdP_2$ lies in the range from 3.93 to 4.17. Thus, this range for the alpha phase of $CdP_2$ lies in the typical range of $B_0'$ from 2 to 6 for solids [220].

**Table 3.3:** At zero pressure, the computed values of bulk modulus $B_0$ (GPa), first pressure derivative $B_0'$ and unit cell volume $V_0$ (Å$^3$) of the α-$CdP_2$ under different functionals

| Scheme | EOS method | $B_0$ | $B_0'$ | $V_0$ |
|---|---|---|---|---|
| PBEsol[3d] | Vinet | 57.88 | 3.94 | 283.526 |
| PBEsol[3d] | Poirier-Tarantola | 57.92 | 3.94 | 283.525 |
| PBEsol[3d] | Birch-Murnaghan | 57.83 | 3.93 | 283.528 |
| PBE | Vinet | 51.99 | 4.13 | 297.066 |
| PBE | Poirier-Tarantola | 52.05 | 4.13 | 297.065 |
| PBE | Birch-Murnaghan | 51.94 | 4.12 | 297.067 |
| PWGGA | Vinet | 52.30 | 4.17 | 296.269 |
| PWGGA | Poirier-Tarantola | 52.36 | 4.17 | 296.269 |
| PWGGA | Birch-Murnaghan | 52.25 | 4.16 | 296.271 |
| LDA PZ | Vinet | 64.37 | 3.99 | 273.573 |
| LDA PZ | Poirier-Tarantola | 64.42 | 4.00 | 273.572 |
| LDA PZ | Birch-Murnaghan | 64.32 | 3.98 | 273.575 |
| LDA VWN | Vinet | 64.52 | 4.02 | 273.218 |
| LDA VWN | Poirier-Tarantola | 64.57 | 4.03 | 273.217 |
| LDA VWN | Birch-Murnaghan | 64.46 | 4.02 | 273.219 |
| B3LYP | Vinet | 52.74 | 4.05 | 304.658 |
| B3LYP | Poirier-Tarantola | 52.79 | 4.05 | 304.658 |
| B3LYP | Birch-Murnaghan | 52.70 | 4.04 | 304.659 |
| B3PW | Vinet | 56.31 | 4.16 | 293.488 |
| B3PW | Poirier-Tarantola | 56.37 | 4.16 | 293.487 |
| B3PW | Birch-Murnaghan | 56.25 | 4.15 | 293.489 |
| PBE0 | Vinet | 58.64 | 4.09 | 290.604 |
| PBE0 | Poirier-Tarantola | 58.70 | 4.10 | 290.604 |
| PBE0 | Birch-Murnaghan | 58.58 | 4.09 | 290.605 |
| HSE06 | Vinet | 58.00 | 4.09 | 291.208 |
| HSE06 | Poirier-Tarantola | 58.06 | 4.09 | 291.208 |
| HSE06 | Birch-Murnaghan | 57.95 | 4.08 | 291.209 |

[3d]Ref. [219].

## 3.3.2 Structural Properties of $ZnP_2$

### 3.3.2.1 Structural Details

Two different crystalline phases of zinc diphosphide are represented as α-$ZnP_2$ and β-$ZnP_2$ [28, 34]. The alpha phase and beta phase of $ZnP_2$ have tetragonal and monoclinic crystal structures, respectively [28, 34]. Stackelberg *et al.* [35] and White [36] reported a tetragonal crystal structure of the alpha phase of $ZnP_2$. The monoclinic structure of $ZnP_2$ has lattice parameters $a$ = 8.85 Å, $b$ = 7.29 Å, $c$ = 7.56 Å and angle $\beta = 102.3°$ [28, 34]. The space group of monoclinic $ZnP_2$ is $P2_1/c$ [34]. In the monoclinic $ZnP_2$, there is tetrahedral coordination for atoms [34]. The tetragonal structure of zinc diphosphide has lattice parameters $a$ = 5.08 Å and $c$ =18.59 Å [36]. Each crystalline phase, α-$ZnP_2$ and β-$ZnP_2$, has 24 atoms in the unit cell [28].

In this work, the structural properties of the alpha phase of $ZnP_2$ are investigated. The conventional cell of α-$ZnP_2$ has eight formula units [28, 36]. Hence, its unit cell has eight Zn and sixteen P atoms [36]. Each Zn atom is bonded to its four nearest P atoms [36]. Also, each P atom is bonded to its two nearest P atoms and two nearest Zn atoms [36]. The study of the alpha phase of $ZnP_2$ (a tetragonal crystal with space group $P4_32_12$ [28, 36]) is carried out with DFT. The α-$ZnP_2$ consists of three nonequivalent atoms, namely, Zn, P(I) and P(II) [36]. The computed fractional coordinates of the conventional cell of α-$ZnP_2$ are shown in **Table 3.4** under the PBE scheme. Optimized lattice parameters of the conventional cell have been investigated using initial geometry data of α-$ZnP_2$ and the obtained results are shown in **Table 3.5**. Our obtained results fairly agree with the other reported results in **Table 3.5**. The volume obtained with LDA functional is the lowest in **Table 3.5**. The conventional cell of the alpha phase of $ZnP_2$ is depicted in **Fig. 3.2** using DLV software [179]. Under the PBE scheme, the crystal structure of the tetragonal unit cell of α-$ZnP_2$ is shown in different planes.

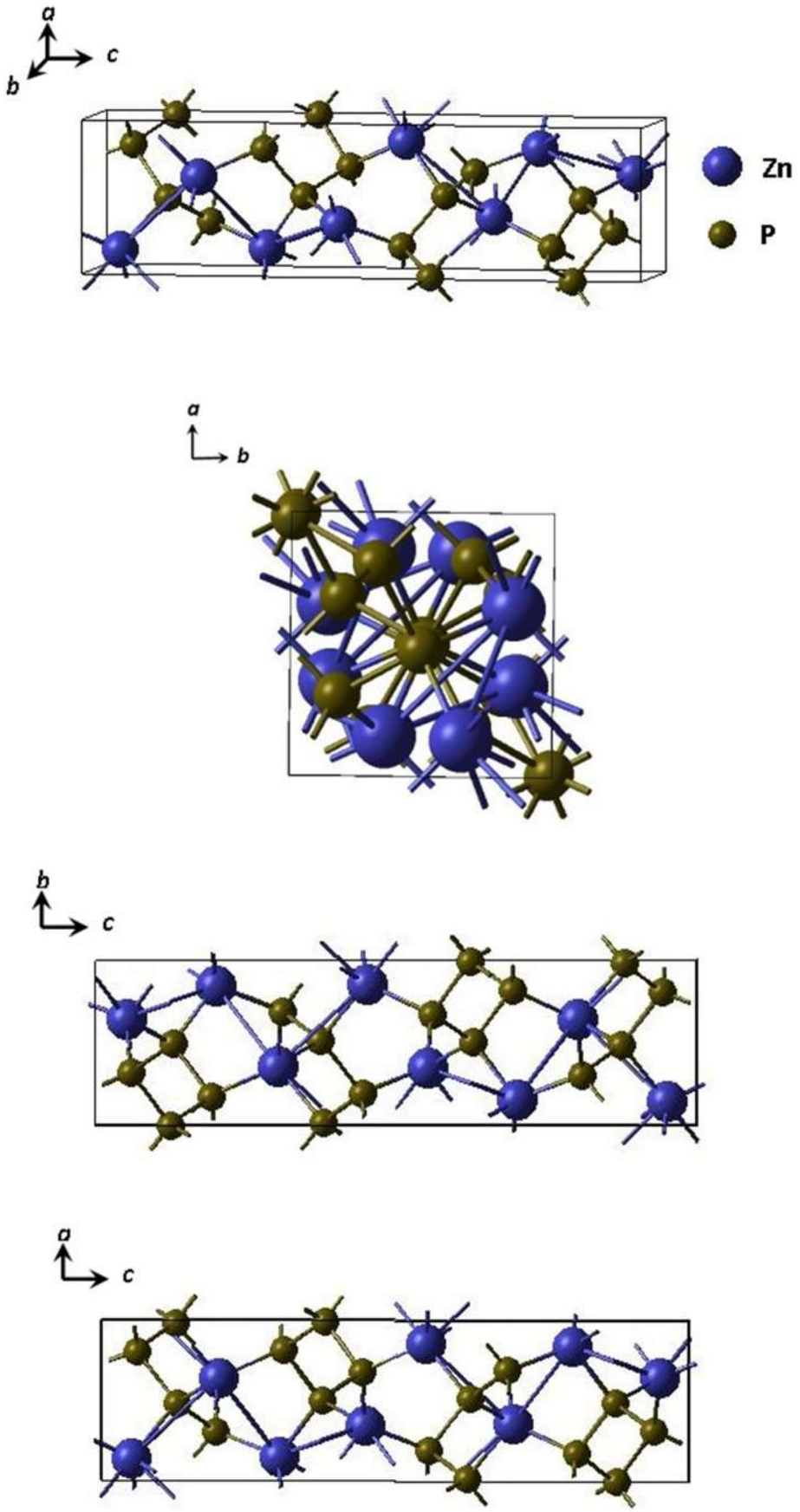


**Figure 3.2:** The crystal structure of a tetragonal unit cell of α-$ZnP_2$. The lengths $a$, $b$ and $c$ are the lattice parameters.

**Table 3.4:** The fractional coordinates of the nonequivalent atoms in the conventional cell of α-$ZnP_2$

| Atom | Fractional coordinates | | | | | |
|---|---|---|---|---|---|---|
| | Present work (PBE scheme) | | | Exp.[3e] | | |
| | *X*/*a* | *Y*/*b* | *Z*/*c* | *X*/*a* | *Y*/*b* | *Z*/*c* |
| Zn | 0.1408 | –0.3476 | 0.0511 | 0.154 | –0.366 | 0.0503 |
| P (I) | –0.0191 | 0.0059 | 0.1229 | –0.010 | –0.020 | 0.1261 |
| P (II) | –0.1943 | 0.3209 | 0.0584 | –0.185 | 0.298 | 0.0597 |

[3e]Ref. [36].

**Table 3.5:** The lattice parameters (*a* and *c* in Å) and volume (*V* in $Å^3$) of the tetragonal unit cell of α-$ZnP_2$ at zero pressure

| Scheme | *a* | *c* | *V* |
|---|---|---|---|
| PBEsol | 5.031 | 18.357 | 464.720 |
| PBE | 5.108 | 18.620 | 485.908 |
| PWGGA | 5.107 | 18.598 | 484.962 |
| LDA PZ | 4.984 | 18.155 | 450.949 |
| LDA VWN | 4.981 | 18.147 | 450.317 |
| B3LYP | 5.170 | 18.823 | 503.161 |
| B3PW | 5.099 | 18.624 | 484.202 |
| PBE0 | 5.083 | 18.595 | 480.410 |
| HSE06 | 5.087 | 18.603 | 481.402 |
| Exp.[3f] | 5.07 | 18.65 | |
| Exp.[3g] | 5.08 | 18.59 | 479.8 |
| Exp.[3h] | 5.0586 | 18.506 | |
| Exp.[3i] | 5.0661 | 18.532 | 475.61 |
| Other Work[3j] | 5.098 | 18.604 | |

[3f]Ref. [35].

[3g]Ref. [36].

[3h]Ref. [61].

[3i]Ref. [222].

[3j]Ref. [88].

The atomic pair distances of α-$ZnP_2$ are shown in **Table 3.6**. The nearest P-P pair distance (about 2.17 Å) is less than the nearest Zn-P (about 2.3 Å) pair distance for LDA scheme. In **Table 3.6**, atomic pair distances between the same pairs under different functional schemes are the lowest for the LDA VWN scheme and the highest for the B3LYP scheme. The nearest neighbor distance between the Cd-P atomic pair in α-$CdP_2$ is greater than the nearest neighbor distance between the Zn-P atomic pair in α-$ZnP_2$. The nearest neighbor distance between the P-P atomic pair in α-$CdP_2$ is not very different from the nearest neighbor distance between the P-P atomic pair in α-$ZnP_2$.

**Table 3.6:** Atomic pair distances (in Å) for the first six nearest atoms in α-$ZnP_2$

| Atom A | Atom B | Cell | Atomic Pair distance | | | | | | | | |
|---|---|---|---|---|---|---|---|---|---|---|---|
| | | | PBEsol | PBE | PWGGA | LDA PZ | LDA VWN | B3LYP | B3PW | PBE0 | HSE06 |
| 1Zn | 22P | (0 0 0) | 2.327 | 2.369 | 2.366 | 2.299 | 2.298 | 2.408 | 2.375 | 2.370 | 2.370 |
| | 11P | (0 –1 0) | 2.345 | 2.383 | 2.381 | 2.320 | 2.319 | 2.416 | 2.388 | 2.384 | 2.385 |
| | 9P | (0 0 0) | 2.349 | 2.391 | 2.388 | 2.322 | 2.321 | 2.426 | 2.396 | 2.391 | 2.392 |
| | 17P | (0 –1 0) | 2.370 | 2.412 | 2.410 | 2.342 | 2.341 | 2.456 | 2.420 | 2.414 | 2.415 |
| | 9P | (0 –1 0) | 3.612 | 3.656 | 3.654 | 3.580 | 3.578 | 3.684 | 3.642 | 3.631 | 3.633 |
| | 19P | (0 –1 0) | 3.623 | 3.661 | 3.660 | 3.594 | 3.592 | 3.684 | 3.644 | 3.633 | 3.636 |
| 9P | 17P | (0 0 0) | 2.183 | 2.198 | 2.198 | 2.171 | 2.169 | 2.202 | 2.182 | 2.176 | 2.178 |
| | 19P | (0 0 0) | 2.251 | 2.275 | 2.275 | 2.234 | 2.233 | 2.278 | 2.249 | 2.238 | 2.242 |
| | 3Zn | (0 0 0) | 2.345 | 2.383 | 2.381 | 2.320 | 2.319 | 2.416 | 2.388 | 2.384 | 2.385 |
| | 1Zn | (0 0 0) | 2.349 | 2.391 | 2.388 | 2.322 | 2.321 | 2.426 | 2.396 | 2.391 | 2.392 |
| | 11P | (0 0 0) | 3.532 | 3.571 | 3.569 | 3.504 | 3.502 | 3.585 | 3.547 | 3.536 | 3.540 |
| | 1Zn | (0 1 0) | 3.585 | 3.656 | 3.654 | 3.546 | 3.545 | 3.684 | 3.642 | 3.631 | 3.633 |
| 17P | 9P | (0 0 0) | 2.183 | 2.198 | 2.198 | 2.171 | 2.169 | 2.202 | 2.182 | 2.176 | 2.178 |
| | 11P | (–1 0 0) | 2.251 | 2.275 | 2.275 | 2.234 | 2.233 | 2.278 | 2.249 | 2.238 | 2.242 |
| | 6Zn | (0 0 0) | 2.327 | 2.369 | 2.366 | 2.299 | 2.298 | 2.408 | 2.375 | 2.370 | 2.370 |
| | 1Zn | (0 1 0) | 2.370 | 2.412 | 2.410 | 2.342 | 2.341 | 2.456 | 2.420 | 2.414 | 2.415 |
| | 19P | (0 0 0) | 3.597 | 3.634 | 3.633 | 3.573 | 3.571 | 3.652 | 3.607 | 3.594 | 3.598 |
| | 3Zn | (0 0 0) | 3.623 | 3.661 | 3.660 | 3.594 | 3.592 | 3.684 | 3.644 | 3.633 | 3.636 |

### 3.3.2.2 Equation of State

By means of the Birch-Murnaghan [124, 132, 133, 134, 135], Vinet [124, 130, 131] and Poirier-Tarantola [124, 132, 136] equations of states, computations [173] for the isothermal bulk modulus $B_0$ and first pressure derivative $B_0'$ are performed for α-$ZnP_2$. In this investigation, with these three EOS schemes, results with the estimated values of $B_0$, $B_0'$ and unit cell volume of α-$ZnP_2$ at zero pressure are shown in **Table 3.7**. All three EOS schemes provide approximately the same estimated values for $B_0$ and $B_0'$ for the given functional scheme. Under GGA functionals, a reasonable consistency is found between our respective estimated values of $B_0$ & $B_0'$ and those of Fan *et al.* [221]. Under the PBE functional, using the Vinet EOS, the plot of relative energy $E$ (per unit cell) of α-$ZnP_2$ versus its unit cell volume is shown in **Fig. 3.3**.

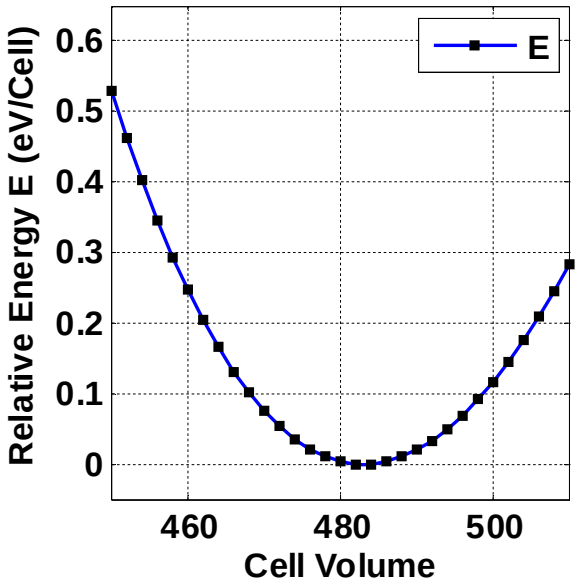


**Figure 3.3:** Under the Vinet EOS scheme, the plot of relative energy per unit cell $E$ (with respect to minimum energy) of α-$ZnP_2$ versus its unit cell volume (Å$^3$). The obtained data points are shown in the volume range of the unit cell from 450 Å$^3$ to 510 Å$^3$.

The typical estimated range of $B_0'$ for the alpha phase of $ZnP_2$ is 4.34−4.58, which lies in the general typical range of $B_0'$ from 2 to 6 for solids [220].

**Table 3.7:** At zero pressure, the computed values of bulk modulus $B_0$(GPa), first pressure derivative $B_0'$ and unit cell volume $V_0$(Å$^3$) of the alpha phase of $ZnP_2$ under different functionals

| Scheme | EOS method | $B_0$ | $B_0'$ | $V_0$ |
|---|---|---|---|---|
| PBEsol | Vinet | 75.33 | 4.48 | 464.716 |
| PBEsol | Poirier-Tarantola | 75.25 | 4.36 | 464.731 |
| PBEsol | Birch-Murnaghan | 75.37 | 4.57 | 464.704 |
| PBE | Vinet | 66.30 | 4.54 | 482.967 |
| PBE | Poirier-Tarantola | 66.42 | 4.52 | 482.970 |
| PBE | Birch-Murnaghan | 66.22 | 4.54 | 482.966 |
| PWGGA | Vinet | 66.63 | 4.55 | 484.835 |
| PWGGA | Poirier-Tarantola | 66.74 | 4.56 | 484.833 |
| PWGGA | Birch-Murnaghan | 66.55 | 4.55 | 484.835 |
| LDA PZ | Vinet | 82.98 | 4.54 | 451.306 |
| LDA PZ | Poirier-Tarantola | 83.12 | 4.55 | 451.303 |
| LDA PZ | Birch-Murnaghan | 82.88 | 4.53 | 451.309 |
| LDA VWN | Vinet | 83.18 | 4.57 | 450.614 |
| LDA VWN | Poirier-Tarantola | 83.33 | 4.58 | 450.611 |
| LDA VWN | Birch-Murnaghan | 83.08 | 4.56 | 450.617 |
| B3LYP | Vinet | 63.97 | 4.35 | 502.939 |
| B3LYP | Poirier-Tarantola | 64.06 | 4.35 | 502.938 |
| B3LYP | Birch-Murnaghan | 63.90 | 4.34 | 502.942 |
| B3PW | Vinet | 70.13 | 4.41 | 484.188 |
| B3PW | Poirier-Tarantola | 70.24 | 4.41 | 484.186 |
| B3PW | Birch-Murnaghan | 70.05 | 4.40 | 484.190 |
| PBE0 | Vinet | 72.68 | 4.35 | 480.485 |
| PBE0 | Poirier-Tarantola | 72.79 | 4.35 | 480.483 |
| PBE0 | Birch-Murnaghan | 72.60 | 4.34 | 480.487 |
| HSE06 | Vinet | 71.90 | 4.35 | 481.450 |
| HSE06 | Poirier-Tarantola | 72.00 | 4.36 | 481.448 |
| HSE06 | Birch-Murnaghan | 71.82 | 4.35 | 481.452 |
| Other Work[3k] | | 76.83 | | |
| Other Work[3l] | | 69 | | 483.6 |
| Other Work[3m] | | 63.13 | 4.445 | |
| Exp.[3n] | | 63.6 | | |

[3k]Ref. [96].
[3l]Ref. [88].
[3m]Ref. [221].
[3n]Ref. [67].

## 3.3.3 Structural Properties of $ZnAs_2$

### 3.3.3.1 Structural Details

In this investigation, the structural properties of $ZnAs_2$ are studied. The crystal structure of $ZnAs_2$ is shown in **Fig. 3.4**. Under the PBE scheme, the crystal structure is shown with the *ab* plane view, *ac* plane view, *bc* plane view and 3D view. The space group of monoclinic $ZnAs_2$ is $P2_1/c$ ($C_{2h}^5$) [46, 47]. $ZnAs_2$ has 08 formula units in the monoclinic unit cell [46]. Monoclinic $ZnAs_2$ has 06 nonequivalent atoms in the unit cell [47, 50]. With the initial geometry data of $ZnAs_2$ [46, 47], the optimized lattice parameters have been computed. The lattice parameters (*a, b, c* and angle $\beta$) and volume of the unit cell under different functional methods are shown in **Table 3.8**. It is evident from **Table 3.8** that volume is the least with LDA functional and volume is the maximum for the B3LYP functional. Using the PBE functional, deviations in the computed lattice parameters *a, b* and *c* with their respective experimental values are about $-0.33\%$, $-0.27\%$ and $0.21\%$, respectively. It is evident from **Table 3.8** that deviations in computed angle $\beta$ with its respective experimental value are small. The maximum deviation in angle $\beta$ is observed for the B3LYP scheme, which is about 0.034%.

**Table 3.8:** The lattice parameters (*a, b* and *c* in Å), angle $\beta$ (in degrees) and volume *V* (in $Å^3$) of the monoclinic unit cell of $ZnAs_2$ at zero pressure

| Scheme | *a* | *b* | *c* | $\beta$ | *V* |
|---|---|---|---|---|---|
| PBEsol[3o] | 9.125 | 7.570 | 7.909 | 102.483 | 533.42 |
| PBE | 9.256 | 7.670 | 8.027 | 102.494 | 556.325 |
| PWGGA | 9.249 | 7.665 | 8.021 | 102.498 | 555.204 |
| LDA PZ | 9.035 | 7.477 | 7.818 | 102.425 | 515.791 |
| LDA VWN | 9.028 | 7.487 | 7.822 | 102.415 | 516.393 |
| B3LYP | 9.342 | 7.741 | 8.088 | 102.501 | 571.051 |
| B3PW | 9.244 | 7.672 | 8.003 | 102.487 | 554.145 |
| PBE0 | 9.221 | 7.649 | 7.977 | 102.475 | 549.314 |
| HSE06 | 9.219 | 7.650 | 7.976 | 102.466 | 549.228 |
| Exp.[3p] | 9.287 | 7.691 | 8.010 | 102.466 | |

[3o]Ref. [223].
[3p]Ref. [47].

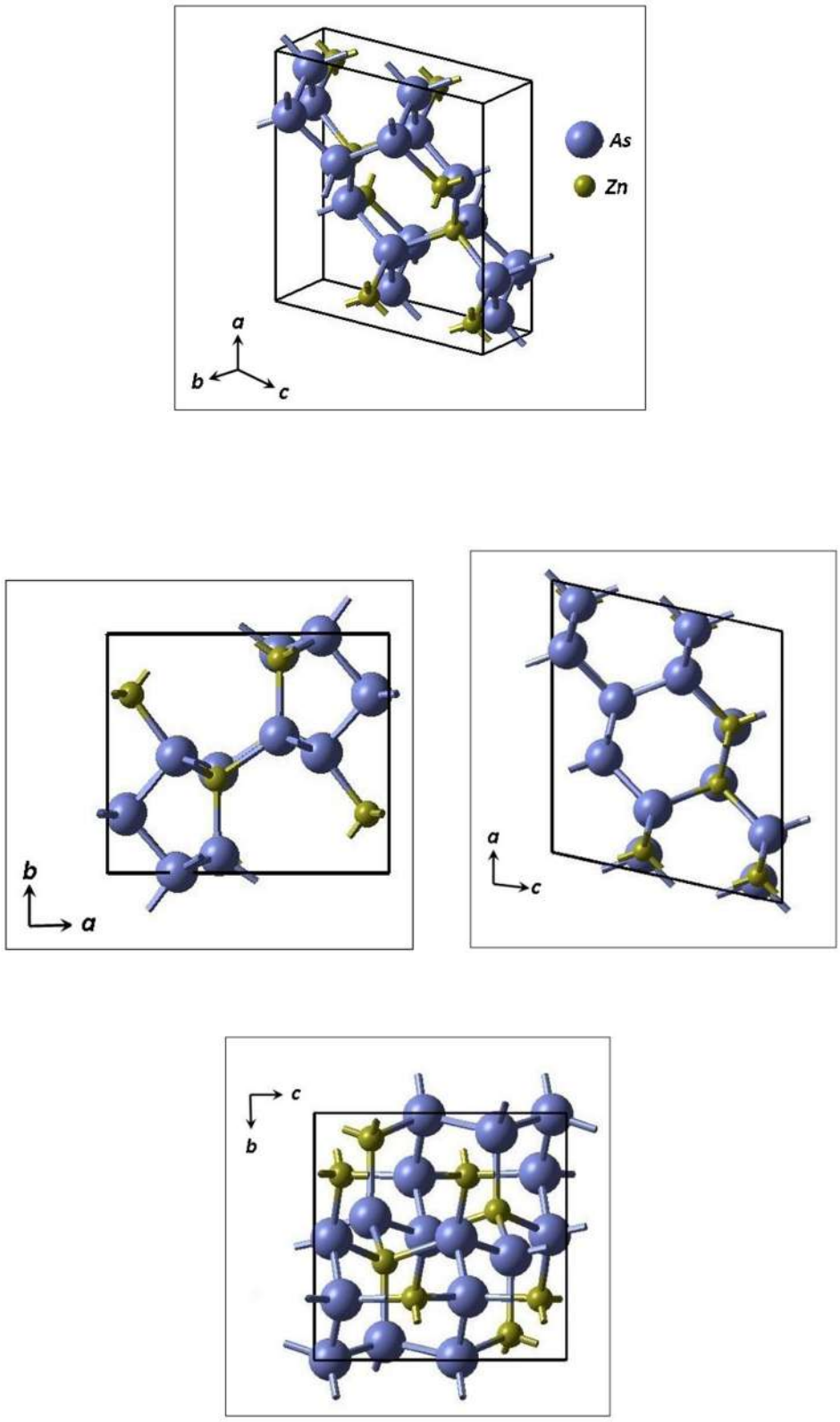


**Figure 3.4:** The crystal structure of a monoclinic unit cell of $ZnAs_2$. The lengths *a*, *b* and *c* are the lattice parameters.

**Table 3.9:** Atomic pair distances (in Å) for the first six nearest atoms in $ZnAs_2$

| Atom A | Atom B | Cell | Atomic Pair Distance | | | | | | | | |
|---|---|---|---|---|---|---|---|---|---|---|---|
| | | | PBEsol | PBE | PWGGA | LDA PZ | LDA VWN | B3LYP | B3PW | PBE0 | HSE06 |
| 1Zn | 22As | (0 0 0) | 2.371 | 2.406 | 2.403 | 2.343 | 2.344 | 2.431 | 2.408 | 2.402 | 2.401 |
| | 23As | (0 0 1) | 2.373 | 2.407 | 2.405 | 2.344 | 2.346 | 2.432 | 2.409 | 2.405 | 2.403 |
| | 17As | (0 –1 0) | 2.412 | 2.449 | 2.446 | 2.378 | 2.383 | 2.476 | 2.452 | 2.447 | 2.443 |
| | 13As | (0 0 0) | 2.416 | 2.455 | 2.452 | 2.382 | 2.386 | 2.486 | 2.460 | 2.455 | 2.450 |
| | 21As | (0 –1 0) | 3.717 | 3.777 | 3.774 | 3.671 | 3.662 | 3.816 | 3.785 | 3.772 | 3.770 |
| | 21As | (0 0 0) | 3.860 | 3.899 | 3.897 | 3.814 | 3.833 | 3.930 | 3.892 | 3.882 | 3.886 |
| 5Zn | 10As | (1 0 0) | 2.406 | 2.444 | 2.442 | 2.374 | 2.374 | 2.471 | 2.450 | 2.441 | 2.440 |
| | 9As | (0 0 0) | 2.420 | 2.454 | 2.453 | 2.396 | 2.393 | 2.487 | 2.460 | 2.453 | 2.458 |
| | 13As | (0 0 0) | 2.442 | 2.482 | 2.479 | 2.409 | 2.411 | 2.511 | 2.486 | 2.481 | 2.477 |
| | 20As | (0 0 0) | 2.446 | 2.485 | 2.483 | 2.412 | 2.417 | 2.515 | 2.489 | 2.483 | 2.480 |
| | 24As | (0 0 0) | 3.637 | 3.679 | 3.680 | 3.603 | 3.601 | 3.709 | 3.676 | 3.669 | 3.667 |
| | 21As | (0 0 0) | 3.679 | 3.712 | 3.712 | 3.645 | 3.651 | 3.737 | 3.703 | 3.697 | 3.697 |
| 9As | 6Zn | (1 1 0) | 2.406 | 2.444 | 2.442 | 2.374 | 2.374 | 2.471 | 2.450 | 2.441 | 2.440 |
| | 5Zn | (0 0 0) | 2.420 | 2.454 | 2.453 | 2.396 | 2.393 | 2.487 | 2.460 | 2.453 | 2.458 |
| | 16As | (0 0 0) | 2.461 | 2.489 | 2.488 | 2.443 | 2.442 | 2.491 | 2.464 | 2.453 | 2.457 |
| | 17As | (0 0 0) | 2.461 | 2.489 | 2.488 | 2.443 | 2.443 | 2.491 | 2.465 | 2.454 | 2.456 |
| | 21 As | (0 0 0) | 3.756 | 3.804 | 3.802 | 3.730 | 3.727 | 3.815 | 3.773 | 3.755 | 3.764 |
| | 24As | (0 0 0) | 3.761 | 3.812 | 3.811 | 3.732 | 3.731 | 3.826 | 3.782 | 3.764 | 3.771 |
| 13As | 1Zn | (0 0 0) | 2.416 | 2.455 | 2.452 | 2.382 | 2.386 | 2.467 | 2.440 | 2.430 | 2.450 |
| | 21As | (0 0 0) | 2.435 | 2.462 | 2.462 | 2.409 | 2.411 | 2.486 | 2.460 | 2.454 | 2.433 |
| | 5Zn | (0 0 0) | 2.442 | 2.482 | 2.479 | 2.417 | 2.417 | 2.491 | 2.465 | 2.455 | 2.477 |
| | 12As | (0 01) | 2.461 | 2.489 | 2.488 | 2.443 | 2.442 | 2.511 | 2.486 | 2.481 | 2.457 |
| | 17As | (0 0 0) | 3.677 | 3.725 | 3.723 | 3.646 | 3.645 | 3.741 | 3.700 | 3.686 | 3.688 |
| | 8Zn | (0 0 1) | 3.792 | 3.830 | 3.830 | 3.760 | 3.761 | 3.857 | 3.819 | 3.811 | 3.814 |
| 17As | 1Zn | (0 1 0) | 2.412 | 2.449 | 2.446 | 2.378 | 2.383 | 2.458 | 2.433 | 2.424 | 2.443 |
| | 21As | (0 0 0) | 2.427 | 2.455 | 2.454 | 2.412 | 2.411 | 2.476 | 2.452 | 2.447 | 2.427 |
| | 8Zn | (0 0 1) | 2.446 | 2.485 | 2.483 | 2.412 | 2.417 | 2.491 | 2.464 | 2.453 | 2.480 |
| | 9As | (0 0 0) | 2.461 | 2.489 | 2.488 | 2.443 | 2.443 | 2.515 | 2.489 | 2.483 | 2.456 |
| | 13As | (0 0 0) | 3.677 | 3.725 | 3.723 | 3.646 | 3.645 | 3.741 | 3.700 | 3.686 | 3.688 |
| | 5Zn | (0 0 0) | 3.787 | 3.827 | 3.827 | 3.755 | 3.756 | 3.857 | 3.817 | 3.809 | 3.810 |
| 21As | 2Zn | (0 0 0) | 2.371 | 2.406 | 2.403 | 2.343 | 2.344 | 2.431 | 2.408 | 2.402 | 2.401 |
| | 3Zn | (0 0 1) | 2.373 | 2.407 | 2.405 | 2.344 | 2.346 | 2.432 | 2.409 | 2.405 | 2.403 |
| | 17As | (0 0 0) | 2.427 | 2.455 | 2.454 | 2.412 | 2.411 | 2.458 | 2.433 | 2.424 | 2.427 |
| | 13As | (0 0 0) | 2.435 | 2.462 | 2.462 | 2.417 | 2.417 | 2.467 | 2.440 | 2.430 | 2.433 |
| | 8Zn | (0 0 1) | 3.637 | 3.679 | 3.680 | 3.603 | 3.601 | 3.709 | 3.676 | 3.669 | 3.667 |
| | 5Zn | (0 0 0) | 3.679 | 3.712 | 3.712 | 3.645 | 3.651 | 3.737 | 3.703 | 3.697 | 3.667 |

Atomic pair distances for monoclinic $ZnAs_2$ for the first 06 nearest atoms are shown in **Table 3.9**. The unit cell of $ZnAs_2$ has 06 nonequivalent atoms [47, 50], namely Zn(I), Zn(II), P(I), P(II), P(III) and P(IV). In general, the nearest atomic pair Zn-As distance is smaller than the nearest atomic pair As-As distance. For example, in **Table 3.9**, the nearest atomic pair Zn-As distance is about 2.34 Å and the nearest atomic pair As-As distance is about 2.41 Å in the LDA functional.

### 3.3.3.2 Equation of State

The Birch-Murnaghan [124, 132, 133, 134, 135], Vinet [124, 130, 131] and Poirier-Tarantola [124, 132, 136] equations of states [173] are utilized for calculations of the isothermal bulk modulus $B_0$ and first pressure derivative $B_0'$. In this work, with these mentioned EOS schemes, the computed values of $B_0$, $B_0'$ and volume of the cell of $ZnAs_2$ at zero pressure are depicted in **Table 3.10**. Under the PBE functional, using the Vinet EOS, the plot of relative energy $E$ (per unit cell) of $ZnAs_2$ versus its monoclinic unit cell volume is shown in **Fig. 3.5**.

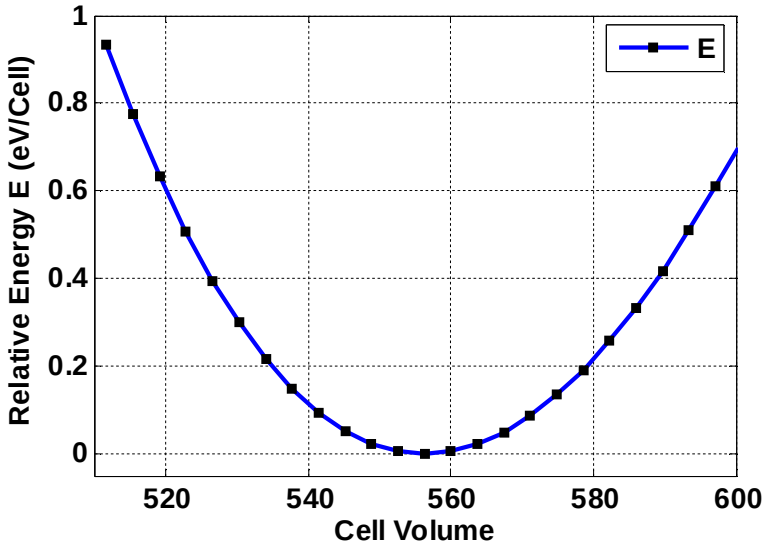


**Figure 3.5:** Under the Vinet EOS scheme, the plot of relative energy per unit cell $E$ (with respect to minimum energy) of $ZnAs_2$ versus its unit cell volume ($Å^3$). The obtained data points are shown in the volume range of the unit cell from 512 $Å^3$ to 600 $Å^3$.

**Table 3.10:** At zero pressure, the computed values of bulk modulus $B_0$ (GPa), first pressure derivative $B_0'$ and unit cell volume $V_0$ (Å$^3$) of $ZnAs_2$ under different functionals

| Scheme | EOS method | $B_0$ | $B_0'$ | $V_0$ |
|---|---|---|---|---|
| PBEsol | Vinet | 79.88 | 3.26 | 531.486 |
| PBEsol | Poirier-Tarantola | 79.89 | 3.26 | 531.484 |
| PBEsol | Birch-Murnaghan | 79.88 | 3.25 | 531.490 |
| PBE | Vinet | 73.31 | 4.01 | 556.253 |
| PBE | Poirier-Tarantola | 73.37 | 4.01 | 556.252 |
| PBE | Birch-Murnaghan | 73.25 | 4.00 | 556.253 |
| PWGGA | Vinet | 73.96 | 3.96 | 553.897 |
| PWGGA | Poirier-Tarantola | 74.02 | 3.97 | 553.896 |
| PWGGA | Birch-Murnaghan | 73.90 | 3.96 | 553.899 |
| LDA PZ | Vinet | 86.05 | 2.73 | 515.507 |
| LDA PZ | Poirier-Tarantola | 86.03 | 2.74 | 515.506 |
| LDA PZ | Birch-Murnaghan | 86.13 | 2.72 | 515.512 |
| LDA VWN | Vinet | 83.54 | 2.62 | 515.248 |
| LDA VWN | Poirier-Tarantola | 83.52 | 2.62 | 515.248 |
| LDA VWN | Birch-Murnaghan | 83.63 | 2.61 | 515.252 |
| B3LYP | Vinet | 72.38 | 4.16 | 569.734 |
| B3LYP | Poirier-Tarantola | 72.46 | 4.16 | 569.733 |
| B3LYP | Birch-Murnaghan | 72.31 | 4.16 | 569.735 |
| B3PW | Vinet | 75.77 | 4.20 | 554.109 |
| B3PW | Poirier-Tarantola | 75.86 | 4.20 | 554.108 |
| B3PW | Birch-Murnaghan | 75.69 | 4.19 | 554.112 |
| PBE0 | Vinet | 79.12 | 3.98 | 547.737 |
| PBE0 | Poirier-Tarantola | 79.26 | 3.98 | 547.736 |
| PBE0 | Birch-Murnaghan | 79.19 | 3.98 | 547.739 |
| HSE06 | Vinet | 78.59 | 3.96 | 548.669 |
| HSE06 | Poirier-Tarantola | 78.65 | 3.96 | 548.667 |
| HSE06 | Birch-Murnaghan | 78.52 | 3.95 | 548.671 |

The typical estimated value of the first pressure derivative for $ZnAs_2$ is 2.61–4.20, which lies in the typical range of $B_0'$ from 2 to 6 for solids [220]. For the given

functional scheme, all three EOS schemes provide nearly the same estimated values for $B_0$, $B_0'$ and unit cell volumes $V_0$. It is evident from **Table 3.10** that the computed value of $B_0'$ is the minimum under the LDA scheme and the maximum under the B3PW scheme.

## 3.4 Conclusions

This chapter explores the structural properties of α-$CdP_2$, α-$ZnP_2$ and $ZnAs_2$ by implementing DFT methods. Our investigation illustrates that atomic pair P-P has the nearest distance of about 2.17 Å, whereas atomic pair Cd-P has the nearest distance of about 2.53 Å in the unit cell of α-$CdP_2$ under LDA scheme. The lattice parameters and volume of the α-$CdP_2$ cell computed from LDA functionals are closer to experimental results. An important feature, such as the pressure derivative in the equation of state, was also elaborated. The values of bulk modulus and first pressure derivative of α-$CdP_2$ computed with EOS (Vinet, Poirier-Tarantola and Birch-Murnaghan) are in the range 51.94–64.57 GPa and in the range 3.93–4.17, respectively, at zero pressure under various functionals. For the alpha phase of $CdP_2$, the first pressure derivative $B_0'$ lies in the general range of $B_0'$ from 2 to 6 for solids.

For atomic pair distances of α-$ZnP_2$, the nearest P-P pair distance is about 2.17 Å and the nearest Zn-P pair distance is about 2.3 Å under LDA functional. The obtained nearest neighbor distance between the P-P atomic pair in α-$ZnP_2$ is not much different from the nearest neighbor distance between the P-P atomic pair in α-$CdP_2$. The nearest neighbor distance between the Zn-P atomic pair in α-$ZnP_2$ is less than the nearest neighbor distance between the Cd-P atomic pair in α-$CdP_2$. The estimated range of the first pressure derivative $B_0'$ for α-$ZnP_2$ is about 4.34–4.58. The computed range of bulk modulus $B_0$ for α-$ZnP_2$ is about 64–83 GPa.

For $ZnAs_2$, deviations in the calculated lattice parameters *a*, *b* and *c* with their respective experimental values are about −0.33%, −0.27% and 0.21%, respectively, under the PBE scheme. The value of computed angle $\beta$ of $ZnAs_2$ is about 102.46° at zero pressure under various functionals. The unit cell of $ZnAs_2$ has 06 nonequivalent atoms, namely Zn(I), Zn(II), P(I), P(II), P(III) and P(IV). The nearest atomic pair As-As distance is larger than the nearest atomic pair Zn-As distance in the unit cell of $ZnAs_2$.

Under the LDA scheme, the nearest atomic pair Zn-As distance is about 2.34 Å and the nearest atomic pair As-As distance is about 2.41 Å in the monoclinic $ZnAs_2$ crystal. The typical calculated value of the first pressure derivative for $ZnAs_2$ is 2.61–4.20. The estimated value of bulk modulus for $ZnAs_2$ lies in the range 72.31–86.13 GPa.

# CHAPTER 4

## ELECTRONIC PROPERTIES OF $CdP_2$, $ZnP_2$ AND $ZnAs_2$ COMPOUNDS

## 4.1 Introduction

Investigation of the density of states and electronic band structures provides information on the electronic properties of materials. Using special $\vec{k}$ points of high symmetry in the reciprocal space, the electronic band structure of the material is plotted. The electronic band structure provides an energy band gap for the material. The direct energy band gaps as well as the indirect energy band gaps of semiconductor compounds may be determined by the electronic band structures. The total DOS (density of states) and the PDOS (partial density of states) are useful in predicting conduction properties. Understanding the electronic band structure of a substance can elucidate its optical properties. The region close to Fermi energy in the band structure has importance in the deduction of important conclusions about electronic properties. The position of Fermi energy in the plot between the density of states and the energy plays an important role in finding out the conduction properties of solids [13].

Contributions to the electronic states of different shells and orbitals may be illustrated by the partial density of states (PDOS). Mulliken population analysis may be utilized to illustrate electronic charge density distribution. Overlap population is useful in predicting the various features of the nature of chemical bonds in substances. An analysis of the overlap population may indicate the covalent and ionic characters of a chemical bond. Mulliken population analysis can also reveal typical atomic charges. Investigations on the electronic properties of II–$V_2$ semiconductor compounds will be useful in the development of semiconductor devices for optoelectronics.

## 4.2 Methodology

Using the CRYSTAL Code [124, 140], electronic properties are investigated. The keyword BAND is used for the analysis of electronic band properties [124]. Band structures are plotted using CRYSPLOT [180]. The plot of the energy of a band state as a function of a wave vector $\vec{k}$ (in the Brillouin zone) forms a band structure [50]. In this work, the density of states is plotted using CRYSPLOT [180]. Mulliken population [126] is analyzed by means of the keyword PPAN [124]. Overlap population and charge transfer are also studied with different functionals. Properties

of the density of states are studied using the keyword DOSS [124]. The energy band range (first and last bands) may be specified for the computation of the density of states. The energy band gaps of compounds are computed with different functionals.

In the present work, computations are performed with the functionals PBE [187, 188], PBEsol [189, 190], PWGGA [191, 192, 193, 194, 195, 196], LDA PZ [197, 198], LDA VWN [197, 199], B3PW [191, 192, 193, 200, 201], B3LYP [199, 200, 202, 203], PBE0 [204, 205, 206, 207] and HSE06 [187, 188, 208, 209, 210, 211,212 213, 214, 215]. In the present investigation, the study of the electronic properties of α-$CdP_2$, α-$ZnP_2$ and $ZnAs_2$ is carried out.

## 4.3 Results and Discussions

### 4.3.1 Electronic Properties of $CdP_2$

#### 4.3.1.1 Band Structure and DOS

The beta phase of cadmium diphosphide has an energy band gap of about 2.02 eV [54, 68, 73]. For polarizations $E \| c$ and $E \perp c$, Sobolev *et al*. studied the energy band gap of β-$CdP_2$ [37]. In the present study, the electronic properties of the alpha phase of $CdP_2$ are investigated. The band structure calculations can provide details about the energy band gap, Fermi energy, band structures, the valence band maxima, the conduction band minima, etc. [224]. The band structure of α-$CdP_2$ is shown in **Fig. 4.1**. The band structure of α-$CdP_2$ is drawn along appropriate paths connecting special points of high symmetry [225].

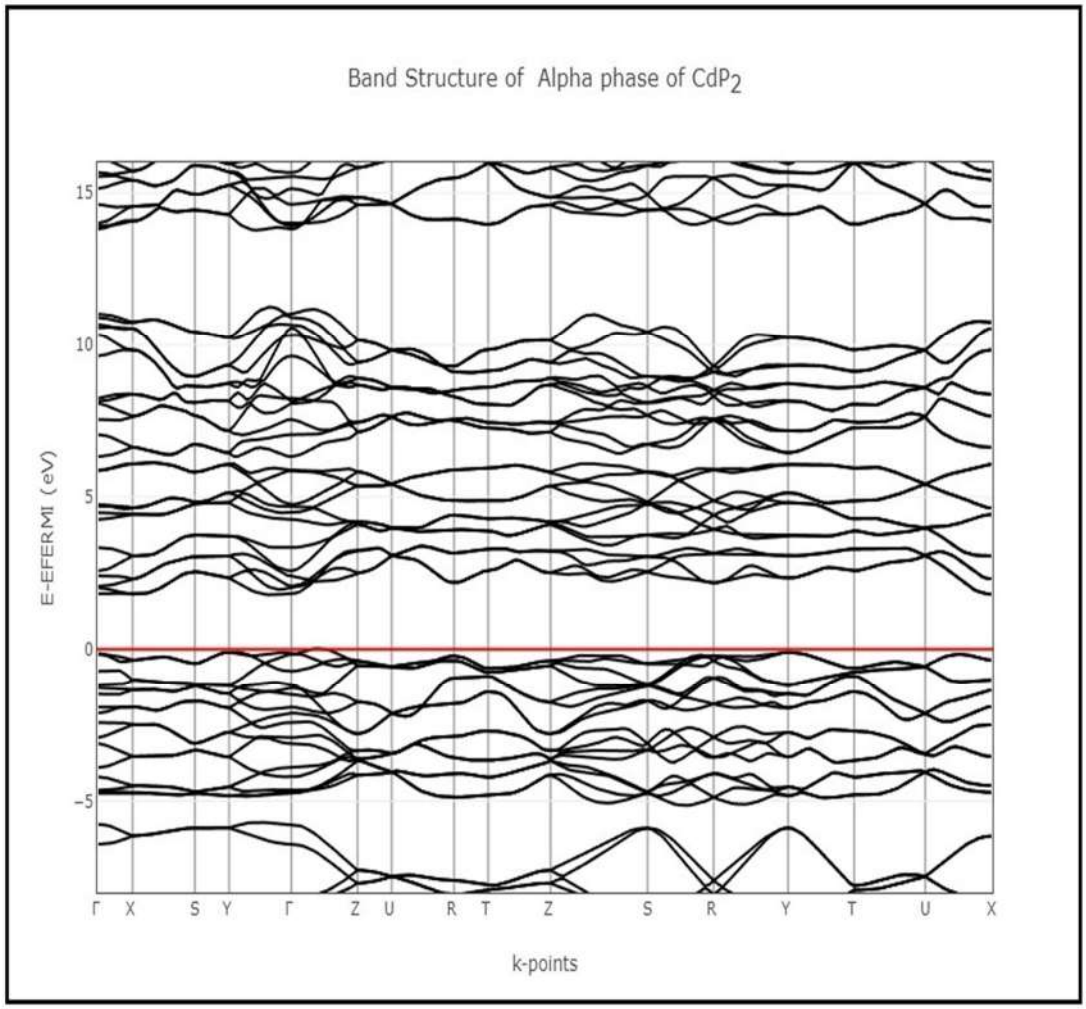


**Figure 4.1:** The band structure of α-$CdP_2$ under the PBE scheme.

The energy band gap of α-$CdP_2$ is 1.79 eV under the PBE scheme. The energy value of 1.79 eV lies in the energy band gap range for semiconductors. The highest point of the valence band can be seen on the path $\Gamma - Z$ in **Fig. 4.1**. It is also evident from **Fig. 4.1** that the lowest point of the conduction band exists near the *X* point. Hence, it shows the indirect energy band gap of 1.79 eV for the alpha phase of cadmium diphosphide. For electronic band structure, computations are performed along high symmetry directions for these special points (namely $X, Z, S, U, Y, R, \Gamma,$ etc.) in the Brillouin zone [4].

Relative to the Fermi energy level, the density of states is plotted from about $-5$ eV to 10 eV, as shown in **Fig. 4.2**. On the *y*-axis, arbitrary units are used for the density of states, but scaling is the same for all the atoms, which are mentioned in **Fig. 4.2**.


**Figure 4.2:** The density of states of α-$CdP_2$ under the PBE scheme.

The total DOS and the density of states of nonequivalent atoms [Cd, P(I) and P(II)] of α-$CdP_2$ are shown in **Fig. 4.2**. Each P(I) and P(II) atom contributes more in comparison to the contribution to the density of states by Cd atom. The density of states lying near the Fermi energy level has importance in determining the electronic properties of materials. The study of the band structure and the density of states for α-$CdP_2$ was carried out with the PBEsol functional in other work [219].

### 4.3.1.2 Mulliken Population Analysis

**Table 4.1** shows the charges of nonequivalent Cd and P atoms in α-$CdP_2$ crystal. The charge transfer in the LDA scheme is less than that in other schemes, as mentioned in **Table 4.1**. The charge transfer values for Cd, P(I) and P(II) are 1.055*e*, 0.536*e* and 0.519*e*, respectively, under the PBE scheme. It is evident from **Table 4.1** that the maximum charge transfer values for Cd, P(I) and P(II) atoms take place under the PBE0 scheme. The energy band gap values for α-$CdP_2$ crystals are shown in **Table 4.2**. The energy band gap value is the least for the LDA scheme and the maximum for the PBE0 scheme, as evident from **Table 4.2**. The overlap population in α-$CdP_2$ crystal for the first six nearest neighbors is shown in **Table 4.3**. In **Table 4.3**, negative values of the overlap population show antibonding [126]. Positive values of the overlap population show bonding [126]. For bonding states, overlap population values for most of the pairs are higher for the LDA scheme, as shown in **Table 4.3**. From **Table 3.2**, it is obvious that pairs 1Cd-7P and 5P-3Cd each have a minimum distance, and the overlap population has a maximum value, as seen in **Table 4.3.** The overlap population for pair 1Cd-7P has a value of 0.148 under the PBE method.

**Table 4.1:** Charges (in terms of *e*) of nonequivalent Cd and P atoms of α-$CdP_2$

| Scheme | Charge Cd | Charge P (I) | Charge P (II) |
|---|---|---|---|
| PBEsol[4a] | 46.977 | 15.522 | 15.502 |
| PBE | 46.945 | 15.536 | 15.519 |
| PWGGA | 46.960 | 15.528 | 15.512 |
| LDA PZ | 47.038 | 15.493 | 15.469 |
| LDA VWN | 47.038 | 15.493 | 15.469 |
| B3LYP | 46.941 | 15.533 | 15.526 |
| B3PW | 46.906 | 15.554 | 15.541 |
| PBE0 | 46.879 | 15.568 | 15.554 |
| HSE06 | 46.887 | 15.564 | 15.549 |

[4a]Ref. [219].

**Table 4.2:** Energy band gap (in eV) of α-$CdP_2$

| PBEsol[4b] | PBE | PWGGA | LDA PZ | LDA VWN | B3LYP | B3PW | PBE0 | HSE06 | Other Work[4c] |
|---|---|---|---|---|---|---|---|---|---|
| 1.76 | 1.79 | 1.78 | 1.71 | 1.71 | 2.90 | 2.97 | 3.25 | 2.60 | 1.49 |

[4b]Ref. [219].

[4c]Ref. [226, 227].

**Table 4.3:** Overlap population for the first six nearest neighbors in α-$CdP_2$

| Atom A | Atom B | Cell | Overlap Population AB | | | | | | | | |
|---|---|---|---|---|---|---|---|---|---|---|---|
| | | | PBEsol[4d] | PBE | PWGGA | LDA PZ | LDA VWN | B3LYP | B3PW | PBE0 | HSE06 |
| 1Cd | 7P | (0 0 0) | 0.154 | 0.148 | 0.150 | 0.164 | 0.164 | 0.148 | 0.146 | 0.144 | 0.145 |
| | 9P | (0 0 0) | 0.139 | 0.134 | 0.136 | 0.145 | 0.145 | 0.136 | 0.132 | 0.129 | 0.129 |
| | 5P | (0 0 1) | 0.141 | 0.136 | 0.138 | 0.148 | 0.148 | 0.135 | 0.132 | 0.130 | 0.130 |
| | 10P | (0 0 0) | 0.135 | 0.128 | 0.130 | 0.144 | 0.144 | 0.128 | 0.127 | 0.125 | 0.125 |
| | 6P | (0 1 0) | –0.009 | –0.008 | –0.008 | –0.009 | –0.010 | –0.007 | –0.008 | –0.008 | –0.008 |
| | 10P | (0 1 0) | –0.010 | –0.008 | –0.008 | –0.010 | –0.011 | –0.008 | –0.009 | –0.009 | –0.009 |
| 5P | 10P | (0 1 –1) | 0.068 | 0.076 | 0.078 | 0.066 | 0.066 | 0.102 | 0.089 | 0.087 | 0.085 |
| | 9P | (0 0 0) | 0.021 | 0.030 | 0.032 | 0.018 | 0.018 | 0.062 | 0.046 | 0.044 | 0.042 |
| | 3Cd | (0 1 0) | 0.154 | 0.148 | 0.150 | 0.164 | 0.164 | 0.148 | 0.146 | 0.144 | 0.145 |
| | 1Cd | (0 0 –1) | 0.141 | 0.136 | 0.138 | 0.148 | 0.148 | 0.135 | 0.132 | 0.130 | 0.130 |
| | 6P | (0 1 0) | –0.066 | –0.060 | –0.059 | –0.069 | –0.069 | –0.056 | –0.066 | –0.071 | –0.069 |
| | 2Cd | (0 1 0) | –0.009 | –0.008 | –0.008 | –0.009 | –0.010 | –0.007 | –0.008 | –0.008 | –0.008 |
| 9P | 6P | (0 1 0) | 0.068 | 0.076 | 0.078 | 0.066 | 0.066 | 0.102 | 0.089 | 0.087 | 0.085 |
| | 5P | (0 0 0) | 0.021 | 0.030 | 0.032 | 0.018 | 0.018 | 0.062 | 0.046 | 0.044 | 0.042 |
| | 1Cd | (0 0 0) | 0.139 | 0.134 | 0.136 | 0.145 | 0.145 | 0.136 | 0.132 | 0.129 | 0.129 |
| | 2Cd | (0 0 0) | 0.135 | 0.128 | 0.130 | 0.144 | 0.144 | 0.128 | 0.127 | 0.125 | 0.125 |
| | 10P | (0 1 0) | –0.069 | –0.062 | –0.062 | –0.072 | –0.072 | –0.060 | –0.070 | –0.074 | –0.072 |
| | 2Cd | (0 1 0) | –0.010 | –0.008 | –0.008 | –0.010 | –0.011 | –0.008 | –0.009 | –0.009 | –0.009 |

[4d]Ref. [219].

## 4.3.2 Electronic Properties of $ZnP_2$

### 4.3.2.1 Band Structure and DOS

The energy band gap of beta modification of $ZnP_2$ (monoclinic) is nearly 1.33−1.37 eV, as reported by Hegyi *et al.* [34]. In the present work, the electronic band structure and the density of states of alpha modification of $ZnP_2$ are studied. The energy band gap (in eV) of the α-$ZnP_2$ crystal under different functionals is shown in **Table 4.4**. It is clear that the energy band gap value is more than 2.3 eV under the B3LYP, B3PW, PBE0, and HSE06 schemes. The value of the energy band gap under the LDA scheme is 1.36 eV. The band structure of α-$ZnP_2$ under PBE scheme is shown in **Fig. 4.3**. The value of the energy band gap under PBE functional is 1.54 eV. The energy band gap value of 1.54 eV corresponds to the IR region. It is evident from **Fig. 4.3** that Brillouin point *M* is the highest point of the valence band for the forbidden region. **Fig. 4.3** shows an indirect energy band gap of 1.54 eV for the alpha phase of $ZnP_2$. Huang *et al.* reported an energy band gap of 1.48 eV for the alpha phase of $ZnP_2$ [88].

**Table 4.4:** Energy band gap (in eV) of α-$ZnP_2$

| PBEsol | PBE | PWGGA | LDA PZ | LDA VWN | B3LYP | B3PW | PBE0 | HSE06 | Exp. Work[4e] | Exp. Work[4f] | Other Work[4g] |
|---|---|---|---|---|---|---|---|---|---|---|---|
| 1.41 | 1.54 | 1.55 | 1.36 | 1.36 | 2.84 | 2.72 | 2.98 | 2.33 | 2.14 | 1.65 | 1.48 |

[4e]Ref. [77].

[4f]Ref. [28, 228].

[4g]Ref. [88].

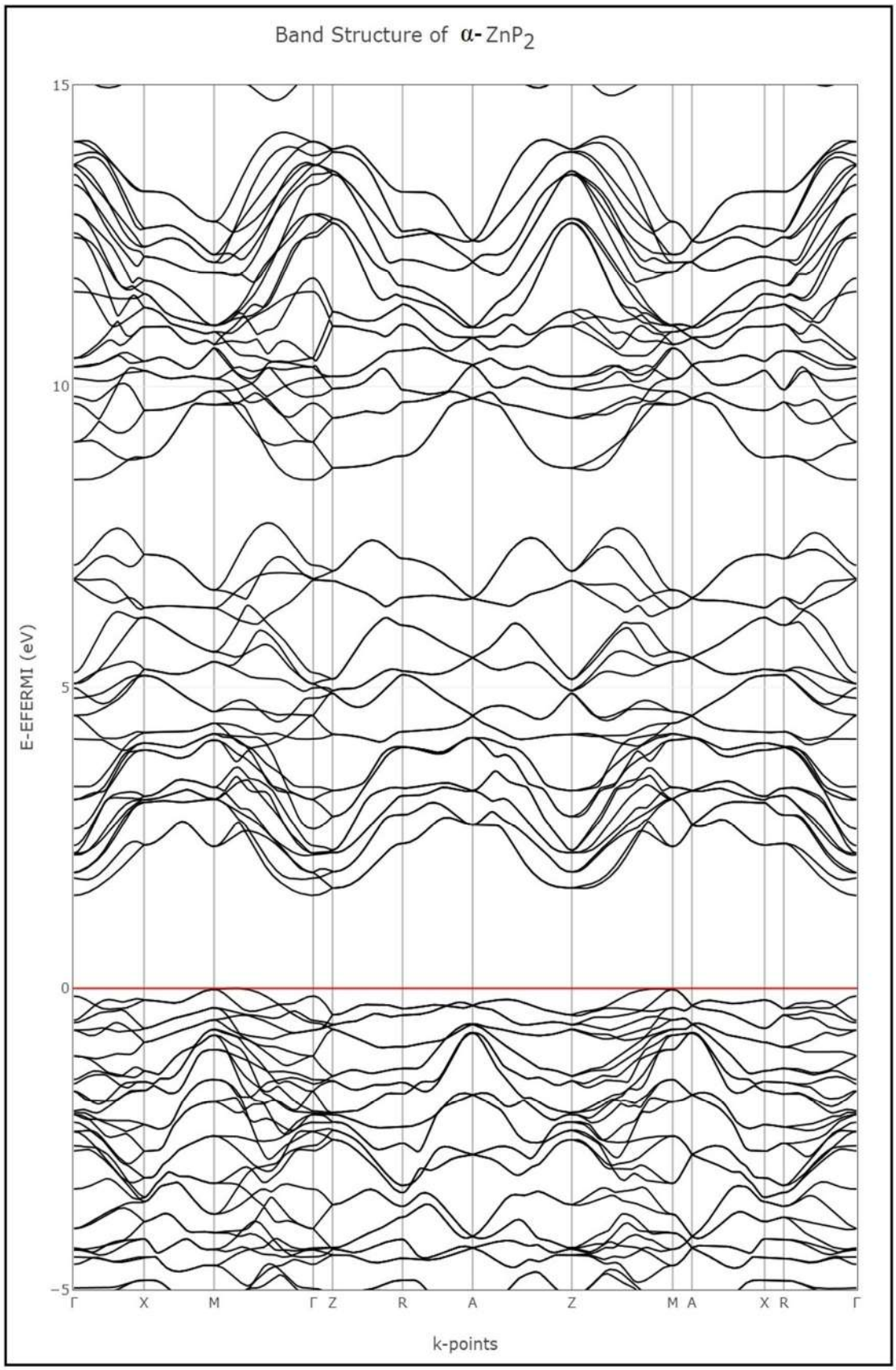


**Figure 4.3:** The band structure of α-$ZnP_2$ under the PBE scheme.

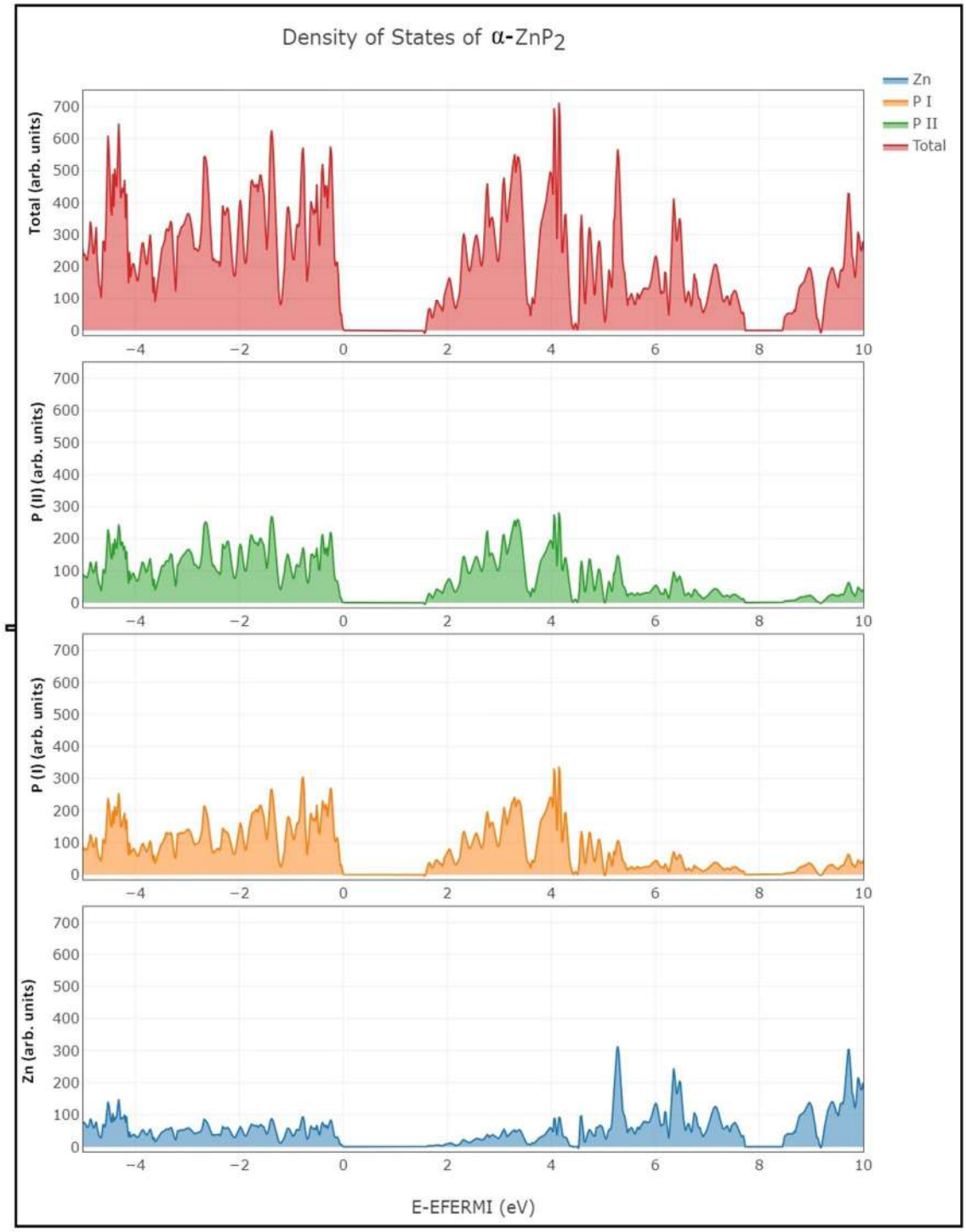


**Figure 4.4:** The density of states of α-$ZnP_2$ under the PBE scheme.

The total density of states and contribution of nonequivalent atoms [Zn, P(I) and P(II)] of α-$ZnP_2$ under the PBE scheme are shown in **Fig. 4.4**. Near the Fermi energy, each P(I) and P(II) atom contributes more to DOS in comparison with Zn atom.

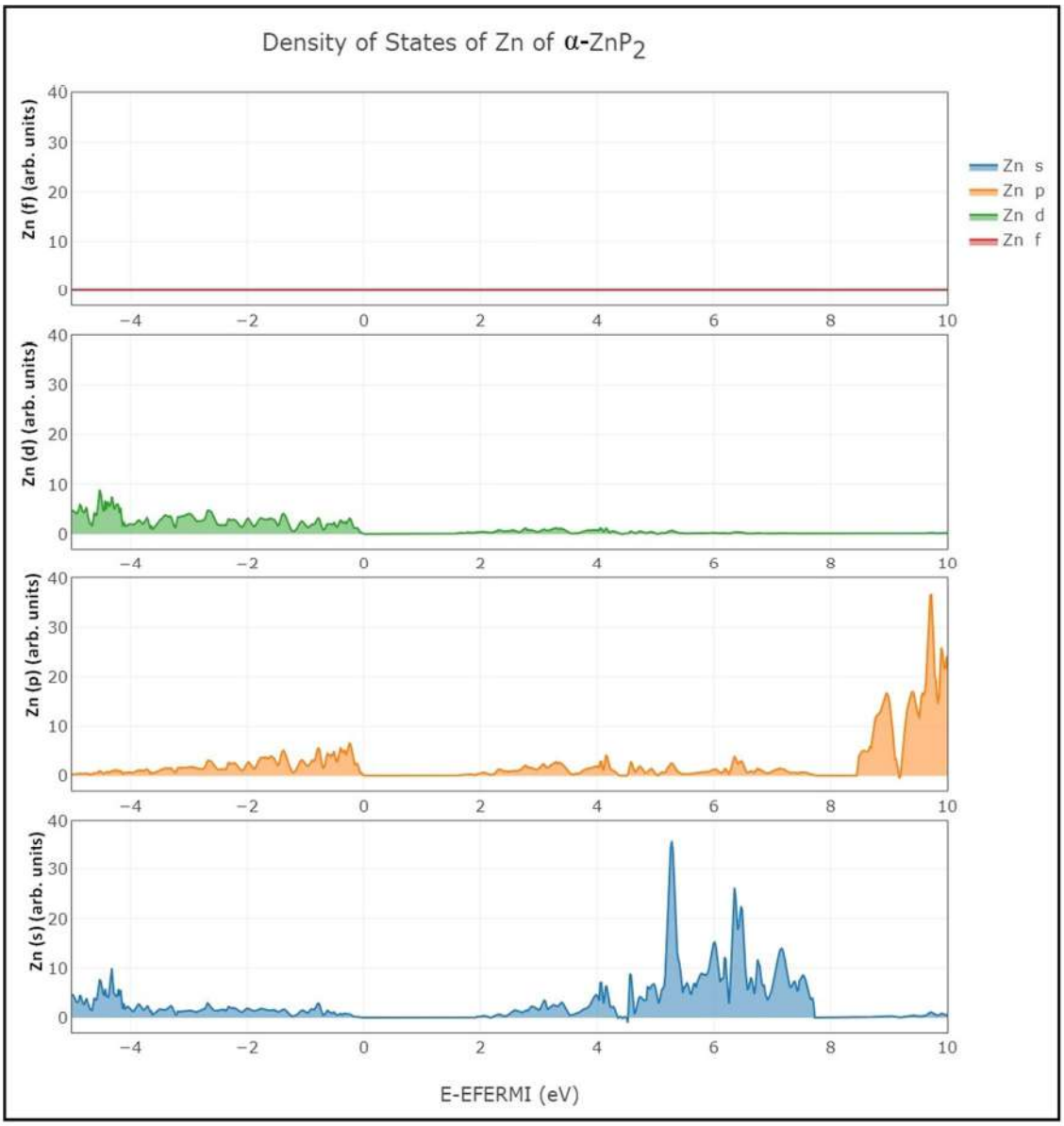


**Figure 4.5:** The density of states of the nonequivalent zinc atom of α-$ZnP_2$ under the PBE scheme.

**Figure 4.5** illustrates the contribution of orbitals (*s*, *p*, *d* and *f* ) of nonequivalent Zn atoms in the density of states. The contribution of *f* orbitals of Zn atom of α-$ZnP_2$ is minimal to the density of states. The contribution of *s* orbitals of Zn atom to the density of states is smaller than the individual contributions of *p* and *d* orbitals near Fermi energy.

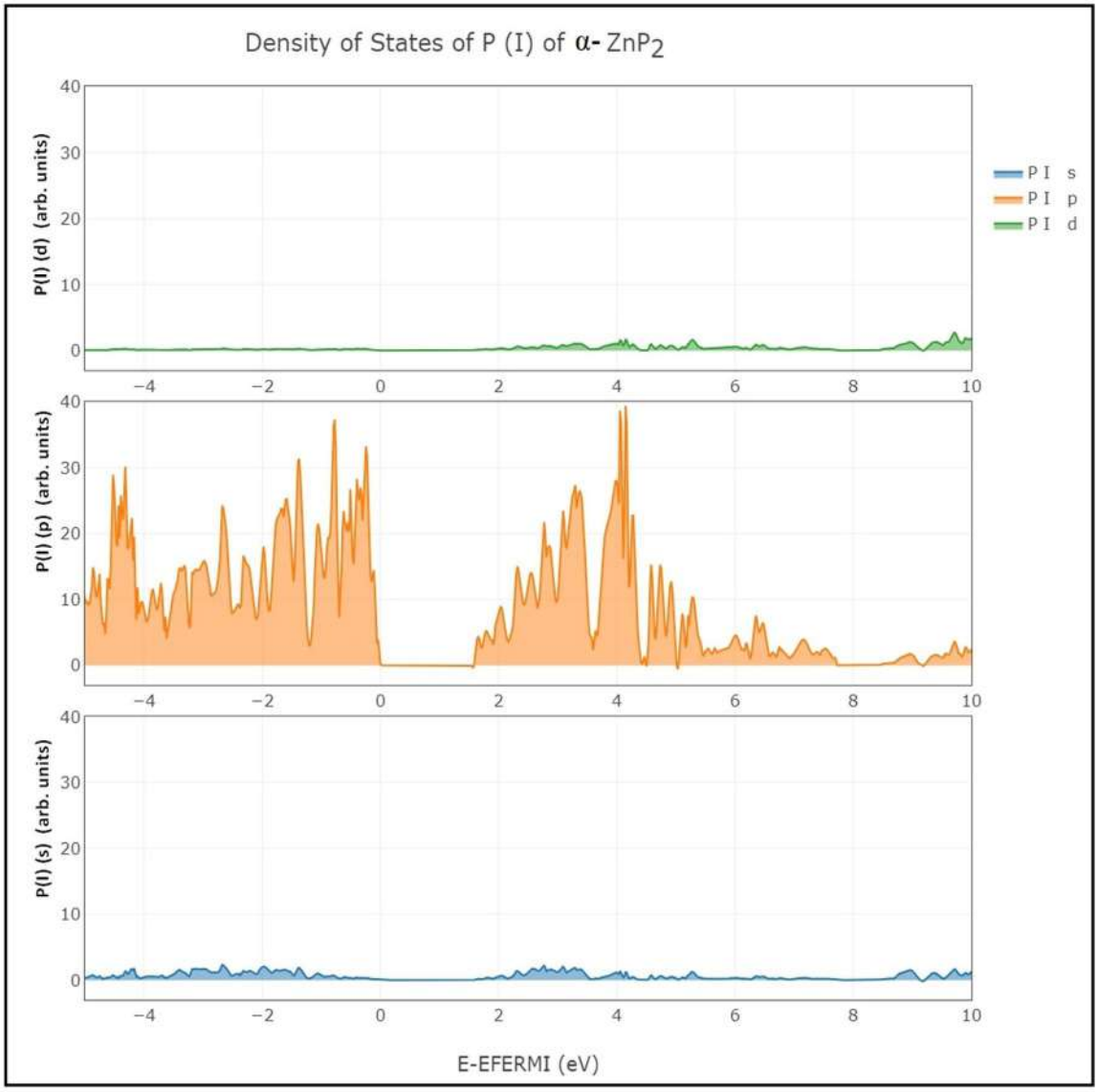


**Figure 4.6:** The density of states of the nonequivalent phosphorus atom [P(I)] of α-$ZnP_2$ under the PBE scheme.

The density of states of the nonequivalent P(I) atom of α-$ZnP_2$ under the PBE scheme is shown in **Fig. 4.6.** For the DOS, the contribution of *p* orbitals of P(I) atom of α-$ZnP_2$ is much higher than that of *s* and *d* orbitals. The contributions of *s* and *d* orbitals of P(I) atom of α-$ZnP_2$ are minimal to the density of states near the Fermi level.

**Figure 4.7** shows the density of states of the nonequivalent P(II) atom of α-$ZnP_2$ under the PBE scheme. The contributions of *s* and *d* orbitals of P(II) atom of α-$ZnP_2$ are minimal to the density of states near the Fermi level. For the DOS, the

contribution of *p* orbitals of P(II) atom of α-$ZnP_2$ is much higher than that of other orbitals of P(II) atom.

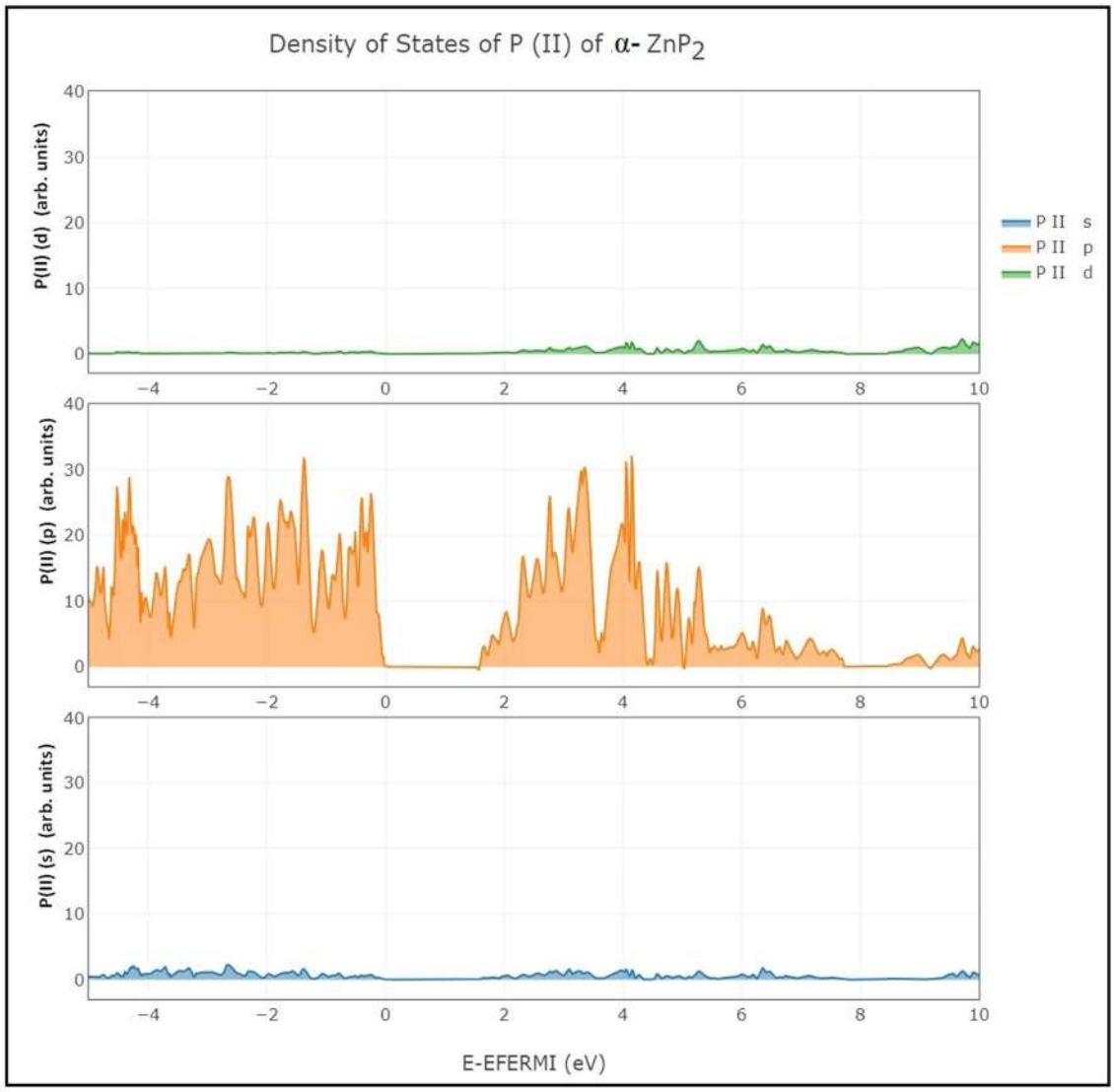


**Figure 4.7:** The density of states of the nonequivalent phosphorus atom [P(II)] of α-$ZnP_2$ under the PBE scheme.

### 4.3.2.2 Mulliken Population Analysis

**Table 4.5** shows the charges of nonequivalent Zn and P atoms in the α-$ZnP_2$ crystal. The amount of charge transfer is relatively small under the LDA functional in comparison to other functionals, as mentioned in **Table 4.5**. For the functionals PBE0 and HSE06, the amount of charge transfer is relatively high in comparison to other functionals, as mentioned in **Table 4.5**. With PBE functional, the charge transfer of

nearly 1.07*e* takes place from Zn atom. Charge transfers of almost 0.52*e* and 0.54*e* take place from P(I) atom and P(II) atom, respectively.

**Table 4.5:** Charges (in terms of *e*) of nonequivalent Zn and P atoms of α-$ZnP_2$

| Scheme | Charge Zn | Charge P (I) | Charge P (II) |
|---|---|---|---|
| PBEsol | 28.957 | 15.510 | 15.533 |
| PBE | 28.932 | 15.524 | 15.544 |
| PWGGA | 28.945 | 15.517 | 15.538 |
| LDA PZ | 29.012 | 15.482 | 15.506 |
| LDA VWN | 29.013 | 15.482 | 15.506 |
| B3LYP | 28.924 | 15.530 | 15.546 |
| B3PW | 28.898 | 15.542 | 15.560 |
| PBE0 | 28.874 | 15.554 | 15.572 |
| HSE06 | 28.880 | 15.551 | 15.570 |

**Table 4.6:** Overlap population for the first six nearest neighbors in α-$ZnP_2$

| Atom A | Atom B | Cell | Overlap Population AB | | | | | | | | |
|---|---|---|---|---|---|---|---|---|---|---|---|
| | | | PBEsol | PBE | PWGGA | LDA PZ | LDA VWN | B3LYP | B3PW | PBE0 | HSE06 |
| 1Zn | 22P | (0 0 0) | 0.180 | 0.171 | 0.173 | 0.188 | 0.188 | 0.164 | 0.166 | 0.164 | 0.164 |
| | 11P | (0 –1 0) | 0.165 | 0.158 | 0.160 | 0.173 | 0.173 | 0.153 | 0.153 | 0.151 | 0.151 |
| | 9P | (0 0 0) | 0.159 | 0.152 | 0.153 | 0.168 | 0.168 | 0.147 | 0.147 | 0.145 | 0.145 |
| | 17P | (0 –1 0) | 0.166 | 0.158 | 0.160 | 0.174 | 0.174 | 0.150 | 0.152 | 0.151 | 0.151 |
| | 9P | (0 –1 0) | –0.008 | –0.007 | –0.007 | –0.009 | –0.009 | –0.007 | –0.007 | –0.008 | –0.007 |
| | 19P | (0 –1 0) | –0.009 | –0.008 | –0.008 | –0.010 | –0.010 | –0.007 | –0.008 | –0.008 | –0.008 |
| 9P | 17P | (0 0 0) | 0.028 | 0.038 | 0.040 | 0.028 | 0.028 | 0.073 | 0.060 | 0.059 | 0.057 |
| | 19P | (0 0 0) | –0.031 | –0.015 | –0.013 | –0.034 | –0.034 | 0.030 | 0.010 | 0.008 | 0.005 |
| | 3Zn | (0 0 0) | 0.165 | 0.158 | 0.160 | 0.173 | 0.173 | 0.153 | 0.153 | 0.151 | 0.151 |
| | 1Zn | (0 0 0) | 0.159 | 0.152 | 0.153 | 0.168 | 0.168 | 0.147 | 0.147 | 0.145 | 0.145 |
| | 11P | (0 0 0) | –0.073 | –0.067 | –0.066 | –0.076 | –0.076 | –0.065 | –0.074 | –0.077 | –0.076 |
| | 11P | (0 –1 0) | –0.032 | | | –0.035 | –0.035 | | | | |
| | 1Zn | (0 1 0) | | –0.007 | –0.007 | | | –0.007 | –0.007 | –0.008 | –0.007 |
| 17P | 9P | (0 0 0) | 0.028 | 0.038 | 0.040 | 0.028 | 0.028 | 0.073 | 0.060 | 0.059 | 0.057 |
| | 11P | (–1 0 0) | –0.031 | –0.015 | –0.013 | –0.034 | –0.034 | 0.030 | 0.010 | 0.008 | 0.005 |
| | 6Zn | (0 0 0) | 0.180 | 0.171 | 0.173 | 0.188 | 0.188 | 0.164 | 0.166 | 0.164 | 0.164 |
| | 1Zn | (0 1 0) | 0.166 | 0.158 | 0.160 | 0.174 | 0.174 | 0.150 | 0.152 | 0.151 | 0.151 |
| | 19P | (0 0 0) | –0.058 | –0.054 | –0.053 | –0.060 | –0.060 | –0.052 | –0.060 | –0.063 | –0.062 |
| | 3Zn | (0 0 0) | –0.009 | –0.008 | –0.008 | –0.010 | –0.010 | –0.007 | –0.008 | –0.008 | –0.008 |

It is evident from **Table 4.6** that in most of the pairs, the magnitude of overlap population is higher under the LDA schemes than other functionals. Under the LDA scheme, the maximum value of the overlap population is found between pairs Zn-P, which is 0.188. Under the LDA scheme, the maximum value of the overlap population between pairs P-P is 0.028. Under the PBE scheme, the maximum values of the overlap populations between pairs Zn-P and pairs P-P are 0.171 and 0.038, respectively. In **Table 4.6**, the overlap population for atomic pair 9P-1Zn is not mentioned under PBEsol scheme, as 1Zn is not the first six nearest neighbors of 9P in α-$ZnP_2$. With different functionals, overlap populations are mentioned only for the pairs under the first six nearest neighbors in **Table 4.6.**

## 4.3.3 Electronic Properties of $ZnAs_2$

### 4.3.3.1 Band Structure and DOS

The energy band gap of the monoclinic $ZnAs_2$ crystal under different functionals is shown in **Table 4.7.** Under the PBE scheme, the energy band gap of $ZnAs_2$ is 0.82 eV. The functionals B3LYP and B3PW give band gaps of 1.79 eV and 1.83 eV, respectively. Under the PBE0 scheme, the energy band gap of $ZnAs_2$ is 2.10 eV. The computed value of the energy band gap is the minimum with the LDA functional, as seen in **Table 4.7. Fig. 4.8** shows the band structure of $ZnAs_2$ under the PBE scheme. For the electronic band structure of $ZnAs_2$, computations are carried out along high symmetry directions for the special points (namely *A, B, C, D, E, Y* and *Z*) in the Brillouin zone [124]. It is clear from **Fig. 4.8** that the Brillouin zone point *Y* is the uppermost point in the valence band region. Relative to the Fermi energy level, the electronic band structure is plotted from nearly −7 eV to 15 eV, as shown in **Fig. 4.8**.

**Table 4.7:** Energy band gap (in eV) of $ZnAs_2$

| PBEsol[4h] | PBE | PWGGA | LDA PZ | LDA VWN | B3LYP | B3PW | PBE0 | HSE06 | Exp.[4i] |
|---|---|---|---|---|---|---|---|---|---|
| ~0.78 | 0.82 | 0.81 | 0.74 | 0.75 | 1.79 | 1.83 | 2.10 | 1.56 | ~1 |

[4h]Ref. [223].

[4i]Ref. [50, 99].

**Figure 4.9** shows the density of states of monoclinic $ZnAs_2$ under the PBE scheme. Relative to Fermi energy level, the density of states is plotted from about −5 eV to 10 eV as shown in **Fig. 4.9**. On the *y*-axis, arbitrary units are used for the density of states, but scaling is the same for all the atoms, which are mentioned in **Fig. 4.9**. It illustrates the contributions of nonequivalent atoms [Zn(I), Zn(II), As(I), As(II), As(III) and As(IV)] of $ZnAs_2$. In the vicinity of Fermi energy, the contribution of each nonequivalent As atom is greater than that of each nonequivalent Zn atom. **Fig. 4.10** describes the density of states of the nonequivalent Zn(I) atom of $ZnAs_2$ under the PBE scheme. Near the Fermi energy, the contributions of *p* and *d* orbitals of Zn(I) atom are greater than those of *s* and *f* orbitals in **Fig. 4.10**. The contribution of the *f* orbitals of Zn(I) atom is negligible. On the *y*-axis, arbitrary units are used for the contribution of orbitals to the density of states, but scaling is the same for all the orbitals, which are mentioned in **Fig. 4.10**.

**Fig. 4.11** illustrates the density of states of the nonequivalent Zn(II) atom of $ZnAs_2$ under the PBE scheme. Regarding the contributions of *s*, *p*, *d* and *f* orbitals of the nonequivalent Zn(II) atom, a nearly similar pattern of the nonequivalent Zn(I) atom is observed. The contribution of the *f* orbitals of Zn(II) atom of $ZnAs_2$ is also negligible.

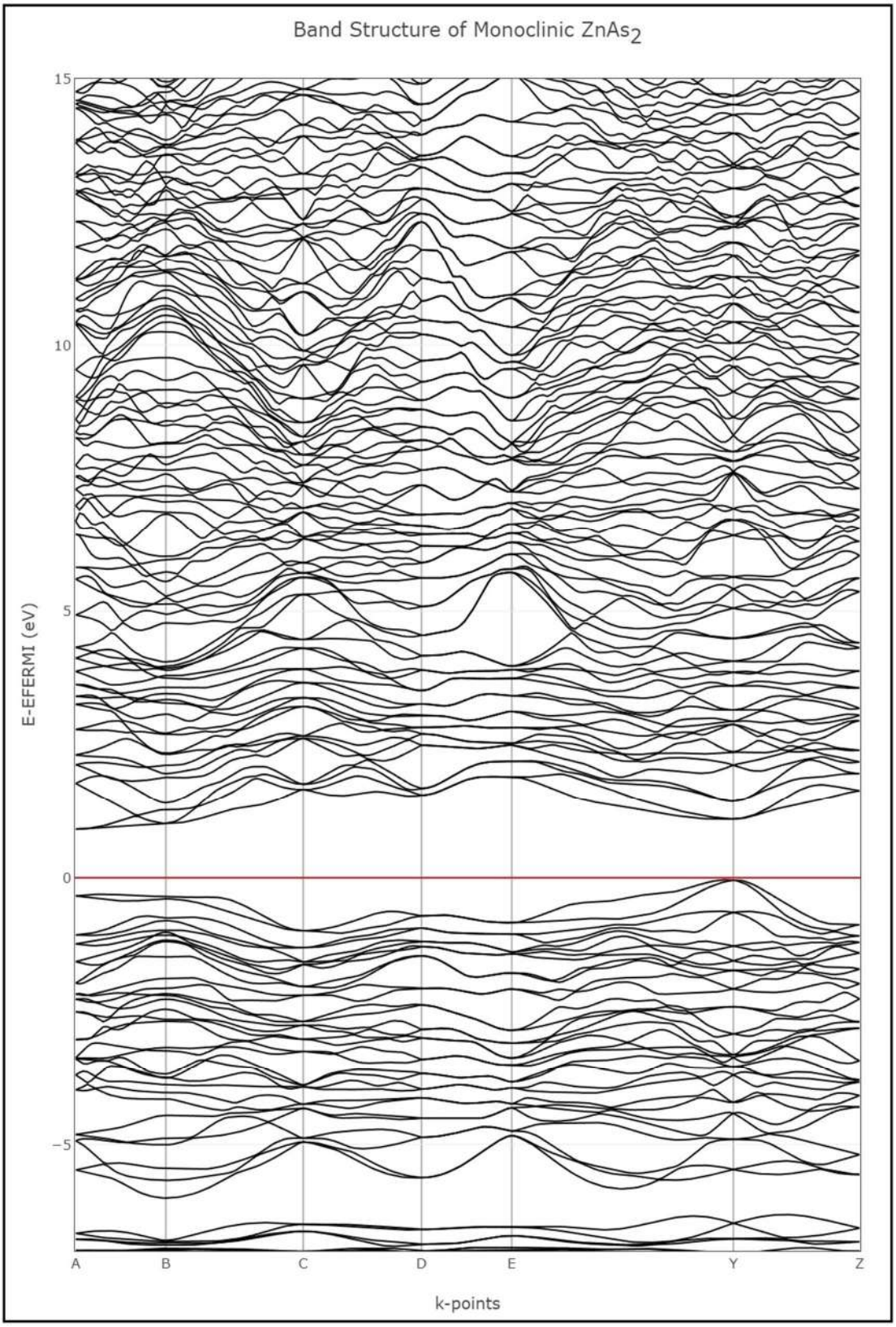


**Figure 4.8:** The band structure of $ZnAs_2$ under the PBE scheme.

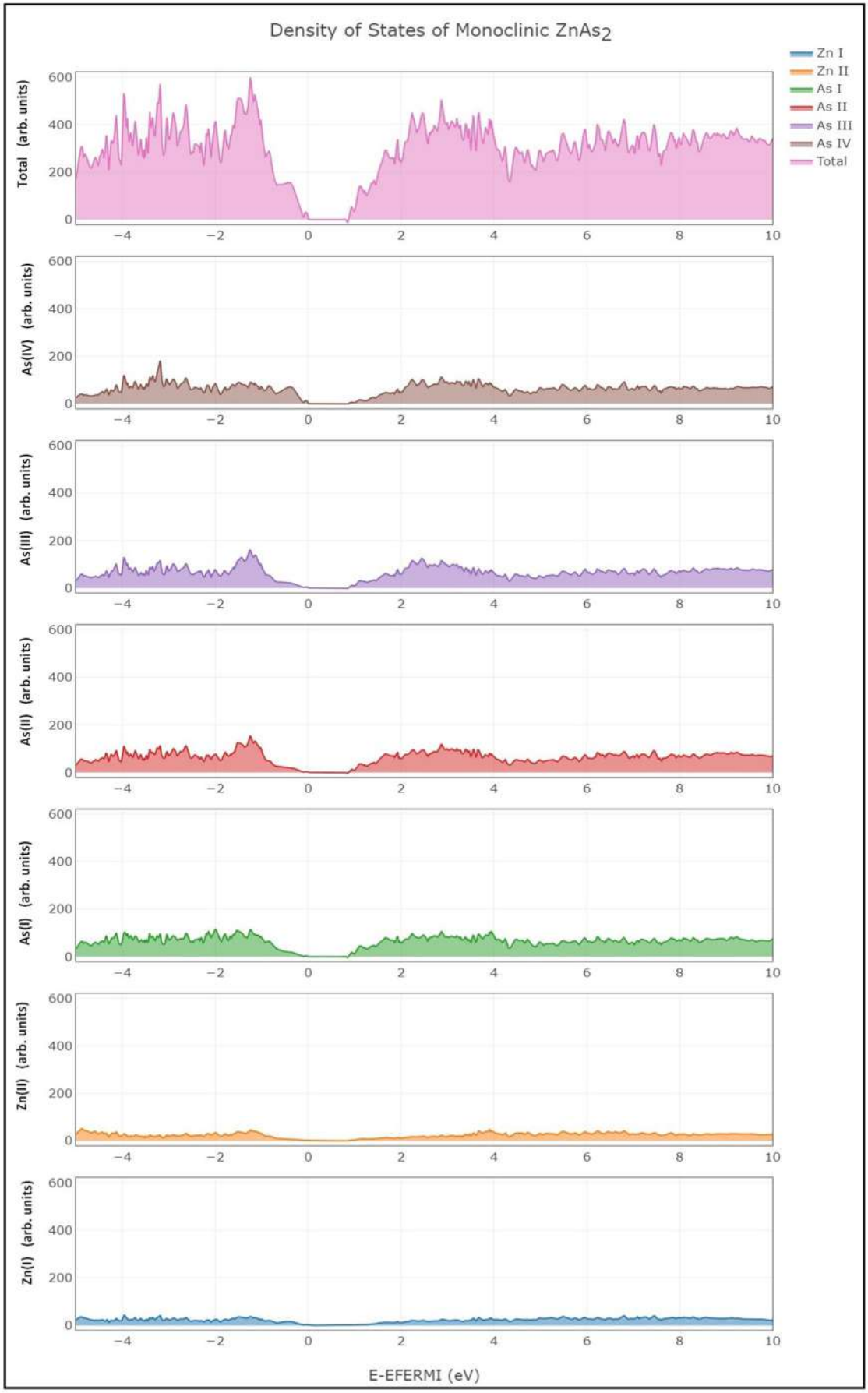


**Figure 4.9:** The density of states of $ZnAs_2$ under the PBE scheme.

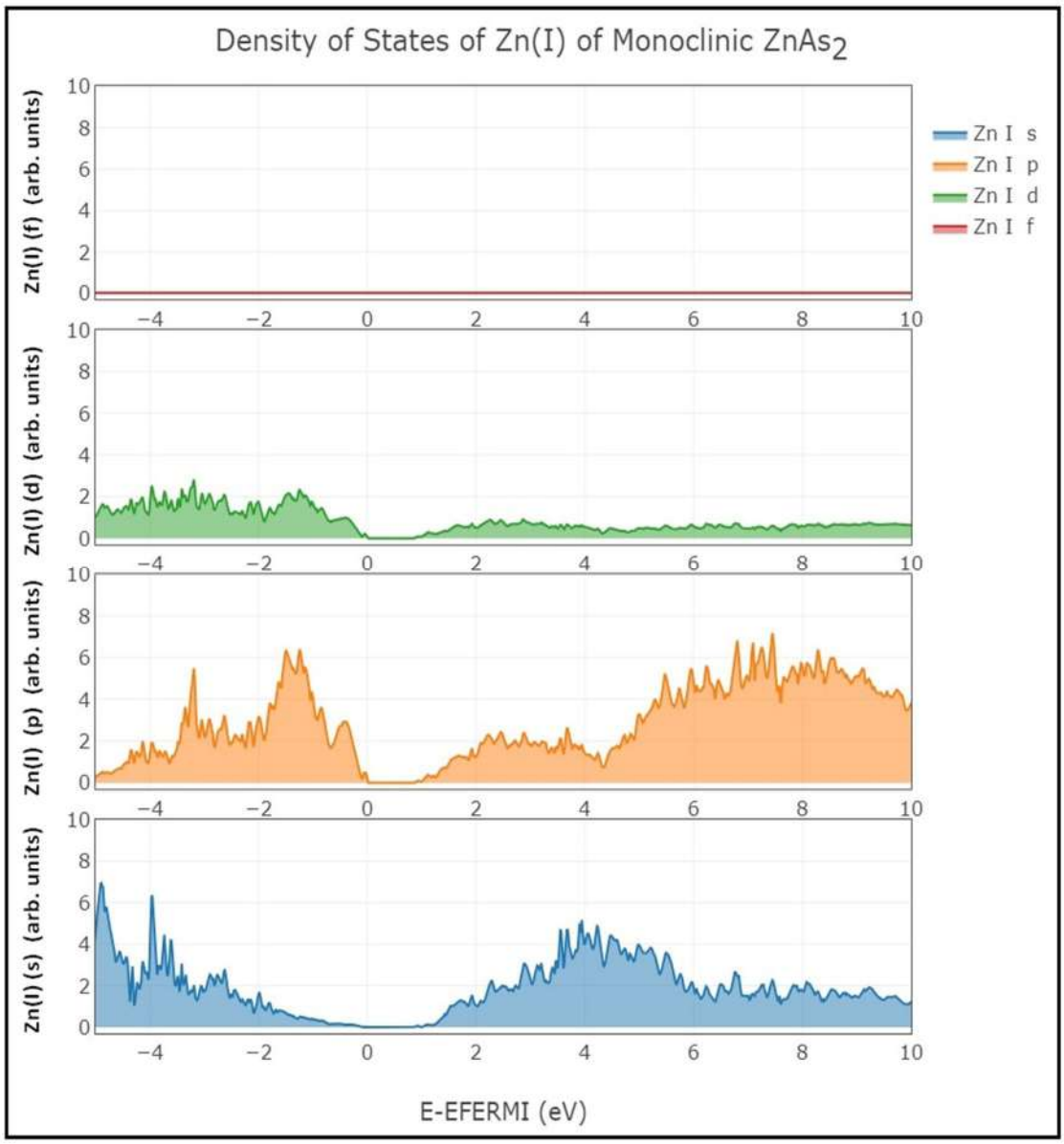


**Figure 4.10:** The density of states of the nonequivalent zinc atom [Zn(I)] of $ZnAs_2$ under the PBE scheme.

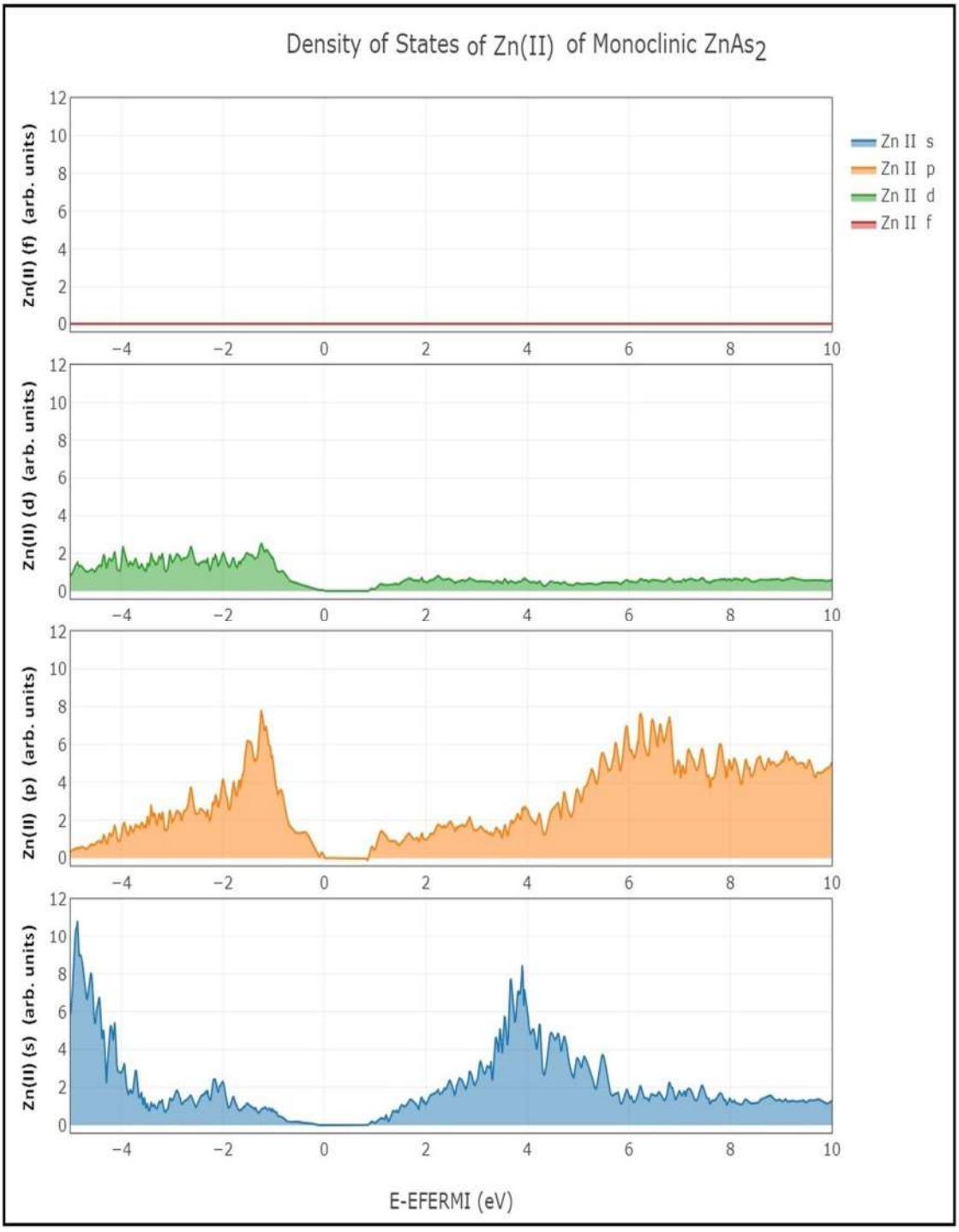


**Figure 4.11:** The density of states of the nonequivalent zinc atom [Zn(II)] of $ZnAs_2$ under the PBE scheme.

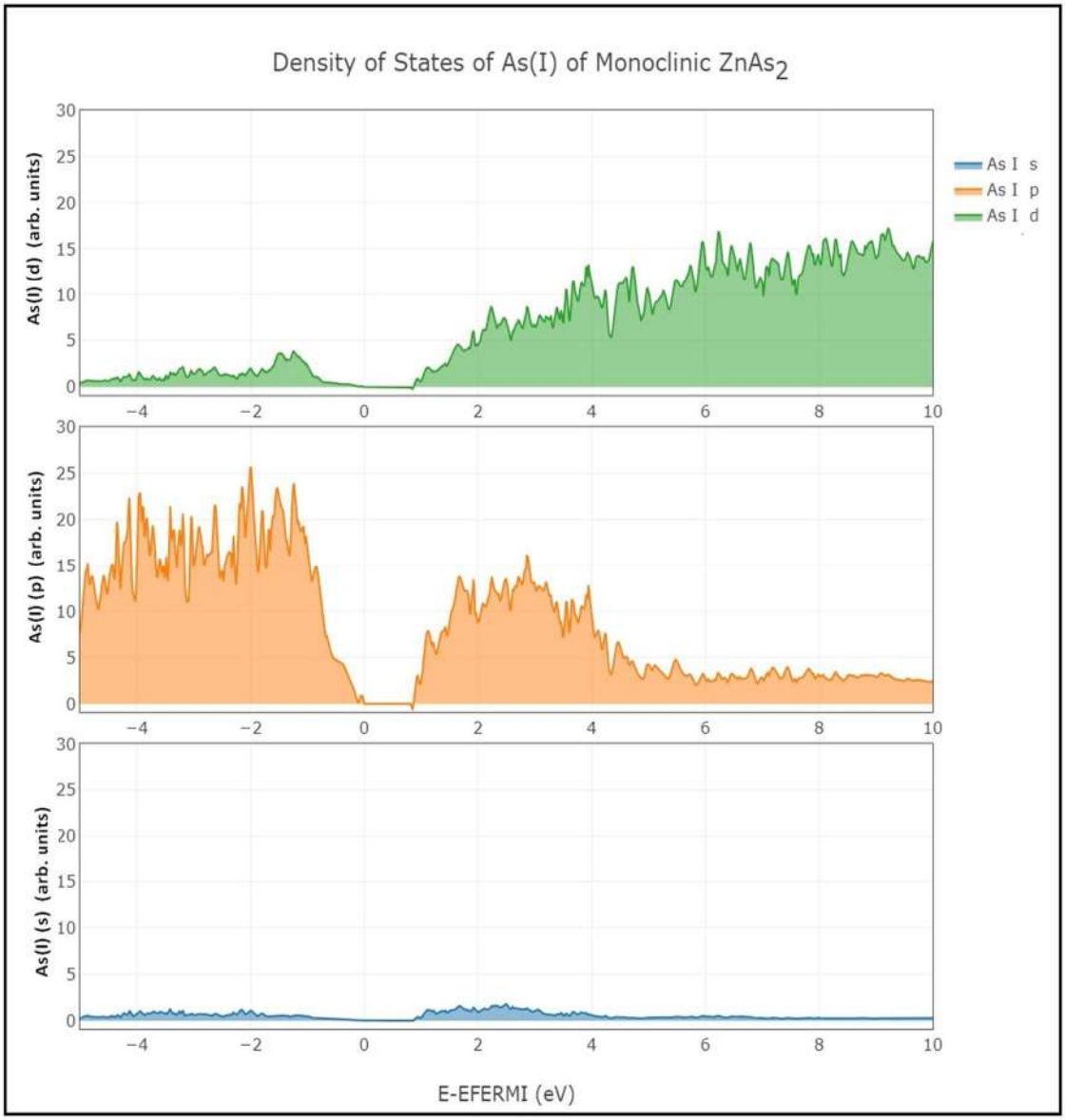


**Figure 4.12:** The density of states of the nonequivalent arsenic atom [As(I)] of $ZnAs_2$ under the PBE scheme.

**Fig. 4.12** shows the density of states of the nonequivalent As(I) atom of $ZnAs_2$ under the PBE scheme. Near the Fermi energy, the contribution of *p* orbitals of As(I) atom is greater than those of *s* and *d* orbitals of As(I) atom in **Fig. 4.12**.

**Fig. 4.13** illustrates the density of states of the nonequivalent As(II) atom of $ZnAs_2$ under the PBE scheme. The density of states of the nonequivalent As(III) and As(IV) atoms of $ZnAs_2$ under the PBE scheme are illustrated in **Fig. 4.14** and **Fig. 4.15**, respectively. The contribution of *p* orbitals of As(III) atom is greater than

those of *s* and *d* orbitals of As(III) in **Fig. 4.14** near the Fermi energy. Similarly, near the Fermi energy, the contribution of *p* orbitals of As(IV) atom is greater than that of *s* and *d* orbitals of As(IV) in **Fig. 4.15.**

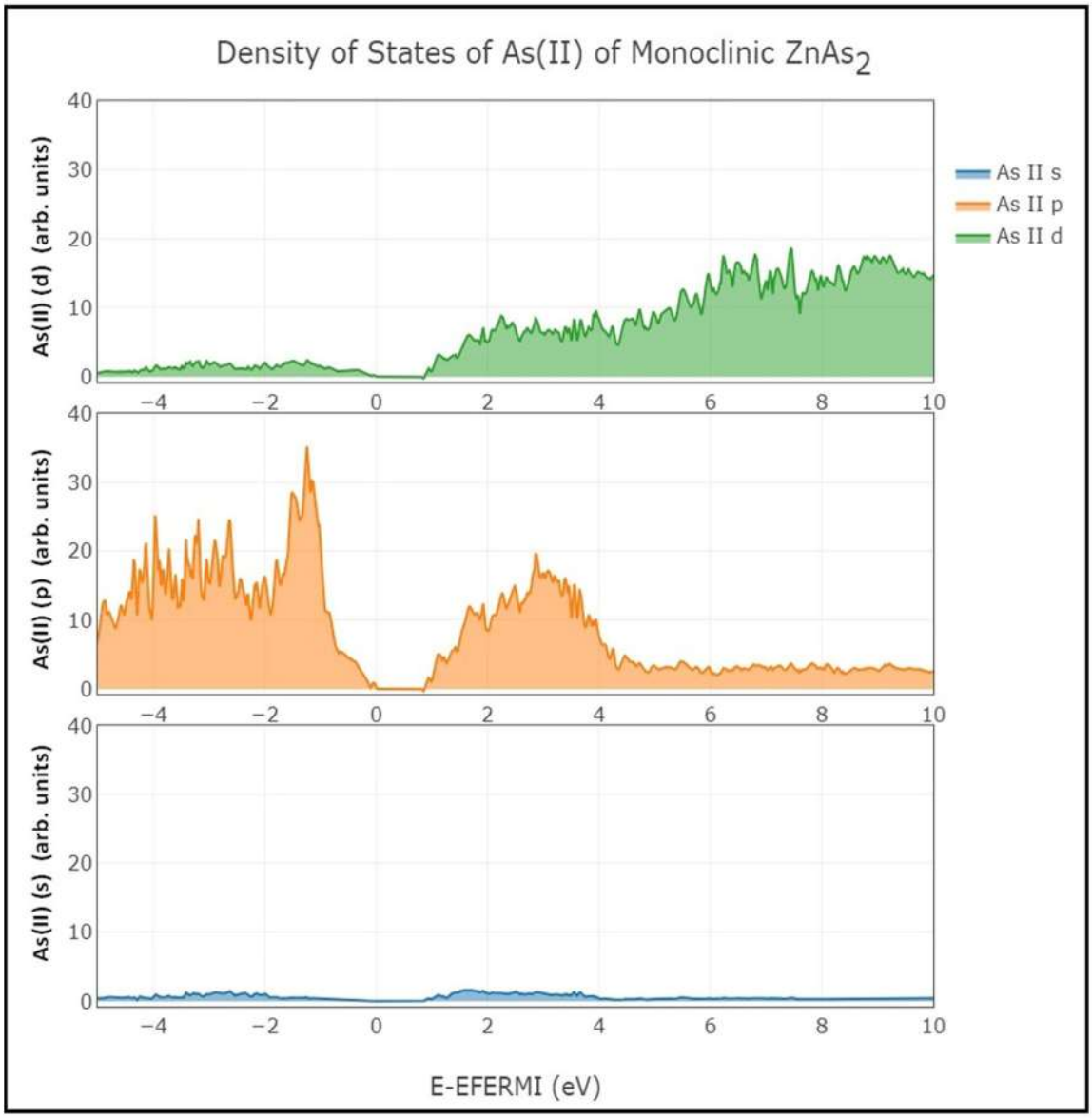


**Figure 4.13:** The density of states of the nonequivalent arsenic atom [As(II)] of $ZnAs_2$ under the PBE scheme.

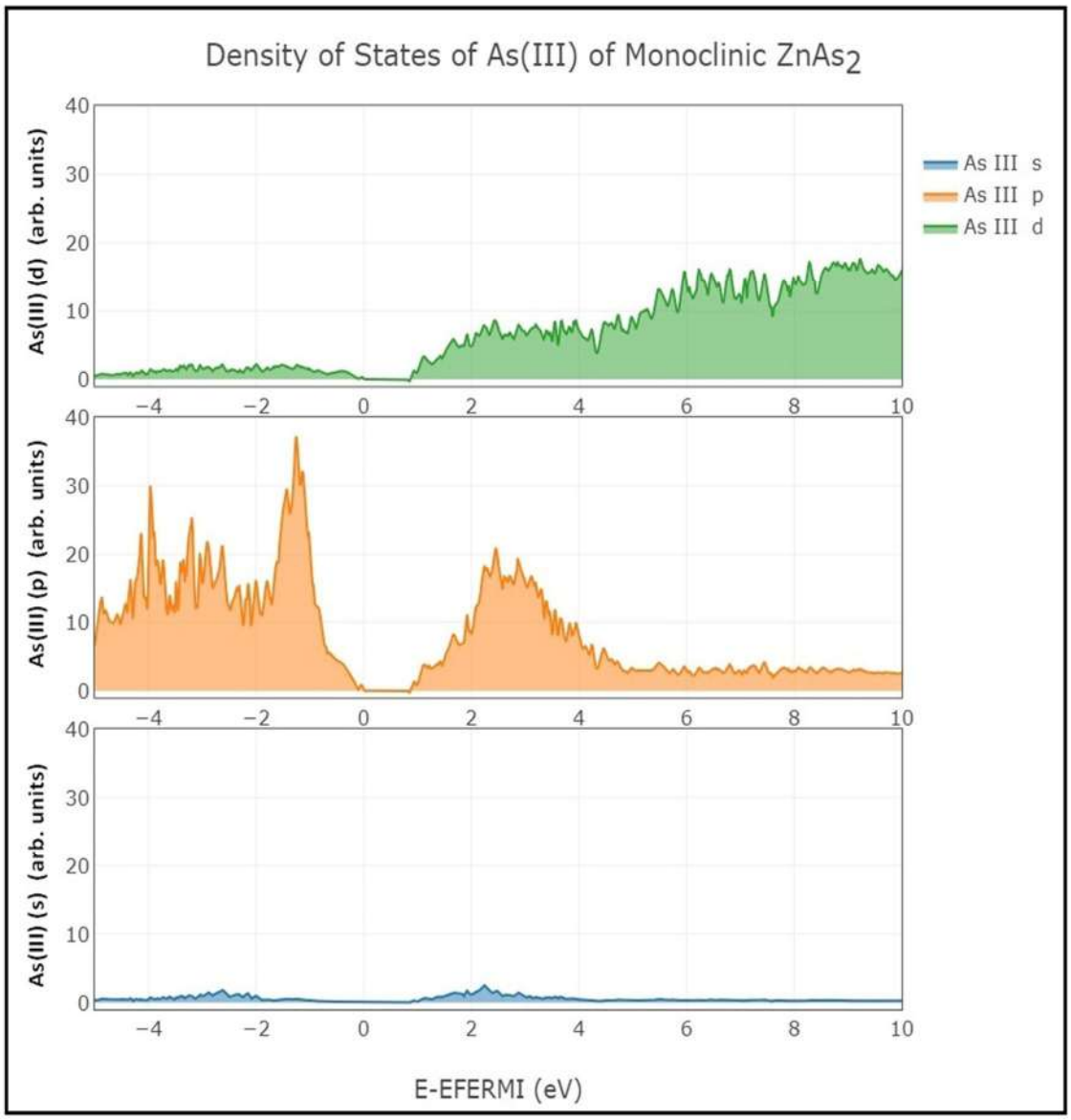


**Figure 4.14:** The density of states of the nonequivalent arsenic atom [As(III)] of $ZnAs_2$ under the PBE scheme.

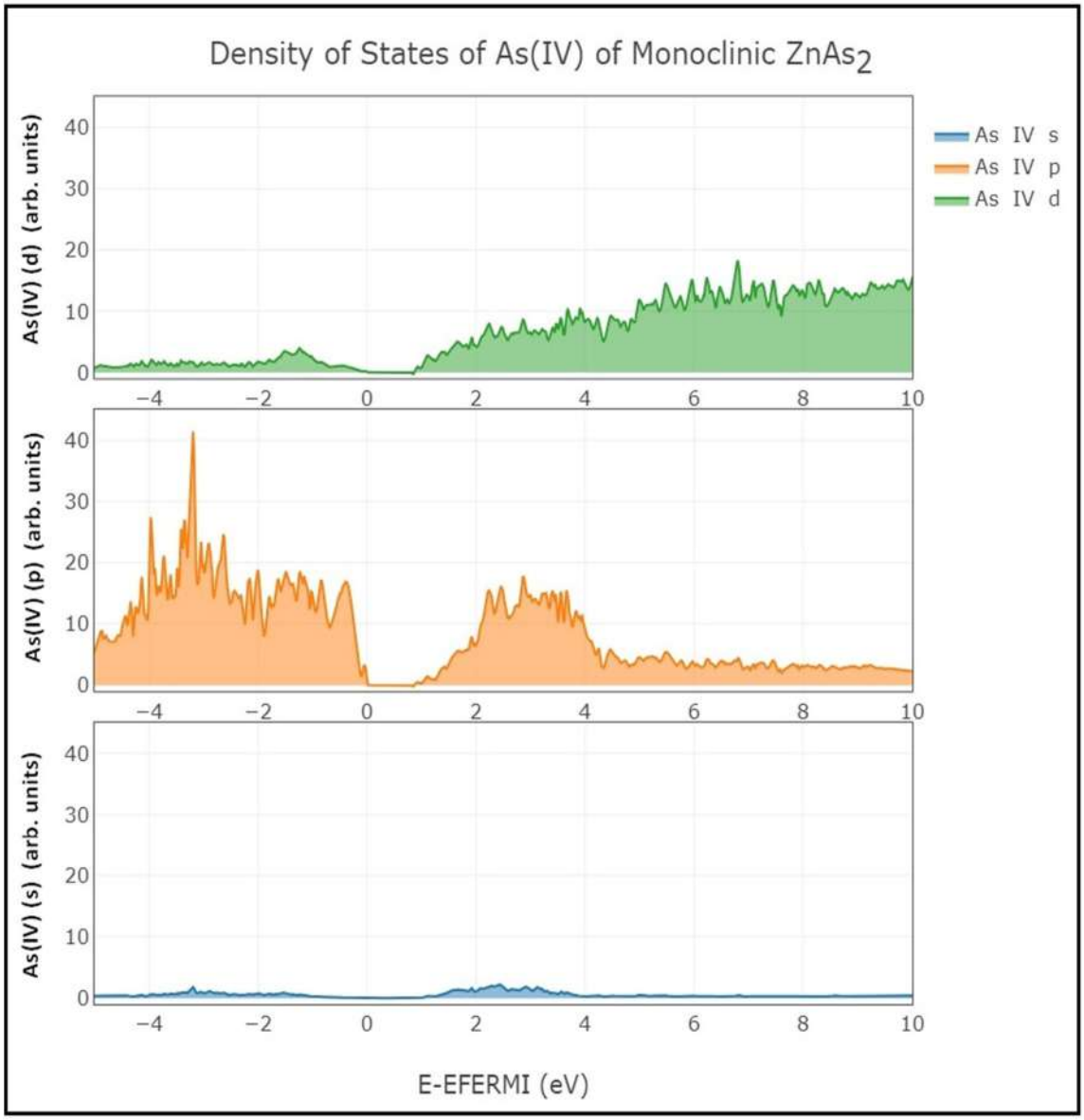


**Figure 4.15:** The density of states of the nonequivalent arsenic atom [As(IV)] of $ZnAs_2$ under the PBE scheme.

### 4.3.3.2 Mulliken Population Analysis

**Table 4.8** shows charges of nonequivalent Zn and As atoms in the $ZnAs_2$ crystal. It is evident from **Table 4.8** that charge transfer in Zn(I) atom is a little more than in Zn(II) atom. Under the LDA scheme, the charge transfer in Zn(I) atom is about 0.9*e*. The obtained charge transfer value is higher under the PBE0 scheme for $ZnAs_2$. It is evident from **Table 4.8** that charge transfer in As(IV) atoms is little more than in other nonequivalent As atoms. Charge transfer values for As(I), As(II) and As(III) are

nearly 0.46*e*, whereas charge transfer value for As(IV) is nearly 0.51*e* under the PBE scheme.

**Table 4.8:** Charges (in terms of *e*) of nonequivalent Zn and As atoms of $ZnAs_2$

| Scheme | Charge Zn(I) | Charge Zn(II) | Charge As (I) | Charge As (II) | Charge As (III) | Charge As (IV) |
|---|---|---|---|---|---|---|
| PBEsol | 29.050 | 29.072 | 33.461 | 33.453 | 33.459 | 33.504 |
| PBE | 29.042 | 29.065 | 33.467 | 33.457 | 33.461 | 33.507 |
| PWGGA | 29.054 | 29.077 | 33.461 | 33.452 | 33.456 | 33.501 |
| LDA PZ | 29.091 | 29.112 | 33.438 | 33.434 | 33.440 | 33.486 |
| LDA VWN | 29.092 | 29.113 | 33.438 | 33.434 | 33.439 | 33.486 |
| B3LYP | 29.041 | 29.065 | 33.463 | 33.459 | 33.463 | 33.509 |
| B3PW | 29.011 | 29.033 | 33.480 | 33.474 | 33.479 | 33.523 |
| PBE0 | 28.986 | 29.009 | 33.492 | 33.485 | 33.491 | 33.537 |
| HSE06 | 28.991 | 29.014 | 33.489 | 33.483 | 33.489 | 33.533 |

**Table 4.9** describes the overlap population for the first six nearest neighbors in the $ZnAs_2$ crystal. Under the PBE scheme, the maximum value of overlap population for Zn-As pair in $ZnAs_2$ is 0.196. The maximum value of overlap population for As-As pair in $ZnAs_2$ is 0.276 under the PBE functional, as shown in **Table 4.9**. Negative values of overlap population between pairs Zn-As and As-As indicate antibonding states.

**Table 4.9:** Overlap population for the first six nearest neighbors in $ZnAs_2$

| Atom A | Atom B | Cell | Overlap Population AB | | | | | | | | |
|---|---|---|---|---|---|---|---|---|---|---|---|
| | | | PBEsol | PBE | PWGGA | LDA PZ | LDA VWN | B3LYP | B3PW | PBE0 | HSE06 |
| 1Zn | 22As | (0 0 0) | 0.202 | 0.196 | 0.197 | 0.208 | 0.208 | 0.186 | 0.187 | 0.186 | 0.186 |
| | 23As | (0 0 1) | 0.200 | 0.195 | 0.195 | 0.207 | 0.206 | 0.184 | 0.186 | 0.184 | 0.185 |
| | 17As | (0 –1 0) | 0.186 | 0.180 | 0.180 | 0.193 | 0.192 | 0.170 | 0.173 | 0.172 | 0.173 |
| | 13As | (0 0 0) | 0.184 | 0.177 | 0.178 | 0.191 | 0.190 | 0.167 | 0.170 | 0.169 | 0.170 |
| | 21As | (0 –1 0) | 0.001 | 0.001 | 0.001 | 0.002 | 0.002 | 0.001 | 0.001 | 0.001 | 0.001 |
| | 21As | (0 0 0) | 0.000 | 0.000 | 0.000 | 0.000 | 0.000 | 0.000 | 0.000 | 0.000 | 0.000 |
| 5Zn | 10As | (1 0 0) | 0.195 | 0.187 | 0.188 | 0.202 | 0.202 | 0.177 | 0.180 | 0.180 | 0.180 |
| | 9As | (0 0 0) | 0.200 | 0.194 | 0.194 | 0.205 | 0.206 | 0.183 | 0.186 | 0.186 | 0.185 |
| | 13As | (0 0 0) | 0.182 | 0.175 | 0.176 | 0.188 | 0.188 | 0.167 | 0.169 | 0.167 | 0.168 |
| | 20As | (0 0 0) | 0.178 | 0.172 | 0.173 | 0.185 | 0.184 | 0.163 | 0.166 | 0.164 | 0.166 |
| | 24As | (0 0 0) | 0.001 | 0.001 | 0.001 | 0.001 | 0.001 | 0.001 | 0.001 | 0.001 | 0.001 |
| | 21As | (0 0 0) | 0.001 | 0.001 | 0.001 | 0.001 | 0.000 | 0.001 | 0.000 | 0.000 | 0.000 |
| 9As | 6Zn | (1 1 0) | 0.195 | 0.187 | 0.188 | 0.202 | 0.202 | 0.177 | 0.180 | 0.180 | 0.180 |
| | 5Zn | (0 0 0) | 0.200 | 0.194 | 0.194 | 0.205 | 0.206 | 0.183 | 0.186 | 0.186 | 0.185 |
| | 16As | (0 0 0) | 0.276 | 0.275 | 0.273 | 0.272 | 0.272 | 0.282 | 0.289 | 0.296 | 0.295 |
| | 17As | (0 0 0) | 0.275 | 0.274 | 0.272 | 0.271 | 0.271 | 0.281 | 0.289 | 0.295 | 0.295 |
| | 21As | (0 0 0) | 0.002 | 0.002 | 0.002 | 0.001 | 0.001 | 0.001 | 0.001 | 0.000 | 0.001 |
| | 24As | (0 0 0) | 0.002 | 0.002 | 0.002 | 0.001 | 0.001 | 0.001 | 0.001 | 0.000 | 0.001 |
| 13As | 1Zn | (0 0 0) | 0.184 | 0.177 | 0.178 | 0.191 | 0.190 | 0.167 | 0.170 | 0.169 | 0.170 |
| | 21As | (0 0 0) | 0.274 | 0.274 | 0.272 | 0.269 | 0.269 | 0.279 | 0.287 | 0.293 | 0.292 |
| | 5Zn | (0 0 0) | 0.182 | 0.175 | 0.176 | 0.188 | 0.188 | 0.167 | 0.169 | 0.167 | 0.168 |
| | 12As | (0 0 1) | 0.276 | 0.275 | 0.273 | 0.272 | 0.272 | 0.282 | 0.289 | 0.296 | 0.295 |
| | 17As | (0 0 0) | –0.005 | –0.003 | –0.003 | –0.006 | –0.006 | –0.004 | –0.005 | –0.006 | –0.005 |
| | 8Zn | (0 0 1) | –0.001 | 0.000 | 0.000 | –0.001 | –0.001 | 0.000 | –0.001 | –0.001 | –0.001 |
| 17As | 1Zn | (0 1 0) | 0.186 | 0.180 | 0.180 | 0.193 | 0.192 | 0.170 | 0.173 | 0.172 | 0.173 |
| | 21As | (0 0 0) | 0.276 | 0.276 | 0.274 | 0.271 | 0.271 | 0.282 | 0.289 | 0.295 | 0.295 |
| | 8Zn | (0 0 1) | 0.178 | 0.172 | 0.173 | 0.185 | 0.184 | 0.163 | 0.166 | 0.164 | 0.166 |
| | 9As | (0 0 0) | 0.275 | 0.274 | 0.272 | 0.271 | 0.271 | 0.281 | 0.289 | 0.295 | 0.295 |
| | 13As | (0 0 0) | –0.005 | –0.003 | –0.003 | –0.006 | –0.006 | –0.004 | –0.005 | –0.006 | –0.005 |
| | 5 Zn | (0 0 0) | 0.000 | 0.000 | 0.000 | –0.001 | –0.001 | 0.000 | –0.001 | –0.001 | –0.001 |
| 21As | 2Zn | (0 0 0) | 0.202 | 0.196 | 0.197 | 0.208 | 0.208 | 0.186 | 0.187 | 0.186 | 0.186 |
| | 3Zn | (0 0 1) | 0.200 | 0.195 | 0.195 | 0.207 | 0.206 | 0.184 | 0.186 | 0.184 | 0.185 |
| | 17As | (0 0 0) | 0.276 | 0.276 | 0.274 | 0.271 | 0.271 | 0.282 | 0.289 | 0.295 | 0.295 |
| | 13As | (0 0 0) | 0.274 | 0.274 | 0.272 | 0.269 | 0.269 | 0.279 | 0.287 | 0.293 | 0.292 |
| | 8Zn | (0 0 1) | 0.001 | 0.001 | 0.001 | 0.001 | 0.001 | 0.001 | 0.001 | 0.001 | 0.001 |
| | 5Zn | (0 0 0) | 0.001 | 0.001 | 0.001 | 0.001 | 0.000 | 0.001 | 0.000 | 0.000 | 0.000 |

## 4.4 Conclusions

The value of the energy band gap of the alpha phase of $CdP_2$ is 1.79 eV under the PBE functional. The contribution to the density of states of each nonequivalent P(I) and P(II) atom is greater in comparison to Cd atom for the alpha phase of $CdP_2$. Typical

values of charge transfer for Cd, P(I) and P(II) are 1.055*e*, 0.536*e* and 0.519*e*, respectively, under the PBE scheme for α-$CdP_2$. The value of the energy band gap under the PBE scheme is 1.54 eV for α-$ZnP_2$. The value of the energy band gap of 1.54 eV corresponds to the IR region of the electromagnetic wave. In the vicinity of Fermi energy, each P(I) and P(II) atom contributes more to DOS in comparison with Zn atom in the α-$ZnP_2$. The contribution of *p* orbitals of P(I) atom of the alpha phase of $ZnP_2$ to the density of states is much higher than that of *s* and *d* orbitals of P(I) atom near the Fermi level. For the density of states, the contribution of the *f* orbitals of Zn atom of α-$ZnP_2$ is negligible. Near the Fermi energy, for the DOS, the contribution of *s* orbitals of Zn atom is smaller than the contributions of *p* and *d* orbitals of Zn atom in the α-$ZnP_2$. The contribution of the *p* orbitals of the P(II) atom of α-$ZnP_2$ is much greater than that of *s* and *d* orbitals of P(II) atom in the vicinity of the Fermi level. For α-$ZnP_2$, the charge transfer of approximately 1.07*e* takes place from Zn atom under the PBE scheme. From P(I) atom and P(II) atom of α-$ZnP_2$, charge transfers of approximately 0.52*e* and 0.54*e*, respectively, take place under the PBE scheme. The maximum value of the overlap population between the Zn-P pair for α-$ZnP_2$ is 0.188 under the LDA functional.

The energy band gap of monoclinic $ZnAs_2$ is 0.82 eV under the PBE functional. For $ZnAs_2$, the contribution of each nonequivalent arsenic atom to DOS is greater than that of each nonequivalent zinc atom near Fermi energy. The contributions of *p* and *d* orbitals of Zn(I) atom are greater than that of *s* and *f* orbitals of Zn(I) atom in $ZnAs_2$. The contribution of *p* orbitals of As(I) atom is greater than that of *s* and *d* orbitals of As(I) atom in $ZnAs_2$ near the Fermi energy under the PBE functional. All As atoms of $ZnAs_2$ also follow nearly the same pattern for DOS in the vicinity of the Fermi level. For $ZnAs_2$, the charge transfer in Zn(I) atom is a little more than in Zn(II) atom. The charge transfer in Zn(I) atom in $ZnAs_2$ is about 0.9*e* under the LDA scheme. The charge transfer values for the nonequivalent As(I), As(II) and As(III) atoms are nearly 0.46e, whereas the charge transfer value for the nonequivalent As(IV) atom is nearly 0.51*e* under the PBE functional for $ZnAs_2$. Under the PBE functional, the maximum value of the overlap population for As-As pair in $ZnAs_2$ is 0.275, whereas the maximum value of the overlap population for Zn-As pair in $ZnAs_2$ is 0.196.

# CHAPTER 5

## ELASTIC PROPERTIES OF $CdP_2$, $ZnP_2$ AND $ZnAs_2$ COMPOUNDS

## 5.1 Introduction

The elastic stiffness coefficients illustrate the response of crystals to stress. A completely asymmetric crystal has 21 independent stiffness constants $C_{ij}$ [16]. Elastic stiffness constants are useful for estimating the mechanical strength of the crystals. Density functional theory has the capability to predict the elastic behavior of crystals. The estimation of the directional elastic properties of crystals under different tensile stresses may play an important role in the device application. A correlation between volume change and applied uniform pressure may be made by means of the bulk modulus $B$. Reuss bulk modulus $B_R$ and Voigt bulk modulus $B_V$ may be represented as [184, 185, 186]

$$B_R = \left[S_{11} + S_{22} + S_{33} + 2S_{12} + 2S_{13} + 2S_{23}\right]^{-1} \tag{5.1}$$

where $S_{ij}$ represents elastic compliance constants.

$$B_V = \frac{1}{9}\left[C_{11} + C_{22} + C_{33} + 2C_{12} + 2C_{13} + 2C_{23}\right] \tag{5.2}$$

Also, Reuss shear modulus $G_R$ and Voigt shear modulus $G_V$ may be expressed as [184, 185, 186]

$$G_R = 15\left[4\left(S_{11} + S_{22} + S_{33}\right) + 3\left(S_{44} + S_{55} + S_{66}\right) - 4\left(S_{12} + S_{13} + S_{23}\right)\right]^{-1} \tag{5.3}$$

$$G_V = \frac{1}{15}\left[C_{11} + C_{22} + C_{33} - C_{12} - C_{13} - C_{23}\right] + \frac{1}{5}\left[C_{44} + C_{55} + C_{66}\right] \tag{5.4}$$

Macroscopic polycrystalline shear modulus $G_H$ and bulk modulus $B_H$ may be represented by Voigt-Reuss-Hill theory in the following manner [184, 185, 186]

$$G_H = \frac{1}{2}\left[G_R + G_V\right] \tag{5.5}$$

$$B_H = \frac{1}{2}\left[B_R + B_V\right] \tag{5.6}$$

Also, polycrystalline Poisson's ratio $v_H$ and Young's modulus $E_H$ may be estimated as [184, 185, 186]

$$\nu_{\mathrm{H}} = \frac{3B_{\mathrm{H}} - 2G_{\mathrm{H}}}{2\left(3B_{\mathrm{H}} + G_{\mathrm{H}}\right)} \tag{5.7}$$

$$E_{\mathrm{H}} = \frac{9B_{\mathrm{H}}G_{\mathrm{H}}}{3B_{\mathrm{H}} + G_{\mathrm{H}}} \tag{5.8}$$

The mechanical elastic behavior of the material is correlated with various elastic quantities, such as bulk modulus, Young's modulus, Poisson's ratio and shear modulus. For design calculations for devices, directional shear modulus, Young's modulus and Poisson's ratio are the key parameters. The proper anisotropic description of elasticity for materials results in noteworthy advantages for the prediction of preferred orientations of crystals for their technological usages. Moreover, understanding the anisotropic behavior of materials assists in improving the durability of the devices, which helps in obtaining the desired electrical and physical properties. The first principle methods in computational materials science play a significant role in predicting the elastic anisotropy of solid materials. It is worthwhile to investigate the anisotropic properties of the materials for microelectromechanical engineering.

## 5.2 Methodology

Elastic properties of the alpha phase of $CdP_2$, the alpha phase of $ZnP_2$ and monoclinic $ZnAs_2$ are investigated with the CRYSTAL package (periodic *ab initio* HF and DFT code) [124, 140]. In the present investigation, computations are performed with the functionals PBE [187, 188], PBEsol [189, 190], PWGGA [191, 192, 193, 194, 195, 196], LDA PZ [197, 198], LDA VWN [197, 199], B3PW [191, 192, 193, 200, 201], B3LYP [199, 200, 202, 203], PBE0 [204, 205, 206, 207] and HSE06 [187, 188, 208, 209, 210, 211,212, 213, 214, 215].

The computations of EOS [173] and elastic properties [171, 172, 173] are performed with the various functionals. Also, the BROYDEN accelerator scheme [124, 140, 154, 155] is implemented. The keyword ELASTCON is employed to analyze the elastic properties. The strain step for this work of elastic calculations is 0.01. The convergence threshold TOLDEE on energy is implemented at $10^{-8}$ Hartree. The ELATE program [181, 182] is also utilized for the determination of the maximum and minimum values of various elastic quantities. The dependence of bulk modulus

on pressure is also obtained using the keyword EOS [173]. To change the default values of truncation tolerances, the keyword TOLINTEG is used in the CRYSTAL CODE [124]. The study of the directional dependence of linear compressibility $\beta$, Poisson's ratio $v$, shear modulus $G$ and Young's modulus $E$ is carried out by plotting polar graphs using the ELATE program [181, 182]. These graphs are plotted under the PBE scheme in this work.

## 5.3 Results and Discussions

### 5.3.1 Elastic Properties of $CdP_2$

#### 5.3.1.1 Elastic Constants

Feng *et al.* [72] computed elastic constants (in GPa) for the beta phase of $CdP_2$, which are $C_{11}=92.6$, $C_{22}=92.6$, $C_{33}=102.2$, $C_{44}=36.2$, $C_{55}=36.2$, $C_{66}=41.1$, $C_{12}=33.2$, $C_{13}=32.3$, and $C_{23}=32.3$. Soshnikov *et al.* [229] reported the elastic compliance constants (in $10^{-11}\,\mathrm{m^2/N}$) of β-$CdP_2$, which are $S_{11}=2.327$, $S_{33}=2.288$, $S_{44}=3.81$, $S_{66}=3.295$, $S_{12}=-0.504$ and $S_{13}=-1.096$. For the beta phase of $CdP_2$, the values of the directional Young modulus (in GPa) are $E_{100}=42.97$ and $E_{101}=43.71$ [229]. The bulk modulus is 64.5 GPa and the shear modulus is 17.97 GPa for β-$CdP_2$ [229]. Poisson's ratios $v_{12}$ and $v_{13}$ are 0.217 and 0.479, respectively, for β-$CdP_2$ [229].

The orthorhombic crystal has 09 independent elastic constants $C_{11}$, $C_{12}$, $C_{13}$, $C_{22}$, $C_{23}$, $C_{33}$, $C_{44}$, $C_{55}$ and $C_{66}$ [16]. The necessary and sufficient elastic stability conditions for the orthorhombic crystal, as stated by Mouhat *et al.* [230], are expressed by the following three conditions:

$$C_{11}>0,\ C_{44}>0,\ C_{55}>0,\ C_{66}>0 \tag{5.9}$$

$$2C_{12}C_{13}C_{23}+C_{11}C_{22}C_{33}-C_{12}^2C_{33}-C_{13}^2C_{22}-C_{23}^2C_{11}>0 \tag{5.10}$$

$$C_{12}^2<C_{11}C_{22} \tag{5.11}$$

The computed elastic constants $C_{11}$, $C_{12}$, $C_{13}$, $C_{22}$, $C_{23}$, $C_{33}$, $C_{44}$, $C_{55}$ and $C_{66}$ under various schemes are shown in **Table 5.1**. In the present study, the obtained elastic

stiffness constants of α-$CdP_2$ (shown in **Table 5.1**) satisfy the mentioned elastic stability conditions. Hence, it asserts the mechanical stability of the α-$CdP_2$ crystal. The computed value of the elastic constant $C_{11}$ is the greatest and $C_{55}$ is the least among the coefficients $C_{11}$, $C_{12}$, $C_{13}$, $C_{22}$, $C_{23}$, $C_{33}$, $C_{44}$, $C_{55}$ and $C_{66}$. The values of $C_{13}$ and $C_{23}$ are nearly equal. It is evident from **Table 5.1** that the LDA functional gives relatively higher values for $C_{11}$, $C_{12}$, $C_{13}$, $C_{22}$, $C_{23}$ and $C_{33}$. In the present work, **Table 5.1** shows that $C_{11} > C_{22} > C_{33} > C_{12}$ and $C_{44} > C_{66} > C_{55}$.

**Table 5.1:** Elastic constants $C_{ij}$ (in GPa) of α-$CdP_2$ at zero pressure

| Scheme | $C_{11}$ | $C_{12}$ | $C_{13}$ | $C_{22}$ | $C_{23}$ | $C_{33}$ | $C_{44}$ | $C_{55}$ | $C_{66}$ |
|---|---|---|---|---|---|---|---|---|---|
| PBEsol[5a] | 105.16 | 50.35 | 43.41 | 86.52 | 41.86 | 74.23 | 33.42 | 24.33 | 27.48 |
| PBE | 95.41 | 43.00 | 36.37 | 81.15 | 36.27 | 69.15 | 32.74 | 23.92 | 27.21 |
| PWGGA | 95.63 | 42.81 | 36.51 | 82.12 | 36.28 | 69.58 | 31.98 | 23.13 | 26.98 |
| LDA PZ | 116.70 | 57.75 | 49.35 | 92.80 | 46.98 | 81.87 | 34.70 | 25.44 | 28.98 |
| LDA VWN | 116.75 | 57.43 | 49.31 | 92.86 | 46.87 | 82.11 | 34.79 | 25.60 | 28.99 |
| B3LYP | 96.58 | 40.13 | 35.08 | 86.08 | 35.63 | 76.68 | 36.26 | 26.26 | 29.04 |
| B3PW | 103.81 | 45.01 | 38.91 | 88.59 | 38.23 | 76.48 | 35.51 | 25.90 | 29.86 |
| PBE0 | 107.59 | 47.61 | 41.43 | 90.36 | 40.35 | 78.18 | 35.45 | 26.04 | 30.19 |
| HSE06 | 106.40 | 47.24 | 40.97 | 89.29 | 39.89 | 77.22 | 35.01 | 25.65 | 29.66 |
| Other Work[5b] | 101.3 | 31.1 | 37.7 | 91.4 | 32.5 | 87.3 | 37.4 | 28.2 | 19.0 |

[5a]Ref. [219].

[5b]Ref. [72].

Elastic compliance constants $S_{11}$, $S_{12}$, $S_{13}$, $S_{22}$, $S_{23}$, $S_{33}$, $S_{44}$, $S_{55}$ and $S_{66}$ of α-$CdP_2$ at zero pressure are shown in **Table 5.2**. The values of elastic coefficients $S_{12}$, $S_{13}$ and $S_{23}$ are negative. It is obvious from **Table 5.2** that the elastic compliance constants $S_{ij}$ of α-$CdP_2$ at zero pressure follow the relation $S_{55} > S_{66} > S_{44} > S_{33} > S_{22} > S_{11}$. Elastic compliance constant $S_{23}$ has the most negative value among elastic compliance constants $S_{12}$, $S_{13}$ and $S_{23}$.

**Table 5.2:** Elastic compliance constants $S_{ij}$ [in $(TPa)^{-1}$] of α-$CdP_2$ at zero pressure

| Scheme | $S_{11}$ | $S_{12}$ | $S_{13}$ | $S_{22}$ | $S_{23}$ | $S_{33}$ | $S_{44}$ | $S_{55}$ | $S_{66}$ |
|---|---|---|---|---|---|---|---|---|---|
| PBEsol[5c] | 14.46 | –5.96 | –5.11 | 18.34 | –6.86 | 20.33 | 29.92 | 41.10 | 36.38 |
| PBE | 14.91 | –5.74 | –4.83 | 18.31 | –6.58 | 20.46 | 30.54 | 41.82 | 36.76 |
| PWGGA | 14.81 | –5.57 | –4.87 | 17.92 | –6.42 | 20.27 | 31.27 | 43.23 | 37.06 |
| LDA PZ | 13.55 | –6.06 | –4.69 | 17.90 | –6.62 | 18.84 | 28.82 | 39.31 | 34.51 |
| LDA VWN | 13.48 | –5.97 | –4.69 | 17.77 | –6.56 | 18.74 | 28.74 | 39.07 | 34.50 |
| B3LYP | 13.82 | –4.74 | –4.12 | 16.01 | –5.27 | 17.38 | 27.58 | 38.09 | 34.43 |
| B3PW | 13.40 | –4.93 | –4.35 | 16.21 | –5.59 | 18.09 | 28.16 | 38.61 | 33.49 |
| PBE0 | 13.20 | –4.98 | –4.43 | 16.26 | –5.75 | 18.11 | 28.21 | 38.40 | 33.13 |
| HSE06 | 13.38 | –5.08 | –4.47 | 16.49 | –5.83 | 18.33 | 28.57 | 38.99 | 33.71 |

[5c]Using Ref. [219].

**Table 5.3:** Young's modulus $E$ (in GPa), bulk modulus $B$ (in GPa) and shear modulus $G$ (in GPa) of α-$CdP_2$ at zero pressure

| Scheme | $B_V$ | $B_R$ | $B_H$ | $G_V$ | $G_R$ | $G_H$ | $E_V$ | $E_R$ | $E_H$ |
|---|---|---|---|---|---|---|---|---|---|
| PBEsol[5d] | 59.68 | 57.81 | 58.75 | 25.73 | 24.74 | 25.23 | 67.50 | 64.94 | 66.22 |
| PBE | 53.00 | 51.65 | 52.32 | 25.44 | 24.56 | 25.00 | 65.80 | 63.61 | 64.71 |
| PWGGA | 53.17 | 51.85 | 52.51 | 25.20 | 24.43 | 24.81 | 65.29 | 63.33 | 64.31 |
| LDA PZ | 66.62 | 64.30 | 65.46 | 26.98 | 25.93 | 26.45 | 71.30 | 68.57 | 69.93 |
| LDA VWN | 66.55 | 64.28 | 65.42 | 27.08 | 26.05 | 26.57 | 71.54 | 68.85 | 70.20 |
| B3LYP | 53.45 | 52.78 | 53.11 | 28.21 | 27.49 | 27.85 | 71.97 | 70.28 | 71.12 |
| B3PW | 57.02 | 55.74 | 56.38 | 28.04 | 27.22 | 27.63 | 72.27 | 70.23 | 71.25 |
| PBE0 | 59.43 | 57.97 | 58.70 | 28.12 | 27.27 | 27.69 | 72.86 | 70.71 | 71.79 |
| HSE06 | 58.79 | 57.32 | 58.06 | 27.72 | 26.88 | 27.30 | 71.86 | 69.73 | 70.80 |

[5d]Using Ref. [219].

Various elastic quantities Young's modulus $E$, bulk modulus $B$ and shear modulus $G$ of α-$CdP_2$ are computed by means of the ELATE program [181, 182] using computed elastic constants $C_{ij}$. These elastic quantities are shown in **Table 5.3**.

It is observed that $E_H > B_H > G_H$. It is evident from **Table 5.3** that the LDA functional gives relatively higher values for $B_H$. The values of $E_H$ and $G_H$ obtained with the schemes B3LYP, B3PW, PBE0, HSE06 are relatively higher in comparison with the respective values of $E_H$ and $G_H$ obtained with the schemes PBEsol, PBE, PWGGA, LDA PZ and LDA VWN.

Poisson's ratios ($\nu_V$, $\nu_R$ and $\nu_H$) of α-$CdP_2$ at zero pressure are computed by means of the ELATE program [181, 182] using obtained elastic constants. These values of Poisson's ratio under different schemes are shown in **Table 5.4**. It is evident from **Table 5.4** that the LDA functional gives relatively higher values for Poisson's ratio $\nu$. **Table 5.4** shows that the obtained values of Poisson's ratios are around 0.3. Thus, computed values of Poisson's ratios lie in the theoretically predicted range [137] for materials.

**Table 5.4:** Poisson's ratio $\nu$ (unitless) of α-$CdP_2$ at zero pressure

| Scheme | $\nu_V$ | $\nu_R$ | $\nu_H$ |
|---|---|---|---|
| PBEsol[5e] | 0.312 | 0.313 | 0.312 |
| PBE | 0.293 | 0.295 | 0.294 |
| PWGGA | 0.295 | 0.296 | 0.296 |
| LDA PZ | 0.322 | 0.322 | 0.322 |
| LDA VWN | 0.321 | 0.321 | 0.321 |
| B3LYP | 0.276 | 0.278 | 0.277 |
| B3PW | 0.289 | 0.290 | 0.289 |
| PBE0 | 0.296 | 0.297 | 0.296 |
| HSE06 | 0.296 | 0.297 | 0.297 |

[5e]Using Ref. [219].

The brittleness and malleability properties of polycrystalline substances may be correlated with the ratio of bulk modulus $B$ to shear modulus $G$ [231]. The malleable nature of a polycrystalline substance is likely to be predicted for a ratio $B/G$ greater than tentatively 1.75 [231]. **Table 5.3** shows that the value of $B_H/G_H$ is about 2.1–2.2. Hence, it predicts the malleable nature of the alpha phase of $CdP_2$.

Using the keyword EOS, variation of bulk modulus with pressure is obtained with the PBE functional under the Vinet [124, 130, 131] scheme. The variation of bulk

modulus with pressure is plotted in **Fig. 5.1**. The variation of bulk modulus with pressure is nearly linear in the given range of pressure, as depicted in **Fig. 5.1**. To our best knowledge, there is no other theoretically or experimentally reported bulk modulus data for α-$CdP_2$ at higher pressures for comparison with our investigation.

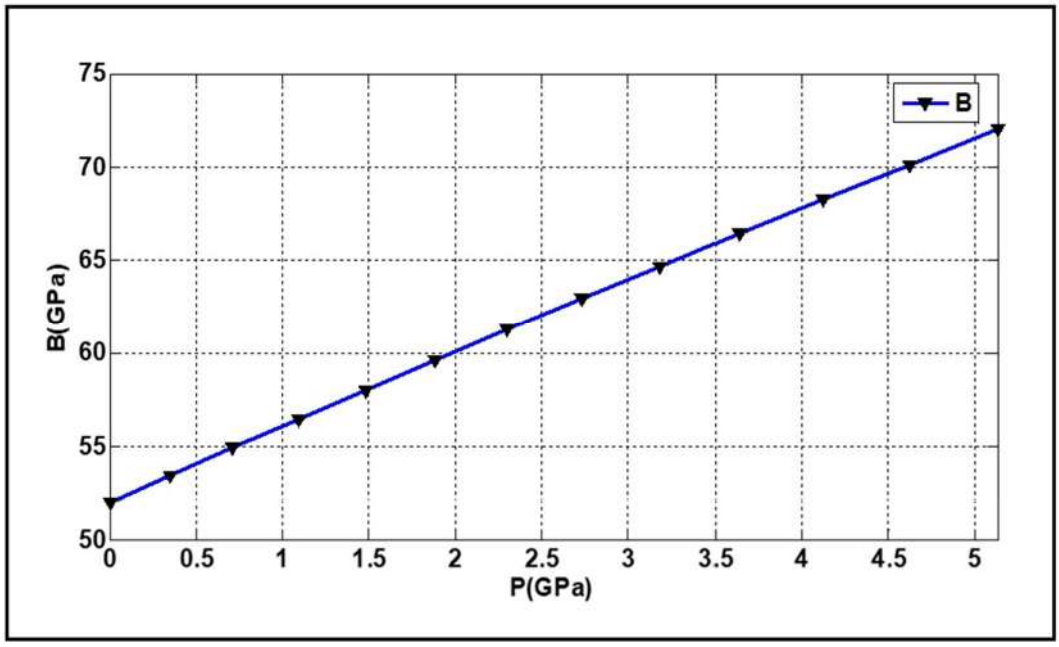


**Figure 5.1:** Computed bulk modulus *B* of α-$CdP_2$ as a function of applied pressure *P*.

### 5.3.1.2 Elastic Anisotropy

In terms of elastic compliance constants $S_{ij}$, Young's modulus *E* along the unit vector $l_i$ for the orthorhombic crystal may be represented as [16]

$$E = \left[ l_1^4 S_{11} + 2l_1^2 l_2^2 S_{12} + 2l_2^2 l_3^2 S_{23} + 2l_1^2 l_3^2 S_{13} + l_2^4 S_{22} + l_3^4 S_{33} + l_1^2 l_3^2 S_{55} + l_2^2 l_3^2 S_{44} + l_1^2 l_2^2 S_{66} \right]^{-1} \tag{5.12}$$

where the direction cosines are denoted by $l_1$, $l_2$ and $l_3$.

The directional linear compressibility $\beta$ along the unit vector $l_i$ for orthorhombic crystal may be represented as [16]

$$\beta = \left(S_{11} + S_{12} + S_{13}\right) l_1^2 + \left(S_{12} + S_{23} + S_{22}\right) l_2^2 + \left(S_{13} + S_{33} + S_{23}\right) l_3^2 \tag{5.13}$$

The elastic anisotropy may be represented in various ways. The degree of elastic anisotropy may be introduced by the following expression [232, 233]

$$A_G = \frac{G_V - G_R}{G_V + G_R} \tag{5.14}$$

The value of $A_G$ is zero in the case of elastic-isotropic materials. For defining the degree of elastic anisotropy for all crystalline symmetry, Ranganathan *et al.* [234] introduced the term universal elastic anisotropy index $A^U$ as

$$A^U = \frac{B_V}{B_R} + 5\frac{G_V}{G_R} - 6 \tag{5.15}$$

Elastic isotropic materials have a value of zero for index $A^U$ [234]. Values of $A^U$ greater than zero reflect the degree of elastic anisotropy in materials. Minimum and maximum values of linear compressibility ($\beta_{min}$ and $\beta_{max}$), Poisson's ratio ($\nu_{min}$ and $\nu_{max}$), shear modulus ($G_{min}$ and $G_{max}$) and Young's modulus ($E_{min}$ and $E_{max}$) of the α-$CdP_2$ crystal are shown in **Table 5.5.** These elastic quantities are calculated by means of the ELATE program [181, 182] using computed values of the α-$CdP_2$ crystal.

From **Table 5.6**, it is evident that the percentage variation of Poisson's ratio relative to its minimum value is higher among the corresponding percentage variations of Young's modulus, linear compressibility, shear modulus and Poisson's ratio for α-$CdP_2$. It is also clear that almost all the anisotropy indices shown in **Table 5.6** have relatively high values under the PBEsol and LDA schemes. Under the B3LYP scheme, almost all the mentioned anisotropy indices have relatively low values.

Polar graphs for the directional-dependent Young's modulus of α-$CdP_2$ at zero pressure under the PBE scheme are depicted in **Fig. 5.2** and **Fig. 5.3** using the ELATE program [181, 182].

**Table 5.5:** Minimum and maximum values of linear compressibility $\beta$ [in $(\mathrm{TPa})^{-1}$], Poisson's ratio $v$ (unitless), shear modulus $G$ (in GPa) and Young's modulus $E$ (in GPa) of α-$CdP_2$

| Scheme | $G_{min}$ | $G_{max}$ | $E_{min}$ | $E_{max}$ | $\beta_{min}$ | $\beta_{max}$ | $v_{min}$ | $v_{max}$ |
|---|---|---|---|---|---|---|---|---|
| PBEsol[5f] | 19.09 | 33.42 | 49.20 | 73.14 | 3.41 | 8.36 | 0.091 | 0.418 |
| PBE | 19.26 | 32.74 | 48.89 | 71.53 | 4.34 | 9.04 | 0.088 | 0.391 |
| PWGGA | 19.59 | 31.98 | 49.32 | 71.00 | 4.37 | 8.99 | 0.104 | 0.387 |
| LDA PZ | 20.01 | 34.70 | 53.07 | 77.28 | 2.80 | 7.53 | 0.102 | 0.447 |
| LDA VWN | 20.15 | 34.79 | 53.36 | 77.37 | 2.82 | 7.49 | 0.103 | 0.443 |
| B3LYP | 22.77 | 36.26 | 57.55 | 79.51 | 4.96 | 7.98 | 0.094 | 0.359 |
| B3PW | 21.99 | 35.51 | 55.30 | 78.33 | 4.12 | 8.14 | 0.099 | 0.376 |
| PBE0 | 21.80 | 35.45 | 55.23 | 78.62 | 3.80 | 7.93 | 0.105 | 0.387 |
| HSE06 | 21.52 | 35.01 | 54.54 | 77.60 | 3.82 | 8.04 | 0.104 | 0.386 |

[5f]Ref. [219].

**Table 5.6:** Elastic anisotropy parameters: ratio of maximum to minimum values of Young's modulus $E$, linear compressibility $\beta$, shear modulus $G$ and Poisson's ratio $v$ for α-$CdP_2$. Elastic anisotropy parameters $A_G$ and $A^U$ for α-$CdP_2$

| Scheme | Anisotropy | | | | | |
|---|---|---|---|---|---|---|
| | $\frac{E_{max}}{E_{min}}$ | $\frac{\beta_{max}}{\beta_{min}}$ | $\frac{G_{max}}{G_{min}}$ | $\frac{v_{max}}{v_{min}}$ | $A_G$ | $A^U$ |
| PBEsol[5g] | 1.49 | 2.45 | 1.75 | 4.59 | 0.020 | 0.234 |
| PBE | 1.46 | 2.08 | 1.70 | 4.44 | 0.018 | 0.205 |
| PWGGA | 1.44 | 2.06 | 1.63 | 3.70 | 0.016 | 0.184 |
| LDA PZ | 1.46 | 2.69 | 1.73 | 4.40 | 0.020 | 0.238 |
| LDA VWN | 1.45 | 2.65 | 1.73 | 4.32 | 0.019 | 0.233 |
| B3LYP | 1.38 | 1.61 | 1.59 | 3.83 | 0.013 | 0.143 |
| B3PW | 1.42 | 1.98 | 1.62 | 3.82 | 0.015 | 0.173 |
| PBE0 | 1.42 | 2.09 | 1.63 | 3.70 | 0.015 | 0.181 |
| HSE06 | 1.42 | 2.10 | 1.63 | 3.70 | 0.015 | 0.182 |

[5g]Using Ref. [219].

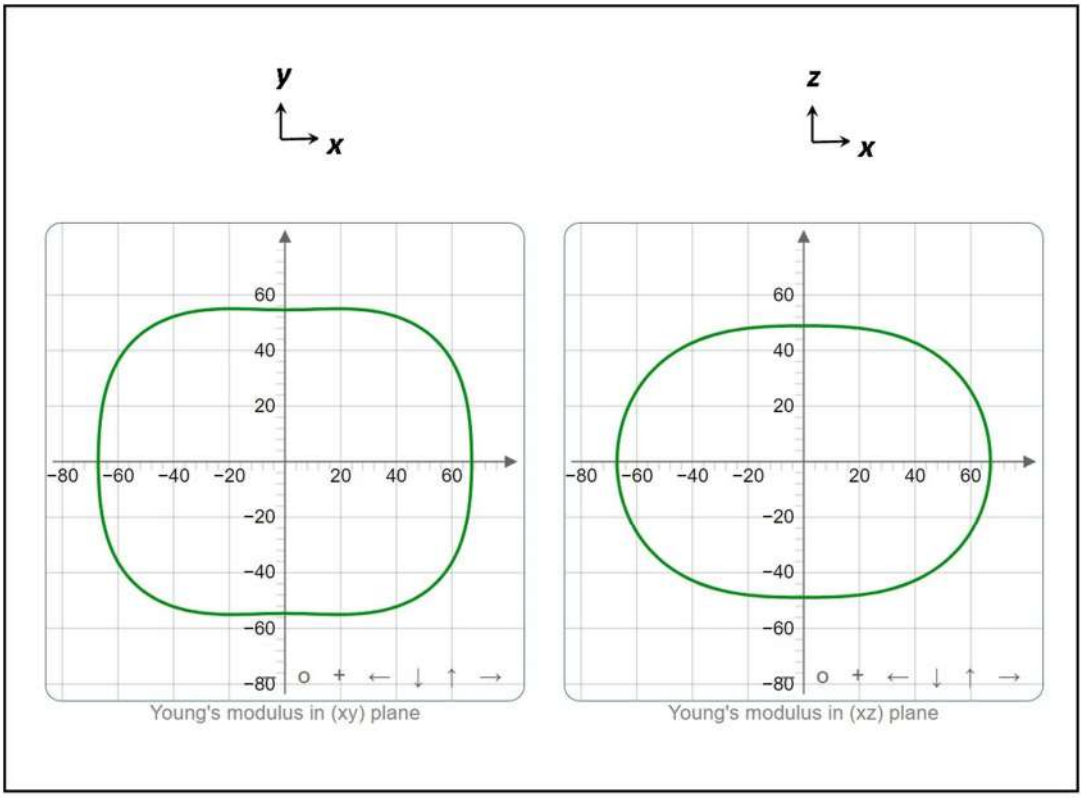


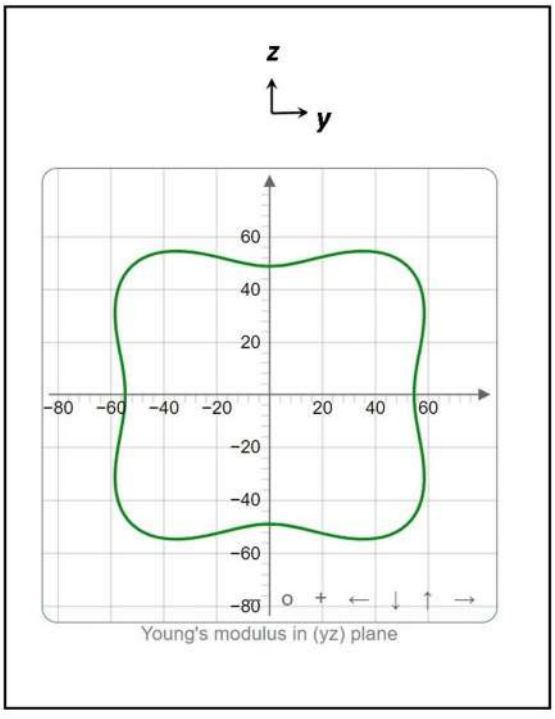


**Figure 5.2:** Polar graphs[5h] (2D view) for the directional-dependent Young's modulus *E* (in GPa) of α-$CdP_2$ at zero pressure under the PBE scheme.

[5h]Using the ELATE program [181, 182].

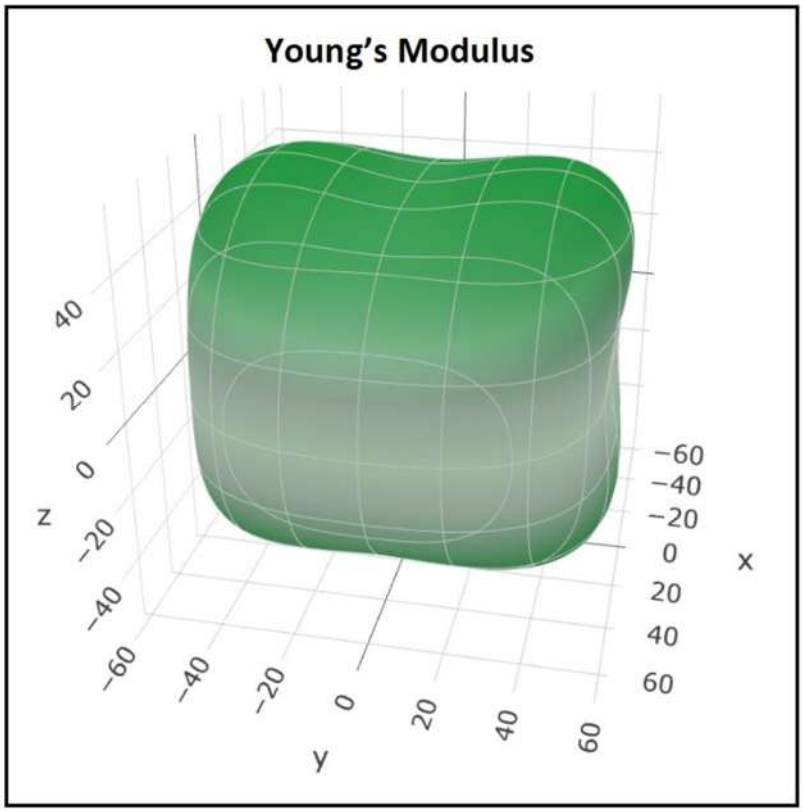


**Figure 5.3:** Polar graph[5i] (3D view) for the directional-dependent Young's modulus *E* (in GPa) of α-$CdP_2$ at zero pressure under the PBE scheme.
[5i]Using the ELATE program [181, 182].

The directional Young's modulus varies from a minimum value of 48.89 GPa to a maximum value of 71.53 GPa under the PBE scheme. Polar graphs for the directional-dependent linear compressibility $\beta$ of α-$CdP_2$ at zero pressure under the PBE scheme are shown in **Fig. 5.4** and **Fig. 5.5** using the ELATE program [181, 182]. The directional shear modulus varies from a minimum value of 19.26 GPa to a maximum value of 32.74 GPa under the PBE method.

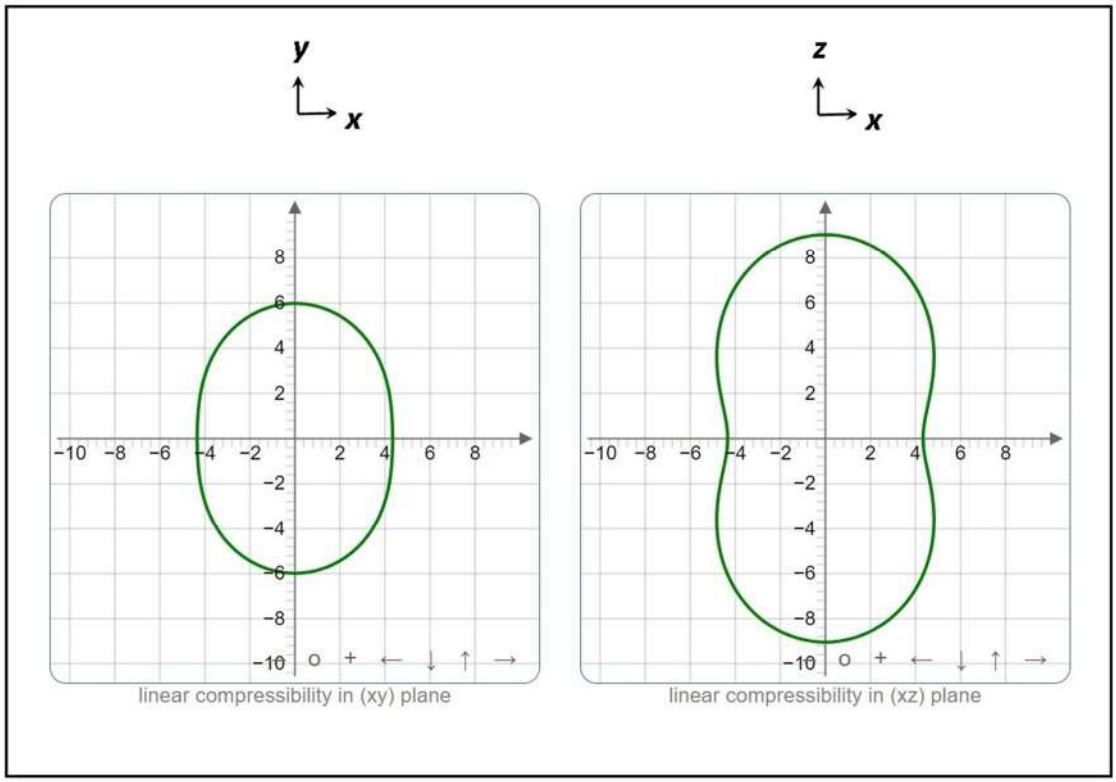


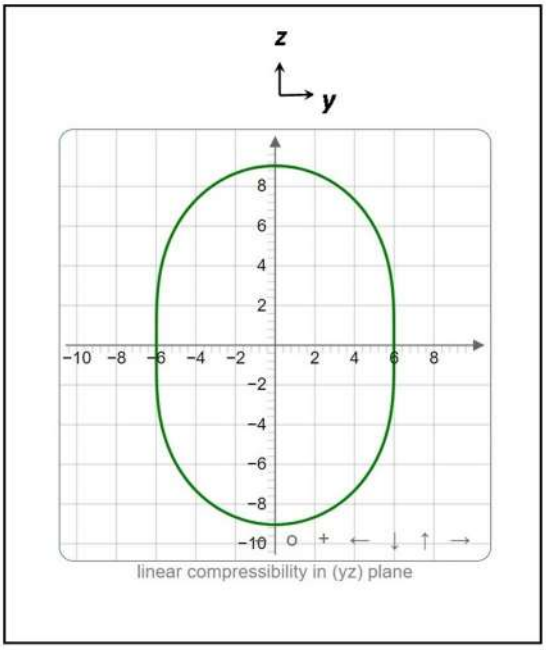


**Figure 5.4:** Polar graphs[5j] (2D view) for the directional-dependent linear compressibility $\beta$ [in $(\mathrm{TPa})^{-1}$] of α-$CdP_2$ at zero pressure under the PBE scheme.

[5j]Using the ELATE program [181, 182].

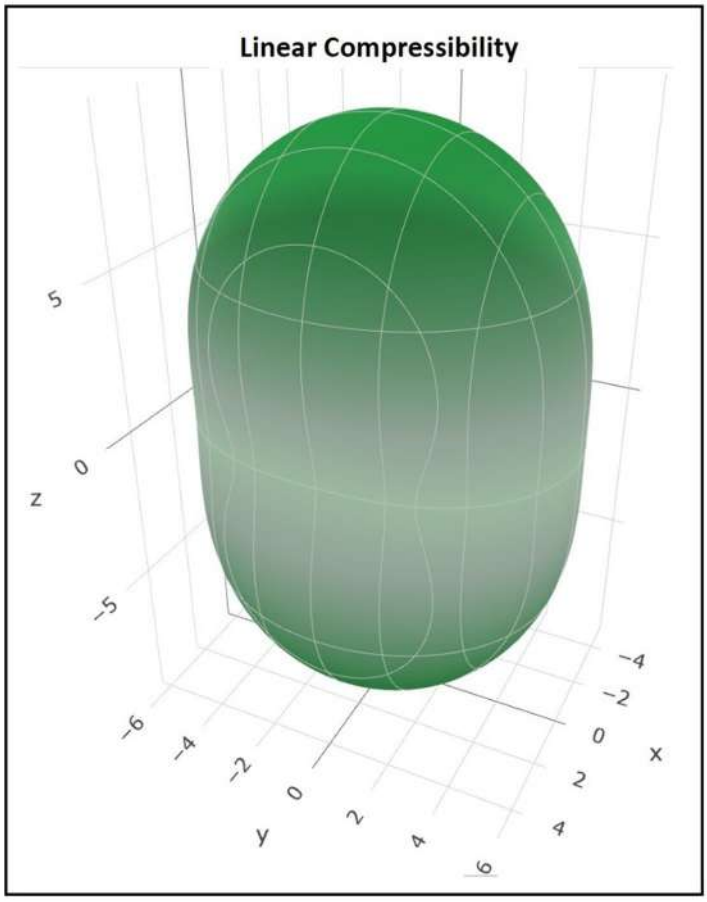


**Figure 5.5:** Polar graph[5k] (3D view) for the directional-dependent linear compressibility $\beta$ [in $(\mathrm{TPa})^{-1}$] of α-$CdP_2$ at zero pressure under the PBE scheme.
[5k]Using the ELATE program [181, 182].

The variation of directional-dependent Poisson's ratio and shear modulus of α-$CdP_2$ at zero pressure under the PBE scheme in polar form are illustrated in **Fig. 5.6**, **Fig. 5.7**, **Fig. 5.8** and **Fig. 5.9**. These polar graphs are plotted as per the convention used for the ELATE program [181, 182]. Variations of Young's modulus and linear compressibility were also plotted with the PBEsol scheme in other work [219].

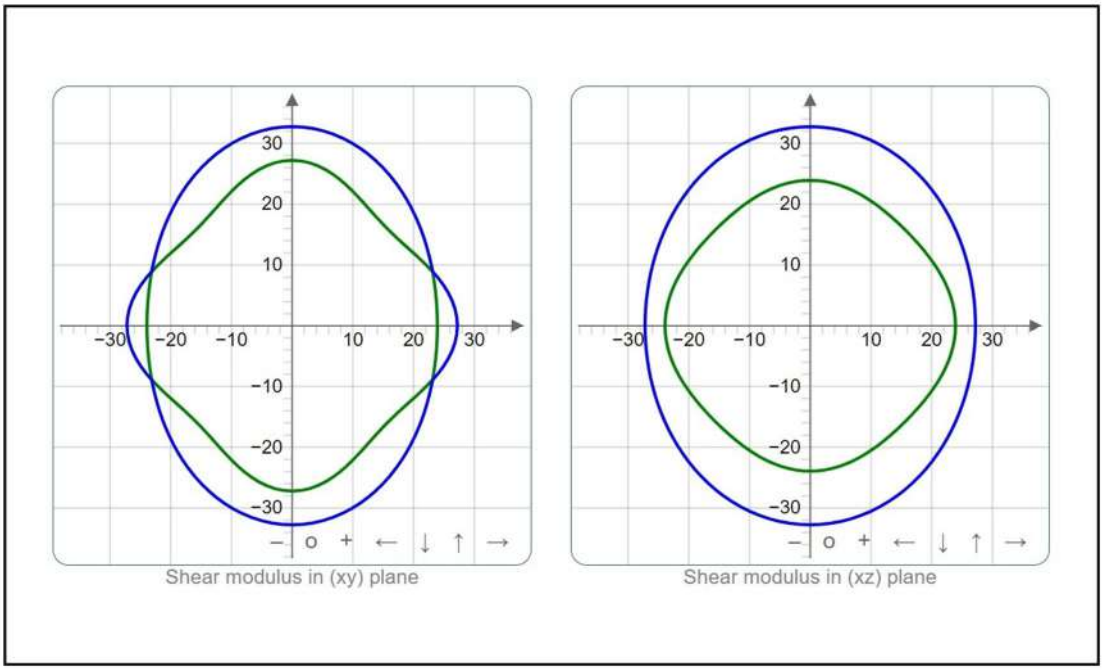


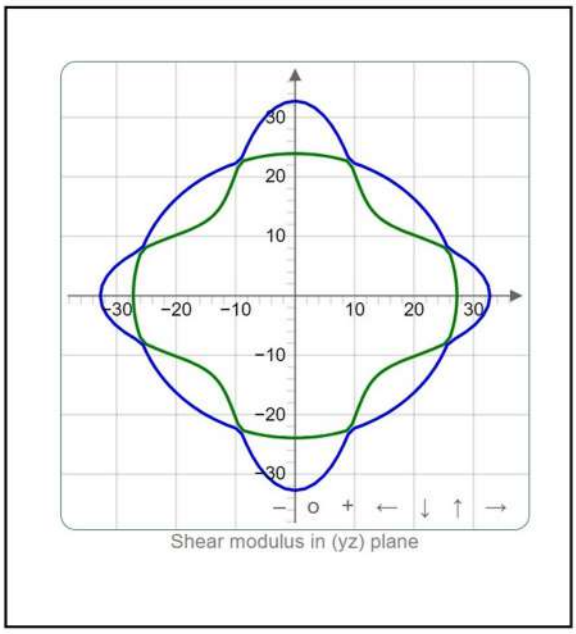


**Figure 5.6:** Polar graphs[51] (2D view) for the directional-dependent shear modulus *G* (in GPa) of α-$CdP_2$ at zero pressure under the PBE scheme.

[51]Using the ELATE program [181, 182].

.

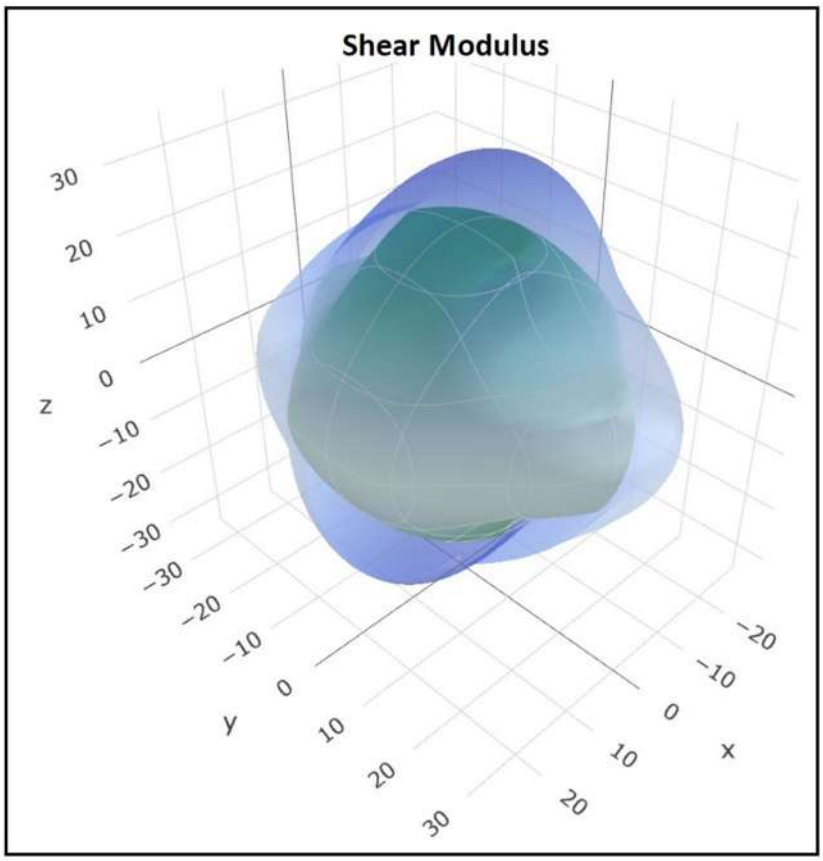


**Figure 5.7:** Polar graph[5m] (3D view) for the directional-dependent shear modulus *G* (in GPa) of α-$CdP_2$ at zero pressure under the PBE scheme.

[5m]Using the ELATE program [181, 182].

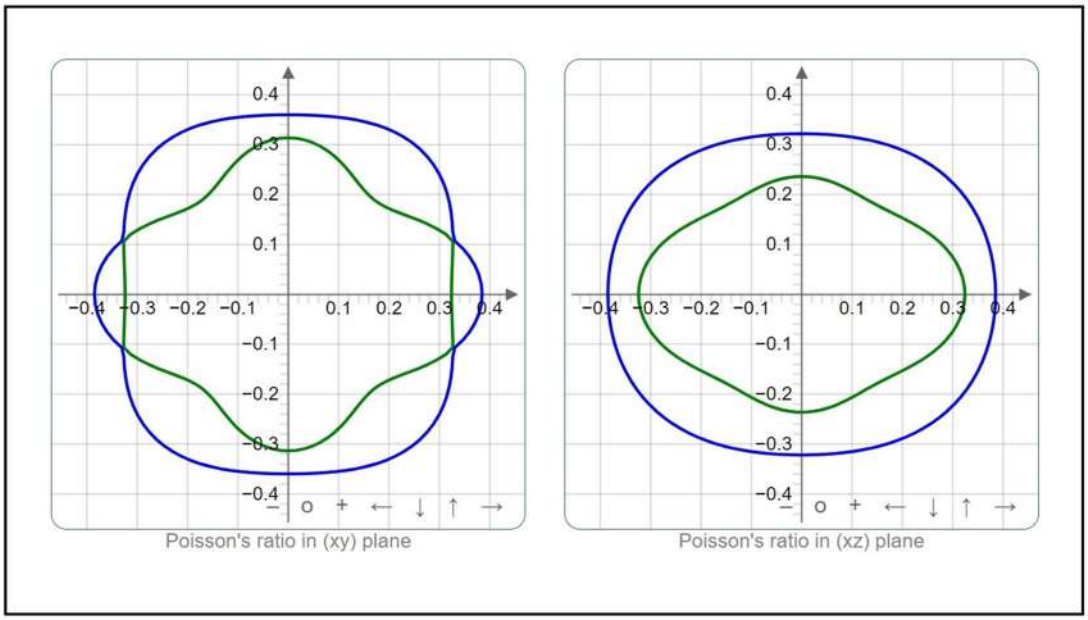


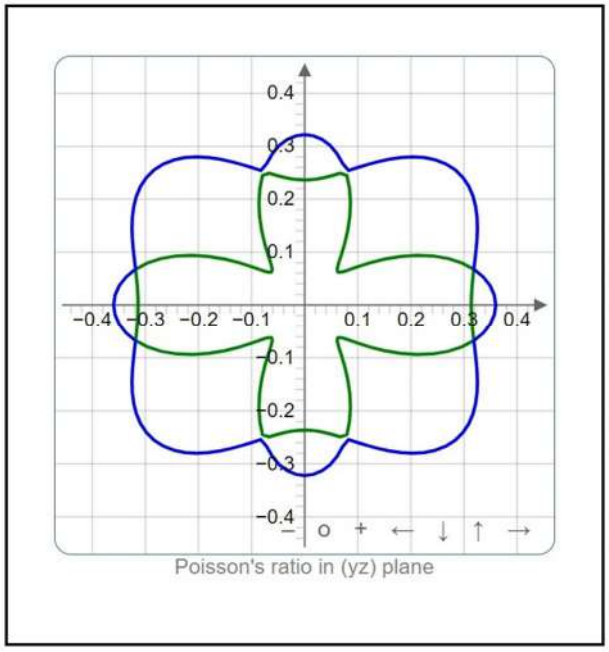


**Figure 5.8:** Polar graphs[5n] (2D view) for the directional-dependent Poisson's ratio *v* (unitless) of α-$CdP_2$ at zero pressure under the PBE scheme.

[5n]Using the ELATE program [181, 182].

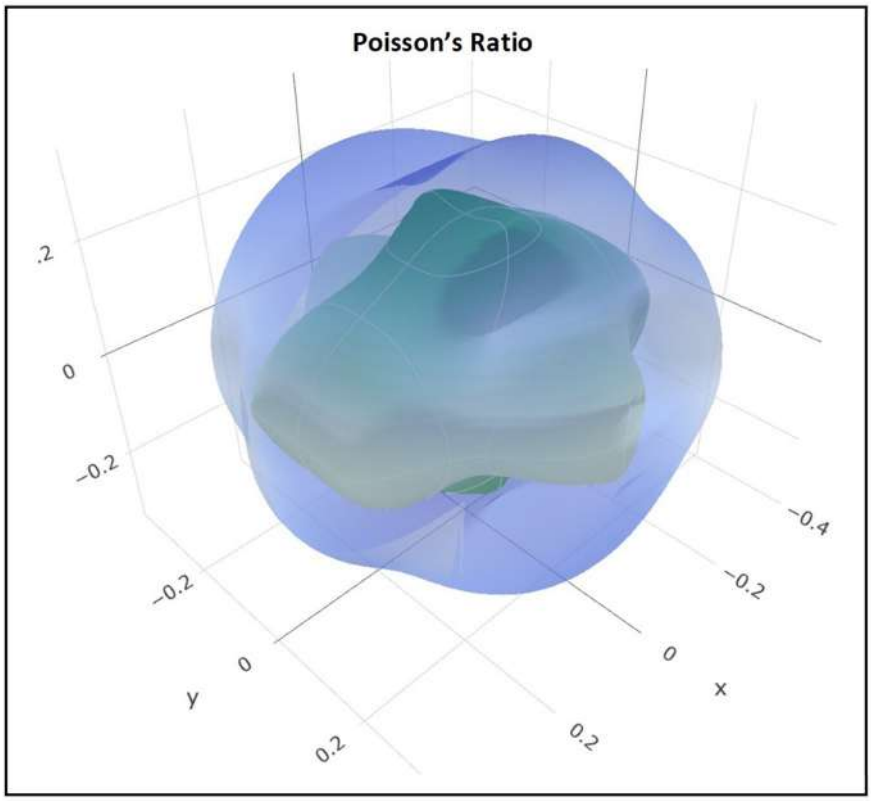


**Figure 5.9:** Polar graph[5o] (3D view) for the directional-dependent Poisson's ratio *v* (unitless) of α-$CdP_2$ at zero pressure under the PBE scheme.

[5o]Using the ELATE program [181, 182].

## 5.3.2 Elastic Properties of $ZnP_2$

### 5.3.2.1 Elastic Constants

The bulk modulus and shear modulus of β-$ZnP_2$ are 68 GPa and 44 GPa, respectively, as reported by Huang *et al.* [88]. Young's modulus and Poisson's ratio of the beta phase of $ZnP_2$ are 110 GPa and 0.23, respectively [88]. The zero pressure elastic constants (in GPa) of β-$ZnP_2$ are $C_{11}=117$, $C_{22}=126$, $C_{33}=136$, $C_{44}=30$, $C_{55}=50$, $C_{66}=54$, $C_{12}=50$, $C_{13}=45$, $C_{23}=22$, $C_{15}=-0.03$, $C_{25}=-0.3$, $C_{35}=-0.4$ and $C_{46}=0$ [88].

In this work, an investigation of the elastic properties of the alpha phase of $ZnP_2$ is carried out. The crystal of the tetragonal (I) class (4/mmm) has six independent elastic stiffness constants $C_{11}$, $C_{12}$, $C_{13}$, $C_{33}$, $C_{44}$ and $C_{66}$ [16]. In the present study, the obtained elastic stiffness constants $C_{ij}$ of α-$ZnP_2$ are shown in **Table 5.7** along with

theoretical [88, 235] and experimental data [229]. As stated by Mouhat *et al.* [230], necessary and sufficient elastic stability conditions for the crystal of the tetragonal (I) class (4/mmm) are expressed by the following four conditions:

$$C_{11} > \left|C_{12}\right| \tag{5.16}$$

$$2C_{13}^2 < C_{33}\left(C_{11} + C_{12}\right) \tag{5.17}$$

$$C_{44} > 0 \tag{5.18}$$

$$C_{66} > 0 \tag{5.19}$$

In this study, the obtained elastic stiffness constants (shown in **Table 5.7**) satisfy these necessary and sufficient elastic stability conditions for the crystal of the tetragonal (I) class (4/mmm). Thus, it asserts the mechanical stability of the α-$ZnP_2$ crystal. At zero pressure, it is obvious that the obtained elastic stiffness constants $C_{ij}$ are in fair agreement with the experimental values [229].

**Table 5.7:** Elastic constants $C_{ij}$ (in GPa) of α-$ZnP_2$ at zero pressure

| Scheme | $C_{11}$ | $C_{12}$ | $C_{13}$ | $C_{33}$ | $C_{44}$ | $C_{66}$ |
|---|---|---|---|---|---|---|
| PBEsol | 117.90 | 55.65 | 51.00 | 129.63 | 47.57 | 66.64 |
| PBE | 108.21 | 46.66 | 42.39 | 118.78 | 44.92 | 62.04 |
| PWGGA | 109.24 | 46.98 | 42.70 | 119.63 | 45.26 | 62.65 |
| LDA PZ | 128.01 | 62.21 | 57.15 | 139.06 | 50.72 | 71.60 |
| LDA VWN | 128.34 | 62.35 | 57.29 | 139.40 | 50.85 | 71.79 |
| B3LYP | 110.24 | 42.25 | 38.22 | 120.05 | 46.07 | 62.85 |
| B3PW | 115.67 | 48.82 | 44.68 | 126.75 | 47.06 | 65.09 |
| PBE0 | 117.95 | 51.43 | 47.44 | 129.75 | 47.29 | 65.71 |
| HSE06 | 116.65 | 50.95 | 46.90 | 128.33 | 46.93 | 64.99 |
| Other Work[5p] | 116.48 | 54.18 | 48.12 | 126.37 | 44.34 | 59.42 |
| Other Work[5q] | 118 | 53 | 45 | 123 | 45 | 60 |
| Exp.[5r] | 102.1 | 30.76 | | 115.7 | 42.85 | 52.08 |

[5p]Ref. [235].

[5q]Ref. [88].

[5r]Ref. [229].

For the crystal of the tetragonal (I) class (4/mmm) $B_R$, $B_V$, $G_R$ and $G_V$ may be represented in the following way [184, 185, 186]

$$B_R = \left[2S_{11} + S_{33} + 2S_{12} + 4S_{13}\right]^{-1} \tag{5.20}$$

$$B_V = \frac{1}{9}\left[2C_{11} + C_{33} + 2C_{12} + 4C_{13}\right] \tag{5.21}$$

$$G_R = 15\left[4\left(2S_{11} + S_{33}\right) + 3\left(2S_{44} + S_{66}\right) - 4\left(S_{12} + 2S_{13}\right)\right]^{-1} \tag{5.22}$$

$$G_V = \frac{1}{15}\left[2C_{11} + C_{33} - C_{12} - 2C_{13}\right] + \frac{1}{5}\left[2C_{44} + C_{66}\right] \tag{5.23}$$

Elastic compliance constants $S_{ij}$ [in $(\text{TPa})^{-1}$] of α-$ZnP_2$ at zero pressure are shown in **Table 5.8**. The computed elastic moduli of α-$ZnP_2$ are reported in **Table 5.9**. The orthorhombic phosphorus crystal has a Young's modulus of 30.4 GPa [29] and a bulk modulus of nearly 36 GPa [236]. The Young's modulus and bulk modulus for zinc crystals are 92.7 GPa and 60.6 GPa, respectively [29]. **Table 5.9** shows that the respective computed values of Young's modulus $E$ and bulk modulus $B$ of α-$ZnP_2$ are higher than those of its constituent elements. In view of resisting structural deformation, the typical bulk modulus of ~66 GPa of α-$ZnP_2$ reflects its considerably ample mechanical strength.

It is evident that the value of $B/G$ is ~1.55 at zero pressure under the PBE scheme. Hence, it suggests the brittle nature of α-$ZnP_2$. Our computed ratio $c/a$ at zero pressure is 3.645 under PBE scheme, which is almost equal to the experimental value of 3.659 [36]. Hence, it is obvious that the computed values of Poisson's ratio lie in the theoretically predicted range [137] for materials. Now, we illustrate the various elastic properties with different functional schemes. It is evident from **Table 5.7** that computation with the LDA functional gives relatively high values of coefficients $C_{11}$, $C_{12}$, $C_{13}$, $C_{33}$, $C_{44}$ and $C_{66}$ for α-$ZnP_2$.

**Table 5.8:** Elastic compliance constants $S_{ij}$ [in $(\text{TPa})^{-1}$] of α-$ZnP_2$ at zero pressure

| Scheme | $S_{11}$ | $S_{12}$ | $S_{13}$ | $S_{33}$ | $S_{44}$ | $S_{66}$ |
|---|---|---|---|---|---|---|
| PBEsol | 11.78 | –4.28 | –2.95 | 10.04 | 21.02 | 15.01 |
| PBE | 12.14 | –4.11 | –2.86 | 10.46 | 22.26 | 16.12 |
| PWGGA | 12.01 | –4.05 | –2.84 | 10.39 | 22.10 | 15.96 |
| LDA PZ | 11.09 | –4.11 | –2.87 | 9.55 | 19.72 | 13.97 |
| LDA VWN | 11.06 | –4.10 | –2.86 | 9.53 | 19.67 | 13.93 |
| B3LYP | 11.26 | –3.45 | –2.48 | 9.91 | 21.71 | 15.91 |
| B3PW | 11.24 | –3.72 | –2.65 | 9.76 | 21.25 | 15.36 |
| PBE0 | 11.23 | –3.80 | –2.71 | 9.69 | 21.15 | 15.22 |
| HSE06 | 11.36 | –3.86 | –2.74 | 9.80 | 21.31 | 15.39 |
| Other Work[5s] | 12.5 | –1.5 | –4.69 | 12.64 | 23.34 | 19.2 |

[5s]Ref. [229].

**Table 5.9:** Young's modulus $E$ (in GPa), bulk modulus $B$ (in GPa) and shear modulus $G$ (in GPa) of α-$ZnP_2$ at zero pressure

| Scheme | $B_V$ | $B_R$ | $B_H$ | $G_V$ | $G_R$ | $G_H$ | $E_V$ | $E_R$ | $E_H$ |
|---|---|---|---|---|---|---|---|---|---|
| PBEsol | 75.64 | 75.59 | 75.61 | 46.21 | 43.32 | 44.77 | 115.17 | 109.12 | 112.16 |
| PBE | 66.45 | 66.41 | 66.43 | 43.96 | 41.64 | 42.80 | 108.05 | 103.33 | 105.70 |
| PWGGA | 66.99 | 66.95 | 66.97 | 44.35 | 42.02 | 43.18 | 108.99 | 104.25 | 106.63 |
| LDA PZ | 83.12 | 83.09 | 83.10 | 49.18 | 45.94 | 47.56 | 123.24 | 116.38 | 119.83 |
| LDA VWN | 83.33 | 83.29 | 83.31 | 49.31 | 46.07 | 47.69 | 123.55 | 116.68 | 120.14 |
| B3LYP | 64.21 | 64.18 | 64.20 | 45.79 | 43.94 | 44.87 | 110.98 | 107.33 | 109.17 |
| B3PW | 70.50 | 70.45 | 70.47 | 46.50 | 44.30 | 45.4 | 114.36 | 109.87 | 112.12 |
| PBE0 | 73.14 | 73.08 | 73.11 | 46.68 | 44.37 | 45.53 | 115.48 | 110.71 | 113.11 |
| HSE06 | 72.34 | 72.29 | 72.32 | 46.23 | 43.93 | 45.08 | 114.33 | 109.59 | 111.97 |
| Other Work[5t] | 73.35 | 73.33 | 73.34 | 43.55 | 41.66 | 42.61 | 109.06 | 105.08 | 107.07 |

[5t]Ref. [235].

**Table 5.8** shows that $S_{12}$ and $S_{13}$ have negative values. Young's modulus ($E_V$, $E_R$ and $E_H$), bulk modulus ($B_V$, $B_R$ and $B_H$), and shear modulus ($G_V$, $G_R$ and $G_H$) of

α-$ZnP_2$ are reported in **Table 5.9**. Poisson's ratio $v$ (unitless) of α-$ZnP_2$ at zero pressure is illustrated in **Table 5.10**. Using the obtained elastic constants, these elastic quantities (shown in **Table 5.9** and **Table 5.10**) are calculated by means of the ELATE program [181, 182]. It is also obvious that the values of elastic quantities obtained in **Table 5.9** and **Table 5.10** have relatively high values under the LDA functionals.

Based on ultrasonic measurements, according to Soshnikov *et al.*, the calculated shear modulus and bulk modulus of the alpha phase of the $ZnP_2$ are 35.7 GPa and 62.91 GPa [229]. According to Huang *et al.* [88], the computed values of shear modulus, bulk modulus, Young's modulus and Poisson's ratio of α-$ZnP_2$ are 44 GPa, 72 GPa, 110 GPa and 0.24, respectively.

**Table 5.10:** Poisson's ratio $v$ (unitless) of α-$ZnP_2$ at zero pressure

| Scheme | $v_V$ | $v_R$ | $v_H$ |
|---|---|---|---|
| PBEsol | 0.246 | 0.259 | 0.253 |
| PBE | 0.229 | 0.241 | 0.235 |
| PWGGA | 0.229 | 0.240 | 0.235 |
| LDA PZ | 0.253 | 0.267 | 0.260 |
| LDA VWN | 0.253 | 0.267 | 0.260 |
| B3LYP | 0.212 | 0.221 | 0.217 |
| B3PW | 0.230 | 0.240 | 0.235 |
| PBE0 | 0.237 | 0.248 | 0.242 |
| HSE06 | 0.237 | 0.247 | 0.242 |

### 5.3.2.2 Elastic Anisotropy

The α-$ZnP_2$ crystal has directional-dependent variations in elastic quantities, such as shear modulus $G$, Young's modulus $E$ and Poisson's ratio $v$. In terms of elastic compliance constants $S_{ij}$, Young's modulus $E$ along the unit vector $l_i$ for the crystal of the tetragonal class (4/mmm) may be represented as [16]

$$E = \left[ l_3^4 S_{33} + \left( l_1^4 + l_2^4 \right) S_{11} + l_1^2 l_2^2 \left( S_{66} + 2S_{12} \right) + l_3^2 \left( 1 - l_3^2 \right) \left( 2S_{13} + S_{44} \right) \right]^{-1} \quad (5.24)$$

where the direction cosines are denoted by $l_1$, $l_2$ and $l_3$.

The directional linear compressibility $\beta$ along the unit vector $l_i$ ,for all classes of tetragonal crystal systems, may be represented as [16]

$$\beta = (S_{11} + S_{13} + S_{12}) - (S_{11} + S_{12} - S_{33} - S_{13}) l_3^2 \tag{5.25}$$

Along different directions, the directional Young's modulus and linear compressibility for α-$ZnP_2$ at zero pressure under the PBE scheme are illustrated in **Table 5.11**.

**Table 5.11:** Under the PBE method, the directional Young's modulus and linear compressibility for α-$ZnP_2$ at zero pressure

| $\frac{E_{[100]}}{(\mathrm{GPa})}$ | $\frac{E_{[010]}}{(\mathrm{GPa})}$ | $\frac{E_{[001]}}{(\mathrm{GPa})}$ | $\frac{E_{[110]}}{(\mathrm{GPa})}$ | $\frac{\beta_{[100]}}{(\mathrm{TPa})^{-1}}$ | $\frac{\beta_{[010]}}{(\mathrm{TPa})^{-1}}$ | $\frac{\beta_{[001]}}{(\mathrm{TPa})^{-1}}$ | $\frac{\beta_{[110]}}{(\mathrm{TPa})^{-1}}$ |
|---|---|---|---|---|---|---|---|
| 82.41 | 82.41 | 95.57 | 124.35 | 5.16 | 5.16 | 4.74 | 5.16 |

Along the different crystallographic directions, the following results about the directional Young's modulus and linear compressibility of the α-$ZnP_2$ crystal may be inferred from our investigation:

$$E_{[100]} = E_{[010]} < E_{[001]} < E_{[110]} \;;\; a = b < c \tag{5.26}$$

$$\beta_{[100]} = \beta_{[010]} = \beta_{[110]} > \beta_{[001]} \;;\; a = b < c \tag{5.27}$$

These substantial differences themselves indicate the existence of considerable elastic anisotropy in the α-$ZnP_2$ crystal. Minimum and maximum values of linear compressibility ($\beta_{\min}$ and $\beta_{\max}$), Poisson's ratio ($v_{\min}$ and $v_{\max}$), shear modulus ($G_{\min}$ and $G_{\max}$) and Young's modulus ($E_{\min}$ and $E_{\max}$) of α-$ZnP_2$ crystal are shown in **Table 5.12**. These elastic quantities are calculated by means of the ELATE program [181, 182] using computed values of the α-$ZnP_2$ crystal.

**Table 5.12:** Minimum and maximum values of linear compressibility $\beta$ [in $(\text{TPa})^{-1}$], Poisson's ratio $v$ (unitless), shear modulus $G$ (in GPa) and Young's modulus $E$ (in GPa) of α-$ZnP_2$

| Scheme | $G_{min}$ | $G_{max}$ | $E_{min}$ | $E_{max}$ | $\beta_{min}$ | $\beta_{max}$ | $v_{min}$ | $v_{max}$ |
|---|---|---|---|---|---|---|---|---|
| PBEsol | 31.13 | 66.64 | 84.90 | 133.35 | 4.14 | 4.55 | 0.0006 | 0.396 |
| PBE | 30.78 | 62.04 | 82.41 | 124.35 | 4.74 | 5.16 | 0.0022 | 0.361 |
| PWGGA | 31.13 | 62.65 | 83.28 | 125.52 | 4.71 | 5.12 | 0.0017 | 0.360 |
| LDA PZ | 32.90 | 71.60 | 90.18 | 143.22 | 3.81 | 4.11 | 0.0002 | 0.407 |
| LDA VWN | 32.99 | 71.79 | 90.42 | 143.58 | 3.80 | 4.10 | 0.0001 | 0.407 |
| B3LYP | 34.00 | 62.85 | 88.85 | 126.92 | 4.94 | 5.32 | 0.0096 | 0.319 |
| B3PW | 33.43 | 65.09 | 88.98 | 131.56 | 4.46 | 4.87 | 0.0107 | 0.349 |
| PBE0 | 33.26 | 65.71 | 89.06 | 133.04 | 4.26 | 4.71 | 0.0123 | 0.360 |
| HSE06 | 32.85 | 64.99 | 88.03 | 131.63 | 4.31 | 4.76 | 0.0127 | 0.361 |

Polar graphs (2D and 3D views) for the directional-dependent various elastic quantities of α-$ZnP_2$ at zero pressure under the PBE scheme are plotted in **Fig. 5.10** to **Fig. 5.17**.

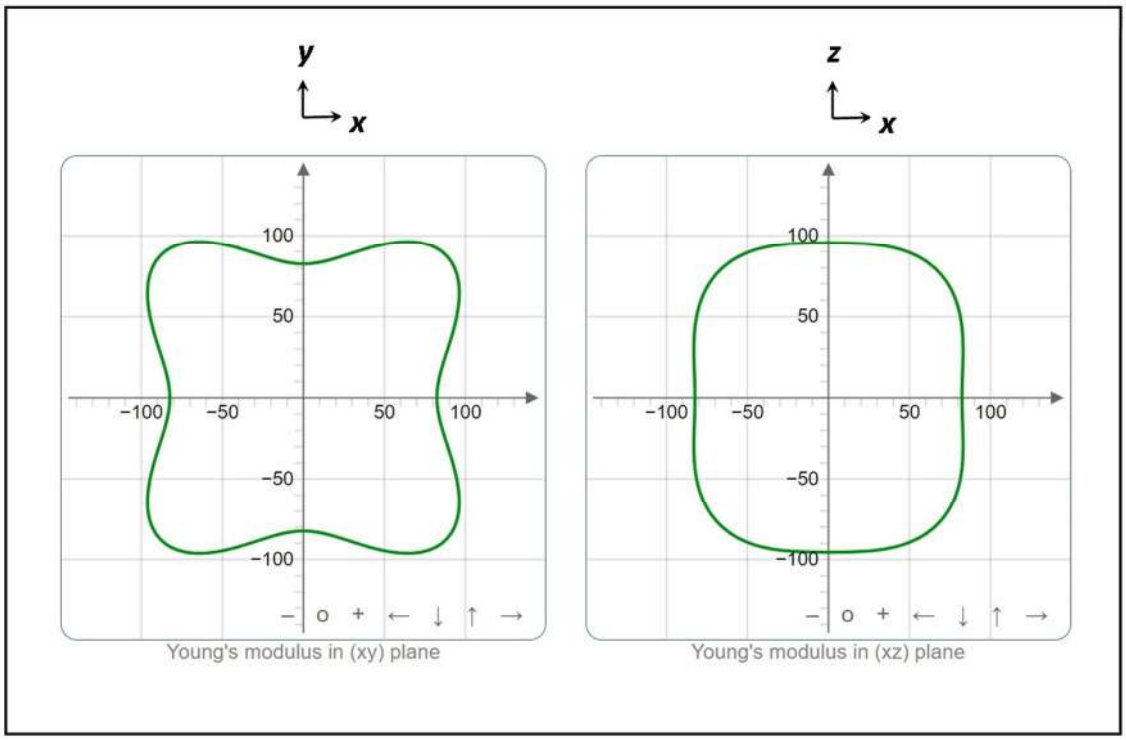


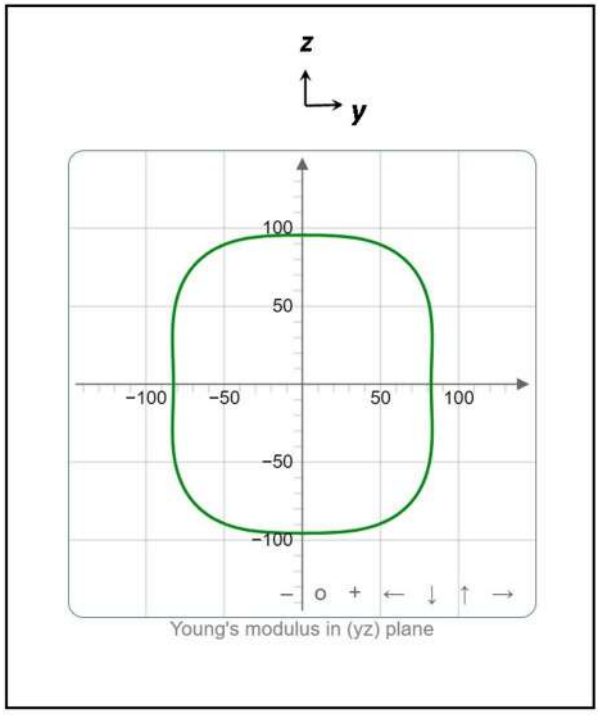


**Figure 5.10:** Polar graphs[5u] (2D view) for the directional-dependent Young's modulus $E$ (in GPa) of α-$ZnP_2$ at zero pressure under the PBE scheme.

[5u]Using the ELATE program [181, 182].

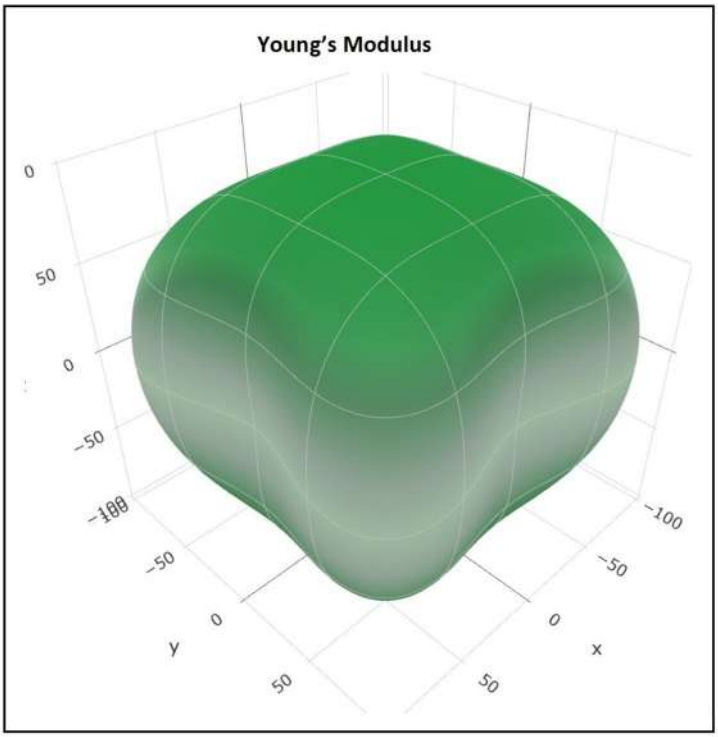


**Figure 5.11:** Polar graph[5v] (3D view) for the directional-dependent Young's modulus *E* (in GPa) of α-$ZnP_2$ at zero pressure under the PBE scheme.
[5v]Using the ELATE program [181, 182].

It is evident from **Fig. 5.10** that the *xy*-plane has greater anisotropy than the *yz*-plane for Young's modulus *E*. In the *yz*-plane, it is observed that *E* increases from 82.41 GPa to about 103.4 GPa (the maximum value in the *yz*-plane) as the angle (with the [010] direction) varies from 0° to about 53.9°, and then *E* decreases from about 103.4 GPa to 95.57 GPa as the angle increases from about 53.9° to 90°. The approximate maximum value of 103.4 GPa of Young's modulus is again found at an angle of about 126.1° in the *yz*-plane. In the *xy*-plane, an increase of the angle (with the [100] direction) from 0° to 45° results in a continuous increase in the value of Young's modulus *E* from 82.41 GPa to 124.35 GPa ($E_{max}$ in **Table 5.12**). Also, as the angle (with the [100] direction) varies from 45° to 90°, *E* decreases continuously from 124.35 GPa to 82.41 GPa ($E_{min}$ in **Table 5.12**). In the *xy*-plane, the maxima of *E* again occur at an angle of 135° (with the [100] direction). For the *yz*- and *xy*- planes, the maximum percentage change in the value of Young's modulus *E* with respect to their minimum values (in the corresponding planes) is about 25.5% and 50.9%, respectively.

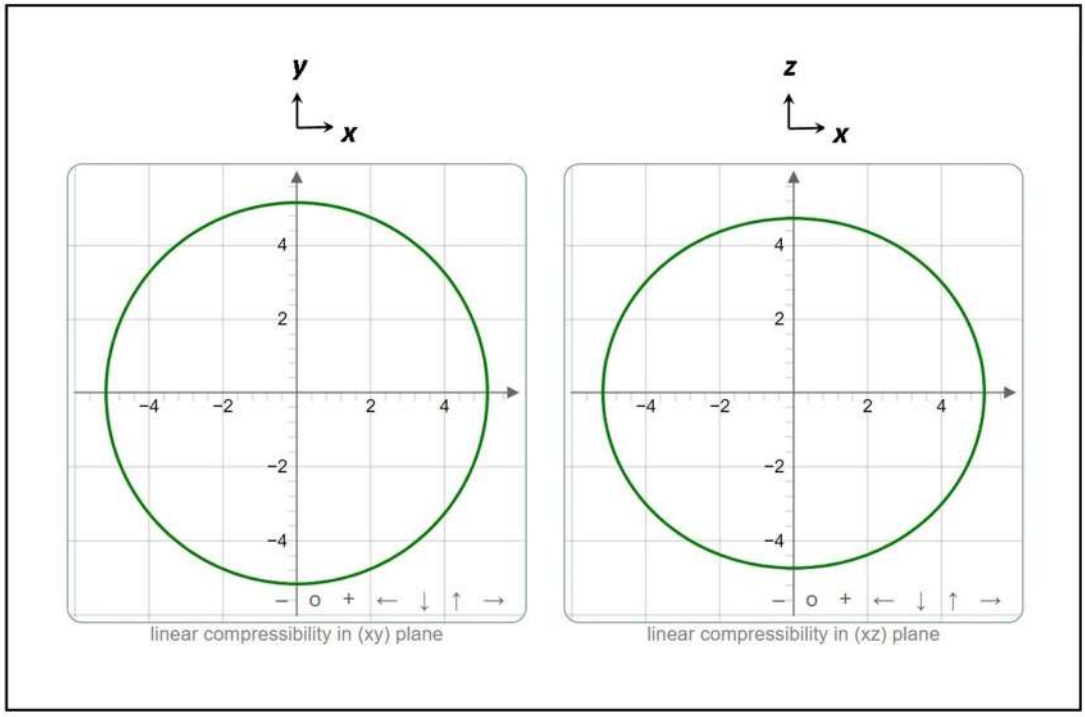


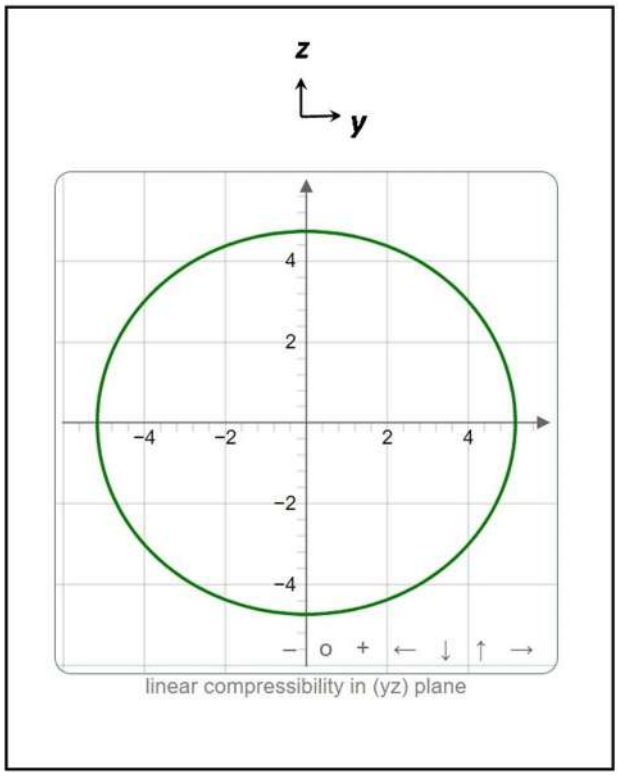


**Figure 5.12:** Polar graphs[5w] (2D view) for the directional-dependent linear compressibility $\beta$ [in $(\mathrm{TPa})^{-1}$] of α-$ZnP_2$ at zero pressure under the PBE scheme.

[5w]Using the ELATE program [181, 182].

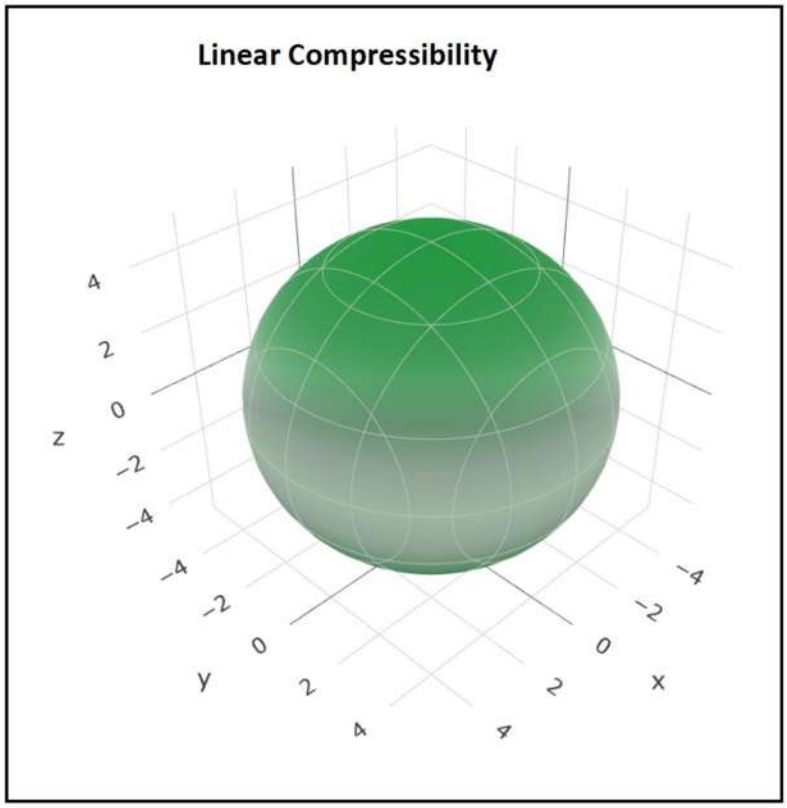


**Figure 5.13:** Polar graph[5x] (3D view) for the directional-dependent linear compressibility $\beta$ [in $(\text{TPa})^{-1}$] of α-$ZnP_2$ at zero pressure under the PBE scheme.
[5x]Using the ELATE program [181, 182].

For linear compressibility $\beta$, no variation of $\beta$ with angle is observed in the *xy*-plane, as apparent from **Fig. 5.12**. In the *xz*-plane, as the angle (with the [100] direction) changes from 0° to 90°, linear compressibility decreases continuously from 5.16 $(\text{TPa})^{-1}$ to 4.74 $(\text{TPa})^{-1}$. Thus, in the case of linear compressibility, the *xz*-plane has anisotropy. For the *xz*-plane, the maximum percentage change in the value of linear compressibility with respect to its minimum value is about 8.9%. Moreover, it can be said that overall, more anisotropy is observed for Young's modulus in comparison to linear compressibility for α-$ZnP_2$.

Directional-dependent Poisson's ratio and shear modulus of α-$ZnP_2$ at zero pressure in polar form are shown from **Fig. 5.14** to **Fig. 5.17**. These polar graphs are plotted under the PBE scheme as per the convention used for the ELATE program [181, 182].

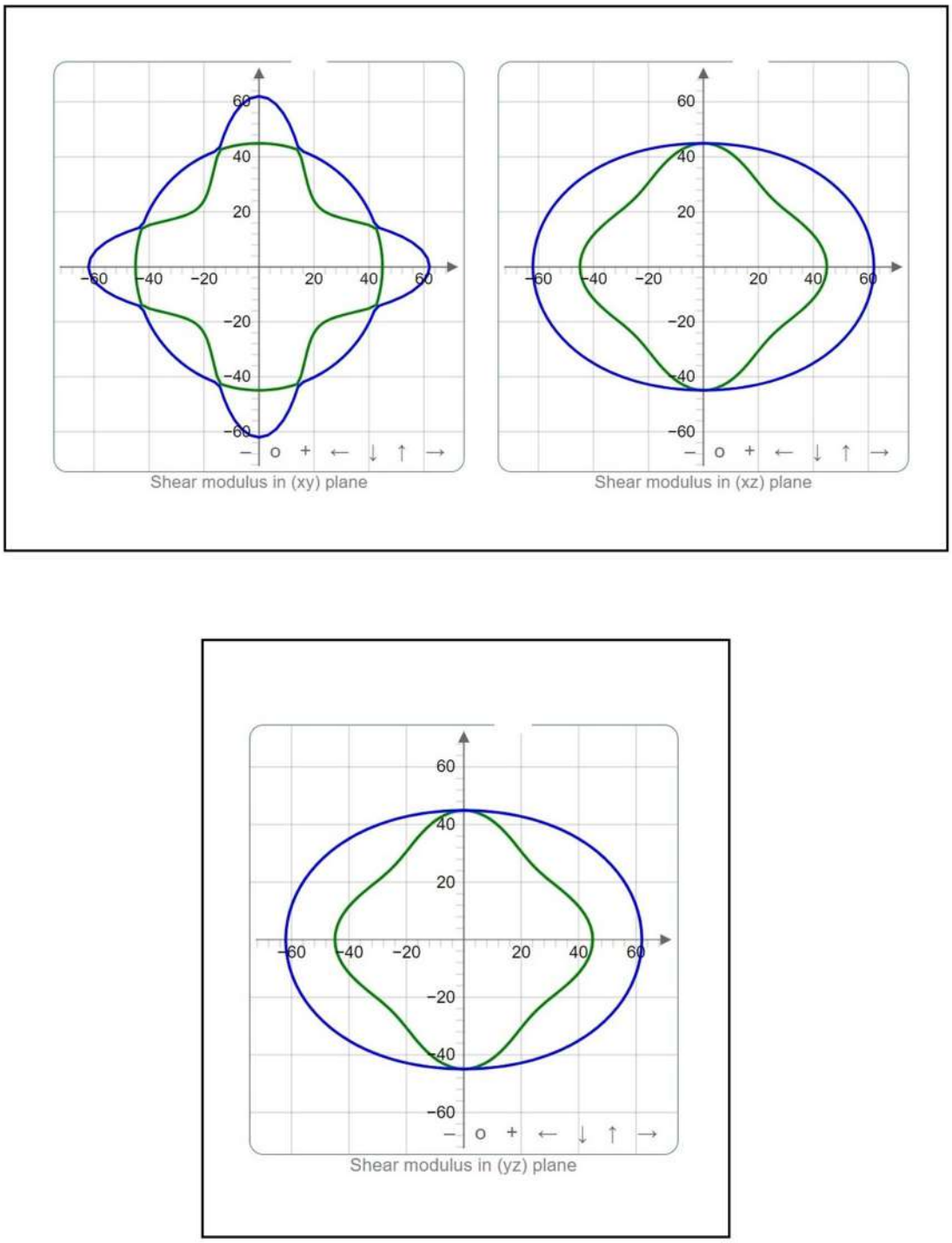


**Figure 5.14:** Polar graphs[5y] (2D view) for the directional-dependent shear modulus *G* (in GPa) of α-$ZnP_2$ at zero pressure under the PBE scheme.

[5y]Using the ELATE program [181, 182].

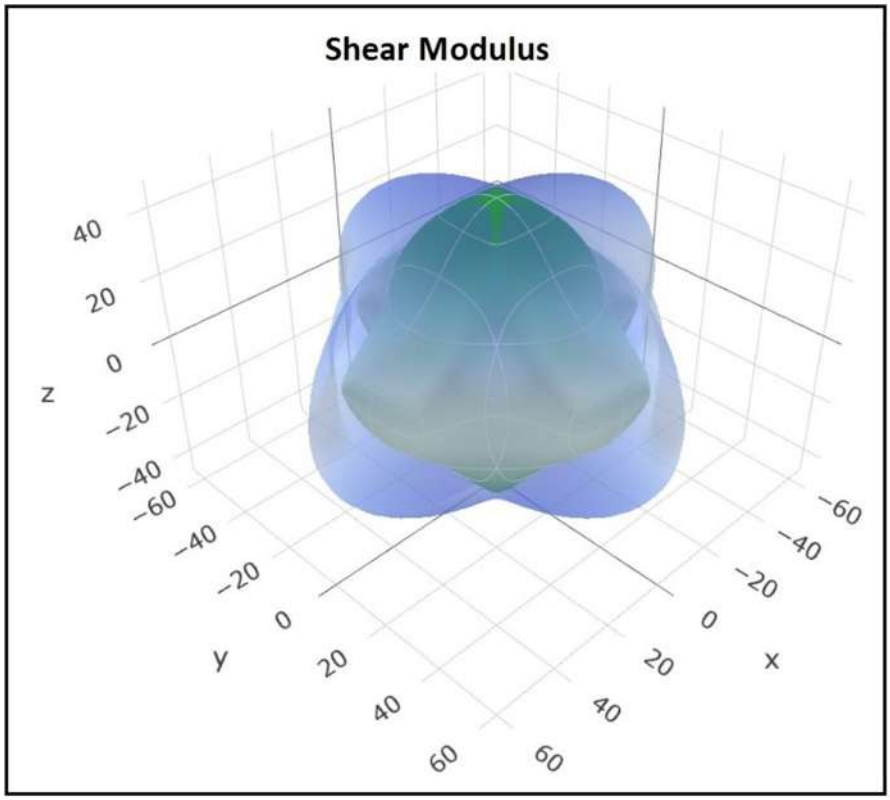


**Figure 5.15:** Polar graph[5z] (3D view) for the directional-dependent shear modulus *G* (in GPa) of α-$ZnP_2$ at zero pressure under the PBE scheme.

[5z]Using the ELATE program [181, 182].

.

As per the convention used in the ELATE program for the plots, the value of the directional shear modulus *G* does not vary with angular variation in the *xy*-plane. In the case of the *yz*-plane, shear modulus *G* varies from 44.92 GPa to 62.04 GPa ($G_{max}$ in **Table 5.12**). For the *yz*-plane, the maximum percentage change in the value of shear modulus *G* relative to its minimum value is 38.1%. For the physical quantities Young's modulus *E* and linear compressibility *β*, this study reveals that the *xy*-plane has a higher level of anisotropy for Young's modulus.

From **Table 5.13**, it is evident that the percentage variations in linear compressibility and Young's modulus are about 10% and 50%, respectively. The shear modulus *G* has around 100% variation relative to its minimum value. Here, anisotropy parameter $A_G$ has relatively higher values in comparison with the alpha phase of $CdP_2$. The variation in Poisson's ratio is more significant in the alpha phase of $ZnP_2$ than in the alpha phase of $CdP_2$.

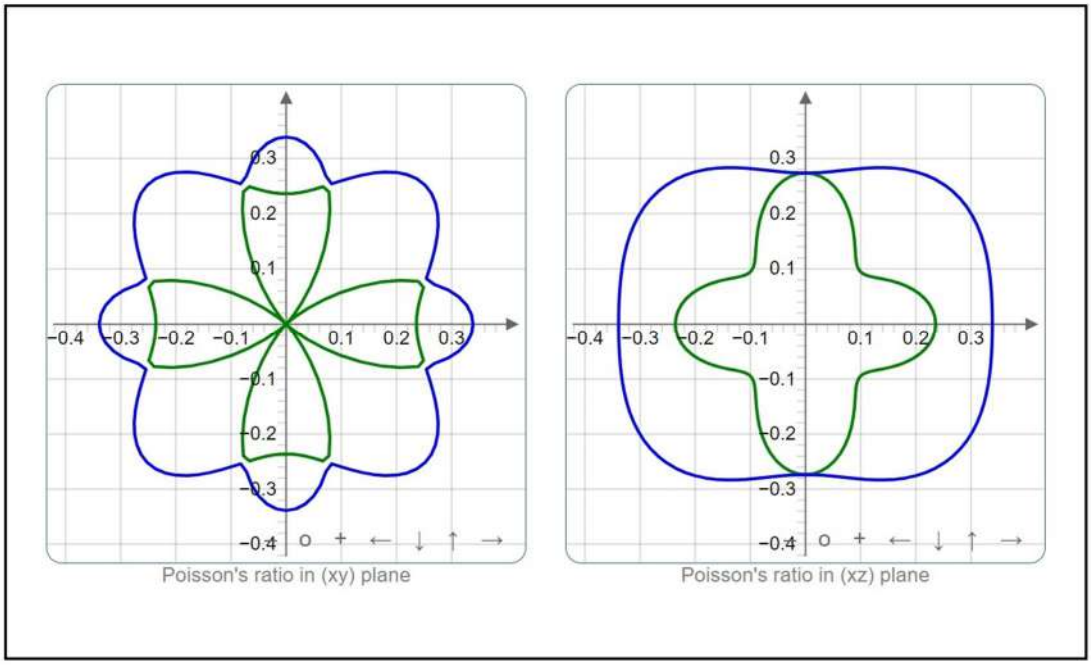


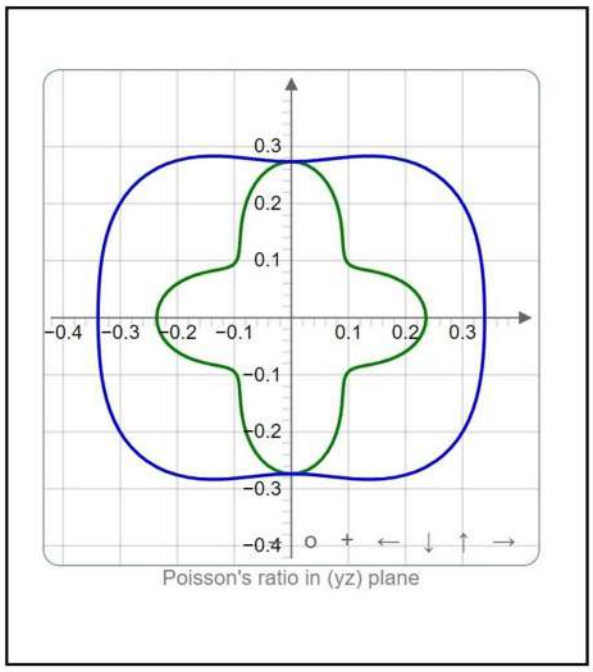


**Figure 5.16:** Polar graphs[5aa] (2D view) for the directional-dependent Poisson's ratio *v* (unitless) of α-$ZnP_2$ at zero pressure under the PBE scheme.

[5aa]Using the ELATE program [181, 182].

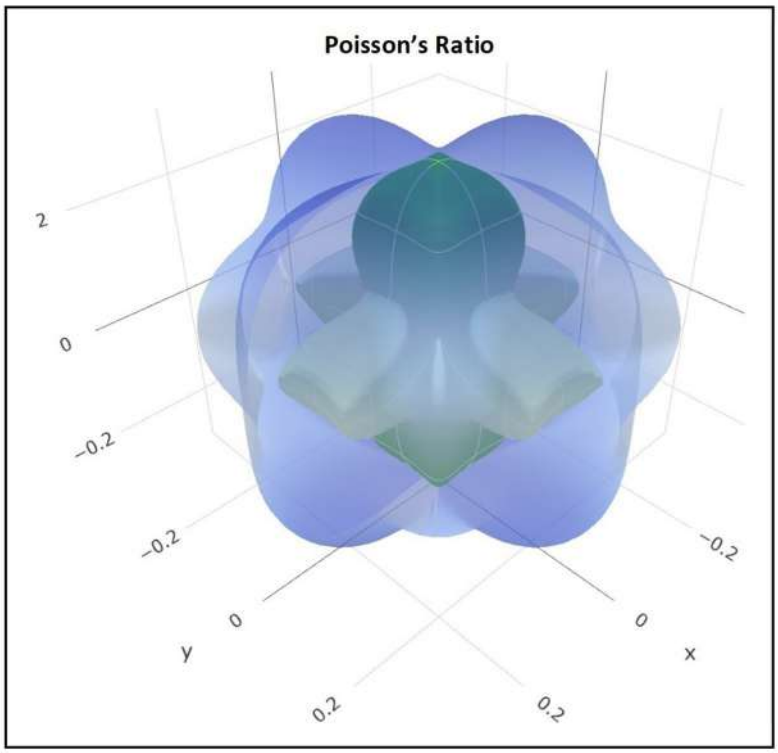


**Figure 5.17:** Polar graph[5bb] (3D view) for the directional-dependent Poisson's ratio $v$ (unitless) of α-$ZnP_2$ at zero pressure under the PBE scheme.

[5bb]Using the ELATE program [181, 182].

**Table 5.13:** Elastic anisotropy parameters: ratio of maximum to minimum values of Young's modulus $E$, linear compressibility $\beta$, shear modulus $G$ and Poisson's ratio $v$ for α-$ZnP_2$. Elastic anisotropy parameters $A_G$ and $A^U$ for α-$ZnP_2$

| Scheme | Anisotropy | | | | | |
|---|---|---|---|---|---|---|
| | $\frac{E_{max}}{E_{min}}$ | $\frac{\beta_{max}}{\beta_{min}}$ | $\frac{G_{max}}{G_{min}}$ | $\frac{v_{max}}{v_{min}}$ | $A_G$ | $A^U$ |
| PBEsol | 1.57 | 1.10 | 2.14 | 706.14 | 0.032 | 0.333 |
| PBE | 1.51 | 1.09 | 2.02 | 162.80 | 0.027 | 0.279 |
| PWGGA | 1.51 | 1.09 | 2.01 | 213.01 | 0.027 | 0.278 |
| LDA PZ | 1.59 | 1.08 | 2.18 | 2379.97 | 0.034 | 0.353 |
| LDA VWN | 1.59 | 1.08 | 2.18 | 4168.02 | 0.034 | 0.352 |
| B3LYP | 1.43 | 1.08 | 1.85 | 33.07 | 0.017 | 0.157 |
| B3PW | 1.48 | 1.09 | 1.95 | 32.71 | 0.024 | 0.249 |
| PBE0 | 1.49 | 1.11 | 1.98 | 29.33 | 0.025 | 0.261 |
| HSE06 | 1.50 | 1.10 | 1.98 | 28.54 | 0.026 | 0.262 |

## 5.3.3 Elastic Properties of $ZnAs_2$

### 5.3.3.1 Elastic Constants

The monoclinic crystal has 13 independent elastic stiffness constants [16], namely $C_{11}$, $C_{12}$, $C_{13}$, $C_{15}$, $C_{22}$, $C_{23}$, $C_{25}$, $C_{33}$, $C_{35}$, $C_{44}$, $C_{46}$, $C_{55}$ and $C_{66}$ for standard orientation. The elastic properties are studied for $ZnAs_2$, which has a monoclinic unit cell. The computations of elastic stiffness constants under various functional schemes are shown in **Table 5.14**. It is quite apparent from **Table 5.14** that the elastic stiffness constants $C_{11}$, $C_{22}$ and $C_{33}$ are significantly greater than the other elastic stiffness constants, such as $C_{12}$, $C_{13}$, $C_{15}$, $C_{23}$, $C_{25}$, $C_{35}$, $C_{44}$, $C_{46}$, $C_{55}$ and $C_{66}$.

**Table 5.14:** Elastic constants $C_{ij}$ (in GPa) of $ZnAs_2$ at zero pressure

| Scheme | $C_{11}$ | $C_{12}$ | $C_{13}$ | $C_{15}$ | $C_{22}$ | $C_{23}$ | $C_{25}$ | $C_{33}$ | $C_{35}$ | $C_{44}$ | $C_{46}$ | $C_{55}$ | $C_{66}$ |
|---|---|---|---|---|---|---|---|---|---|---|---|---|---|
| PBEsol[5cc] | 126.72 | 63.47 | 59.95 | –4.41 | 136.81 | 38.35 | 6.07 | 145.84 | 1.75 | 26.73 | 4.23 | 44.58 | 44.18 |
| PBE | 117.83 | 56.74 | 53.64 | –4.90 | 126.51 | 32.57 | 5.71 | 136.43 | 1.71 | 25.50 | 3.92 | 42.95 | 41.65 |
| PWGGA | 117.87 | 56.70 | 53.71 | –4.55 | 126.63 | 33.52 | 5.53 | 135.11 | 1.64 | 25.61 | 3.92 | 42.20 | 42.37 |
| LDA PZ | 136.26 | 70.03 | 66.34 | –3.61 | 146.28 | 43.81 | 6.91 | 156.69 | 2.11 | 27.72 | 4.87 | 45.98 | 47.66 |
| LDA VWN | 134.95 | 68.87 | 65.20 | –3.63 | 146.97 | 42.65 | 6.94 | 156.59 | 2.30 | 27.89 | 4.65 | 46.66 | 46.87 |
| B3LYP | 119.12 | 53.06 | 50.94 | –5.22 | 126.78 | 29.48 | 5.48 | 138.05 | 1.51 | 27.30 | 3.92 | 44.91 | 43.75 |
| B3PW | 123.83 | 56.94 | 53.76 | –5.06 | 131.85 | 32.60 | 5.62 | 142.25 | 1.73 | 28.15 | 4.04 | 45.77 | 45.29 |
| PBE0 | 127.56 | 59.81 | 56.46 | –4.98 | 135.93 | 34.90 | 5.88 | 146.12 | 1.82 | 28.33 | 4.13 | 46.55 | 45.95 |
| Other Work[5dd] | 95.63 | 31.47 | | | 102.5 | | | 112.7 | | 20.76 | | | 40.45 |

[5cc]Ref. [237].

[5dd]Ref. [67, 238].

**Table 5.15:** Elastic compliance constants $S_{ij}$ [in $(\text{TPa})^{-1}$] of $ZnAs_2$ at zero pressure

| Scheme | $S_{11}$ | $S_{12}$ | $S_{13}$ | $S_{15}$ | $S_{22}$ | $S_{23}$ | $S_{25}$ | $S_{33}$ | $S_{35}$ | $S_{44}$ | $S_{46}$ | $S_{55}$ | $S_{66}$ |
|---|---|---|---|---|---|---|---|---|---|---|---|---|---|
| PBEsol[5ee] | 12.06 | –4.63 | –3.76 | 1.97 | 9.71 | –0.63 | –1.75 | 8.58 | –0.62 | 37.98 | –3.64 | 22.89 | 22.98 |
| PBE | 12.63 | –4.78 | –3.86 | 2.23 | 10.27 | –0.55 | –1.89 | 8.99 | –0.73 | 39.80 | –3.74 | 23.82 | 24.36 |
| PWGGA | 12.59 | –4.71 | –3.86 | 2.13 | 10.26 | –0.65 | –1.83 | 9.11 | –0.68 | 39.60 | –3.66 | 24.19 | 23.94 |
| LDA PZ | 11.45 | –4.48 | –3.62 | 1.74 | 9.26 | –0.67 | –1.71 | 8.11 | –0.56 | 36.73 | –3.75 | 22.17 | 21.36 |
| LDA VWN | 11.44 | –4.40 | –3.59 | 1.72 | 9.13 | –0.63 | –1.67 | 8.06 | –0.58 | 36.45 | –3.61 | 21.84 | 21.69 |
| B3LYP | 11.87 | –4.24 | –3.50 | 2.02 | 9.86 | –0.52 | –1.68 | 8.65 | –0.63 | 37.11 | –3.32 | 22.73 | 23.15 |
| B3PW | 11.59 | –4.24 | –3.43 | 1.93 | 9.63 | –0.59 | –1.63 | 8.47 | –0.63 | 35.99 | –3.21 | 22.29 | 22.37 |
| PBE0 | 11.41 | –4.22 | –3.42 | 1.89 | 9.44 | –0.60 | –1.62 | 8.32 | –0.62 | 35.76 | –3.21 | 21.91 | 22.05 |

[5ee]Using Ref. [237].

**Table 5.15** illustrates the elastic compliance constants under various functional schemes. It is evident that values of $S_{12}$, $S_{13}$, $S_{23}$, $S_{25}$, $S_{35}$ and $S_{46}$ are negative**.**

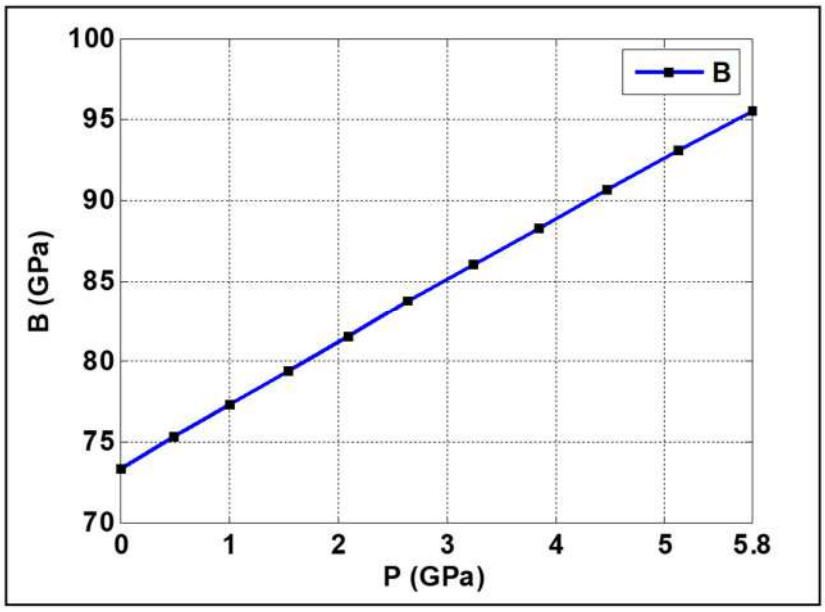


**Figure 5.18:** Computed bulk modulus $B$ of $ZnAs_2$ as a function of applied pressure $P$ under the PBE functional.

The computed bulk modulus $B$ of monoclinic $ZnAs_2$ increases with applied pressure $P$. To our best knowledge, there is no other experimentally or theoretically

reported data on elastic stiffness constants for monoclinic $ZnAs_2$ at higher pressures for comparison with our work. It is obvious from **Fig. 5.18** that bulk modulus shows a significant variation with pressure.

**Table 5.16:** Computed values of Young's modulus $E$ (in GPa), bulk modulus $B$ (in GPa) and shear modulus $G$ (in GPa) of $ZnAs_2$ at zero pressure

| Scheme | $B_V$ | $B_R$ | $B_H$ | $G_V$ | $G_R$ | $G_H$ | $E_V$ | $E_R$ | $E_H$ |
|---|---|---|---|---|---|---|---|---|---|
| PBEsol[5ff] | 81.44 | 81.28 | 81.36 | 39.60 | 36.67 | 38.14 | 102.24 | 95.63 | 98.95 |
| PBE | 74.08 | 73.91 | 73.99 | 37.87 | 35.03 | 36.45 | 97.08 | 90.75 | 93.93 |
| PWGGA | 74.16 | 74.01 | 74.09 | 37.75 | 35.06 | 36.40 | 96.82 | 90.83 | 93.84 |
| LDA PZ | 88.84 | 88.62 | 88.73 | 41.54 | 38.35 | 39.95 | 107.82 | 100.54 | 104.20 |
| LDA VWN | 87.99 | 87.81 | 87.90 | 41.74 | 38.57 | 40.15 | 108.12 | 100.93 | 104.54 |
| B3LYP | 72.32 | 72.15 | 72.24 | 39.89 | 37.17 | 38.53 | 101.08 | 95.17 | 98.14 |
| B3PW | 76.06 | 75.89 | 75.97 | 40.82 | 38.10 | 39.46 | 103.87 | 97.91 | 100.91 |
| PBE0 | 79.11 | 78.93 | 79.02 | 41.40 | 38.58 | 39.99 | 105.74 | 99.518 | 102.64 |

[5ff]Ref. [237].

The computed elastic moduli of monoclinic $ZnAs_2$ under various functional schemes are reported in **Table 5.16**. Young's modulus ($E_V$, $E_R$ and $E_H$), bulk modulus ($B_V$, $B_R$ and $B_H$), and shear modulus ($G_V$, $G_R$ and $G_H$) of $ZnAs_2$ are reported in **Table 5.16**. Using the obtained elastic constants, these elastic quantities are calculated by means of the ELATE program [181, 182].

Poisson's ratio $v$ (unitless) of monoclinic $ZnAs_2$ at zero pressure is reported in **Table 5.17**. These values of Poisson's ratio ($v_V$, $v_R$ and $v_H$) of $ZnAs_2$ at zero pressure are computed by means of the ELATE program [181, 182] using the obtained elastic constants. It is noteworthy to examine the ratio $B/G$ for $ZnAs_2$. The ratio $B/G$ for the $ZnAs_2$ crystals has a value of about 2. It indicates the malleable nature of polycrystalline $ZnAs_2$. From **Table 5.17**, it is also obvious that the computed values of Poisson's ratio lie in the theoretically predicted range [137] for materials.

**Table 5.17:** Computed values of Poisson's ratio $v$ (unitless) of $ZnAs_2$ at zero pressure

| Scheme | $v_V$ | $v_R$ | $v_H$ |
|---|---|---|---|
| PBEsol[5gg] | 0.291 | 0.304 | 0.297 |
| PBE | 0.282 | 0.295 | 0.288 |
| PWGGA | 0.282 | 0.295 | 0.289 |
| LDA PZ | 0.298 | 0.311 | 0.304 |
| LDA VWN | 0.295 | 0.308 | 0.302 |
| B3LYP | 0.267 | 0.280 | 0.274 |
| B3PW | 0.272 | 0.285 | 0.279 |
| PBE0 | 0.277 | 0.290 | 0.284 |

[5gg]Ref. [237].

### 5.3.3.2 Elastic Anisotropy

To study the anisotropy of monoclinic $ZnAs_2$ at zero pressure, directional Young's modulus, shear modulus and linear compressibility have been investigated and their polar graphs have been plotted in different crystallographic planes.

The minimum and maximum values of the linear compressibility ($\beta_{min}$ and $\beta_{max}$), Poisson's ratio ($v_{min}$ and $v_{max}$), shear modulus ($G_{min}$ and $G_{max}$) and Young's modulus ($E_{min}$ and $E_{max}$) of monoclinic $ZnAs_2$ are shown in **Table 5.18**. These elastic quantities are calculated by means of the ELATE program [181, 182] using the computed values for the $ZnAs_2$ crystal.

**Table 5.19** illustrates that the percentage variations in the linear compressibility and Young's modulus are about 25% and 70%, respectively. The shear modulus $G$ has around 100% variation relative to its minimum value. It is obvious from **Table 5.19** that the anisotropy parameter $A^U$ of monoclinic $ZnAs_2$ have relatively higher values in comparison with alpha phase $CdP_2$. **Table 5.19** shows that the variation in Poisson's ratio is more significant in the monoclinic $ZnAs_2$ crystal than in the alpha phase of $CdP_2$.

**Table 5.18:** Minimum and maximum values of linear compressibility $\beta$ [in $(\mathrm{TPa})^{-1}$], Poisson's ratio $v$ (unitless), shear modulus $G$ (in GPa) and Young's modulus $E$ (in GPa) of $ZnAs_2$

| Scheme | $G_{min}$ | $G_{max}$ | $E_{min}$ | $E_{max}$ | $\beta_{min}$ | $\beta_{max}$ | $v_{min}$ | $v_{max}$ |
|---|---|---|---|---|---|---|---|---|
| PBEsol[5hh] | 25.76 | 51.76 | 70.92 | 121.47 | 3.60 | 4.45 | 0.051 | 0.491 |
| PBE | 24.60 | 49.67 | 67.29 | 116.32 | 3.95 | 4.95 | 0.038 | 0.481 |
| PWGGA | 24.74 | 48.93 | 67.70 | 114.39 | 3.96 | 4.90 | 0.049 | 0.479 |
| LDA PZ | 26.60 | 54.13 | 73.82 | 127.71 | 3.23 | 4.11 | 0.059 | 0.510 |
| LDA VWN | 26.82 | 54.84 | 74.41 | 129.00 | 3.31 | 4.10 | 0.055 | 0.504 |
| B3LYP | 26.41 | 51.70 | 71.56 | 120.17 | 4.09 | 5.09 | 0.039 | 0.454 |
| B3PW | 27.25 | 52.43 | 73.82 | 122.84 | 3.88 | 4.80 | 0.048 | 0.458 |
| PBE0 | 27.42 | 53.29 | 74.66 | 125.17 | 3.71 | 4.61 | 0.051 | 0.468 |

[5hh]Ref. [237].

**Table 5.19:** Elastic anisotropy parameters: ratio of maximum to minimum values of Young's modulus $E$, linear compressibility $\beta$, shear modulus $G$ and Poisson's ratio $v$ for $ZnAs_2$. Elastic anisotropy parameters $A_G$ and $A^U$ for $ZnAs_2$

| Scheme | Anisotropy | | | | | |
|---|---|---|---|---|---|---|
| | $\frac{E_{max}}{E_{min}}$ | $\frac{\beta_{max}}{\beta_{min}}$ | $\frac{G_{max}}{G_{min}}$ | $\frac{v_{max}}{v_{min}}$ | $A_G$ | $A^U$ |
| PBEsol[5ii] | 1.71 | 1.24 | 2.01 | 9.59 | 0.019 | 0.402 |
| PBE | 1.73 | 1.25 | 2.02 | 12.59 | 0.020 | 0.408 |
| PWGGA | 1.69 | 1.24 | 1.98 | 9.77 | 0.037 | 0.386 |
| LDA PZ | 1.73 | 1.27 | 2.04 | 8.65 | 0.040 | 0.419 |
| LDA VWN | 1.73 | 1.24 | 2.05 | 9.12 | 0.040 | 0.413 |
| B3LYP | 1.68 | 1.25 | 1.96 | 11.72 | 0.035 | 0.368 |
| B3PW | 1.66 | 1.24 | 1.92 | 9.60 | 0.034 | 0.359 |
| PBE0 | 1.68 | 1.24 | 1.94 | 9.20 | 0.035 | 0.368 |

[5ii]Using Ref. [237].

The obtained value of the elastic anisotropy index $A^U$ is nearly 0.41 at zero pressure under the PBE method. The theoretically predicted maximum and minimum values of directional elastic quantities have a correlation with elastic anisotropy. **Table 5.18** illustrates that $G$, $E$ and $\beta$ have significant differences between their

respective maximum and minimum values. Hence, it is inferred that bulk anisotropy, as well as shear anisotropy, are exhibited by monoclinic $ZnAs_2$. Ranganathan's universal elastic anisotropy index $A^U$ has a higher value for monoclinic $ZnAs_2$ in comparison with α-$CdP_2$ and α-$ZnP_2$.

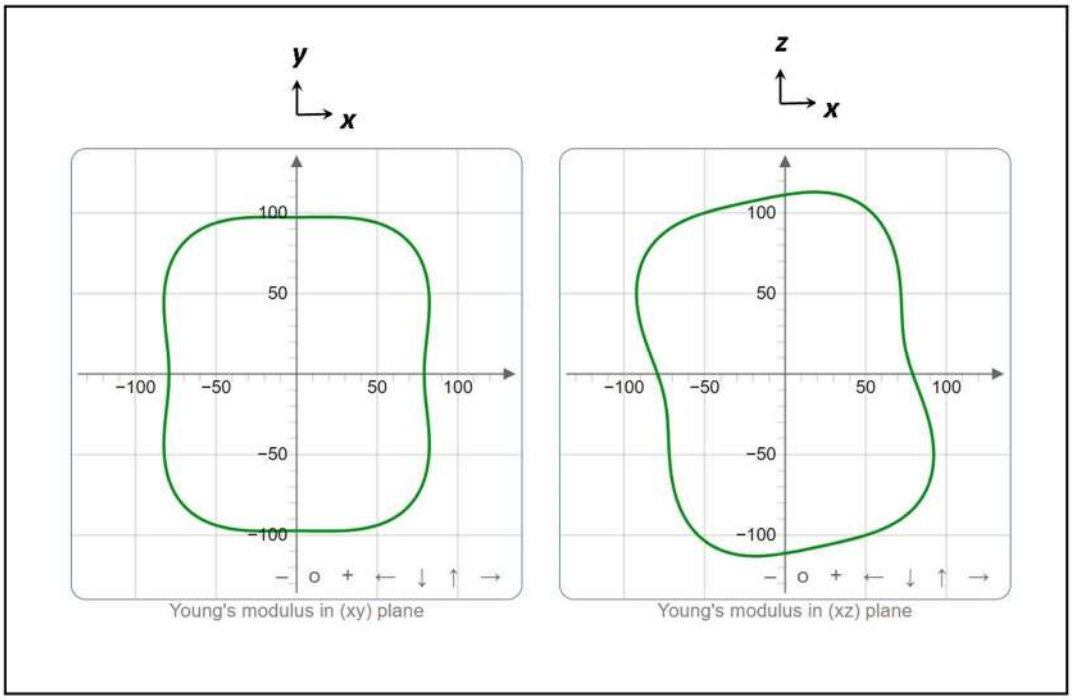


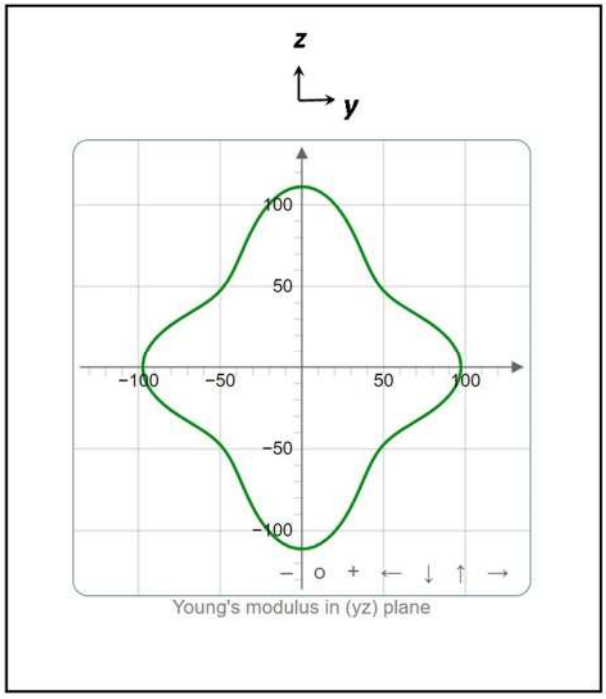


**Figure 5.19:** Polar graphs[5jj] (2D view) for the directional-dependent Young's modulus $E$ (in GPa) of $ZnAs_2$ at zero pressure under the PBE scheme.

[5jj]Using the ELATE program [181, 182].

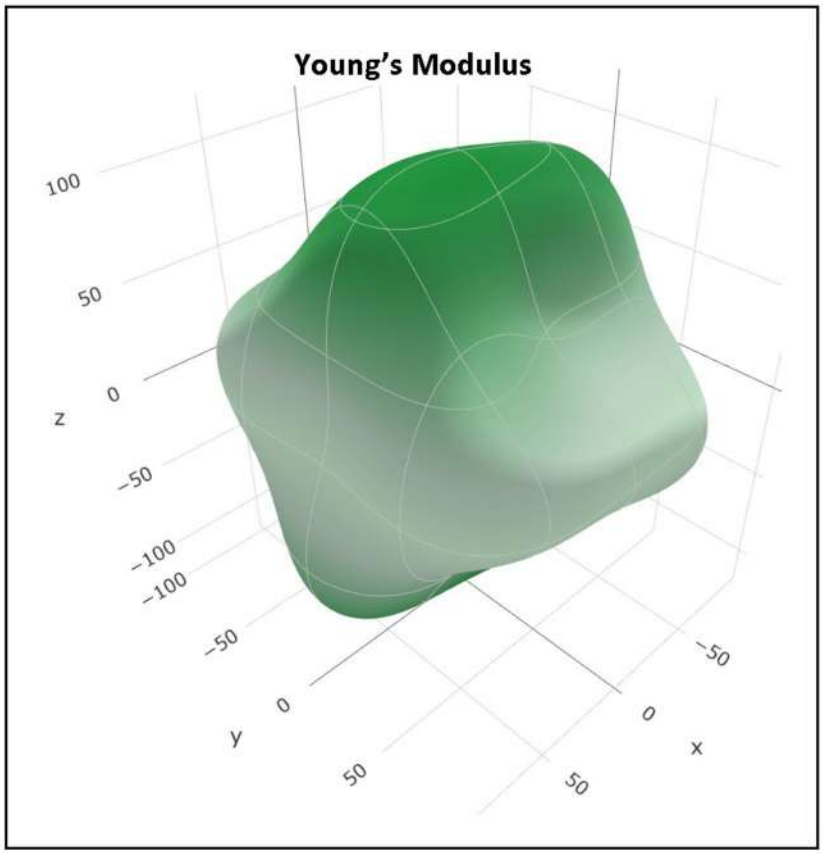


**Figure 5.20:** Polar graph[5kk] (3D view) for the directional-dependent Young's modulus *E* (in GPa) of $ZnAs_2$ at zero pressure under the PBE scheme.

[5kk]Using the ELATE program [181, 182].

The plots of the directional Young's modulus, shear modulus and linear compressibility could provide valuable insights about the elastic anisotropy of the crystals. It is apparent from **Fig. 5.19** to **Fig. 5.22** that the polar plots of the directional Young's modulus and linear compressibility are not in a circular shape. Therefore, the presence of finite elastic anisotropy is inferred for monoclinic $ZnAs_2$. In the *xy*-plane, Young's modulus *E* first increases and then decreases continuously as the angle (with the *x*-direction) increases from 0° to 90°.

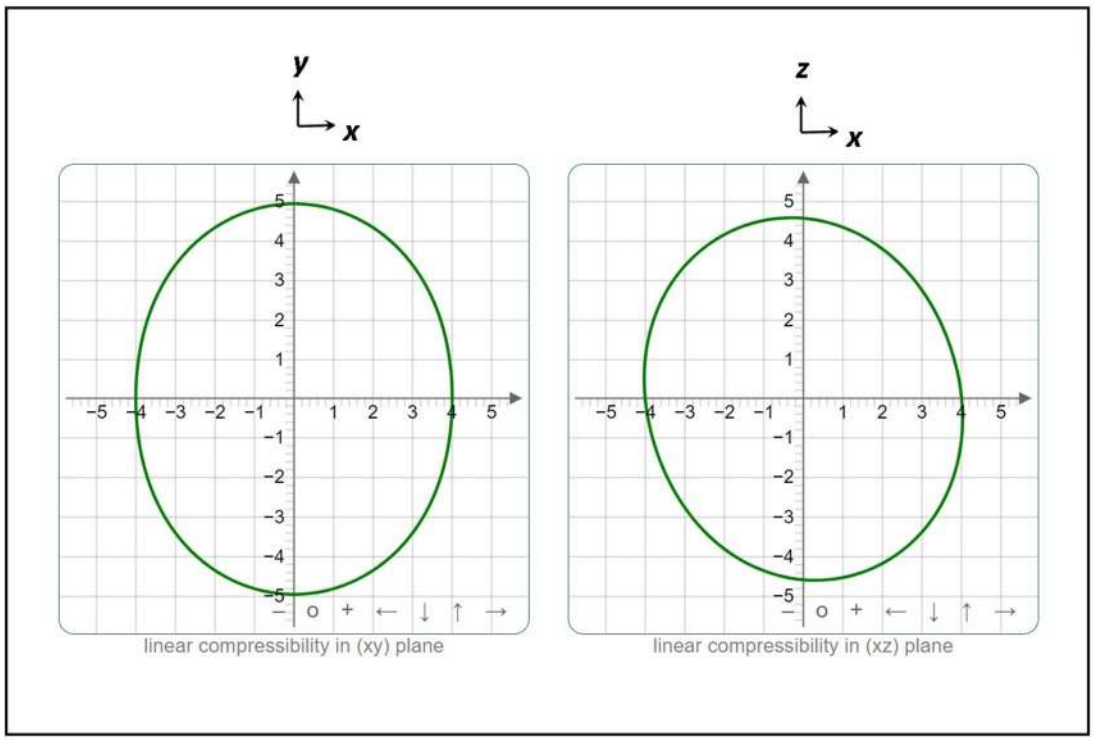


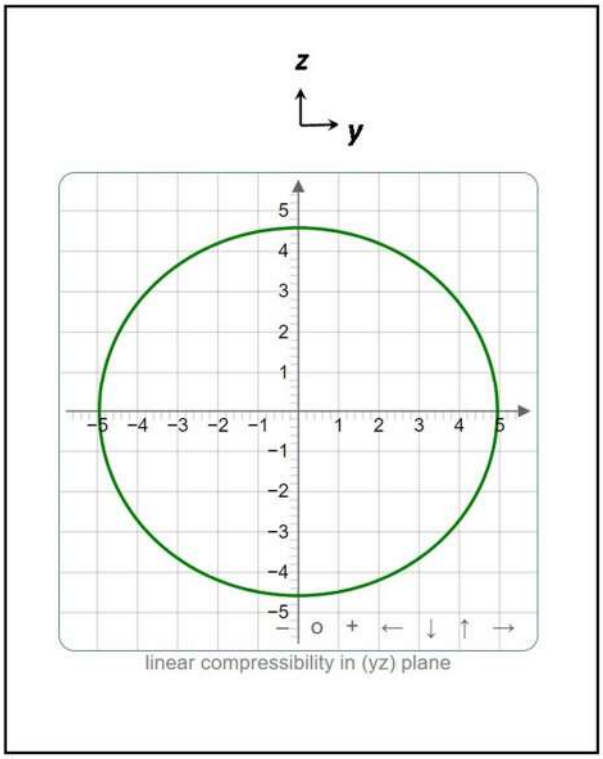


**Figure 5.21:** Polar graphs[5ll] (2D view) for the directional-dependent linear compressibility $\beta$ [in $(\mathrm{TPa})^{-1}$] of $ZnAs_2$ at zero pressure under the PBE scheme.

[5ll]Using the ELATE program [181, 182].

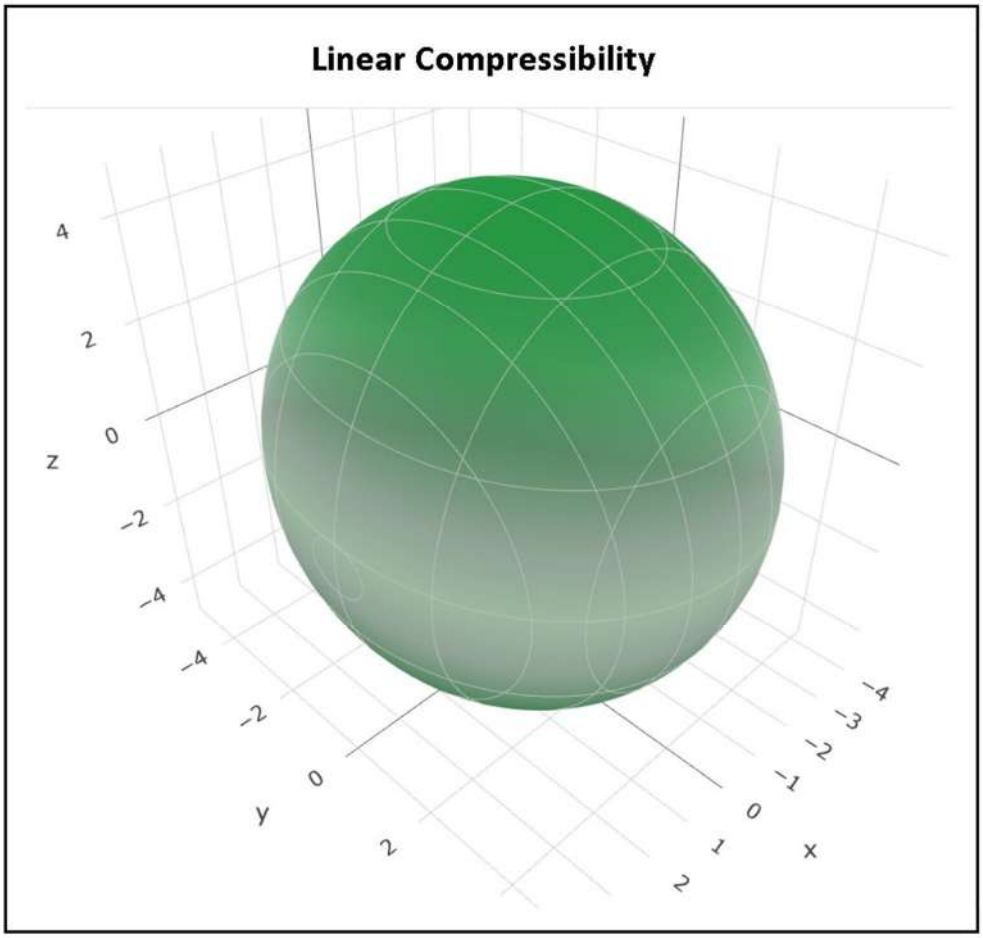


**Figure 5.22:** Polar graph[5mm] (3D view) for the directional-dependent linear compressibility $\beta$ [in $(\mathrm{TPa})^{-1}$] of $ZnAs_2$ at zero pressure under the PBE scheme.
[5mm]Using the ELATE program [181, 182].

The polar graphs of Young's modulus and linear compressibility for $ZnAs_2$ were plotted with the PBEsol scheme in other work [237]. The directional-dependent Poisson's ratio and shear modulus of monoclinic $ZnAs_2$ at zero pressure under the PBE scheme in polar form are depicted in **Fig. 5.23** to **Fig. 5.26**. These polar graphs have been plotted as per the convention used for the ELATE program [181, 182].

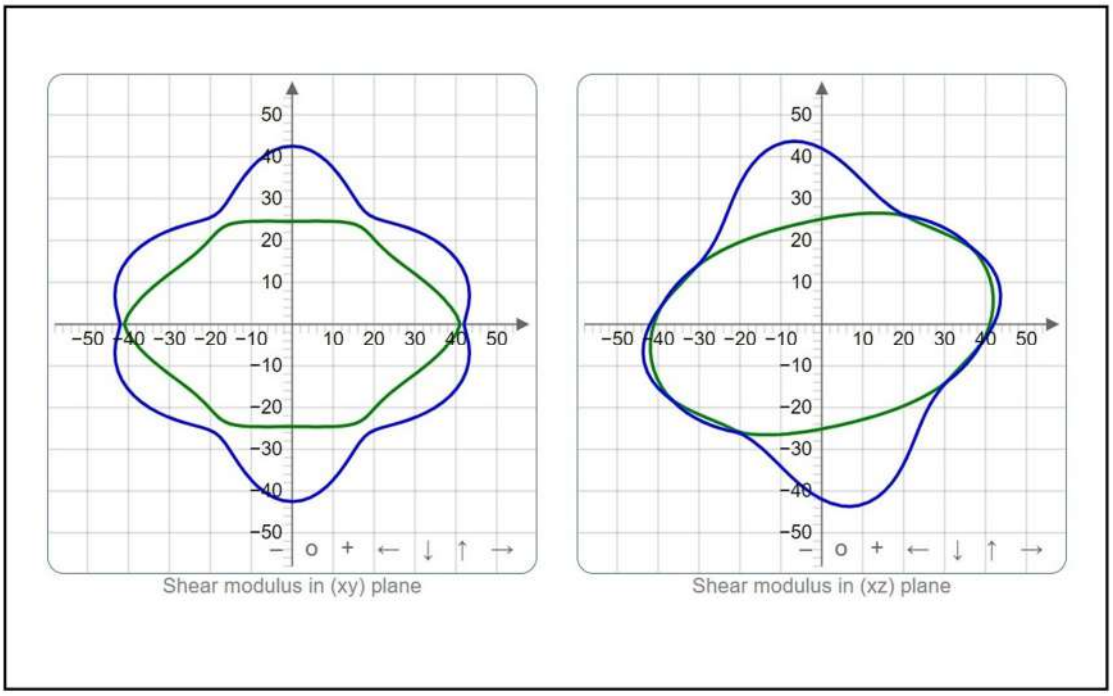


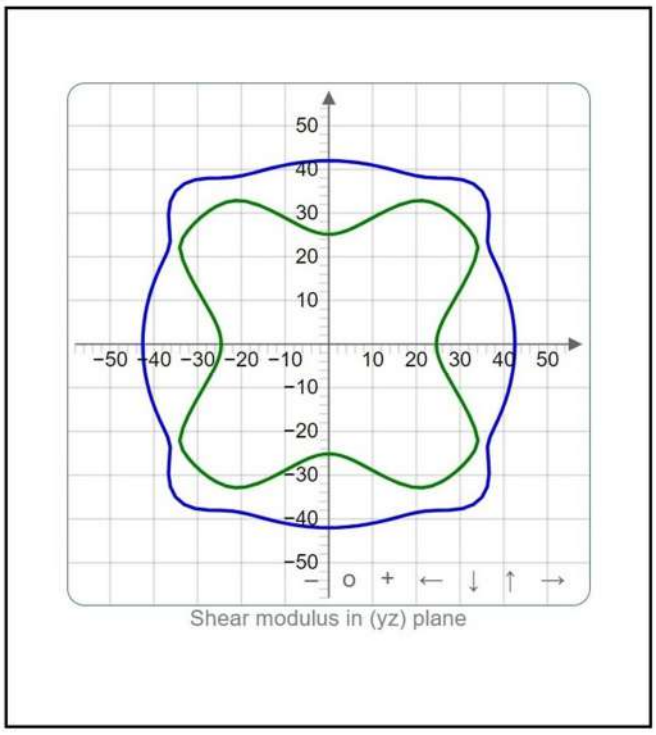


**Figure 5.23:** Polar graphs[5nn] (2D view) for the directional-dependent shear modulus *G* (in GPa) of $ZnAs_2$ at zero pressure under the PBE scheme.

[5nn]Using the ELATE program [181, 182].

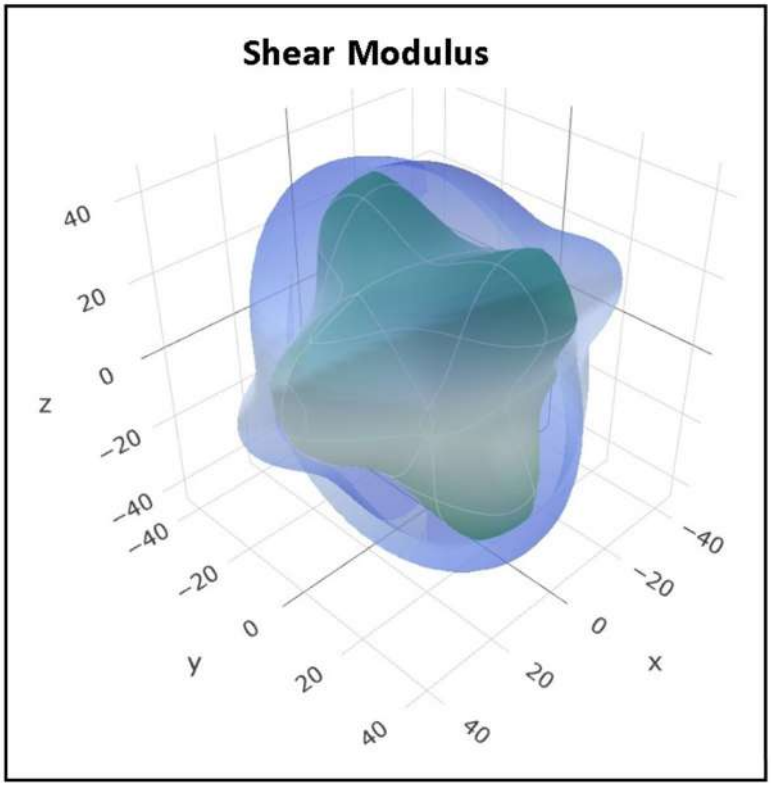


**Figure 5.24:** Polar graph[5oo] (3D view) for the directional-dependent shear modulus *G* (in GPa) of $ZnAs_2$ at zero pressure under the PBE scheme.

[5oo]Using the ELATE program [181, 182].

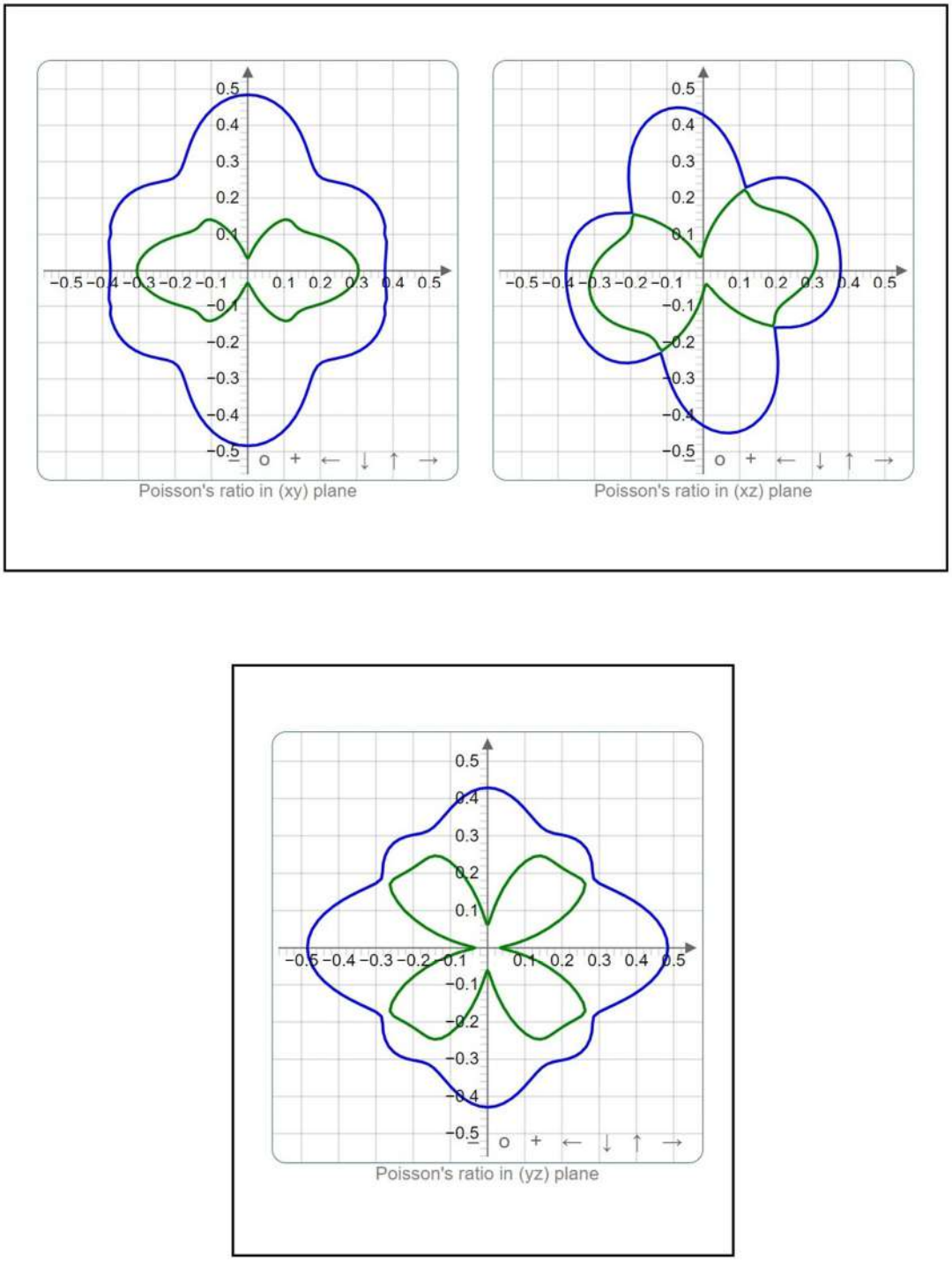


**Figure 5.25:** Polar graphs[5pp] (2D view) for the directional-dependent Poisson's ratio *v* (unitless) of $ZnAs_2$ at zero pressure under the PBE scheme.

[5pp]Using the ELATE program [181, 182].

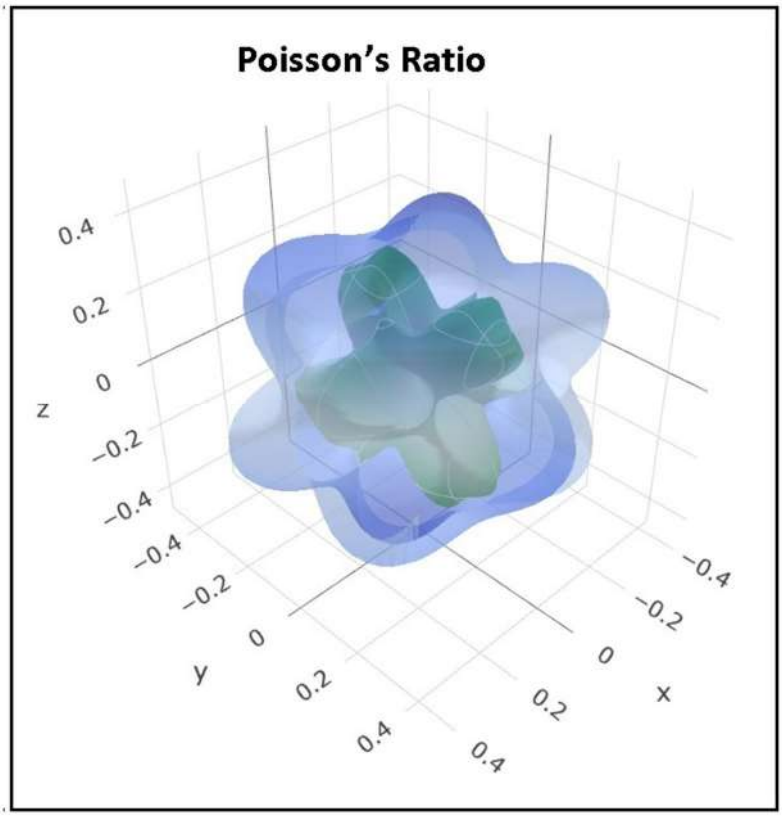


**Figure 5.26:** Polar graph[5qq] (3D view) for the directional-dependent Poisson's ratio *v* (unitless) of $ZnAs_2$ at zero pressure under the PBE scheme.
[5qq]Using the ELATE program [181, 182].

## 5.4 Conclusions

The projections (polar graphs) of Young's modulus on the different *xy*-, *xz*- and *yz*-planes provide insight into the variation in Young's modulus. Our study reveals the malleable nature of α-$CdP_2$ at zero pressure. The directional Young's modulus of α-$CdP_2$ varies from 48.89 GPa to 71.53 GPa under the PBE method. The directional shear modulus of α-$CdP_2$ varies from 19.26 GPa to 32.74 GPa under the PBE method. For α-$ZnP_2$, the values of the elastic constants $C_{11}$ and $C_{33}$ are substantially greater in comparison to the other elastic stiffness constants, such as $C_{12}$, $C_{13}$, $C_{44}$ and $C_{66}$. The calculated values of the Young's modulus and bulk modulus for polycrystalline α-$ZnP_2$ are 105.70 GPa and 66.43 GPa, respectively, under the PBE method. The value of Young's modulus is indicative of the stiffness of the substance. Therefore, it

may be concluded that the α-$ZnP_2$ crystal has enough stiffness. Our present findings show that α-$CdP_2$, α-$ZnP_2$ and monoclinic $ZnAs_2$ crystal systems have definite elastic anisotropies. The calculated value of the elastic anisotropy index $A^U$ is 0.279 at zero pressure in the case of α-$ZnP_2$ under the PBE scheme. For α-$ZnP_2$, the angular variation of Young's modulus $E$ is similar in the *xz*-plane and in the *yz*-plane. For α-$ZnP_2$, the *yz*-plane has higher elastic anisotropy in comparison with the *xy*-plane for linear compressibility. In the case of Young's modulus of α-$ZnP_2$, the *xy*-plane has greater anisotropy than the *yz*-plane. Substantial differences are present among the calculated values of the directional Young's moduli $E_{[100]}$, $E_{[001]}$ and $E_{[110]}$ for α-$ZnP_2$. In general, our calculated elastic moduli of α-$ZnP_2$ are in reasonably fair agreement with the existing available experimental data. Our investigation also shows that the *yz*-plane has remarkable anisotropy for the shear modulus of α-$ZnP_2$. This comprehensive computational study of the anisotropic properties of the alpha phase of $ZnP_2$ may bestow a prophecy about the favored orientation of the α-$ZnP_2$ crystal for devising optoelectronic instruments. Our computational outcome on the elastic properties of α-$ZnP_2$ might provide a guiding point for experimentalists.

The elastic anisotropy index $A^U$ has a higher value for monoclinic $ZnAs_2$ in comparison with α-$CdP_2$ and α-$ZnP_2$. Our investigation illustrates that the percentage variation in Poisson's ratio is higher in monoclinic $ZnAs_2$ than in α-$CdP_2$. The polycrystalline bulk modulus $B_H$ has a higher value for monoclinic $ZnAs_2$ in comparison with α-$CdP_2$ and α-$ZnP_2$. The value of polycrystalline Young's modulus $E_H$ is relatively high for α-$ZnP_2$ in comparison with α-$CdP_2$ and monoclinic $ZnAs_2$. The polycrystalline shear modulus $G_H$ has a higher value for α-$ZnP_2$ in comparison with α-$CdP_2$ and monoclinic $ZnAs_2$. The polar graphs in the *xz*-plane for the directional-dependent linear compressibility $\beta$ show that α-$CdP_2$ has more anisotropy than α-$ZnP_2$.

# CHAPTER 6

# CONCLUSIONS AND FUTURE SCOPE

## 6.1 Conclusions

The present investigation illustrates the structures of the orthorhombic $CdP_2$, tetragonal $ZnP_2$ and monoclinic $ZnAs_2$ crystals. Our work shows that the atomic pair P-P has the nearest distance of about 2.19 Å and the atomic pair Cd-P has the nearest distance of about 2.61 Å in the alpha phase of $CdP_2$ under PBE scheme. The values of the isothermal bulk modulus $B_0$ of α-$CdP_2$ are calculated with EOS (Birch-Murnaghan, Vinet and Poirier-Tarantola) and these values lie in the range 51.94–64.57 GPa. At zero pressure, the first pressure derivative of bulk modulus of the orthorhombic α-$CdP_2$ crystal is in the range 3.93–4.17. The computed first pressure derivative $B_0'$ of α-$ZnP_2$ is about 4.5. The bulk modulus $B_0$ for the alpha phase of $ZnP_2$ is about 64–83 GPa. In the alpha phase of $ZnP_2$, the nearest P-P atomic pair distance is about 2.17 Å and the nearest Zn-P atomic pair distance is about 2.3 Å under LDA scheme. The computed nearest neighbor distance between the P-P atomic pair in the alpha phase of $CdP_2$ is not much different from the nearest neighbor distance between the P-P atomic pair in the alpha phase of $ZnP_2$. At zero pressure, the obtained value of the calculated angle $\beta$ for $ZnAs_2$ is around 102.46.° The nearest atomic pair Zn-As distance is around 2.41 Å and the nearest atomic pair As-As distance is around 2.46 Å in the $ZnAs_2$ crystal under PBE scheme. The estimated value of the first pressure derivative of the monoclinic $ZnAs_2$ crystal lies in the approximate range of 2.61 to 4.20. The computed value of bulk modulus for the $ZnAs_2$ crystal is in the range 72.31–86.13 GPa. In the $ZnAs_2$ crystal, the nearest atomic pair As-As distance is larger than the nearest atomic pair Zn-As distance. The estimated first pressure derivatives $B_0'$ of α-$CdP_2$, α-$ZnP_2$ and $ZnAs_2$ lie in the general range of $B_0'$ from 2 to 6 for solids. Among α-$CdP_2$, α-$ZnP_2$ and $ZnAs_2$, bulk modulus is found to have a low value for α-$CdP_2$. The first pressure derivative is the highest for α-$ZnP_2$ among α-$CdP_2$, α-$ZnP_2$ and $ZnAs_2$.

The present work explores the electronic properties of α-$CdP_2$, α-$ZnP_2$ and $ZnAs_2$. In the vicinity of Fermi energy, the contribution to the density of states of each Cd atom is less in comparison to that of each nonequivalent phosphorus atom [P(I) and P(II)] in α-$CdP_2$. The estimated approximate charge transfer values for Cd, P(I) and P(II) are 1.06*e*, 0.54*e* and 0.52*e*, respectively, for α-$CdP_2$. The value of the maximum

overlap population for pair Cd-P is nearly 0.148 and for pair P-P, it is 0.076 in α-$CdP_2$ under PBE scheme. The value of the energy band gap of the alpha phase of $CdP_2$ is almost 1.78 eV under the GGA functionals (PBE, PBEsol and PWGGA).

For α-$ZnP_2$, near the Fermi energy level, the contribution of each Zn atom is lower in comparison with each P atom. In the vicinity of the Fermi level, for the P atom of the alpha phase of $ZnP_2$, the contribution of *s* and *d* orbitals is much lower than that of *p* orbitals to the density of states. It can be said that the contribution of *s* and *d* orbitals of P atom is negligible near Fermi energy. In a similar way, the contribution of the *f* orbitals of Zn atom of α-$ZnP_2$ to DOS is insignificant. The *p* and *d* orbitals of Zn atom contributes to the density of states more than that of *s* orbitals of Zn atom in α-$ZnP_2$ in the vicinity of Fermi energy. Near the bottom of the conduction band region and the top of the valence band, *p* orbitals of P atoms mainly contribute to the density of states for α-$ZnP_2$, i.e., specified band regions have mostly P-*p* characters. The energy band gap of α-$ZnP_2$ is about 1.5 eV under the GGA functional. Charge transfers take place about 1.07*e*, 0.52*e* and 0.54*e* for Zn atom, P(I) atom and P(II) atom, respectively, in the alpha phase of $ZnP_2$. For α-$ZnP_2$, the value of the maximum overlap population between pairs Zn-P is nearly 0.17 under PBE functional. The value of the maximum overlap population between pairs P-P is of the order of 0.04 for α-$ZnP_2$.

In the vicinity of the Fermi energy level, the contributions of each nonequivalent arsenic atom to the density of states are more significant than those of each nonequivalent zinc atom in the $ZnAs_2$ crystal. Near the Fermi energy, for DOS, the contribution of *p* orbitals is greater than that of *s* and *d* orbitals of the nonequivalent As(I) atoms in monoclinic $ZnAs_2$. In the vicinity of the Fermi energy level, all the arsenic atoms follow nearly the same pattern for the density of states in $ZnAs_2$. The contributions of *s* and *f* orbitals of the nonequivalent Zn(I) atom to DOS are less than that of *p* and *d* orbitals of the nonequivalent Zn(I) atom in $ZnAs_2$. The computed charge transfer values for the nonequivalent atoms Zn(I) and Zn(II) are nearly 0.96*e* and 0.94*e*, respectively, for $ZnAs_2$. The estimated values of charge transfer for the nonequivalent atoms As(I), As(II), As(III) and As(IV) are nearly 0.46*e*, 0.46*e*, 0.46*e* and 0.51*e*, respectively, for the monoclinic $ZnAs_2$ crystal. The value of energy band gap under the GGA functionals is about 0.81 eV for $ZnAs_2$. The value of the

maximum overlap population for pair As-As is about 0.27 and for pair Zn-As, it is about 0.20 in $ZnAs_2$.

Our study provides insight into the elastic properties of the semiconductor compounds α-$CdP_2$, α-$ZnP_2$ and $ZnAs_2$. The present work reveals the malleable nature of the alpha phase of $CdP_2$. The value of the elastic constant $C_{11}$ is the maximum among the other elastic constants of α-$CdP_2$. The elastic constants $C_{22}$ and $C_{33}$ are substantially greater than other elastic stiffness constants, such as $C_{12}$, $C_{13}$, $C_{23}$, $C_{44}$, $C_{55}$ and $C_{66}$ in the alpha phase of $CdP_2$. Our results show that $C_{11} > C_{22} > C_{33} > C_{12}$ and $C_{44} > C_{66} > C_{55}$ for α-$CdP_2$. It is observed that elastic moduli $E_H > B_H > G_H$ for α-$CdP_2$. The estimated Poisson's ratio $\nu_H$ for α-$CdP_2$ is about 0.28–0.32. The elastic anisotropy parameters ratio of the maximum to minimum values of Young's modulus, linear compressibility, shear modulus and Poisson's ratio for α-$CdP_2$ are nearly 1.46, 2.08, 1.70 and 4.44, respectively, under PBE scheme. In the case of Young's modulus of α-$CdP_2$, the *yz*-plane has greater anisotropy than the *xy*-plane.

Our study illustrates $C_{33} > C_{11} > C_{66} > C_{44}$ for the alpha phase of $ZnP_2$. For α-$ZnP_2$, the values of the elastic constants $C_{11}$ and $C_{33}$ are sufficiently greater than the other elastic stiffness constants, such as $C_{12}$, $C_{13}$, $C_{44}$ and $C_{66}$. It is also observed that elastic moduli $E_H > B_H > G_H$ for α-$ZnP_2$. The computed value of Poisson's ratio $\nu_H$ for α-$ZnP_2$ is in the range 0.21–0.26. This work indicates the brittle nature of the alpha phase of $ZnP_2$.

Along different crystallographic directions, the directional Young's modulus of the α-$ZnP_2$ crystal follows the relation $E_{[100]} = E_{[010]} < E_{[001]} < E_{[110]}$ ; $a = b < c$, whereas linear compressibility follows the relation $\beta_{[100]} = \beta_{[010]} = \beta_{[110]} > \beta_{[001]}$. The elastic anisotropy parameters ratios of the maximum to minimum values of Young's modulus, linear compressibility and shear modulus for α-$ZnP_2$ are nearly 1.51, 1.09 and 2.02, respectively. The ratio of the maximum to minimum value of Poisson's ratio for α-$ZnP_2$ is much greater than that of α-$CdP_2$. For the Young's modulus of α-$ZnP_2$, the *yz*-plane has a smaller anisotropy than the *xy*-plane. The *yz*-plane has substantial anisotropy for shear modulus for the alpha phase of $ZnP_2$.

Our present work illustrates $C_{11}$, $C_{22}$ and $C_{33}$ are much greater than other elastic constants, such as $C_{44}$, $C_{55}$, $C_{66}$, $C_{12}$, $C_{13}$, $C_{23}$, $C_{25}$, $C_{35}$ and $C_{46}$ for $ZnAs_2$ crystals. For $ZnAs_2$, it is observed that elastic moduli $E_H > B_H > G_H$. The computed value of Poisson's ratio $\nu_H$ for $ZnAs_2$ is in the range of 0.27–0.31. The elastic anisotropy parameters ratios of maximum to minimum values of Young's modulus, linear compressibility, shear modulus and Poisson's ratio for $ZnAs_2$ are 1.73, 1.25, 2.02 and 12.59, respectively, under PBE scheme.

The bulk modulus $B_H$ of $ZnAs_2$ has a higher value than that of α-$CdP_2$ and α-$ZnP_2$. Polycrystalline shear modulus $G_H$ has a higher value for α-$ZnP_2$ in comparison with α-$CdP_2$ and $ZnAs_2$. The obtained values of Poisson's ratios $\nu_H$ for α-$CdP_2$, α-$ZnP_2$ and $ZnAs_2$ lie in the theoretically predicted range. This investigation shows that α-$CdP_2$, α-$ZnP_2$ and $ZnAs_2$ crystal systems have definite elastic anisotropy. This investigation on the anisotropic properties of the semiconductor compounds $ZnAs_2$, α-$CdP_2$ and α-$ZnP_2$ might give a guiding point for the favoured orientations of these crystals for devising optoelectronic instruments. In the case of the requirement of malleable nature of the materials for device fabrication, α-$CdP_2$ and $ZnAs_2$ have advantages over α-$ZnP_2$. If a device requires more stiffness for linear compression (i.e., large value of Young's modulus), then α-$ZnP_2$ has advantages over α-$CdP_2$ and $ZnAs_2$. In the case of the requirement of a low value of transverse strain (for a given longitudinal strain) for the polycrystalline materials, then α-$ZnP_2$ should be preferred over α-$CdP_2$ and $ZnAs_2$, as α-$ZnP_2$ has a relatively low value of Poisson's ratio. Our comprehensive computational results about the elastic properties of α-$CdP_2$, α-$ZnP_2$ and $ZnAs_2$ crystals might be useful for experimentalists. The DFT method in computational materials science played an important role in calculating the elastic anisotropy of these compounds. The present study of these semiconducting compounds is likely to be beneficial for further research in optoelectronic device applications.

## 6.2 Future Scope

Concerning future scope, our findings would be useful to explore the properties of II-$V_2$ semiconductors through further experiments. Semiconducting compounds $CdP_2$, $ZnP_2$ and $ZnAs_2$ may be studied with the doping of suitable elements. Investigations

may be carried out with different amounts of doping. The properties of $CdP_2$, $ZnP_2$ and $ZnAs_2$ with doping may also be investigated with temperature variations. Further research might reveal the properties of these compounds for doping. More DFT work is needed to explore the temperature-dependent structural, electronic and elastic properties of these compounds. Pressure-dependent structural, electronic and elastic properties of these compounds may also be explored.

The photoelastic properties of these compounds have yet to be investigated by researchers. Investigation of the piezoelectric tensor of the semiconducting compounds $CdP_2$, $ZnP_2$ and $ZnAs_2$ is to be explored. A thorough investigation of dielectric properties, such as reflection coefficient, absorptivity, etc., should be carried out. The thermoelectric properties of these semiconducting compounds have yet to be thoroughly investigated. Electron thermal conductivity, Seebeck coefficient and power factor have not yet been studied thoroughly for these compounds. Furthermore, the calculation of effective mass should be explored in future research. The properties of the nano phase of these compounds may be studied to expand different perspectives on technological applications. There are some other II-$V_2$ semiconducting compounds, such as $ZnSb_2$, $CdSb_2$, $CdAs_2$, $ZnN_2$ and $CdN_2$. Investigators gave scant attention to the compounds $ZnSb_2$, $CdSb_2$, $CdAs_2$, $ZnN_2$ and $CdN_2$. There is a lot of scope for investigating the unexplored properties of these compounds in future research. Our investigation might stimulate further experimental research on these compounds.

# SUMMARY

# *SUMMARY*

This thesis deals with an *Ab-Initio* investigation of some II-$V_2$ semiconducting compounds. A DFT study of mainly α-$CdP_2$, α-$ZnP_2$ and $ZnAs_2$ has been carried out in the present investigation. The usefulness of semiconductors in devices has encouraged accelerated research endeavors to characterize their properties better [2]. A quantum mechanical *Ab-Initio* computer program provides the computation scheme to investigate many properties of crystalline systems [3]. Semiconductors have many technological utilizations, such as transistors, photoconductors, solar cells, strain gauges, charge-coupled devices, light-emitting diodes (LEDs), etc. [8]. Generally, semiconductor devices have reliability and these devices are also relatively economical [8]. Applications of the optical properties of solids are commercially valuable [9]. For optical integrated circuits, photonics has become an important area of research nowadays [9]. The level of Fermi energy in the DOS (density of states) versus the energy plot plays an important role to determine the electronic transport properties of solids [13]. For the deformation of matter, the theory of elasticity forms a mathematical model [18]. In general, crystals are said to be anisotropic because of their direction-dependent properties. II-$V_2$ semiconducting compounds are made from the $12^{th}$ and $15^{th}$ column elements of the periodic table. These compounds are useful in the fabrication of optoelectronic devices [25, 26, 27].

The thesis consists mainly of six chapters. **In Chapter 1**, Group II and Group V elements for II-$V_2$ semiconducting compounds have been discussed. A brief overview of some II-$V_2$ semiconducting compounds, such as II-$V_2$ phosphides and II-$V_2$ arsenides, is provided in Chapter 1. A special attention has been given to the review of the literature on $CdP_2$, $ZnAs_2$ and $ZnP_2$. Motivation for research work and an outline of the thesis are also provided in the first chapter.

In **Chapter 2**, the basic theoretical framework and computational software/ tools are illustrated. Chapter 2 describes DFT (Density Functional Theory), LCAO (Linear Combination of Atomic Orbitals), Basis Sets, Mulliken population, equation of state (EOS), computation cost, elastic stiffness and compliance constants. Useful software/tools CRYSTAL Program, DL Visualize (DLV), CRYSPLOT and ELATE are introduced in Chapter 2.

The structural, electronic and elastic properties of α-$CdP_2$, α-$ZnP_2$ and $ZnAs_2$ are studied with the CRYSTAL code (periodic *ab-initio* HF and DFT code) [124, 140]. In this study, computations are carried out with the GGA functionals (PBE [187, 188], PBEsol [189, 190] and PWGGA [191, 192, 193, 194, 195, 196]), LDA functionals (LDA PZ [197, 198] and LDA VWN [197, 199]), global hybrid functionals (B3PW [191, 192, 193, 200, 201], B3LYP [199, 200, 202, 203] and PBE0 [204, 205, 206, 207]) and range-separated hybrid functional (HSE06 [187, 188, 208, 209, 210, 211, 212, 213, 214, 215]). In the present investigation, the basis sets for cadmium, zinc, phosphorus and arsenic atoms are used from the CRYSTAL-Basis Set Library of the Torino group [124, 140]. An $8\times8\times8$ Monkhorst-Pack *k*-point mesh [139] is implemented for computation. The Fock/Kohn-Sham matrix mixing factor is utilized as a convergence tool for computations. Electronic properties, such as the density of states and band structures, Mulliken population, etc., are investigated by means of the CRYSTAL Code [124, 140]. Unit cell parameters and atom coordinates can be optimized under the full geometry optimization process [124] by means of the CRYSTAL program. The CRYSTAL program can also explore the dielectric [168, 169, 170], elastic [171, 172, 173, 174], and piezoelastic [174, 177, 178] properties of the substances.

DL Visualize (DLV) is a graphical user interface (GUI) that provides the facility of displaying and editing the structures of molecules, periodic structures of surfaces and crystals [179]. DLV facilitates the GUI to CRYSTAL Code [124, 140, 179].

CRYSPLOT [180] is an online tool to plot different specified features of crystals computed with the CRYSTAL Program [124, 140]. It provides a plotting option for the total and projected density of states for atoms [180]. The CRYSPLOT also allows plotting the density of states and band structure in a single combined plot [180]. The Fermi energy line in the band structure can be displayed through the CRYSPLOT [180].

ELATE [181, 182] is an online tool that is used for the exploration of elastic tensors. The maximum and minimum values of elastic moduli may be obtained using the ELATE software [181]. The EALTE software also gives the values of the anisotropy parameters. Directional variations of shear modulus, Young's modulus, linear compressibility and Poisson's ratio are analyzed and visualized by means of the ELATE software [181]. Visualizations of 2D and 3D plots may be obtained using the ELATE program [181].

In **Chapter 3**, the optimized lattice parameters of conventional cells have been investigated using initial geometry data of II-$V_2$ semiconducting compounds by means of CRYSTAL Code [124, 140]. Atomic pair distances for the first 06 nearest atoms in compounds are computed. Plots of relative energy per unit cell of the compound versus its unit cell volume are illustrated in this work.

The computation of the Birch-Murnaghan [124, 132, 133, 134, 135], Vinet [124, 130, 131] and Poirier-Tarantola [124, 132, 136] equations of states [173] is carried out. Two crystalline phases of cadmium diphosphide, namely, alpha and beta, are reported [40, 41, 50]. The α-$CdP_2$ crystal has an orthorhombic crystal structure at room temperature [41]. A tetragonal crystal structure is reported for the beta phase of $CdP_2$ [35, 45]. The reported space group of α-$CdP_2$ is $Pna2_1$ [40, 41]. The lattice parameters of α-$CdP_2$ are $a$ = 9.90 Å, $b$ = 5.408 Å and $c$ = 5.171 Å, as stated by Goodyear *et al.* [40]. The α-$CdP_2$ comprises three nonequivalent atoms, namely, Cd, P(I) and P(II) [40]. The atomic pair P-P has the nearest distance of nearly 2.19 Å, whereas atomic pair Cd-P has the nearest distance of about 2.61 Å under PBE scheme. The computed values of bulk modulus of α-$CdP_2$ are in the range 51.94–64.57 GPa. The computed values of the first pressure derivative $B_0'$ of α-$CdP_2$ are around 4.05. Hence, this range for α-$CdP_2$ lies in the general typical range of $B_0'$ from 2 to 6 for solids [220].

Two different crystalline phases of $ZnP_2$ are shown as α-$ZnP_2$ and β-$ZnP_2$ [28, 34]. The α-$ZnP_2$ and β-$ZnP_2$ crystals have tetragonal and monoclinic crystal structures, respectively [28, 34]. α-$ZnP_2$ has lattice parameters $a$ = 5.08 Å and $c$ =18.59 Å [36]. The conventional unit cell of the alpha phase of $ZnP_2$ has 08 formula units [28, 36]. The estimated computed range of the first pressure derivative for α-$ZnP_2$ is 4.34–4.58. The estimated range of bulk modulus for α-$ZnP_2$ is 63.9–83.3 GPa.

The space group of monoclinic $ZnAs_2$ is $P2_1/c$ ($C_{2h}^5$) [46, 47]. The monoclinic unit cell of $ZnAs_2$ has 08 formula units [46]. The conventional unit cell of $ZnAs_2$ has six nonequivalent atoms [47, 50]. The computed angle $\beta$ of monoclinic $ZnAs_2$ is around 102.46.° The typical computed value of the first pressure derivative for $ZnAs_2$ is 2.61–4.20. The estimated values of bulk modulus for $ZnAs_2$ are in the range of 72.31–86.13 GPa.

**Chapter 4** addresses the study of the electronic properties of α-$CdP_2$, α-$ZnP_2$ and $ZnAs_2$. The energy band gaps of these compounds have been computed under various functional schemes. For α-$CdP_2$, the highest point of the valence band is found on the path $\Gamma - Z$ and the lowest point of the conduction band is found near the $X$ point. For α-$CdP_2$, computations have been performed along high symmetry directions for special points (namely $X, Z, S, U, Y, R, \Gamma$, etc.) in the Brillouin zone [4]. So, it illustrates the indirect energy band gap for α-$CdP_2$. The density of states of nonequivalent atoms in the alpha phase of $CdP_2$ is studied. Each P(I) and P(II) atom contributes more in comparison to the contribution to the density of states (DOS) by Cd atom. Under PBE scheme, the computed values of charge transfer for P(I), P(II) and Cd atoms are about 0.54*e*, 0.52*e* and 1.06*e*, respectively, in the alpha phase of α-$CdP_2$. The value of the maximum overlap population for the pair Cd-P is found to be nearly 0.148 under PBE functional. The present study shows that the energy band gap of α-$CdP_2$ is almost 1.78 eV under the GGA functionals (PBEsol, PBE and PWGGA).

The energy band gap value for the alpha phase of $ZnP_2$ under the PBE functional is 1.54 eV, which is an indirect energy band gap. For α-$ZnP_2$, point *M* is the highest point in the valence band. The contributions of *s* and *d* orbitals of P(I) atom of α-$ZnP_2$ are minimal to the density of states near the Fermi level. Also, the contribution of *p* orbitals of P(I) atom of α-$ZnP_2$ is much higher than that of *s* and *d* orbitals to DOS. For α-$ZnP_2$, the contribution of the *f* orbitals of Zn atom to DOS is negligible. In α-$ZnP_2$ under PBE scheme, charge transfers take place about 1.07*e*, 0.52*e* and 0.54*e* for Zn atom, P(I) atom and P(II) atom, respectively. The maximum overlap population between pairs Zn-P is about 0.17 in α-$ZnP_2$ under PBE scheme.

For the monoclinic $ZnAs_2$, the energy band gap under the GGA functionals is about 0.81 eV. The value of the maximum overlap population for pair Zn-As is about 0.20 and for pair As-As, it is about 0.27 in $ZnAs_2$.

The contributions of each nonequivalent arsenic atom to the density of states near Fermi energy are more significant than those of each nonequivalent zinc atom in $ZnAs_2$. In the vicinity of the Fermi energy, for DOS, the contribution of *p* orbitals of nonequivalent As(I) atom is more significant than that of *s* and *d* orbitals of nonequivalent As(I) atom in the $ZnAs_2$ crystal. Also, the contributions of *s* and *f* orbitals of nonequivalent Zn(I) atom to DOS are less than those of *p* and *d* orbitals of

nonequivalent Zn(I) atom in monoclinic $ZnAs_2$. The computed values of charge transfer for nonequivalent atoms As(I), As(II), As(III) and As(IV) are nearly 0.46*e*, 0.46*e*, 0.46*e* and 0.51*e*, respectively, for $ZnAs_2$. The calculated charge transfer values for the nonequivalent atoms Zn(I) and Zn(II) are about 0.96*e* and 0.94*e*, respectively, for $ZnAs_2$.

In **Chapter 5**, elastic constants $C_{ij}$ and elastic compliance constants $S_{ij}$ are computed for α-$CdP_2$, α-$ZnP_2$ and $ZnAs_2$. For these compounds, the investigation of the directional dependence of linear compressibility, Poisson's ratio, shear modulus and Young's modulus is carried out by plotting polar graphs. Minimum and maximum values of linear compressibility $\beta$, Poisson's ratio $v$, shear modulus $G$ and Young's modulus $E$ of these compounds are computed under various functionals.

The variation of the bulk modulus of the II-$V_2$ compounds with pressure is studied using the keyword EOS [173]. The elastic quantities Young's modulus $E$, bulk modulus $B$ and shear modulus $G$ are computed by utilizing the ELATE program [181, 182]. For these compounds, it is observed that $E_H > B_H > G_H$. The brittleness and malleability properties of the polycrystalline substances are correlated with the ratio of bulk modulus $B$ to shear modulus $G$ [231]. The malleable nature of a polycrystalline substance is likely to be predicted for a ratio $B/G$ greater than nearly 1.75 [231]. Ranganathan's term universal elastic anisotropy index $A^U$ [234] is calculated for these compounds.

The orthorhombic $CdP_2$ crystal has nine independent elastic constants $C_{11}$, $C_{12}$, $C_{13}$, $C_{22}$, $C_{23}$, $C_{33}$, $C_{44}$, $C_{55}$ and $C_{66}$ [16]. The necessary and sufficient elastic stability conditions for the orthorhombic crystal, as stated by Mouhat *et al.* [230], are followed by the alpha phase of $CdP_2$.

The crystal of the tetragonal (I) class (4/mmm) has 06 independent elastic stiffness constants $C_{11}$, $C_{12}$, $C_{13}$, $C_{33}$, $C_{44}$ and $C_{66}$ [16]. In view of the resisting structural deformation, the bulk modulus of nearly 66 GPa of the alpha phase of $ZnP_2$ shows its considerably ample mechanical strength. In the case of α-$ZnP_2$, the *xy*-plane has greater anisotropy than the *yz*-plane for Young's modulus $E$. The maximum percentage change in the value of linear compressibility of α-$ZnP_2$ with respect to its minimum value is about 8.9% for the *xz*-plane.

The thirteen independent elastic stiffness constants, namely $C_{11}$, $C_{12}$, $C_{13}$, $C_{15}$, $C_{22}$, $C_{23}$, $C_{25}$, $C_{33}$, $C_{35}$, $C_{44}$, $C_{46}$, $C_{55}$ and $C_{66}$ are reported for standard orientation of

monoclinic crystal [16]. In the present study, the calculated bulk modulus *B* of $ZnAs_2$ increases with applied pressure (P from 0 to 6 GPa). The shear modulus *G* has around 100% variation relative to its minimum value for $ZnAs_2$. The anisotropy index $A^U$ has a higher value for $ZnAs_2$ in comparison with α-$CdP_2$ and α-$ZnP_2$.

In **Chapter 6**, conclusions and future scope are illustrated. The present investigation on the anisotropic properties of the semiconducting compounds α-$CdP_2$, α-$ZnP_2$ and $ZnAs_2$ might provide a guiding point for the favored orientation of these crystals for devising optoelectronic instruments. This study of these semiconducting compounds is likely to be beneficial for further research in optoelectronic device applications.

# *BIBLIOGRAPHY*


[1] Vasiliev, V.V. and Morozov, E.V., 2001. *Mechanics and Analysis of Composite Materials.* Oxford: Elsevier Science Ltd.

[2] Azaroff, L.V., 2002. *Introduction to Solids.* New Delhi: Tata McGraw Hill.

[3] Rérat, M., D'Arco, P., Lacivita, V., Pascale, F. and Dovesi, R., 2020. From anisotropy of dielectric tensors to birefringence: a quantum mechanics approach. *Rendiconti Lincei. Scienze Fisiche e Naturali*, 31(3), pp.835-851. https://doi.org/10.1007/s12210-020-00931-9

[4] Kaxiras, E., 2003. *Atomic and Electronic Structure of Solids.* New York: Cambridge University Press.

[5] Kasap, S.O., 2002. *Principles of Electronic Materials and Devices*. 2nd ed. New Delhi: Tata McGraw Hill.

[6] Atkins, P. and de Paula, J., 2006. *Physical Chemistry*. 8th ed. New York: W. H. Freeman and Company.

[7] Litvinchuk, A.P. and Valakh, M.Y., 2020. Raman and infrared phonons in tetragonal $ZnP_2$ and $CdP_2$ crystals: a density functional study. *Journal of Physics: Condensed Matter*, 32(44), p.445401.

[8] Patterson, J.D. and Bailey, B.C., 2018. *Solid-State Physics: Introduction to the Theory*. 3rd ed. Switzerland: Springer International Pulishing AG.

[9] Smart, L.E. and Moore, E.A., 2005. *Solid State Chemistry: An Introduction*. 3rd ed. Boca Raton: CRC press.

[10] Himanshu, Patel, S.L., Thakur, A., Kannan, M.D. and Dhaka, M.S., 2020. Analysis of different annealing conditions on physical properties of Bi doped CdTe thin films for potential absorber layer in solar cells. *Solar Energy*, 199, pp.772-781. https://doi.org/10.1016/j.solener.2020.02.066

[11] Omar, M.A., 2000. *Elementary Solid State Physics: Principles and Applications*. India: Pearson Education Asia Pte. Ltd.

[12] Atkins, P. and Friedman, R, 2011. *Molecular Quantum Mechanics*. 4th ed. New York: Oxford University Press Inc.

[13] Hofmann, P., 2015. *Solid State Physics*. 2nd ed. Wiley-VCH Verlag GmbH & Co.KGaA, Boschstr.

[14] Sólyom, J., 2009. *Fundamentals of the Physics of Solids: Volume II: Electronic Properties.* Springer-Verlag Berlin Heidelberg.

[15] Ashcroft, N.W. and Mermin, N.D., 2001. *Solid State Physics*. Singapore: Harcourt Asia Pte. Ltd.

[16] Nye, J.F., 1985. *Physical Properties of Crystals: Their Representation by Tensors and Matrices.* New York: Oxford University Press Inc.

[17] Kittel, C., 1999. *Introduction to Solid State Physics*. 7th ed. Singapore: John Wiley & Sons (ASIA) Pte. Ltd.

[18] Sadd, M.H., 2009. *Elasticity: Theory, Applications, and Numerics*. Oxford: Elsevier Butterworth-Heinemann.

[19] Teodorescu, P.P., 2013. *Treatise on Classical Elasticity: Theory and Related Problems*. Dordrecht: Springer Science+Business Media

[20] Vannucci, P., 2018. *Anisotropic Elasticity*. Singapore: Springer Nature.

[21] Li, R., Shao, Q., Gao, E. and Liu, Z., 2020. Elastic anisotropy measure for two-dimensional crystals. *Extreme Mechanics Letters*, 34, p.100615. https://doi.org/10.1016/j.eml.2019.100615

[22] Javanbakht, M. and Adaei, M., 2019. Investigating the effect of elastic anisotropy on martensitic phase transformations at the nanoscale. *Computational Materials Science*, 167, pp.168-182.

[23] Daniel, R., Meindlhumer, M., Baumegger, W., Todt, J., Zalesak, J., Ziegelwanger, T., Mitterer, C. and Keckes, J., 2019. Anisotropy of fracture toughness in nanostructured ceramics controlled by grain boundary design. *Materials & Design*, 161, pp.80-85. https://doi.org/10.1016/j.matdes.2018.11.028

[24] Aboudi, J., Arnold, S.M. and Bednarcyk, B.A., 2013. *Micromechanics of Composite Materials: A Generalized Multiscale Analysis Approach*. Oxford: Butterworth-Heinemann.

[25] Rud', V.Y., Rud', Y.V. and Bodnar', I.V., 2010. Growth of Tetragonal $CdP_2$ Single Crystals and the Properties of Barriers on Their Basis. *Technical Physics*, 55(4), pp.517-520. https://doi.org/10.1134/S1063784210040146

[26] Fekeshgazi, I.V., Sidenko, T.S., Czitrovszky, A., Veresh, M., Trukhan, V.M. and Shoukavaya, T.V., 2015. Raman Spectra of Gyrotropic Cadmium Diphosphide Crystals. *Journal of Applied Spectroscopy*, 82(3), pp.367-373.

https://doi.org/10.1007/s10812-015-0114-z

[27] Beril, S.I., Stamov, I.G., Syrbu, N.N. and Zalamai, V.V., 2013. Birefringence and band structure of $CdP_2$ crystals. *Physica B:Condensed Matter*,422,pp.12-19. https://doi.org/10.1016/j.physb.2013.04.029

[28] Zdanowicz, W. and Zdanowicz, L., 1975. Semiconducting Compounds of the $A^{II}$ $B^{V}$ Group. *Annual Review of Materials Science*, 5(1), pp.301-328. https://doi.org/10.1146/annurev.ms.05.080175.001505

[29] Warlimont, H. and Martienssen, W. (Eds.), 2018. *Springer Handbook of Materials Data*. 2nd ed. Springer Cham. https://doi.org/10.1007/978-3-319-69743-7

[30] Kramida, A., Ralchenko, Y., Reader, J., and NIST ASD Team, 2023. *NIST Atomic Spectra Database* (ver. 5.11), [Online]. Available: https://physics.nist.gov/asd [2023, December 25]. National Institute of Standards and Technology, Gaithersburg, MD. https://doi.org/10.18434/T4W30F

[31] Haynes, W.M. (Ed.), 2016. *CRC Handbook of Chemistry and Physics*. 97th ed. Boca Raton: CRC Press. https://doi.org/10.1201/9781315380476

[32] https://www.rsc.org/periodic-table

[33] http://www.nist.gov

[34] Hegyi, I.J., Loebner, E.E, Poor Jr., E.W. and White, J.G., 1963. Two crystal forms of $ZnP_2$, their preparation, structure, and optoelectronic properties. *Journal of Physics and Chemistry of Solids*, 24(2), pp.333-337. https://doi.org/10.1016/0022-3697(63)90140-9

[35] Stackelberg, M.V. and Paulus, R., 1935. Untersuchungen an den Phosphiden und Arseniden des Zinks und Cadmiums. Das $Zn_3P_2$-Gitter. *Zeitschrift für Physikalische Chemie*, 28B(1), pp.427-460. https://doi.org/10.1515/zpch-1935-2841

[36] White, J.G., 1965. The Crystal Structure of the Tetragonal Modification of $ZnP_2$. *Acta Crystallographica*, 18(2), pp.217-220. https://doi.org/10.1107/S0365110X6500049X

[37] Sobolev, V.V., Syrbu, N.N. and Sushkevich, T.N., 1971. Energy Band Structure of the Tetragonal Crystals $ZnP_2$ and $CdP_2$. *Physica Status Solidi (b)*, 43(1), pp.73-81.

https://doi.org/10.1002/pssb.2220430107

[38] Sobolev, V.V. and Syrbu, N.N., 1972. Optical Spectra and Energy Band Structure of the Monoclinic Crystals $ZnP_2$ and $ZnAs_2$. *Physica Status Solidi (b)*, 51(2), pp.863-872.
https://doi.org/10.1002/pssb.2220510244

[39] Tanaka, Y., 1969. Chemical reaction at high temperature and high pressure VI: Polymorphic Transition in $ZnP_2$ at High Temperature and High Pressure. *The Review of Physical Chemistry of Japan*, 38(2), pp.151-169.

[40] Goodyear, J. and Steigmann, G.A., 1969. The Crystal Structure of α-$CdP_2$. *Acta Crystallographica Section B*, 25(11), pp.2371-2374.
https://doi.org/10.1107/S0567740869005723

[41] Eckstein, N., Krüger, I., Bachhuber, F., Weihrich, R., Barquera-Lozada, J.E., van Wüllen, L. and Nilges, T., 2015. Low-activated Li-ion mobility and metal to semiconductor transition in $CdP_2$@ Li phases. *Journal of Materials Chemistry A*, 3(12), pp.6484-6491.
https://doi.org/10.1039/C5TA00471C

[42] Borshch, V.V., Koval, V.S., Potykevich, I.V. and Fekeshgazi, I.V., 1977. Birefringence and Optical Activity of $CdP_2$. *Physica Status Solidi (a)*, 44(1), pp.K15-K19.
https://doi.org/10.1002/pssa.2210440148

[43] Dmitruk, N.L., Zuev, V.A. and Stepanova, M.A., 1991. Spectral Distribution of The Photoconductivity of Cadmium Diphosphide. *Soviet Physics Journal*, 34(7), pp.642-644.
https://doi.org/10.1007/BF00898000

[44] Garasevich, S., Gubanov, V., Korenyuk, P., Koryakov, S., Slobodyanyuk, A. and Yanchuk, Z., 2004. Two-phonon Raman spectra of tetragonal crystals $ZnP_2$, $CdP_2$, and $TeO_2$. *Proceedings SPIE* 5507, *XVI International Conference on Spectroscopy of Molecules and Crystals*, 5507, pp.26-34.
https://doi.org/10.1117/12.569596

[45] Červinka, L. and Hrubý, A., 1970. The crystal structure of $CdAs_2$. *Acta Crystallographica Section B*, 26(4), pp.457-458.
https://doi.org/10.1107/S0567740870002650

[46] Senko, M.E., Dunn, H.M., Weidenborner, J. and Cole, H., 1959. Lattice parameters of $ZnAs_2$. *Acta Crystallographica*, 12(1), p.76.

https://doi.org/10.1107/S0365110X59000214

[47] Fleet, M.E., 1974. The crystal structure of $ZnAs_2$. *Acta Crystallographica Section B*, 30(1), pp.122-126. https://doi.org/10.1107/S0567740874002329

[48] Marenkin, S.F., Morozova, V.A. and Koshelev, O.G., 2010. Structural Defects and Band-Structure Parameters of $CdAs_2$, $ZnAs_2$, $Cd_{1-x}$ $Zn_xAs_2$, and $Zn_{1-x}Cd_xAs_2$ Single Crystals. *Inorganic Materials*, 46(9), pp.1001-1006. https://doi.org/10.1134/S0020168510090153

[49] Marenkin, S.F. and Morozova, V.A., 2000. Zinc and Cadmium Diarsenides Single Crystals and Films: Synthesis and Physicochemical Properties. *Russian Journal of Inorganic Chemistry*, 45(Suppl. 1).

[50] Madelung, O., 2004. *Semiconductors: Data Handbook*. 3rd ed. Springer-Verlag Berlin Heidelberg. https://doi.org/10.1007/978-3-642-18865-7

[51] Ril', A.I. and Marenkin, S.F., 2021. Cadmium Arsenides: Structure, Synthesis of Bulk and Film Crystals, Magnetic and Electrical Properties (Review). *Russian Journal of Inorganic Chemistry*, 66(14), pp.2005-2016. https://doi.org/10.1134/S0036023621140059

[52] Berak, J. and Pruchnik, Z., 1969. Phase Equilibria in the Zinc-Cadmium-Phosphorus System. Part 2: The Zinc-Phosphorus System. *Roczniki Chemii*, 43, pp.1141-1146.

[53] Olofsson, O. and Gullman, J., 1970. A note on the crystal structure of α-$CdP_2$. *Acta Crystallographica Section B*, 26(11), pp.1883-1884. https://doi.org/10.1107/S056774087000506X

[54] Borshch, V.V., Lisitsa, M.P., Mozol, P.E., and Fekeshgazi, I.V., 1978. Self-induced rotation of the direction of polarization of light in crystals of 422 symmetry. *Soviet Journal of Quantum Electronics*, 8(3), pp.393-395. https://doi.org/10.1070/QE1978v008n03ABEH010035

[55] Gorban, I.S., Gorinya, V.A., Dashkovskaya, R.A., Lugovoi, V.I., Makovetskaya, A.P. and Tichina, I.I., 1978. One-and Two-Phonon States in Tetragonal $ZnP_2$ and $CdP_2$ Crystals. *Physica Status Solidi (b)*, 86(1), pp.419-423. https://doi.org/10.1002/pssb.2220860149

[56] Smolyarenko, E.M. and Trukhan, V.M., 1985. Phase diagrams of the $ZnP_2$-$ZnAs_2$ and $ZnP_2$-$CdP_2$ systems. *Thermochimica Acta*, 93, pp.677-680. https://doi.org/10.1016/0040-6031(85)85170-4

[57] Babonas, G., Korets, N.S. and Marcinkevičius, S., 1983. Dispersion of Optical Constants in $CdP_2$. *Physica Status Solidi (b)*, 117(2), pp.477-481. https://doi.org/10.1002/pssb.2221170206

[58] Manolikas, C., van Tendeloo, J. and Amelinckx, S., 1986. The "Devil's Staircase" in $CdP_2$ and $ZnP_2$. *Physica Status Solidi (a)*, 97(1), pp.87-102. https://doi.org/10.1002/pssa.2210970106

[59] Sheleg, A.U., Soshnikov, L.E. and Plyushch, O.B., 1989. Thermal expansion and elastic properties of the crystals with modulated structure. *Phase Transitions*, 16(1-4), pp.463-467. https://doi.org/10.1080/01411598908245722

[60] Polygalov, Y.I. and Poplavnoi, A.S., 1994. Electron density and chemical bonding in tetragonal $A_2B_2^5$ crystals. II. $ZnP_2$ and $CdP_2$. *Journal of Structural Chemistry*, 34(5), pp.696-700. https://doi.org/10.1007/BF00753569

[61] Aleinikova, K.B., Kozlov, A.I., Kozlova, S.G. and Sobolev, V.V., 2002. Electronic and Crystal Structures of Isomorphic $ZnP_2$ and $CdP_2$. *Physics of the Solid State*, 44(7), pp.1257-1262. https://doi.org/10.1134/1.1494619

[62] Kozlov, A.I., Kozlova, S.G. and Sobolev, V.V., 2002. Anisotropy of optical spectra of tetragonal cadmium diphosphide. *Moldavian Journal of the Physical Sciences*, 1(4), pp.92-95.

[63] Gnatyuk, V.A., Borshch, V.V., Kuzmenko, M.G., Gorodnychenko, O.S. and Yuryev, S.O., 2004. Dispersion of Optical Characteristics of Anisotropic $CdP_2$ Single Crystals. *Physics and Chemistry of Solid State*, 5(2), pp.256-259.

[64] Trukhan, V.M., Sheleg, A.U. and Fekeshgazi, I.F., 2004. Cadmium Diphosphide and Zinc Diarsenide Single Crystals-Promising Materials for Electronic Engineering. *Photoelectronics*, 13, pp.15-17.

[65] Bodnar, I.T., Trukhan, V.M. and Sheleg, A.U., 2005. Temperature anomalies of optical properties in cadmium diphosphide crystal. *Moldavian Journal of the Physical Sciences*, 4(2), pp.197-200.

[66] Kopytov, A.V., Polygalov, Y.I. and Tkachenko, V.N., 2005. Dynamics of the Lattice and Thermal Capacity of $ZnP_2$ and $CdP_2$ Tetragonal Crystals. *Russian Physics Journal*, 48(7), pp.679-682. https://doi.org/10.1007/s11182-005-0186-y

[67] Soshnikov, L.E., Trukhan, V.M., Haliakevich, T.V. and Soshnikava, H.L., 2005. Dielectric and elastic properties of $CdP_2$, $ZnP_2$ and $ZnAs_2$ single crystals. *Moldavian Journal of the Physical Sciences*, 4(2), pp.201-210.

[68] Trukhan, V.M., Soshnikov, L.E., Marenkin, S.F. and Haliakevich, T.V., 2005. Crystal Growth and Electrical Properties of β-$CdP_2$ Single Crystals. *Inorganic Materials*, 41(9), pp.901-905. https://doi.org/10.1007/s10789-005-0233-7

[69] Yeshchenko, O.A., Dmitruk, I.M., Koryakov, S.V. and Galak, M.P., 2005. Fabrication, study of optical properties and structure of most stable $(CdP_2)_n$ nanoclusters. *Physica E: Low-dimensional Systems and Nanostructures*, 30(1-2), pp.25-30. https://doi.org/10.1016/j.physe.2005.07.019

[70] Stamov, I.G. and Tkachenko, D.V., 2006. Effect of the Levels of Intrinsic Defects in the $CdP_2$ Band Gap on Electrical Characteristics of Corresponding Structures with the Schottky Barrier. *Semiconductors*, 40(10), pp.1165-1172. https://doi.org/10.1134/S1063782606100083

[71] Feng, S.Q. and Cheng, X.L., 2011. Theoretical study on electronic properties and pressure-induced phase transition in β-$CdP_2$. *Computational and Theoretical Chemistry*, 966(1-3), pp.149-153. https://doi.org/10.1016/j.comptc.2011.02.028

[72] Feng, S.Q., Wang, L.L., Jiang, X.X., Li, H.N., Cheng, X.L. and Su, L., 2017. High-pressure dynamic, thermodynamic properties, and hardness of $CdP_2$. *Chinese Physics B*, 26(4), p.046301. https://doi.org/10.1088/1674-1056/26/4/046301

[73] Shportko, K.V., 2017. The cation and the anion vacancies in cadmium diphosphide: A NIR-VIS, IR, and Raman study. *Vibrational Spectroscopy*, 92, pp.230-233. https://doi.org/10.1016/j.vibspec.2017.08.004

[74] Popov, P.A., Oleinik, E.A., Trukhan, V.M., Izotov, A.D. and Marenkin, S.F., 2018. Thermal Conductivity of Tetragonal Cadmium Diphosphide Crystals. *Inorganic Materials*, 54(3), pp.237-239. https://doi.org/10.1134/S0020168518030123

[75] Zavada, M., Konoreva, O., Lytovchenko, P., Opilat, V., Pinkovska, M., Radkevych, O. and Tartachnyk, V., 2018. Self-organization in irradiated semiconductor crystals caused by thermal annealing. *Semiconductor Physics, Quantum Electronics & Optoelectronics*, 21(2), pp.130-133.

[76] Chen, J., Lin, C., Xu, F., Yang, S., Sun, Y., Zhao, X., Jiang, X., Li, B., Yan, T. and Ye, N., 2020. α-$CdP_2$: Large SHG Effect Originating from the Synergism of Parallel $^{1}_{\infty}\left[P^{-1}\right]$ Polyanion Chains and Distorted $CdP_4$ Tetrahedra. *Chemistry of Materials*, 32(23), pp.10246-10253. https://doi.org/10.1021/acs.chemmater.0c04255

[77] Rubenstein, M. and Dean, P.J., 1970. Preparation of Zinc Diphosphides and the Low Temperature Luminescence and Absorption of the Tetragonal Polymorph. *Journal of Applied Physics*, 41(4), pp.1777-1786. https://doi.org/10.1063/1.1659103

[78] Rubenstein, M. and Ryan, F.M., 1965. Electro- and Photoluminescence in Tetragonal $ZnP_2$. *Journal of Applied Physics*, 36(9), p.2971. http://doi.org/10.1063/1.1714623

[79] Jordan, A.S., 1971. Some Thermodynamic Properties of $Zn_3As_2$, $Cd_3As_2$, and $ZnP_2$. *Journal of The Electrochemical Society*, 118(8), pp.1362-1365. https://doi.org/10.1149/1.2408323

[80] Wardzyński, W., Wojakowski, A. and Źdanowicz, W., 1969. Pair spectra in tetragonal zinc diphosphide ($ZnP_2$) and cadmium diphosphide ($CdP_2$) single crystals. *Physics Letters A*, 29(9), pp.547-548. https://doi.org/10.1016/0375-9601(69)90429-0

[81] Sheleg, A.U., Kutas, A.A. and Tekhanovich, N.P., 1980. X-Ray Study of Lattice Parameters and Thermal Expansion Coefficients of Zinc Diphosphide over the Range 80 to 320 K. *Physica Status Solidi (a)*, 58(2), pp.K179-K183. https://doi.org/10.1002/pssa.2210580264

[82] Januskevicius, Z., Karalkeviciute, V. and Sakalas, A., 1985. The Nature of Acceptor Centres in Zinc and Cadmium Diphosphide. *Physica Status Solidi (a)*, 89(1), pp.K65-K69.
https://doi.org/10.1002/pssa.2210890159

[83] Sobolev, V.V., Kozlov, A.I., Tychina, I.I., Romanik, P.A. and Smolyarenko, E.M., 1981. Free exciton and exciton-impurity complexes of monoclinic zinc diphosphide. *Pis'ma v Zhurnal Èksperimental'noi i Teoreticheskoi Fiziki*, 34(3), pp.115-118.

[84] Jayaraman, A., Maines, R.G. and Chattopadhyay, T., 1986. Effect of high pressure on the vibrational modes and the energy gap of $ZnP_2$. *Pramana: Journal of Physics*, 27(1-2), pp.291-297.
https://doi.org/10.1007/BF02846343

[85] Rubtsov, V.A., Smoljarenko, E.M., Trukhan, V.M., Yakimovich, V.N. and Orlik, L.K., 1989. $ZnP_2$ Crystal Structure under High Pressure. *Crystal Research and Technology*, 24(1), pp.55-58.
https://doi.org/10.1002/crat.2170240111

[86] Aleynikova, K.B., Kozlov, A.I., Kozlova, S.G. and Sobolev, V.V., 2004. Crystal Chemistry and Optical Properties of Monoclinic Zinc Diphosphide. *Moldavian Journal of the Physical Sciences*, 3(2), pp.137-148

[87] Shportko, K.V., Izotov, A.D., Trukhan, V.M., Shelkovaya, T.V. and Venger, E.F., 2014. Effect of Temperature on the Region of Residual Rays of $CdP_2$ and $ZnP_2$ Single Crystals. *Russian Journal of Inorganic Chemistry*, 59(9), pp.986-991.
https://doi.org/10.1134/S0036023614090204

[88] Huang, H.M., Li, Y.L. and Zeng, Z., 2013. Structural, elastic, and electronic properties of compressed $ZnP_2$. *Physica B: Condensed Matter*, 419, pp.112-115.
https://doi.org/10.1016/j.physb.2013.03.036

[89] Stamov, I.G., Syrbu, N.N. and Dorogan, A.V., 2013. Photodetectors and birefringence in $ZnP_2$–$C_{2h}^5$ crystals. *Physica B: Condensed Matter*, 412, pp.130-137.
https://doi.org/10.1016/j.physb.2012.11.033

[90] Shportko, K.V., Rueckamp, R., Shoukavaya, T.V., Trukhan, V.M., El-Nasser, H.M. and Venger, E.F., 2016. Effect of the low temperatures on the Raman

active vibrational modes in $ZnP_2$ and $CdP_2$. *Vibrational Spectroscopy*, 87, pp.173-181.
https://doi.org/10.1016/j.vibspec.2016.09.024

[91] Trukhan, V.M., Izotov, A.D. and Shoukavaya, T.V., 2014. Compounds and Solid Solutions of the Zn-Cd-P-As System in Semiconductor Electronics. *Inorganic Materials*, 50(9), pp.868-873.
https://doi.org/10.1134/S0020168514090143

[92] Stamov, I.G., Syrbu, N.N. and Zalamai, V.V., 2014. Optical properties and band structure of $ZnP_2$-$D_4^8$. *Journal of Luminescence*, 149, pp.19-27.
https://doi.org/10.1016/j.jlumin.2013.11.078

[93] Shportko, K.V., 2016. How the phosphorus chains impact on the vibrational properties of diphosphides $ZnP_2$ and $CdP_2$ at low temperatures. *Semiconductor Physics, Quantum Electronics & Optoelectronics*, 19(4), pp.377-383.
https://doi.org/10.15407/spqeo19.04.377

[94] Dorogan, A., 2018. Optical anisotropy in optoelectronics. *6th International Conference Telecommunications, Electronics and Informatics* (ICTEI), *Chisinau, Moldova*, pp. 67-71.

[95] Dorogan, A.V., Beril, S.I., Stamov, I.G. and Syrbu, N.N., 2019. Me-$ZnP_2$ Diodes Sensible to Optical Gyration. *4th International Conference on Nanotechnologies and Biomedical Engineering (ICNBME), Chisinau, Moldova, IFMBE Proceedings*, Springer Cham, 77, pp.167–171.
https://doi.org/10.1007/978-3-030-31866-6

[96] Živković, A., Farkaš, B., Uahengo, V., de Leeuw, N.H. and Dzade, N.Y., 2019. First-principles DFT insights into the structural, elastic, and optoelectronic properties of α and β-$ZnP_2$: implications for photovoltaic applications. *Journal of Physics: Condensed Matter*, 31(26), p.265501.
https://doi.org/10.1088/1361-648X/ab111c

[97] Nam, K.H., Hwa, Y. and Park, C.M., 2020. Zinc Phosphides as Outstanding Sodium-Ion Battery Anodes. *ACS Applied Materials & Interfaces*, 12(13), pp.15053-15062.
https://doi.org/10.1021/acsami.9b21803

[98] Oh, S.H. and Kim, Y., 2021. Cubic $ZnP_2$ nanowire growth catalysed by bismuth. *CrystEngComm*, 23(11), pp.2297-2303.

https://doi.org/10.1039/D1CE00029B

[99] Weszka, J., Mazurak, Z. and Pishchikov, D.I., 1992. FIR absorption in Monoclinic $ZnAs_2$. *Physica Status Solidi (b)*, 170(1), pp.89-92. https://doi.org/10.1002/pssb.2221700110

[100] Matveeva, L.A. and Matiyuk, I.M., 2001. Surface characterization of the photorefractive crystals $CdAs_2$ and $ZnAs_2$ using electroreflectance. *Eighth International Conference on Nonlinear Optics of Liquid and Photorefractive Crystals. SPIE Proceedings*, 4418, pp.230-233. https://doi.org/10.1117/12.428319

[101] Mollaev, A.Y., Saypulaeva, L.A., Arslanov, R.K., Gabibov, S.F. and Marenkin, S.F., 2002. Electrophysical Properties of $ZnAs_2$ and $CdAs_2$ at Hydrostatic Pressure up to 9 GPa. *High Pressure Research*, 22(1), pp.181-184. https://doi.org/10.1080/08957950211335

[102] Morozova, V.A., Marenkin, S.F. and Koshelev, O.G., 2002. Energy Levels of Structural Defects in $ZnAs_2$. *Inorganic Materials*, 38(4), pp.325-330. https://doi.org/10.1023/A:1015137301787

[103] Yakushev, M.V., Mudryi, A.V., Martin, R.W. and Feofanov, Y., 2003. Comparative study of Er-implanted Si, $ZnAs_2$ and $CuInSe_2$. *Materials Science and Engineering: B*, 105 (1-3), pp.175-178. https://doi.org/10.1016/j.mseb.2003.08.040

[104] Nikolaev, Y.A., Rud', V.Y., Rud', Y.V. and Terukov, E.I., 2009. Polarization Photosensitivity of Schottky Barriers on Monoclinic $ZnAs_2$ Crystals. *Technical Physics*, 54(11), pp.1597-1601. https://doi.org/10.1134/S1063784209110073

[105] Morozova, V.A., Marenkin, S.F. and Koshelev, O.G., 1999. Transmission Spectra of $ZnAs_2$ in the Extrinsic Absorption Region. *Inorganic Materials*, 35(7), pp.661-663.

[106] Marenkin, S.F., Ril, A.I. and Fedorchenko, I.V., 2018. Phase diagram of $ZnAs_2$–MnAs system. *Mendeleev Communications*, 28(2), pp.219-221. https://doi.org/10.1016/j.mencom.2018.03.038

[107] Stamov, I.G., Sîrbu, N.N., Ursaki, V. V. and Dorogan, A.V., 2017. Excitonic polaritons in $ZnAs_2$ nanocrystals. *European Exhibition of Creativity and Innovation: Proceedings of the 9th ed. EUROINVENT, Iasi, Romania*, p.169.

[108] Kidari, O. and Chartrand, P., 2023. Thermodynamic Evaluation and Optimization of the As–Cd, As–Zn and As–Cd–Zn Systems. *Metallurgical and Materials Transactions B*, 54(5), pp.2793-2814. https://doi.org/10.1007/s11663-023-02875-5

[109] Syrbu, N.N., Stamov, I.G., Zalamai, V.V. and Dorogan, A., 2017. Excitonic polaritons of zinc diarsenide single crystals. *Physica B: Condensed Matter*, 506, pp.183-191. https://doi.org/10.1016/j.physb.2016.11.022

[110] Stamov, I.G., Tkachenko, D.V. and Strel'chuk, Y., 2022. Characteristics of Surface-Barrier Structures on Zinc Diarsenide with Hole Conductivity. *5th International Conference on Nanotechnologies and Biomedical Engineering: Proceedings of ICNBME-2021,Chisinau, Moldova*. *IFMBE Proceedings*, Springer, Cham, 87, pp.92-99. https://doi.org/10.1007/978-3-030-92328-0_13

[111] Cramer, C.J., 2004. *Essentials of Computational Chemistry: Theories and Models.* 2nd ed. England: John Wiley & Sons Ltd.

[112] Fermi, E., 1928. Eine statistische Methode zur Bestimmung einiger Eigenschaften des Atoms und ihre Anwendung auf die Theorie des periodischen Systems der Elemente. *Zeitschrift für Physik*, 48(1), pp.73-79. https://doi.org/10.1007/BF01351576

[113] Thomas, L.H., 1927. The calculation of atomic fields. *Mathematical Proceedings of the Cambridge Philosophical Society*, 23(5), pp.542-548. https://doi.org/10.1017/S0305004100011683

[114] Lewars, E.G., 2011. *Computational Chemistry: Introduction to the Theory and Applications of Molecular and Quantum Mechanics*. 2nd ed. Springer Dordrecht Heidelberg London New York. https://doi.org/10.1007/978-90-481-3862-3

[115] Jensen, F., 2007. *Introduction to Computational Chemistry*. 2nd ed. England: John Wiley & Sons Ltd.

[116] Kohn, W., 1999. Nobel Lecture: Electronic structure of matter-wave functions and density functionals. *Reviews of Modern Physics*, 71(5), pp.1253-1266. https://doi.org/10.1103/RevModPhys.71.1253

[117] Hohenberg, P. and Kohn, W., 1964. Inhomogeneous Electron Gas. *Physical Review*, 136(3B), pp.B864-B871.

https://doi.org/10.1103/PhysRev.136.B864

[118] Young, D.C., 2001. *Computational Chemistry: A Practical Guide for Applying Techniques to Real-World Problems.* John Wiley & Sons, Inc.

[119] Kohn, W. and Sham, L.J., 1965. Self-Consistent Equations Including Exchange and Correlation Effects. *Physical Review*, 140(4A), pp.A1133-A1138.
https://doi.org/10.1103/PhysRev.140.A1133

[120] Thijssen, J., 2012. *Computational Physics.* 2nd ed. UK: Cambridge University Press.

[121] Levine, I.N., 2014. *Quantum Chemistry.* 7th ed. USA: Pearson Prentice Hall.

[122] Ibach, H. and Luth, H., 1996. *Solid State Physics: An Introduction to Principles of Materials Science.* 2nd ed. Springer-Verlag Berlin Heidelberg.

[123] Slater, J.C. and Koster, G.F., 1954. Simplified LCAO Method for the Periodic Potential Problem. *Physical Review,* 94(6), pp.1498-1524.
https://doi.org/10.1103/PhysRev.94.1498

[124] Dovesi, R., Saunders, V.R., Roetti, C., Orlando, R., Zicovich-Wilson, C.M., Pascale, F., Civalleri, B., Doll, K., Harrison, N.M., Bush, I.J., D'Arco, P., Llunell, M. , Causà, M., Noël, Y., Maschio, L., Erba, A., Rérat, M., Casassa, S., 2017. *CRYSTAL17 User's Manual,* University of Torino, Torino.

[125] Fiolhais, C., Nogueira, F. and Marques, M. (Eds.), 2003. *A Primer in Density Functional Theory.* Springer-Verlag Berlin Heidelberg.

[126] Mulliken, R.S., 1955. Electronic Population Analysis on LCAOMO Molecular Wave Functions. I. *The Journal of Chemical Physics,* 23(10), pp.1833-1840.
https://doi.org/10.1063/1.1740588

[127] Segall, M.D., Shah, R., Pickard, C.J. and Payne, M.C., 1996. Population analysis of plane-wave electronic structure calculations of bulk materials. *Physical Review B,* 54(23), pp.16317-16320.
https://doi.org/10.1103/PhysRevB.54.16317

[128] Coulson, C.A., 1969. d Electrons and Molecular Bonding. *Nature,* 221(5186), pp.1106-1110.
https://doi.org/10.1038/2211106a0

[129] Louisnathan, S.J. and Gibbs, G.V., 1972. The Effect of Tetrahedral Angles on Si-O Bond Overlap Populations for Isolated Tetrahedra. *American Mineralogist,* 57(11-12), pp.1614-1642.

[130] Vinet, P., Ferrante, J., Rose, J.H. and Smith, J.R., 1987. Compressibility of Solids. *Journal of Geophysical Research: Solid Earth*, 92(B9), pp.9319-9325. https://doi.org/10.1029/JB092iB09p09319

[131] Vinet, P., Smith, J.R., Ferrante, J. and Rose, J.H., 1987. Temperature effects on the universal equation of state of solids. *Physical Review B*, 35(4), pp.1945-1953. https://doi.org/10.1103/PhysRevB.35.1945

[132] Poirier, J.P., 2000. *Introduction to the Physics of the Earth's Interior*. 2nd ed. Cambridge University Press.

[133] Birch, F., 1947. Finite Elastic Strain of Cubic Crystals. *Physical Review*, 71(11), pp.809-824. https://doi.org/10.1103/PhysRev.71.809

[134] Birch, F., 1952. Elasticity and constitution of the Earth's interior. *Journal of. Geophysical Research*, 57(2), pp.227-286. https://doi.org/10.1029/JZ057i002p00227

[135] Birch, F., 1978. Finite Strain Isotherm and Velocities for Single-Crystal and Polycrystalline NaCl at High Pressures and $300^{O}$ K. *Journal of Geophysical Research : Solid Earth*, 83(B3), pp.1257-1268. https://doi.org/10.1029/JB083iB03p01257

[136] Poirier, J.P. and Tarantola, A., 1998. A logarithmic equation of state. *Physics of the Earth and Planetary Interiors*, 109(1-2), pp.1-8. https://doi.org/10.1016/S0031-9201(98)00112-5

[137] Love, A.E.H., 1892. *A Treatise on the Mathematical Theory of Elasticity*. Cambridge University Press.

[138] Ting, T.C.T., 1996. *Anisotropic Elasticity: Theory and Applications*. Oxford University Press.

[139] Monkhorst, H.J. and Pack, J.D., 1976. Special points for Brillouin-zone integrations. *Physical Review B*, 13(12), pp.5188-5192. https://doi.org/10.1103/PhysRevB.13.5188

[140] Dovesi, R., Erba, A., Orlando, R., Zicovich-Wilson, C.M., Civalleri, B., Maschio, L., Rérat, M., Casassa, S., Baima, J., Salustro, S. and Kirtman, B., 2018. Quantum-Mechanical Condensed Matter Simulations with

CRYSTAL. *Wiley Interdisciplinary Reviews: Computational Molecular Science*, 8(4), p.e1360.
https://doi.org/10.1002/wcms.1360

[141] Dovesi, R., Pisani, C., Roetti, C., Causa, M. and Saunders V.R., 1989. CRYSTAL88, An Ab Initio All-Electron LCAO Hartree-Fock Program for Periodic Systems. *Quantum Chemistry Program Exchange*, QCPE Pgm N.577, Indiana: Indiana University, Bloomington.

[142] Pisani, C., Dovesi, R. and Roetti, C., 1988. *Hartree-Fock Ab Initio Treatment of Crystalline Systems, Lecture Notes in Chemistry Series.* Vol. 48, Heidelberg-Berlin: Springer-Verlag.
https://doi.org/10.1007/978-3-642-93385-1

[143] Dovesi R., Roetti C. and Saunders V. R., 1992. *CRYSTAL92 User's Manual.* Universita di Torino and SERC Daresbury Laboratory.

[144] Dovesi, R., Saunders, V. R., Roetti, C., Causa, M., Harrison, N. M., Orlando, R. and Apra, E., 1996. *CRYSTAL95 User's Manual*. Universita di Torino, Torino.

[145] Saunders, V. R., Dovesi, R., Roetti, C., Causa, M., Harrison, N. M., Orlando, R. and Zicovich-Wilson, C. M., 1998. *CRYSTAL98 User's Manual*. Universita di Torino, Torino.

[146] Saunders, V. R., Dovesi, R., Roetti, C., Orlando, R., Zicovich-Wilson, C. M., Harrison, N. M., Doll, K., Civalleri, B., Bush, I., D'Arco, Ph. and Llunell, M., 2003. *CRYSTAL03 User's Manual.* Universita di Torino, Torino.

[147] Dovesi, R., Saunders, V. R., Roetti, C., Orlando, R., Zicovich-Wilson, C. M., Pascale, F., Civalleri, B., Doll, K., Harrison, N. M., Bush, I. J., D'Arco, Ph. and Llunell, M., 2006. *CRYSTAL06 User's Manual*. Universita di Torino, Torino.

[148] Dovesi, R., Orlando, R., Civalleri, B., Roetti, C., Saunders, V.R. and Zicovich-Wilson, C.M., 2005. CRYSTAL: a computational tool for the *ab initio* study of the electronic properties of crystals. *Zeitschrift für Kristallographie-Crystalline Materials*, 220(5-6), pp.571-573.
https://doi.org/10.1524/zkri.220.5.571.65065

[149] Dovesi, R., Saunders, V.R., Roetti, C., Orlando, R., Zicovich-Wilson, C. M., Pascale, F., Civalleri, B., Doll, K., Harrison, N.M., Bush, I.J., D'Arco, Ph. and Llunell, M., 2009. *CRYSTAL09 User's Manual*, University of Torino, Torino.

[150] Dovesi, R., Orlando, R., Erba, A., Zicovich-Wilson, C.M., Civalleri, B., Casassa, S., Maschio, L., Ferrabone, M., De La Pierre, M., D'Arco, P., Noël, Y., Causà, M., Rérat, M. and Kirtman, B., 2014. CRYSTAL14: A Program for the *Ab Initio* Investigation of Crystalline Solids. *International Journal of Quantum Chemistry*, 114(19), pp.1287-1317. https://doi.org/10.1002/qua.24658

[151] Dovesi, R., Saunders, V.R., Roetti, C., Orlando, R., Zicovich-Wilson, C. M., Pascale, F., Civalleri, B., Doll, K., Harrison, N.M., Bush, I.J., D'Arco, Ph., Llunell, M., Caus`a, M. and No¨el, Y., 2014. *CRYSTAL14 User's Manual*, University of Torino, Torino.

[152] Erba, A., Desmarais, J.K., Casassa, S., Civalleri, B., Donà, L., Bush, I.J., Searle, B., Maschio, L., Edith-Daga, L., Cossard, A., Ribaldone, C., Ascrizzi, E., Marana, N.L., Flament, J.-P. and Kirtman B., 2023. CRYSTAL23: A Program for Computational Solid State Physics and Chemistry. *Journal of Chemical Theory and Computation*, 19(20), pp.6891-6932. https://doi.org/10.1021/acs.jctc.2c00958

[153] Dovesi, R., Saunders, V.R., Roetti, C., Orlando, R., Zicovich-Wilson, C. M., Pascale, F., Civalleri, B., Doll, K., Harrison, N.M., Bush, I.J., D'Arco, Ph., Llunell, M., Causa, M., Noel, Y., Maschio, L., Erba, A., Rerat, M., Casassa, S., Searle, B.G. and Desmarais J.K., 2022. *CRYSTAL23 User's Manual*. University of Torino, Torino.

[154] Broyden, C.G., 1965. A Class of Methods for Solving Nonlinear Simultaneous Equations. *Mathematics of Computation*, 19(92), pp.577-593. https://doi.org/10.1090/S0025-5718-1965-0198670-6

[155] Johnson, D.D., 1988. Modified Broyden's method for accelerating convergence in self-consistent calculations. *Physical Review B*, 38(18), pp.12807-12813. https://doi.org/10.1103/PhysRevB.38.12807

[156] Shanno, D.F., 1970. Conditioning of Quasi-Newton Methods for Function Minimization. *Mathematics of Computation*, 24(111), pp.647-656. https://doi.org/10.1090/S0025-5718-1970-0274029-X

[157] Broyden, C.G., 1970. The Convergence of a Class of Double-rank Minimization Algorithms 1. General Considerations. *IMA Journal of Applied Mathematics*, 6(1), pp.76-90.

https://doi.org/10.1093/imamat/6.1.76

[158] Broyden, C.G., 1970. The Convergence of a Class of Double-rank Minimization Algorithms: 2. The New Algorithm. *IMA Journal of Applied Mathematics*, 6(3), pp.222-231. https://doi.org/10.1093/imamat/6.3.222

[159] Fletcher, R., 1970. A new approach to variable metric algorithms. *The Computer Journal*, 13(3), pp.317-322. https://doi.org/10.1093/comjnl/13.3.317

[160] Goldfarb, D., 1970. A Family of Variable-Metric Methods Derived by Variational Means. *Mathematics of Computation*, 24(109), pp.23-26. https://doi.org/10.1090/S0025-5718-1970-0258249-6

[161] Pulay, P. and Fogarasi, G., 1992. Geometry optimization in redundant internal coordinates. *The Journal of Chemical Physics*, 96(4), pp.2856-2860. https://doi.org/10.1063/1.462844

[162] Zicovich-Wilson, C.M., San Román, M.L. and Ramírez-Solís, A., 2010. Mechanism of $F^-$ Elimination from Zeolitic D4R Units: A Periodic B3LYP Study on the Octadecasil Zeolite. *The Journal of Physical Chemistry C*, 114(7), pp.2989-2995. https://doi.org/10.1021/jp9088244

[163] Erba, A., Pisani, C., Casassa, S., Maschio, L., Schütz, M. and Usvyat, D., 2010. MP2 versus density-functional theory study of the Compton profiles of crystalline urea. *Physical Review B*, 81(16), p.165108. https://doi.org/10.1103/PhysRevB.81.165108

[164] Erba, A. and Pisani, C., 2012. Evaluation of the Electron Momentum Density of Crystalline Systems from *Ab Initio* Linear Combination of Atomic Orbitals Calculations. *Journal of Computational Chemistry*, 33(8), pp.822-831. https://doi.org/10.1002/jcc.22907

[165] Pisani, C., Erba, A., Casassa, S., Itou, M. and Sakurai, Y., 2011. Anisotropy of the electron momentum distribution in α-quartz investigated by Compton scattering and *ab initio* simulations. *Physical Review B*, 84(24), p.245102. https://doi.org/10.1103/PhysRevB.84.245102

[166] Pascale, F., Zicovich-Wilson, C.M., López Gejo, F., Civalleri, B., Orlando, R. and Dovesi, R., 2004. The Calculation of the Vibrational Frequencies of

Crystalline Compounds and Its Implementation in the CRYSTAL code. *Journal of Computational Chemistry*, 25(6), pp.888-897. https://doi.org/10.1002/jcc.20019

[167] Zicovich-Wilson, C.M., Pascale, F., Roetti, C., Saunders, V.R., Orlando, R. and Dovesi, R., 2004. Calculation of the Vibration Frequencies of α-Quartz: The Effect of Hamiltonian and Basis Set. *Journal of Computational Chemistry*, 25(15), pp.1873-1881. https://doi.org/10.1002/jcc.20120

[168] Ferrero, M., Rérat, M., Orlando, R. and Dovesi, R., 2008. Coupled perturbed Hartree-Fock for periodic systems: The role of symmetry and related computational aspects. *The Journal of Chemical Physics*, 128(1), p.014110. https://doi.org/10.1063/1.2817596

[169] Ferrero, M., Rérat, M., Orlando, R. and Dovesi, R., 2008. The Calculation of Static Polarizabilities of 1-3D Periodic Compounds. The Implementation in the CRYSTAL Code. *Journal of Computational Chemistry*, 29(9), pp.1450-1459. https://doi.org/10.1002/jcc.20905

[170] Ferrero, M., Rérat, M., Kirtman, B. and Dovesi, R., 2008. Calculation of first and second static hyperpolarizabilities of one-to three-dimensional periodic compounds. Implementation in the CRYSTAL code. *The Journal of Chemical Physics*, 129(24), p.244110. https://doi.org/10.1063/1.3043366

[171] Perger, W.F., Criswell, J., Civalleri, B. and Dovesi, R., 2009. Ab-initio calculation of elastic constants of crystalline systems with the CRYSTAL code. *Computer Physics Communications*, 180(10), pp.1753-1759. https://doi.org/10.1016/j.cpc.2009.04.022

[172] Erba, A., Mahmoud, A., Orlando, R. and Dovesi, R., 2014. Elastic properties of six silicate garnet end members from accurate ab initio simulations. *Physics and Chemistry of Minerals*, 41(2), pp.151-160. https://doi.org/10.1007/s00269-013-0630-4

[173] Erba, A., Mahmoud, A., Belmonte, D. and Dovesi, R., 2014. High pressure elastic properties of minerals from *ab initio* simulations: The case of pyrope,

grossular and andradite silicate garnets. *The Journal of Chemical Physics*, 140(12), p.124703.
https://doi.org/10.1063/1.4869144

[174] Erba, A., Ferrabone, M., Baima, J., Orlando, R., Rérat, M. and Dovesi, R., 2013. The vibration properties of the (n, 0) boron nitride nanotubes from *ab initio* quantum chemical simulations. *The Journal of Chemical Physics*, 138(5), p.054906.
https://doi.org/10.1063/1.4788831

[175] Erba, A. and Dovesi, R., 2013. Photoelasticity of crystals from theoretical simulations. *Physical Review B*, 88(4), p.045121.
https://doi.org/10.1103/PhysRevB.88.045121

[176] Erba, A., Ruggiero, M.T., Korter, T.M. and Dovesi, R., 2015. Piezo-optic tensor of crystals from quantum-mechanical calculations. *The Journal of Chemical Physics*, 143(14), p.144504.
https://doi.org/10.1063/1.4932973

[177] Noel, Y., Zicovich-Wilson, C.M., Civalleri, B., D'arco, Ph. and Dovesi, R., 2001. Polarization properties of ZnO and BeO: An *ab initio* study through the Berry phase and Wannier functions approaches. *Physical Review B*, 65(1), p.014111.
https://doi.org/10.1103/PhysRevB.65.014111

[178] Erba, A., El-Kelany, Kh.E., Ferrero, M., Baraille, I. and Rérat, M., 2013. Piezoelectricity of $SrTiO_3$: An *ab initio* description. *Physical Review B*, 88(3), p.035102.
https://doi.org/10.1103/PhysRevB.88.035102

[179] Searle, B.G., 2001. DL Visualize. *Computer Physics Communications*, 137(1), pp.25-32.
https://doi.org/10.1016/S0010-4655(01)00170-9

[180] Beata, G., Perego, G. and Civalleri, B., 2019. CRYSPLOT: A New Tool to Visualize Physical and Chemical Properties of Molecules, Polymers, Surfaces, and Crystalline Solids. *Journal of Computational Chemistry*, 40(26), pp.2329-2338.
https://doi.org/10.1002/jcc.25858

[181] Gaillac, R., Pullumbi, P. and Coudert, F.X., 2016. ELATE: An open-source online application for analysis and visualization of elastic tensors. *Journal of Physics: Condensed Matter*, 28(27), p.275201. https://doi.org/10.1088/0953-8984/28/27/275201

[182] http://progs.coudert.name/elate

[183] Marmier, A., Lethbridge, Z.A.D., Walton, R.I., Smith, C.W., Parker, S.C. and Evans, K.E., 2010. ElAM: A computer program for the analysis and representation of anisotropic elastic properties. *Computer Physics Communications*, 181(12), pp.2102-2115. https://doi.org/10.1016/j.cpc.2010.08.033

[184] Voigt, W., 1928. *Lehrbuch der Kristallphysik*. BG Teubner, Leipzig und Berlin.

[185] Reuss, A. and Angew, Z., 1929. Berechnung der Fliesgrenze von Mischkristallen auf Grund der Plastizatsberechnung fur Einkristalle. *Journal of Applied Mathematics and Mechanics*, 9(1), pp.49–58. https://doi.org/10.1002/zamm.19290090104

[186] Hill, R., 1952. The Elastic Behaviour of a Crystalline Aggregate. *Proceedings of the Physical Society, Section A*, 65(5), p.349-354. https://doi.org/10.1088/0370-1298/65/5/307

[187] Perdew, J.P., Burke, K. and Ernzerhof, M., 1996. Generalized Gradient Approximation Made Simple. *Physical Review Letters*, 77(18), pp.3865- 3868. https://doi.org/10.1103/PhysRevLett.77.3865

[188] Perdrew, J.P., Burke, K. and Ernzerhof, M., 1997. Erratum: Generalized Gradient Approximation Made Simple [*Physical Review Letters*, 77, 3865 (1996)]. *Physical Review Letters*, 78(7), p.1396. https://doi.org/10.1103/PhysRevLett.78.1396

[189] Perdew, J.P., Ruzsinszky, A., Csonka, G.I., Vydrov, O.A., Scuseria, G.E., Constantin, L.A., Zhou, X. and Burke, K., 2008. Restoring the Density-Gradient Expansion for Exchange in Solids and Surfaces. *Physical Review Letters*, 100(13), p.136406. https://doi.org/10.1103/PhysRevLett.100.136406

[190] Perdew, J.P., Ruzsinszky, A., Csonka, G.I., Vydrov, O.A., Scuseria, G.E., Constantin, L.A., Zhou, X. and Burke, K., 2009. Erratum: Restoring the Density-Gradient Expansion for Exchange in Solids and Surfaces [*Physical*

*Review Letters*, 100(13), p.136406 (2008)]. *Physical Review Letters*, 102(3), p.039902.
https://doi.org/10.1103/PhysRevLett.102.039902

[191] Perdew, J.P. and Yue, W., 1986. Accurate and simple density functional for the electronic exchange energy: Generalized gradient approximation. *Physical Review B*, 33(12), pp.8800-8802.
https://doi.org/10.1103/PhysRevB.33.8800

[192] Perdew, J.P. and Yue, W., 1989. Erratum: Accurate and simple density functional for the electronic exchange energy: Generalized gradient approximation [*Physical Review B*, 33(12), pp.8800-8802 (1986)] *Physical Review B*, 40(5), p. 3399.
https://doi.org/10.1103/PhysRevB.40.3399

[193] Perdew, J.P. and Wang, Y., 1992. Accurate and simple analytic representation of the electron-gas correlation energy. *Physical Review B*, 45(23), pp.13244-13249.
https://doi.org/10.1103/PhysRevB.45.13244

[194] Perdew, J.P. and Wang, Y., 2018. Erratum: Accurate and simple analytic representation of the electron-gas correlation energy [*Physical Review B*, *45*(23), pp.13244-13249 (1992)] *Physical Review B*, 98(7), p.079904.
https://doi.org/10.1103/PhysRevB.98.079904

[195] Perdew, J.P., Chevary, J.A., Vosko, S.H., Jackson, K.A., Pederson, M.R., Singh, D.J. and Fiolhais, C., 1992. Atoms, molecules, solids, and surfaces: Applications of the generalized gradient approximation for exchange and correlation. *Physical Review B*, 46(11), pp.6671-6687.
https://doi.org/10.1103/PhysRevB.46.6671

[196] Perdew, J.P., Chevary, J.A., Vosko, S.H., Jackson, K.A., Pederson, M.R., Singh, D.J. and Fiolhais, C., 1993. Erratum: Atoms, molecules, solids, and surfaces: Applications of the generalized gradient approximation for exchange and correlation [*Physical Review B*, *46*(11), pp.6671-6687 (1992)] *Physical Review B*, 48(7), p.4978.
https://doi.org/10.1103/PhysRevB.48.4978.2

[197] Dirac, P.A.M., 1930. Note on exchange phenomena in the Thomas atom. *Mathematical Proceedings of the Cambridge Philosophical Society*, 26(3), pp. 376-385.

https://doi.org/10.1017/S0305004100016108

[198] Perdew, J.P. and Zunger, A., 1981. Self-interaction correction to density-functional approximations for many-electron systems. *Physical Review B*, 23(10), pp.5048-5079.
https://doi.org/10.1103/PhysRevB.23.5048

[199] Vosko, S.H., Wilk, L. and Nusair, M., 1980. Accurate spin-dependent electron liquid correlation energies for local spin density calculations: a critical analysis. *Canadian Journal of Physics*, 58(8), pp.1200-1211.
https://doi.org/10.1139/p80-159

[200] Becke, A.D., 1993. Density-functional thermochemistry. III. The role of exact exchange. *The Journal of Chemical Physics*, 98(7) 5648-5652.
https://doi.org/10.1063/1.464913

[201] Perdew, J.P., 1991. Unified theory of exchange and correlation beyond the local density approximation. *Electronic Structure of Solids' 91: Proceedings of the* 75, (Eds. Ziesche, P. and Eschrig, H.), Akademie Verlag, Berlin.

[202] Stephens, P.J., Devlin, F.J., Chabalowski, C.F. and Frisch, M.J., 1994. *Ab Initio* Calculation of Vibrational Absorption and Circular Dichroism Spectra Using Density Functional Force Fields. *The Journal of Physical Chemistry*, 98(45), pp.11623-11627.
https://doi.org/10.1021/j100096a001

[203] Lee, C., Yang, W. and Parr, R.G., 1988. Development of the Colle-Salvetti correlation-energy formula into a functional of the electron density. *Physical Review B*, 37(2), pp.785-789.
https://doi.org/10.1103/PhysRevB.37.785

[204] Adamo, C. and Barone, V., 1999. Toward reliable density functional methods without adjustable parameters: The PBE0 model. *The Journal of Chemical Physics*, 110(13), pp.6158-6170.
https://doi.org/10.1063/1.478522

[205] Perdew, J.P., Ernzerhof, M. and Burke, K., 1996. Rationale for mixing exact exchange with density functional approximations. *The Journal of Chemical Physics*, 105(22), pp.9982-9985.
https://doi.org/10.1063/1.472933

[206] Ernzerhof, M. and Scuseria, G.E., 1999. Assessment of the Perdew–Burke–Ernzerhof exchange-correlation functional. *The Journal of Chemical Physics*, 110(11), pp.5029-5036. https://doi.org/10.1063/1.478401

[207] Ernzerhof, M., Perdew, J.P. and Burke, K., 1997. Coupling-Constant Dependence of Atomization Energies. *International Journal of Quantum Chemistry*, 64(3), pp.285-295. https://doi.org/10.1002/(SICI)1097-461X(1997)64:3%3C285::AID-QUA2%3E3.0.CO;2-S

[208] Krukau, A.V., Vydrov, O.A., Izmaylov, A.F. and Scuseria, G.E., 2006. Influence of the exchange screening parameter on the performance of screened hybrid functionals. *The Journal of Chemical Physics*, 125(22), p.224106. https://doi.org/10.1063/1.2404663

[209] Heyd, J., Scuseria, G.E. and Ernzerhof, M., 2003. Hybrid functionals based on a screened Coulomb potential. *The Journal of Chemical Physics*, 118(18), pp.8207-8215. https://doi.org/10.1063/1.1564060

[210] Heyd, J., Scuseria, G.E. and Ernzerhof, M., 2006. Erratum: Hybrid functionals based on a screened Coulomb potential [*The Journal of Chemical Physics*, 118(18), pp.8207-8215 (2003)]. *The Journal of Chemical Physics*, 124(21), p.219906. https://doi.org/10.1063/1.2204597

[211] Heyd, J., Peralta, J.E., Scuseria, G.E. and Martin, R.L., 2005. Energy band gaps and lattice parameters evaluated with the Heyd-Scuseria-Ernzerhof screened hybrid functional. *The Journal of Chemical Physics*, 123(17), p.174101. https://doi.org/10.1063/1.2085170

[212] Paier, J., Marsman, M., Hummer, K., Kresse, G., Gerber, I.C. and Ángyán, J.G., 2006. Screened hybrid density functionals applied to solids. *The Journal of Chemical Physics*, 124(15), p.154709. https://doi.org/10.1063/1.2187006

[213] Paier, J., Marsman, M., Hummer, K., Kresse, G., Gerber, I.C. and Ángyán, J.G., 2006. Erratum: Screened hybrid density functionals applied to solids

[*The Journal of Chemical Physics*, 124, p.154709 (2006)]. *The Journal of Chemical Physics*, 124(24), p.249901.
https://doi.org/10.1063/1.2403866

[214] Heyd, J. and Scuseria, G.E., 2004. Assessment and validation of a screened Coulomb hybrid density functional. *The Journal of Chemical Physics*, 120(16), pp.7274-7280.
https://doi.org/10.1063/1.1668634

[215] Heyd, J. and Scuseria, G.E., 2004. Efficient hybrid density functional calculations in solids: Assessment of the Heyd–Scuseria–Ernzerhof screened Coulomb hybrid functional. *The Journal of Chemical Physics*, 121(3), pp.1187-1192.
https://doi.org/10.1063/1.1760074

[216] Vilela Oliveira, D., Laun, J., Peintinger, M.F. and Bredow, T., 2019. BSSE-Correction Scheme for Consistent Gaussian Basis Sets of Double-and Triple-Zeta Valence with Polarization Quality for Solid-State Calculations. *Journal of Computational Chemistry*, 40(27), pp.2364-2376.
https://doi.org/10.1002/jcc.26013

[217] Zicovich-Wilson, C.M., Bert, A., Roetti, C., Dovesi, R. and Saunders, V.R., 2002. Characterization of the electronic structure of crystalline compounds through their localized Wannier functions. *The Journal of Chemical Physics*, 116(3), pp.1120-1127.
https://doi.org/10.1063/1.1425406

[218] Dou, Y., Egdell, R.G., Law, D.S.L., Harrison, N.M. and Searle, B.G., 1998. An experimental and theoretical investigation of the electronic structure of CdO. Journal of Physics: Condensed Matter, 10(38), pp.8447-8458.
https://doi.org/10.1088/0953-8984/10/38/006

[219] Rajpurohit, S., Kabra, K. and Sharma, G., 2020. DFT investigation of electronic and elastic properties of α-$CdP_2$. *Materials Research Express*, 7(9), p.095901.
https://doi.org/10.1088/2053-1591/abb0ad

[220] Hofmeister, A.M., 1991. Pressure Derivatives of the Bulk Modulus. *Journal of Geophysical Research: Solid Earth*, 96(B13), pp.21893-21907.
https://doi.org/10.1029/91JB02157

[221] Fan, C.L., Cheng, X.L. and Zhang, H., 2009. First-principles study of the structural and electronic properties of the α modification of zinc diphosphide. *Physica Status Solidi (b)*, 246(1), pp.77-81. https://doi.org/10.1002/pssb.200844007

[222] Zanin, I.E., Aleinikova, K.B. and Antipin, M.Y., 2003. Analysis of Chemical Bonding in the α and β Modifications of Zinc Diphosphide from X-ray Diffraction Data. *Crystallography Reports*, 48(2), pp.199-204. https://doi.org/10.1134/1.1564195

[223] Rajpurohit S. and Sharma G., 2023. DFT investigation of structural and dielectric properties of monoclinic $ZnAs_2$. *National Conference on Recent Advances in Science and Technology: Proceedings of NCRAST 2023, Kota,*Vital Biotech Publication, pp.252-256

[224] Setyawan, W. and Curtarolo, S., 2010. High-throughput electronic band structure calculations: Challenges and tools. *Computational Materials Science, 49*(2), pp.299-312. https://doi.org/10.1016/j.commatsci.2010.05.010

[225] Pisani, C. (ed.), 1996. *Lecture Notes in Chemistry: Quantum-Mechanical Ab-initio Calculation of the Properties of Crystalline Materials.* Vol. 67, Heidelberg-Berlin: Springer-Verlag. https://doi.org/10.1007/978-3-642-61478-1

[226] Jain, A., Ong, S.P., Hautier, G., Chen, W., Richards, W.D., Dacek, S., Cholia, S., Gunter, D., Skinner, D., Ceder, G. and Persson, K.A., 2013. Commentary: The Materials Project: A materials genome approach to accelerating materials innovation. *APL materials, 1*(1), p. 011002 https://doi.org/10.1063/1.4812323

[227] Data retrieved from the Materials Project for $CdP_2$ (mp-402) from database version v2023.11.1. https://doi.org/10.17188/1207767

[228] Sobolev, V.V. and Syrbu, N.N., 1971. Anisotropy of Edge Absorption and Photoluminescence of Tetragonal $ZnP_2$ and $CdP_2$ Single Crystals. *Physica Status Solidi (b),*43(1), pp.K87-K91 https://doi.org/10.1002/pssb.2220430168

[229] Soshnikov, L.E., Trukhan, V.M., Golyakevich, T.V. and Soshnikova, H.L., 2005. Elastic and Dielectric Properties of $A^{II}B_2^V$ (A= Cd or Zn, B= P or As) Single Crystals. Crystallography Reports, 50 (Suppl.1), pp.S37-S45. https://doi.org/10.1134/1.2133970

[230] F. Mouhat, F.X. Coudert, Necessary and sufficient elastic stability conditions in various crystal systems. Phys. Rev. B, 90 (22) (2014) 224104. https://doi.org/10.1103/PhysRevB.90.224104

[231] Pugh, S.F., 1954. XCII. Relations between the Elastic Moduli and the Plastic Properties of Polycrystalline Pure Metals. *The London, Edinburgh, and Dublin Philosophical Magazine and Journal of Science*, 45(367), pp.823-843. https://doi.org/10.1080/14786440808520496

[232] Chung, D.H. and Buessem, W.R., 1967. The Elastic Anisotropy of Crystals. *Journal of Applied Physics*, 38(5), pp.2010-2012. https://doi.org/10.1063/1.1709819

[233] Chung, D.H. and Buessem, W.R., 1968. Anisotropy in Single Crystal Refractory Compounds: Vol. 2. (Eds. Vahldiek, F.W. and Mersol, S.A.), New York: Plenum Press. pp. 217–246

[234] Ranganathan, S.I. and Ostoja-Starzewski, M., 2008. Universal Elastic Anisotropy Index. *Physical Review Letters*, 101(5), p.055504. https://doi.org/10.1103/PhysRevLett.101.055504

[235] Yang, Z., Wang, X., Liu, L., Yang, S. and Su, X., 2011. Density functional theory studies on elastic and electronic properties of tetragonal $ZnP_2$. *Solid State Sciences*, 13(8), pp.1604-1607. https://doi.org/10.1016/j.solidstatesciences.2011.06.008

[236] Kikegawa, T. and Iwasaki, H., 1983. An X-ray Diffraction Study of Lattice Compression and Phase Transition of Crystalline Phosphorus. *Acta Crystallographica Section B*, 39(2), pp.158-164. https://doi.org/10.1107/S0108768183002220

[237] Rajpurohit, S. and Sharma, G., 2023. Ab-initio Investigation of Elastic Properties of Monoclinic $ZnAs_2$ Crystal. *Journal of Condensed Matter*, 1(02), pp.56-60. https://doi.org/10.61343/jcm.v1i02.34

[238] Balazuk ,V .N., Bogachev, G. U., Kuryachii, V. Y., Marenkin, S. F., Mihalchenko, V. P., Pishikov, D. I. and Rarenko, A. I., 1982. *Solid State Physics (in Russian)*, 33(9), p. 2777.

## *RESEARCH PUBLICATIONS IN REFERRED JOURNALS*

**(i)** Paper Title: *DFT investigation of electronic and elastic properties of α-$CdP_2$.*
Authors: S Rajpurohit, K Kabra and G Sharma
Published on 02.09.2020
Journal: Materials Research Express, Vol. 7, No. 09
(Journal indexed in Web of Science)
ISSN: 2053-1591
Publisher: IOP Publishing Ltd., United Kingdom
DOI: https://dx.doi.org/10.1088/2053-1591/abb0ad

**(ii)** Paper Title: *Ab-initio Investigation of Elastic Properties of Monoclinic $ZnAs_2$ Crystal.*
Authors: S Rajpurohit and G Sharma
Published on 01.12.2023
Journal: Journal of Condensed Matter, Vol. 1, No. 02
(Peer Reviewed and Referred Journal)
ISSN: 2583-9152
Publisher: Condensed Matter Research Society, India
DOI: https://doi.org/10.61343/jcm.v1i02.34

## *PAPER PRESENTATIONS IN CONFERENCES / SEMINARS &*

## *CONFERENCES / SEMINARS / WEBINARS ETC. ATTENDED*

### *Paper Presented (by Sushil Rajpurohit) in Conferences & Attended Conferences*

(i) Presented paper title: *DFT Investigation of Structural and Dielectric Properties of Monoclinic $ZnAs_2$*
Authors: S Rajpurohit and G Sharma
National Conference on Recent Advances in Science and Technology (NCRAST- 2023)
Venue: Department of Chemistry, Government College Kota
Date 6th to 7th October 2023

(ii) Presented paper title: *Ab-initio Investigation of Elastic Properties of Monoclinic $ZnAs_2$ Crystal*
Authors: S Rajpurohit and G Sharma
4th International Conference on Condensed Matter & Applied Physics (ICC 2023)
Venue: Engineering College, Bikaner
Date 9th to10th October 2023

(iii) Presented paper title: *Ab-Initio Investigation of Dielectric Properties of $\alpha$-$CdP_2$*
*Authors: S Rajpurohit and G Sharma*
XXXXII Annual National Conference of the Indian Council of Chemists
Venue: University of Kota, Kota
Date 20th to 22nd December 2023

### *Workshop Attended*

A Workshop on *Academic Ethics and Integrity*
Venue: University of Kota, Kota
Date 27th July 2017

IOP Publishing Mater. Res. Express 7 (2020) 095901 https://doi.org/10.1088/2053-1591/abb0ad

Materials Research Express

PAPER

# DFT investigation of electronic and elastic properties of $\alpha$ -$CdP_2$

**S Rajpurohit**[1], **K Kabra**[2] and **G Sharma**[2]

[1] School of Science and Technology, Vardhman Mahaveer Open University, Kota 324010, India
[2] Department of Pure and Applied Physics, University of Kota, Kota 324005, India

**E-mail:** sushilrajpurohit21@gmail.com

**Keywords:** $CdP_2$, *ab initio*, electronic structure, elastic properties, EOS, Mulliken population

OPEN ACCESS

RECEIVED
12 March 2020

REVISED
7 August 2020

ACCEPTED FOR PUBLICATION
19 August 2020

PUBLISHED
2 September 2020



## Abstract

The energy bands, density of states, charge density, Mulliken population, equation of state and elastic properties of $\alpha$-$CdP_2$ have been studied. Exchange correlation functional PBEsol is utilized in this study. The optimized equilibrium lattice parameters of the conventional cell have been obtained. The present investigation indicates the existence of an indirect band gap of 1.76 eV in $\alpha$-$CdP_2$ crystal. Elastic calculations show the mechanical stability of the alpha phase of $CdP_2$ crystal. This work provides an analysis of directional Young's modulus and linear compressibility for $\alpha$-$CdP_2$. The study of the elastic anisotropy parameters shows that the alpha phase has a definite elastic anisotropy. The calculated Debye temperature of $\alpha$-$CdP_2$ is 288.1 K.

## 1. Introduction

Cadmium diphosphide (II-$V_2$ group semiconducting compound) is reported to be a good feasible material for device application in the field of optoelectronics [1–3] and thermal sensors [4]. The optical properties of $CdP_2$ enable it to be used in the fabrication of solar cells [5]. $CdP_2$ is also useful as a dopant compound for the fabrication of nGaAs/InP PIN photodetector arrays by the metal-organic chemical vapor deposition technique [6]. $CdP_2$ exists in two different crystalline phases, namely alpha and beta [7]. The alpha phase of $CdP_2$ is an orthorhombic structure at room temperature [7]. The $\alpha$-$CdP_2$ crystal structure has a space group $Pna2_1$ with four formula units in the conventional unit cell [8]. A pronounced structural character in the alpha phase of $CdP_2$ is a helical $^1_\infty[P^-]$ -chain coordinated to cadmium ions [7]. The peculiarity of the $\alpha$-$CdP_2$ structure is chains of P atoms existing parallel to each other in the ***c*** direction in the crystal [9]. DFT calculation showed the piezoelectricity in the alpha phase of $CdP_2$ [10–12]. This piezoelectric characteristic opens the doors for the future possibility of using $\alpha$-$CdP_2$ in designing piezoelectric devices such as piezoelectric sensors, transducers, etc. The piezoelectric effect is closely related to basic mathematical formulations based on elastic stiffness constants and dielectric susceptibility. Our elastic characterization and interpretation may get considerable practical utility in the field of piezoelectric device technology for future research. The experimental and theoretical investigations of tetragonal $\beta$-$CdP_2$ have been carried out by several researchers [13–16]. To the best of our knowledge, thorough experimental and theoretical investigations of the alpha phase of $CdP_2$ have not yet been reported. The first principle method within density functional theory has been applied to explore the structural properties, energy bands, density of states, charge density, Mulliken population [17] and elastic properties of $\alpha$-$CdP_2$. Our present *ab initio* study is able to explore the unrevealed properties of $\alpha$-$CdP_2$. Our attempt to fill the existing research gap in the study of the alpha phase of $CdP_2$ crystal is likely to be advantageous for researchers to carry out further investigations for application in optoelectronics and piezoelectric device technologies. The article thereon is organized as follows: In section 2, computational techniques are described. This is followed by results and discussion in section 3. Finally, we discuss conclusions in section 4.

## 2. Computational details

In this study, all the calculations are performed with CRYSTAL Program [18, 19] which is an *ab initio* quantum mechanical program. CRYSTAL Program (periodic *ab initio* HF and DFT code) uses a localized Gaussian type

**Table 1.** The lattice parameters ($a$, $b$ and $c$ in Å) and volume $V$ (Å$^3$) of the conventional cell of $\alpha$-$CdP_2$.

| | Scheme | $a$ | $b$ | $c$ | $V$ |
|---|---|---|---|---|---|
| Present work | PBEsol | 10.0051 | 5.4924 | 5.1603 | 283.5689 |
| Exp.[a] | | 9.90 | 5.408 | 5.171 | 276.85 |
| Other work[b] | | | | | 286.0 |

[a] Reference [8].
[b] Reference [15].

**Table 2.** The fractional coordinates of the nonequivalent atoms in the unit cell of $\alpha$-$CdP_2$.

| Atom | Fractional coordinates | | | | | | | | |
|---|---|---|---|---|---|---|---|---|---|
| | Present work (PBEsol scheme) | | | Exp.[a] | | | Other work[b] | | |
| | $X/a$ | $Y/b$ | $Z/c$ | $X/a$ | $Y/b$ | $Z/c$ | $X/a$ | $Y/b$ | $Z/c$ |
| Cd | 0.1502 | 0.1050 | 0.2621 | 0.1529 | 0.1016 | 0.2606 | 0.1529 | 0.1011 | 0.2606 |
| P (I) | 0.1222 | 0.4441 | –0.3924 | 0.1186 | 0.4458 | 0.5850 | 0.1185 | 0.4442 | 0.5957 |
| P (II) | –0.0091 | 0.2722 | –0.0916 | –0.0074 | 0.2697 | –0.0676 | –0.0064 | 0.2693 | –0.1036 |

[a] Reference [8].
[b] Reference [9].

basis set to form the sets of Bloch functions. In this computational work, the DFT exchange-correlation functional GGA (Generalized Gradient Approximation) is implemented. The study of geometrical optimization, EOS (equation of state), bands, DOS (density of states), Mulliken population and elastic constants is carried out with PBEsol [20] method. The basis sets (for Cd and P atoms) have been employed from CRYSTAL-basis set library of Torino group [18, 19]. We use the basis set of 36 orbitals for Cd atom [21] and the basis set of 18 orbitals for P atom [22]. The calculations are performed using an $8 \times 8 \times 8$ Monkhorst-Pack **k**-point mesh [23] that corresponds to 125 **k**-points in the irreducible Brillouin zone (IBZ). The SCF convergence threshold on the total energy is set to $10^{-10}$ Hartree. The BROYDEN parameter [18, 19, 24, 25] is employed to achieve the rapid convergence of the self-consistent iterations. The Fock/Kohn–Sham matrix mixing factor (FMIXING) [18, 19] of 40% has become useful for the calculations of geometry optimization. The optimized structure is utilized to determine bulk modulus and its first pressure derivative by deploying the EOS within $\pm$8% variation of the volume of optimized geometry. Furthermore, electronic and elastic properties [26, 27] are investigated at the equilibrium volume. The magnitude of the strain step for elastic calculations is 0.01. The unit cell is drawn using DLV software [28]. We use a web-oriented tool CRYSPLOT [29] for charge density and energy band structures.

## 3. Results and discussion

### 3.1. Structural details

The structure of $\alpha$-$CdP_2$ comes under the orthorhombic space group $Pna2_1$ with approximate values of lattice parameters $a = 9.90$ Å, $b = 5.408$ Å and $c = 5.171$ Å [8]. Its unit cell consists of four Cd and eight P atoms [8]. Using the available geometry of $\alpha$-$CdP_2$ [8], we have obtained the optimized lattice parameters and fractional coordinates of the atoms for the unit cell of $\alpha$-$CdP_2$ as shown in the tables 1 and 2. The deviations in the calculated lattice parameters ($a$, $b$ and $c$) from the experimental values [8] are within 1.6% and deviation in conventional cell volume is 2.43%. From table 1, it is obvious that our calculation of cell volume of $\approx$283.57 Å$^3$ is in accordance with other DFT work [15] with a small deviation of 0.86%. Thus, our computed results are in good agreement with the other reported results in tables 1 and 2. The unit cell of $\alpha$-$CdP_2$ with optimized lattice parameters is shown in figure 1. There exist deformed tetrahedral bonds [8] as depicted in figure 1. Each cadmium atom is bonded to its four nearest phosphorus atoms. It is also evident from figure 1 that each P atom is bonded to two nearest Cd atoms and two nearest P atoms. Table 5 shows that atom $P_5$ (nonequivalent atom P-I) has the first four nearest neighbors $P_{10}$, $P_9$, $Cd_3$ and $Cd_1$ atoms. Atom $P_9$ (nonequivalent atom P-II) has the first four nearest neighbors $P_6$, $P_5$, $Cd_1$ and $Cd_2$ atoms.

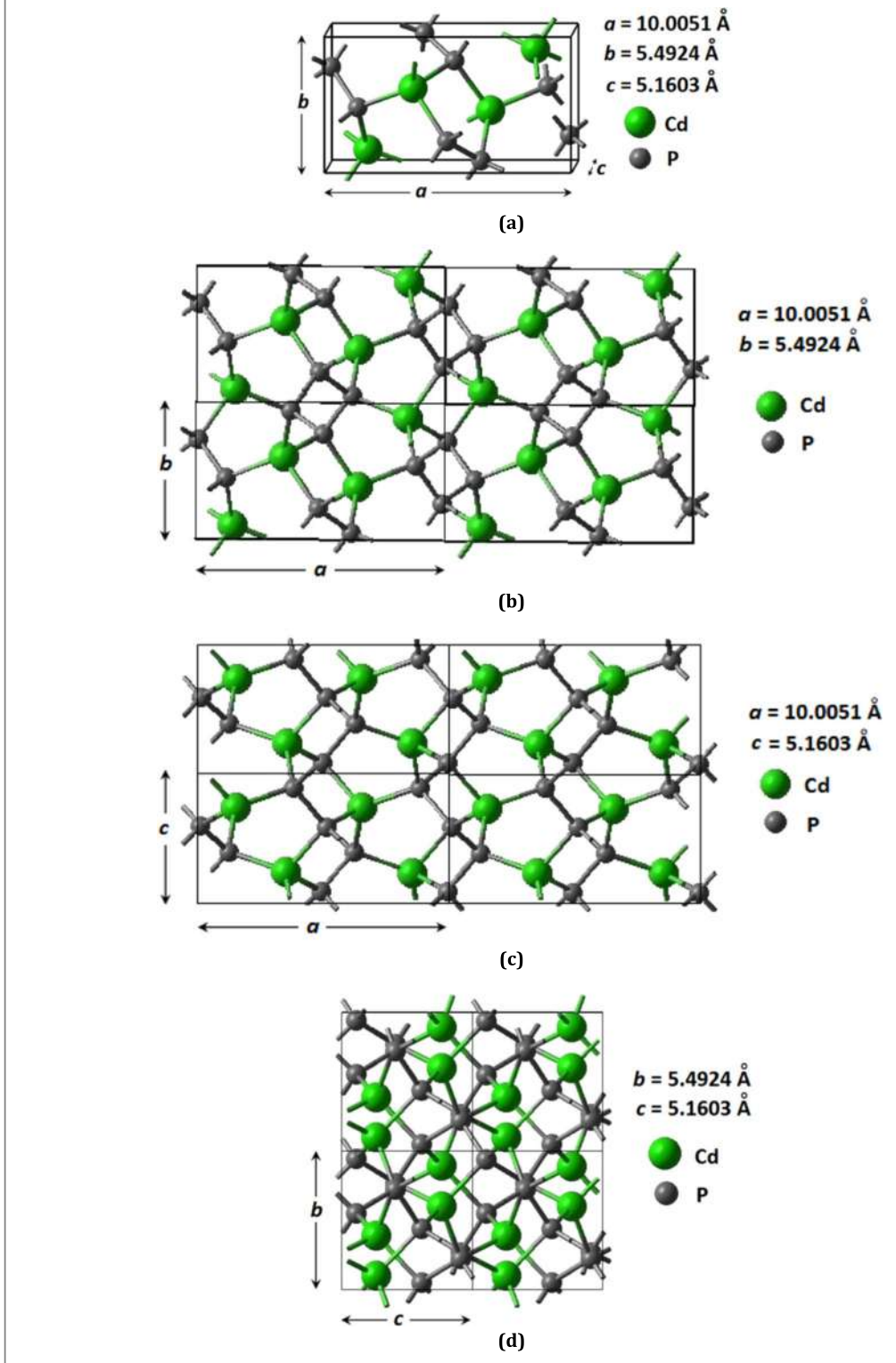


**Figure 1.** Schematic representation of the crystal structure of $\alpha$-$CdP_2$. The lengths *a, b* and *c* are lattice parameters. (a) Schematic 3D view of the conventional cell of $\alpha$-$CdP_2$. (b) Side view (*ab* plane) of $\alpha$-$CdP_2$ crystal structure. (c) Side view (*ac* plane) of $\alpha$-$CdP_2$ crystal structure. (d) Side view (*bc* plane) of $\alpha$-$CdP_2$ crystal structure.

### 3.2. Equation of state

In this study, the EOS computations for the alpha phase are performed using its computed optimized lattice parameters and fractional coordinates of atoms. The isothermal bulk modulus $B_0$ and its first pressure derivative $B'_0$ are computed using Vinet [30], Poirier-Tarantola [31] and Birch-Murnaghan [32] EOSs. These estimated values of $B_0$ and $B'_0$ are shown in table 3. In this present work, it is evident from table 3 that our computed values of $B_0$ and $B'_0$ of $\alpha$-$CdP_2$ at zero pressure with Vinet, Poirier-Tarantola and Birch-Murnaghan EOSs are ≈57.88 GPa and ≈3.94, respectively. Almost the same findings each for $B_0$, $B'_0$ and $V_0$ (equilibrium

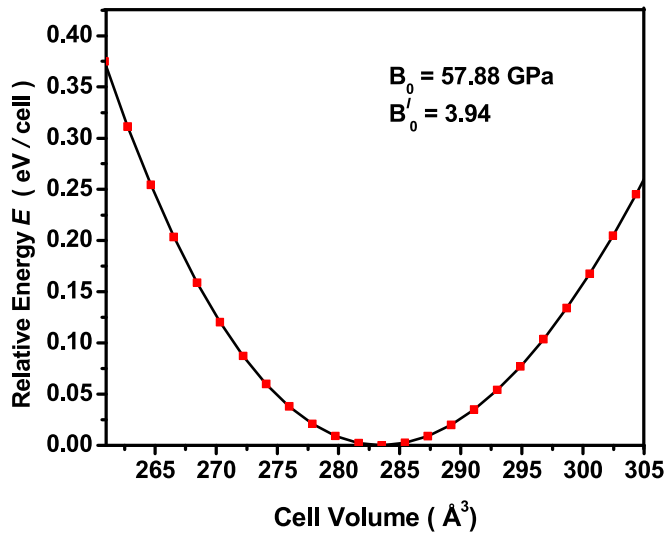


**Figure 2.** The variation of relative energy $E$ (per unit cell) of $\alpha$-$CdP_2$ with its cell volume taking the minimal value in the set of calculations as zero. The curve shows the Vinet EOS fits the computed data points (■) in the approximate range of 261 Å$^3$ to 305 Å$^3$.

**Table 3.** Bulk moduli ($B_0$), their first pressure derivatives ($B'_0$) and equilibrium cell volumes ($V_0$) of $\alpha$-$CdP_2$ at zero pressure using PBEsol scheme.

| | EOS method | $B_0$ (GPa) | $B'_0$ | $V_0$ (Å$^3$) |
|---|---|---|---|---|
| Present work | Vinet | 57.88 | 3.94 | 283.5264 |
| Present work | Poirier-Tarantola | 57.92 | 3.94 | 283.5254 |
| Present work | Birch-Murnaghan | 57.83 | 3.93 | 283.5277 |

cell volume) are obtained using these three EOS schemes. For the unit cell of the alpha $CdP_2$, with respect to minimum energy, the curve of relative energy $E$ (per unit cell) against its cell volume is plotted by means of Vinet EOS as shown in figure 2. The quantities $B_0$ and $B'_0$ are not mere coefficients in the equation of states, furthermore, they are physical characteristics of the materials which depend on the structural composition of the materials [33]. The most common typical range of $B'_0$ for solid materials is from 2 to 6 [33], so obtained value 3.94 of $B'_0$ for $\alpha$-$CdP_2$ is quite physically reasonable in this study.

### 3.3. Band structure and DOS

A study of electronic structure and density of states is useful in the determination of the semiconducting properties of a material. In figure 3, the electronic band structure is plotted along suitable paths connecting eight special points of high symmetry [23, 34] in the reciprocal space. The highest point of the valance band lies on a path $\Gamma$-$Z$ and the lowest point of conduction band lies close to X point in the reciprocal space. Figure 3 indicates the existence of an indirect band gap, $E_g$ of 1.76 eV in the orthorhombic phase of $CdP_2$. The value 1.76 eV falls within the typical range of energy band gap of semiconductor substances. A band gap of 1.439 eV was reported in other computational work [10, 11].

To reveal the distribution of electronic states, the computed total DOS along with the partial density of states (PDOS) of Cd and P atoms are depicted in figure 4. In the immediate vicinity of the top of the valence band region and the bottom of the conduction band region, p orbitals of phosphorus atoms predominantly contribute to DOS. With regard to DOS, the contribution of P(II) atom, in general, is larger than that of P(I) atom, but overall PDOS patterns due to the individual nonequivalent P atoms are broadly similar. We pay particular attention to DOS lying near the Fermi level, as these DOS are important with reference to the electronic properties of solids. In our investigation, we also observed about PDOS that chiefly *p* orbitals of the second and third *sp* shells (shown in table 4) of phosphorus atoms contribute to DOS lying near the Fermi level in the valence region and furthermore, the contribution of the third *sp* shell (having more diffused orbitals) is larger than that of the corresponding second *sp* shell of that P atom. Besides, contribution to DOS from Cd

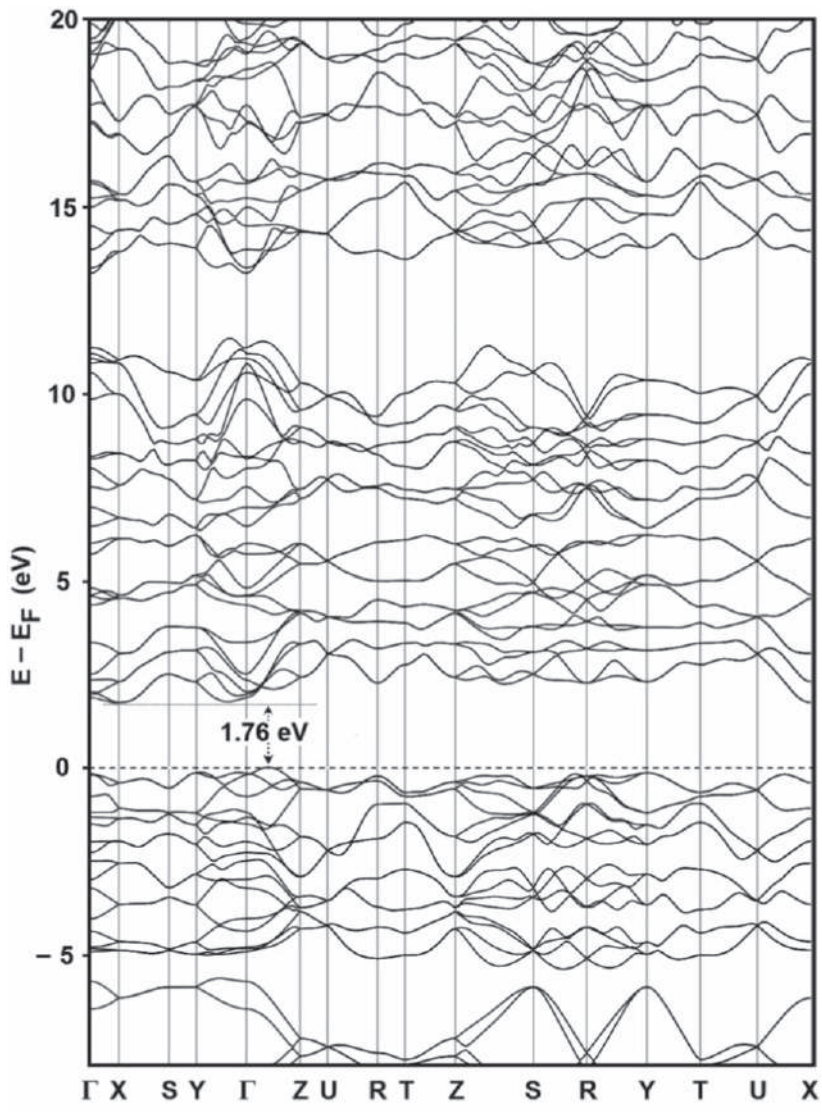


**Figure 3.** Under PBEsol scheme, the energy band structure of $\alpha$-$CdP_2$ (in the range of –8 to 20 eV relative to Fermi energy level $E_F$).

atoms is relatively low at the top of the valence band as well as at the bottom of the conduction band. Hence, the top of the valence band and the bottom of the conduction band are mostly of P-*p* characters.

### 3.4. Charge density and Mulliken population analysis

The computed total electron density map for (010) plane is shown in figure 5. The isodensity contour lines for the total electron density map are sketched at intervals of 0.02 e/Bohr$^3$. Furthermore, the total distribution of electronic charge density is predicted through the Mulliken population analysis. There exist two crystallographically nonequivalent distinct sites of P atom, therefore the charge distribution is accordingly influenced by the orientation of the respective atom in the unit cell, as evident from table 4. In the present investigation, CRYSTAL Code shows 288 orbitals for the unit cell. In table 4, orbitals and shells along with corresponding charges are shown and it is obvious that there is also a small charge transfer of about 0.041e to *d* shell of the associated basis set of each P atom in the $\alpha$-$CdP_2$ crystal.

Many physical properties of a material are correlated to its constituent chemical bonds. Mulliken population analysis plays an important role to predict the characteristics of the chemical bonding in the materials. Mulliken overlap populations for $\alpha$-$CdP_2$ are illustrated in table 5. The positive value of the total overlap population corresponds to bonding, whereas the negative value of the total overlap population corresponds to antibonding [17]. Mulliken population analysis is an important tool for the estimation of the distribution of charges in the atomic orbitals. In our study, for the one formula unit of $\alpha$-$CdP_2$, there is total charge transfer of about 1.02 electrons from one Cd atom to two P atoms as evident from table 4. On the basis of the result of charge transfer, an approximated effective valence state of $\alpha$-$CdP_2$ may be represented as $Cd^{+1.02}P^{-0.52}P^{-0.50}$. Thus, it indicates the reasonable presence of ionic character in the Cd-P bonding. The Mulliken overlap population also

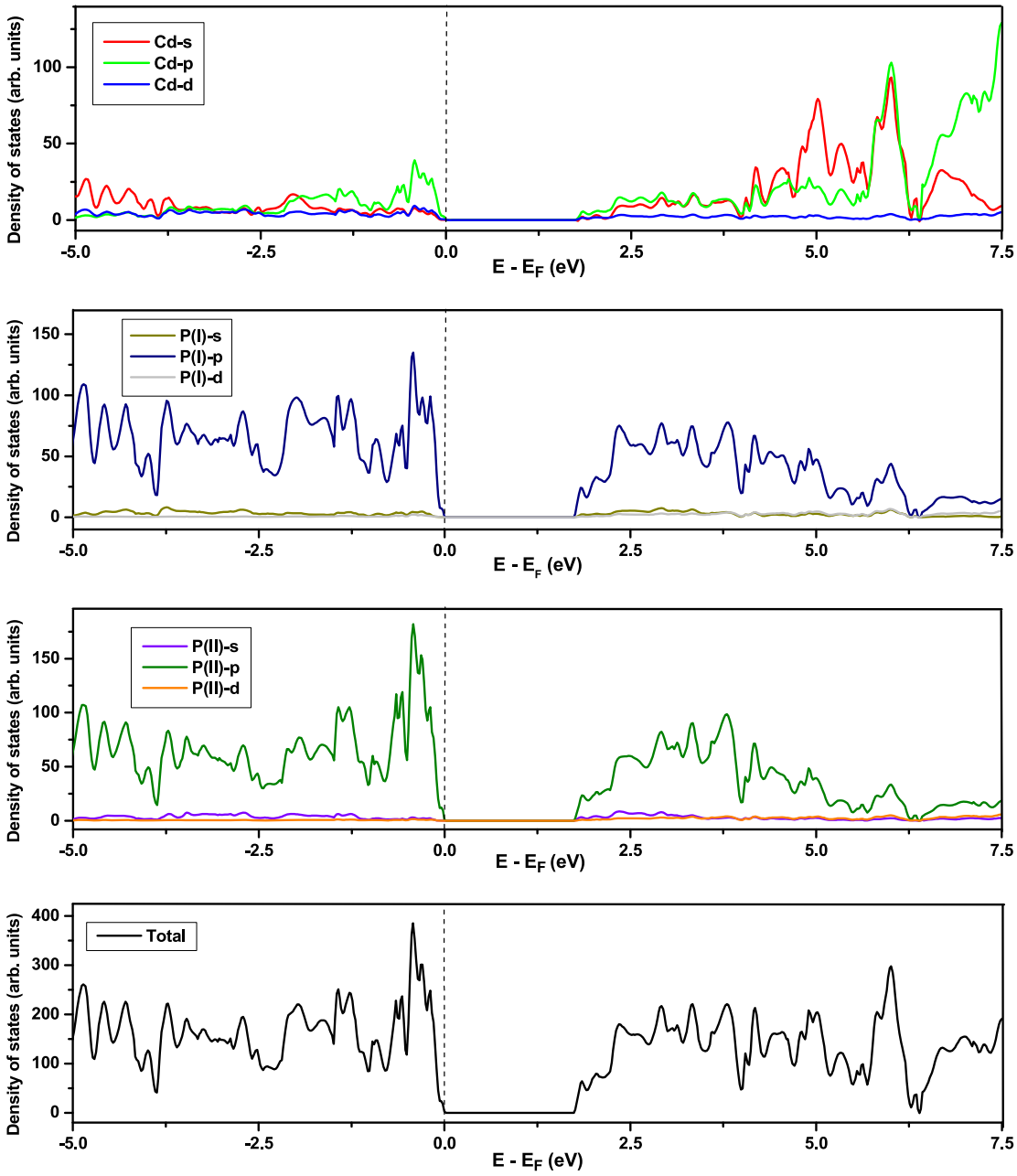


**Figure 4.** The plot of total DOS along with contributions from s, p and d orbitals of the nonequivalent atoms of $\alpha$-$CdP_2$ (in the range of –5 to 7.5 eV relative to Fermi energy level $E_F$). On the *y*-axis all arb. units are identical. Fermi level is shown by vertical dashed lines at 0 eV.

provides a good estimation of the covalent bonding [17]. A high level of overlap population reflects the high level of covalent character of a chemical bond [35]. In the present study, the overlap population between Cd atom and immediate neighboring P atom is about 0.14 as shown in table 5. This value 0.14 is reasonably small compared to 1 and it can be inferred that the Cd-P bonds are also partially covalent in nature. The present study suggests the existence of mixed ionic-covalent character of bonds (Cd-P) in the alpha phase of $CdP_2$. Furthermore, the Mulliken overlap population is useful to reflect its correlation with the strength of the bond. A comparison of hardness $H_v^\mu$ of the bonds (between Cd atom and its immediate neighboring P atoms) is carried out using the expression $H_v^\mu(\text{GPa}) = AP^\mu(v_b^\mu)^{-5/3}$ [36] where, $v_b^\mu$ and $P^\mu$ denote, respectively, the volume and Mulliken overlap population of the $\mu$ type bond and $A$ is the proportional coefficient. In the present study, results show that the computed hardness of bonds $Cd_1$-$P_7$, $Cd_1$-$P_9$, $Cd_1$-$P_5$ and $Cd_1$-$P_{10}$ are in the ratio 1.254 : 1.082 : 1.094 : 1.000. The higher level of hardness of the bond $Cd_1$-$P_7$ among these mentioned Cd-P bonds may be attributed to its relatively high Mulliken overlap population and short bond length.

As reported by Olofsson and Gullman [9], the bond distance (Cd-P) between close neighbor cadmium and phosphorus atoms ranges from 2.562 Å to 2.619 Å and the bond distance (P-P) between close neighbor

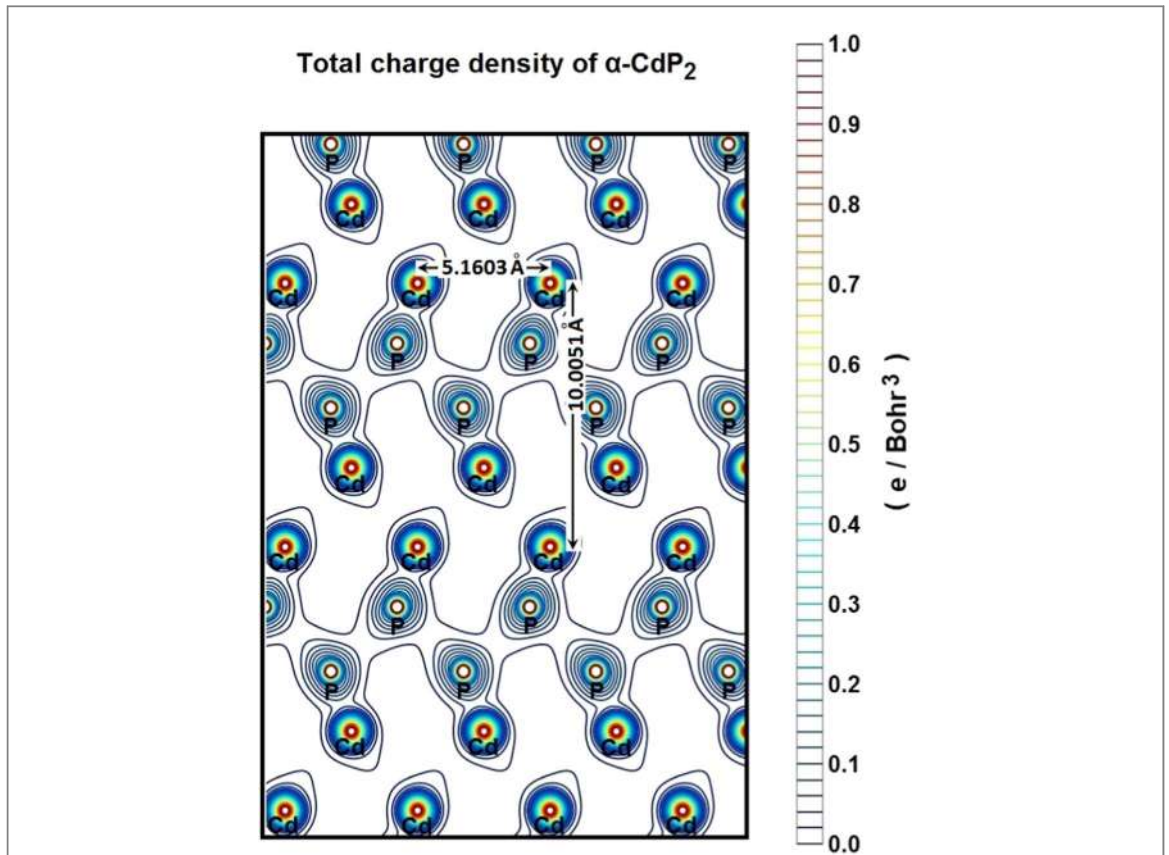


**Figure 5.** Computed total electron density map of $\alpha$-$CdP_2$ for (010) plane using PBEsol method. Lattice parameters $a = 10.0051$ Å and $c = 5.1603$ Å.

**Table 4.** Mulliken population analysis for $\alpha$-$CdP_2$ using PBEsol method. Charges are indicated in the unit of elementary charge *e*.

| Cd | | | P(I) | | | P(II) | | |
|---|---|---|---|---|---|---|---|---|
| Total charge (N. electrons) = 46.977 | | | Total charge (N. electrons) = 15.522 | | | Total charge (N. electrons) = 15.502 | | |
| Orbital No. | Shell | Shell charge | Orbital No. | Shell | Shell charge | Orbital No. | Shell | Shell charge |
| 1 | ***s*** | 2.000 | 145 | ***s*** | 2.000 | 217 | ***s*** | 2.000 |
| 2–5 | First ***sp*** | 7.998 | 146–149 | First ***sp*** | 7.824 | 218–221 | First ***sp*** | 7.824 |
| 6–9 | Second ***sp*** | 7.983 | 150–153 | Second ***sp*** | 2.000 | 222–225 | Second ***sp*** | 2.001 |
| 10–14 | ***d*** | 9.994 | 154–157 | Third ***sp*** | 3.657 | 226–229 | Third ***sp*** | 3.637 |
| 15–18 | Third ***sp*** | 6.539 | 158–162 | ***d*** | 0.042 | 230–234 | ***d*** | 0.041 |
| 19–22 | Fourth ***sp*** | 1.426 | | | | | | |
| 23–26 | Fifth ***sp*** | 1.077 | | | | | | |
| 27–31 | ***d*** | 8.767 | | | | | | |
| 32–36 | ***d*** | 1.193 | | | | | | |

phosphorus atoms ranges from 2.167 Å to 2.20 Å. It is evident from table 5 that our calculated values of bond distances are in fair agreement with the mentioned ranges [9].

### 3.5. Elastic properties

*3.5.1. Elastic constants and mechanical stability*

The study of elastic properties is extremely useful for understanding the ability of the material to resist the deformation. The direction-dependent elastic stretchability of crystals under different tensile strains can shed light on its advantages for engineering applications. A high value of the ratio of bulk modulus to shear modulus enables the crystal to meet various requirements of curvilinear shape for practical applications. Also, piezoelectricity is dependent on the intermingling of elastic and electric phenomena. In view of the device application of $\alpha$-$CdP_2$ crystal, it is necessary to estimate its elastic constants so that its mechanical stability and elastic properties may be examined. The orthorhombic crystal system has nine independent elastic stiffness

**Table 5.** Mulliken overlap populations for $\alpha$-$CdP_2$ using PBEsol scheme.

| Atomic pair AB | Distance AB (Å) | Overlap population AB |
|---|---|---|
| $Cd_1$-$P_7$ | 2.569 | 0.154 |
| $Cd_1$-$P_9$ | 2.592 | 0.139 |
| $Cd_1$-$P_5$ | 2.594 | 0.141 |
| $Cd_1$-$P_{10}$ | 2.618 | 0.135 |
| $Cd_1$-$P_6$ | 3.768 | −0.009 |
| $P_5$-$P_{10}$ | 2.183 | 0.068 |
| $P_5$-$P_9$ | 2.242 | 0.021 |
| $P_5$-$Cd_3$ | 2.569 | 0.154 |
| $P_5$-$P_6$ | 3.608 | −0.066 |
| $P_5$-$Cd_2$ | 3.768 | −0.009 |
| $P_9$-$P_6$ | 2.183 | 0.068 |
| $P_9$-$Cd_2$ | 2.618 | 0.135 |
| $P_9$-$P_{10}$ | 3.599 | −0.069 |

**Table 6.** Elastic stiffness constants (in GPa) of $\alpha$-$CdP_2$ at zero pressure.

| | Scheme | $C_{11}$ | $C_{12}$ | $C_{13}$ | $C_{22}$ | $C_{23}$ | $C_{33}$ | $C_{44}$ | $C_{55}$ | $C_{66}$ |
|---|---|---|---|---|---|---|---|---|---|---|
| Present Work | PBEsol | 105.163 | 50.352 | 43.412 | 86.520 | 41.857 | 74.230 | 33.418 | 24.329 | 27.482 |
| Other Work[a] | PBE | 101.3 | 31.1 | 37.7 | 91.4 | 32.5 | 87.3 | 37.4 | 28.2 | 19.0 |

[a] Reference [15].

coefficients due to its orthorhombic symmetry [37]. These computed elastic stiffness coefficients $C_{ij}$ of $\alpha$-$CdP_2$ are reported in table 6. According to Mouhat *et al* [38], necessary and sufficient elastic stability conditions for an orthorhombic system are given by the following expressions [from (1) to (3)]:

$$C_{11}C_{22} > C_{12}^2 \tag{1}$$

$$C_{11}C_{22}C_{33} + 2C_{12}C_{13}C_{23} - C_{11}C_{23}^2 - C_{22}C_{13}^2 - C_{33}C_{12}^2 > 0 \tag{2}$$

$$C_{11} > 0,\ C_{44} > 0,\ C_{55} > 0,\ C_{66} > 0 \tag{3}$$

The computed elastic stiffness constants (given in table 6) satisfy these necessary and sufficient elastic stability conditions for the orthorhombic system. It shows the mechanical stability of the alpha phase of $CdP_2$ crystal.

In terms of elastic stiffness constants $C_{ij}$ and elastic compliance constants $S_{ij}$, more quantities such as bulk modulus, shear modulus and Poisson's ratio may be represented. Voigt bulk modulus $B_V$ and Reuss bulk modulus $B_R$ can be expressed as [39, 40]

$$B_V = \frac{1}{9}[C_{11} + C_{22} + C_{33} + 2C_{12} + 2C_{13} + 2C_{23}] \tag{4}$$

$$B_R = [S_{11} + S_{22} + S_{33} + 2S_{12} + 2S_{13} + 2S_{23}]^{-1} \tag{5}$$

Similarly, Voigt shear modulus $G_V$ and Reuss shear modulus $G_R$ are given by [39, 40]

$$G_V = \frac{1}{15}[C_{11} + C_{22} + C_{33} - C_{12} - C_{13} - C_{23}] + \frac{1}{5}[C_{44} + C_{55} + C_{66}] \tag{6}$$

$$G_R = 15[4(S_{11} + S_{22} + S_{33}) + 3(S_{44} + S_{55} + S_{66}) - 4(S_{12} + S_{13} + S_{23})]^{-1} \tag{7}$$

According to the Voigt-Reuss-Hill approximation, polycrystalline bulk and shear moduli can be estimated as [39–41]

$$B_H = \frac{1}{2}[B_R + B_V] \tag{8}$$

$$G_H = \frac{1}{2}[G_R + G_V] \tag{9}$$

Macroscopic polycrystalline Young's modulus $E_H$ and Poisson's ratio $\nu_H$ can be expressed as [39–41]

$$E_H = \frac{9B_H G_H}{3B_H + G_H} \tag{10}$$

$$\nu_H = \frac{3B_H - 2G_H}{2(3B_H + G_H)} \tag{11}$$

**Table 7.** Using PBEsol method, computed values of bulk modulus $B$ (in GPa), shear modulus $G$ (in GPa), Young's modulus $E$ (in GPa), Poisson's ratio $\nu$ (unitless) of $\alpha$-$CdP_2$ according to Voigt-Reuss-Hill notations[a].

| | $B_V$ | $B_R$ | $B_H$ | $G_V$ | $G_R$ | $G_H$ | $E_V$ | $E_R$ | $E_H$ | $\nu_V$ | $\nu_R$ | $\nu_H$ |
|---|---|---|---|---|---|---|---|---|---|---|---|---|
| Present work | 59.684 | 57.807 | 58.745 | 25.732 | 24.735 | 25.233 | 67.496 | 64.942 | 66.219 | 0.3115 | 0.3128 | 0.3121 |

[a] Values of $B$, $G$, $E$ and $\nu$ have been obtained using ELATE software [46, 47].

To investigate the mechanical properties of $\alpha$-$CdP_2$, various elastic moduli are determined from elastic constants and are summarized in table 7. The value of bulk modulus is 58.745 GPa which indicates that the material has sufficient mechanical strength to resist structural deformation. The Cd crystal has bulk modulus of ≈46.7 GPa [42] and Young's modulus of ≈62.3 GPa [42]. The values of bulk modulus and Young's modulus for orthorhombic P crystal are ≈36 GPa [43] and ≈30.4 GPa [42] respectively. It can be seen in table 7 that the calculated values of Young's modulus and bulk modulus of $\alpha$-$CdP_2$ are greater than the respective values of Young's moduli and bulk moduli of constituent elements (Cd and P crystals). But, in comparison to the typical values of bulk modulus ≈97.8 GPa [44] and Young's modulus ≈163 GPa [45] of the semiconductor Si, it is obvious that our calculated respective values of bulk modulus 58.745 GPa and Young's modulus 66.219 GPa of $\alpha$-$CdP_2$ are considerably smaller. Since Young's modulus reflects the stiffness of the material, so $\alpha$-$CdP_2$ crystal has less stiffness than Si crystal.

It is also obvious from table 7 that the values of computed Poisson's ratios are about 0.31. Therefore these calculated values of Poisson's ratios are within the theoretically essential limits [48] for materials. In general, the ratio of bulk modulus $B$ to shear modulus $G$ may be used to make predictions about the nature of polycrystalline material in terms of brittleness and malleability [49]. A high value of $B/G$ indicates the malleable nature of the polycrystalline materials [49]. For a value of $B/G$ greater than about 1.75, malleable characteristics of a polycrystalline material is expected [49]. In the present study, the value of $B_H/G_H$ is 2.328 which is greater than 1.75, therefore it indicates the malleable nature of $\alpha$-$CdP_2$. Thus the value 2.328 of B/G for the alpha phase of $CdP_2$ crystal indicates that the crystal has reasonable malleability and this favorable property opens the possibility to allow the curved shape of $\alpha$-$CdP_2$ crystal in the semiconductor devices.

*3.5.2. Elastic anisotropy*

Most of the materials show elastic anisotropic behavior. Atomic bonding arrangement in different crystalline planes is an important factor for the determination of the elastic anisotropy. Elastic anisotropy plays a key role in various directional dependent mechanical-physical phenomena. Elastic constants such as Young's modulus, shear modulus and Poisson's ratio may have directional dependent variations, hence they have an influence on the mechanical characteristics of the crystalline materials. With the help of the theory of micro-cracks analysis from the elastic anisotropy, the enhancement in the mechanical durability of the crystals for device application may be understood [50]. A comprehensive understanding of the elastic anisotropy of the materials is of great significance because it has an important outlook for device designing. The preferred orientation of the crystals is a vital aspect for optimum technological usage of the materials in microelectromechanical systems, hence the knowledge of the elastic anisotropy is essential for imparting the desired physical and electrical properties to devices. For an orthorhombic crystal system, the directional Young's modulus $E$ in the direction of the unit vector $l_i$ is given by the expression [37]

$$E = [l_1^4 S_{11} + 2l_1^2 l_2^2 S_{12} + 2l_1^2 l_3^2 S_{13} + l_2^4 S_{22} + 2l_2^2 l_3^2 S_{23} + l_3^4 S_{33} + l_2^2 l_3^2 S_{44} + l_1^2 l_3^2 S_{55} + l_1^2 l_2^2 S_{66}]^{-1} \quad (12)$$

where $l_1$, $l_2$ and $l_3$ are direction cosines and quantity $S_{ij}$ are known as elastic compliance constants.

For an orthorhombic crystal system, the directional linear compressibility $\beta$ in the direction of the unit vector $l_i$ is given by the expression [37]

$$\beta = (S_{11} + S_{12} + S_{13})l_1^2 + (S_{12} + S_{22} + S_{23})l_2^2 + (S_{13} + S_{23} + S_{33})l_3^2 \quad (13)$$

Table 8 shows the computed Young's Modulus and linear compressibility of $\alpha$-$CdP_2$ along [100], [010] and [001] crystallographic directions. Figure 6 shows the variations of Young's modulus with direction. Figures 6(a) and 7(a) are plotted using ELATE software. It is evident from the figures 6(a) and 7(a) that schematic plots of directional Young's modulus and linear compressibility are not spherical in shape; therefore, they reflect the finite elastic anisotropy for the alpha phase of $CdP_2$. The elastic anisotropy of a crystal may be characterized by different approaches. For instance, to compute the elastic anisotropy, the degree of elastic anisotropy may be defined by expressions [51, 52]

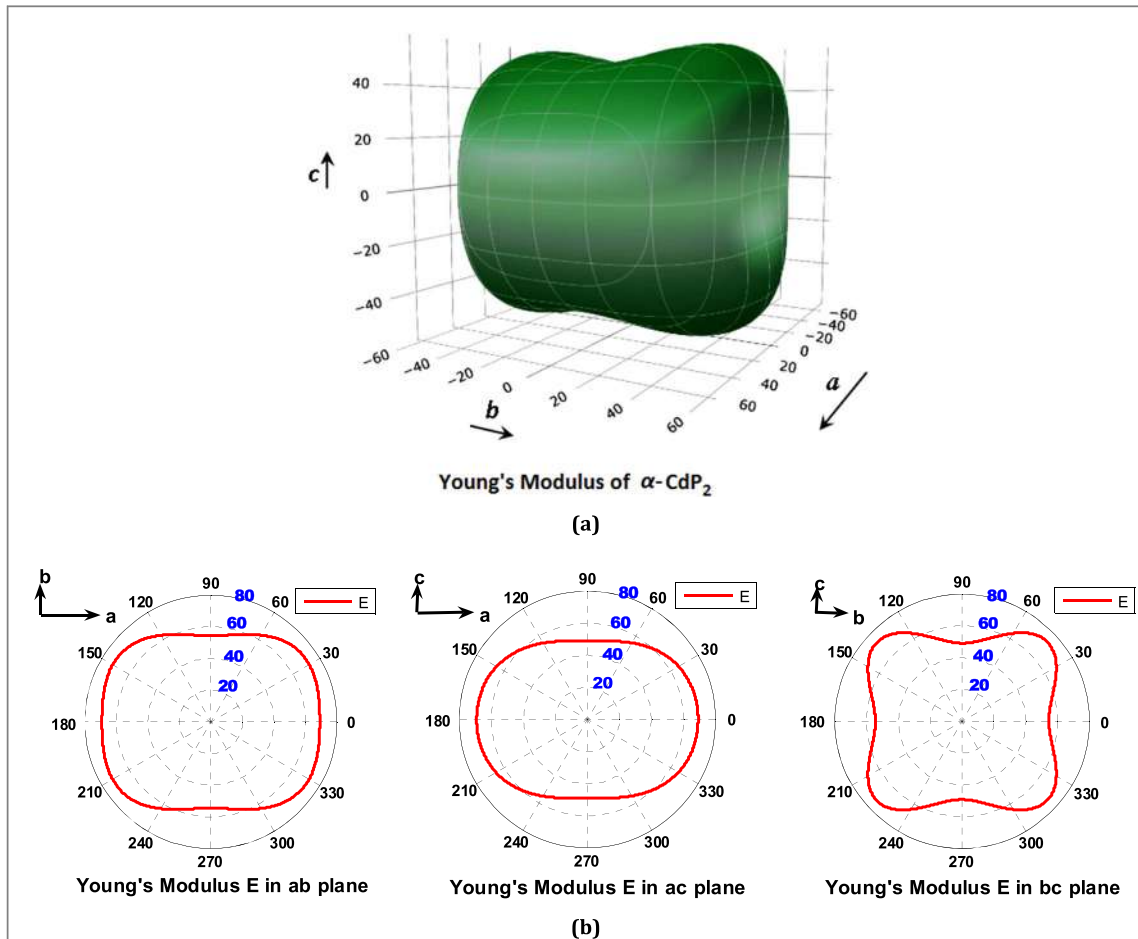


**Figure 6.** Directional dependence (polar graph) of the computed Young's modulus $E$ (in GPa) of $\alpha$-$CdP_2$. (a) 3D View representation of directional Young's modulus (b) Projections of directional Young's modulus on *ab*, *ac* and *bc* planes.

**Table 8.** The computed values of directional Young's modulus, linear compressibility and elastic anisotropy parameters for $\alpha$-$CdP_2$ under PBEsol scheme.

| | $E_{100}$ (GPa) | $E_{010}$ (GPa) | $E_{001}$ (GPa) | $\beta_{100}$ $(TPa)^{-1}$ | $\beta_{010}$ $(TPa)^{-1}$ | $\beta_{001}$ $(TPa)^{-1}$ | $A_B$ (in%) | $A_G$ (in %) | $A^U$ |
|---|---|---|---|---|---|---|---|---|---|
| Present work | 69.135 | 54.526 | 49.195 | 3.411 | 5.529 | 8.359 | 1.60 | 1.98 | 0.234 |

$$A_B = \frac{B_V - B_R}{B_V + B_R} \tag{14}$$

$$A_G = \frac{G_V - G_R}{G_V + G_R} \tag{15}$$

For elastic isotropic materials, both $A_B$ and $A_G$ are zero. Our calculated values of $A_B$ and $A_G$ for the degree of elastic anisotropy are shown in table 8. It is evident from table 8 that values of $A_B$ and $A_G$ are nonzero, therefore, $\alpha$-$CdP_2$ crystal has finite bulk anisotropy as well as shear anisotropy. In different way, Ranganathan *et al* [53] defined the universal elastic anisotropy index as

$$A^U = \frac{B_V}{B_R} + 5\frac{G_V}{G_R} - 6 \tag{16}$$

The index $A^U$ is applicable to all crystalline symmetry and its minimum value is zero for elastic isotropic materials [53]. Table 8 shows the calculated value of 0.234 of $A^U$ for the alpha phase of $CdP_2$. Both tables 8 and 9 illustrate the presence of finite elastic anisotropy characteristics in $\alpha$-$CdP_2$.

Significant differences are found among the computed values of $E_{100}$, $E_{010}$ and $E_{001}$ as shown in table 8. From figures 6 and 7 as well as from table 8, the following conclusions about directional Young's modulus and linear compressibility of $\alpha$-$CdP_2$ crystal are drawn:

$$E_{100} > E_{010} > E_{001};\ a > b > c$$

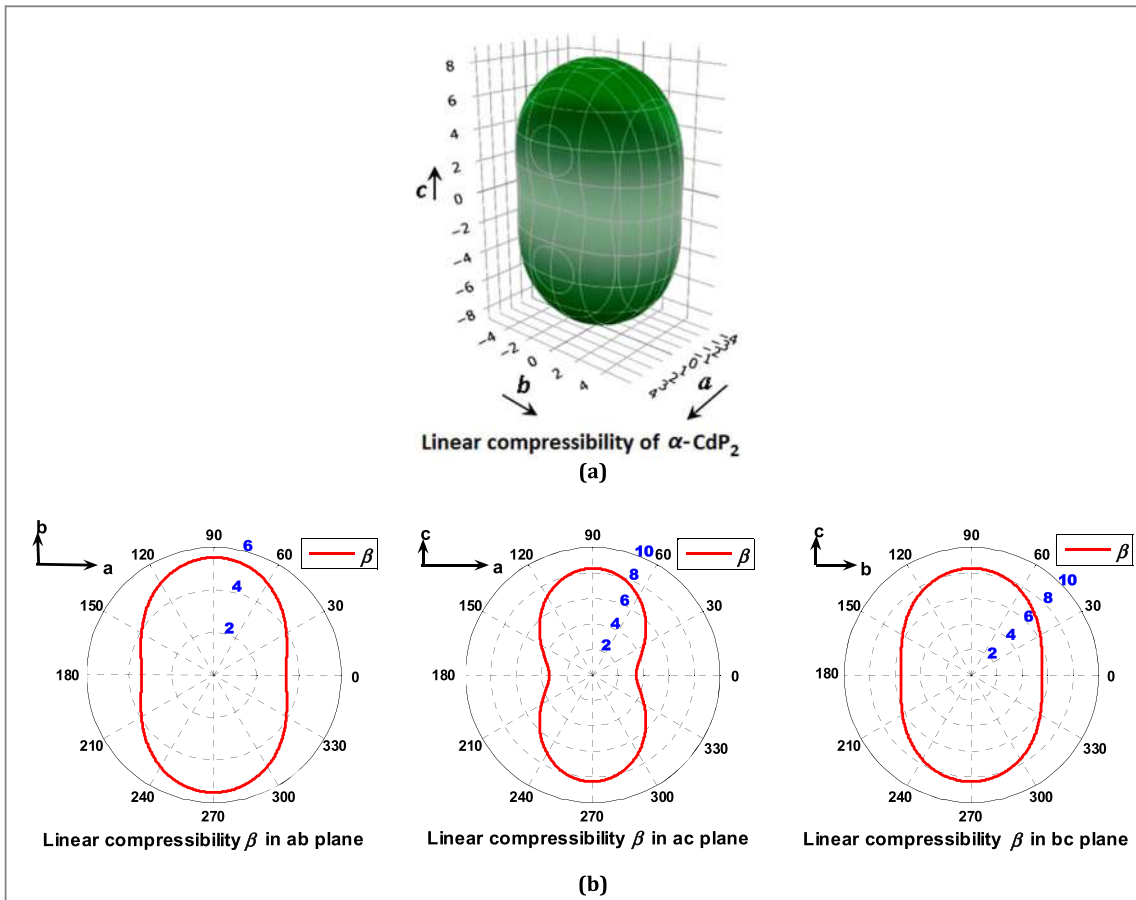


**Figure 7.** Directional dependence (polar graph) of the computed linear compressibility $\beta$ [in $(TPa)^{-1}$] of $\alpha$-$CdP_2$. (a) 3D View representation of directional linear compressibility (b) Projections of directional linear compressibility on *ab*, *ac* and *bc* planes.

**Table 9.** Variations of the shear modulus $G$ (in GPa), Young's modulus $E$ (in GPa), linear compressibility $\beta$ [in $(TPa)^{-1}$] and Poisson's ratio $\nu$ (unitless) of $\alpha$-$CdP_2$ using PBEsol method[a].

| | $G_{min}$ | $G_{max}$ | $E_{min}$ | $E_{max}$ | $\beta_{min}$ | $\beta_{max}$ | $\nu_{min}$ | $\nu_{max}$ |
|---|---|---|---|---|---|---|---|---|
| Present work | 19.087 | 33.418 | 49.195 | 73.140 | 3.411 | 8.359 | 0.0908 | 0.4179 |

[a] Minimum and maximum values of $G$, $E$, $\beta$ and $\nu$ have been obtained using ELATE software.

$$\beta_{100} < \beta_{010} < \beta_{001};\ a > b > c$$

Hence, crystal has more hardness (less compressible) along *a* axis than along *b* and *c* axes. It is evident from table 9 that there is a substantial difference between the minimum and maximum values of the directional shear modulus $G$. This is also the case for Young's modulus $E$ and linear compressibility $\beta$. For $G$, $E$ and $\beta$, respective maximum variations are 75.08%, 48.67% and 145.06% relative to their minimum values. These variations themselves reveal the presence of considerable elastic anisotropy in the alpha phase of $CdP_2$.

For Young's modulus $E$, it is readily apparent from the figure 6(b) that anisotropy is greater in *bc* plane than in *ab* and *ac* planes, since the angular variation of $E$ in *bc* plane is more pronounced among *ab*, *bc* and *ac* planes. In *ab* plane, $E$ increases from 69.135 GPa to ≈72 GPa (maximum value in *ab* plane) as the angle (with *a* axis) increases from 0° to ≈31°, then $E$ decreases from ≈72 GPa to 54.526 GPa as the angle varies from ≈31° to 90°. The maximum value ≈72 GPa of $E$ is again observed at an angle (with *a* axis) of ≈149° in the *ab* plane. It is observed in the *ac* plane that $E$ decreases continuously from 69.135 GPa to 49.195 GPa ($E_{min}$ in table 9) as the angle (with *a* axis) increases from 0° to 90°. In the *bc* plane, $E$ increases from 54.526 GPa to 73.140 GPa as the angle (with *b* axis) increases from 0° to ≈47°. Furthermore, as the angle increases from ≈47° to 90° in the *bc* plane, the value of $E$ decreases from 73.140 GPa to 49.195 GPa ($E_{min}$ in table 9). The maximum value 73.140 GPa ($E_{max}$ in table 9) of $E$ is observed at the angles (with *b* axis) of ≈47° and ≈133° in *bc* plane.

In the case of linear compressibility $\beta$, it emerges clearly from figure 7(b) that the *ac* plane has greater anisotropy than *ab* and *bc* planes. For the *ab* plane, $\beta$ increases continuously from 3.411 $(TPa)^{-1}$ ($\beta_{min}$ in table 9) to 5.529 $(TPa)^{-1}$ as the angle (with *a* axis) increases from 0° to 90°. In *ac* plane, an increase of the angle (with *a* axis)

**Table 10.** The computed values of density, Debye temperature, shear sound velocity, longitudinal sound velocity and average sound velocity of $\alpha$-$CdP_2$ under PBEsol method.

| | $\rho$(kg m$^{-3}$) | $\nu_s$ (m s$^{-1}$) | $\nu_l$ (m s$^{-1}$) | $\nu_m$ (m s$^{-1}$) | $\theta_D$ (K) |
|---|---|---|---|---|---|
| Present work | 4119 | 2475 | 4736 | 2769 | 288.1 |

from 0° to 90° results in a continuous increase of linear compressibility $\beta$ from 3.411 (TPa)$^{-1}$ to 8.359 (TPa)$^{-1}$ ($\beta_{max}$ in table 9). In the case of *bc* plane, as the angle (with *b* axis) varies from 0° to 90°, $\beta$ increases continuously from 5.529 (TPa)$^{-1}$ to 8.359 (TPa)$^{-1}$. The different types of physical quantities may have different levels of anisotropy corresponding to a given plane of the same material. The present investigation shows that among *ab*, *ac* and *bc* planes, the anisotropy is high in *ac* plane for linear compressibility, whereas the anisotropy is high in *bc* plane for Young's modulus.

*3.5.3. Debye temperature*

Debye temperature, which is a useful variable, correlates the thermodynamic properties with elastic properties of the crystal [54]. The Debye temperature of the material is related to its thermal conductivity [55]. Thermal conductivity is an important parameter for heat transfer phenomena. Hence, concerning the dissipation of heat, the thermal conductivity is a significant factor for determining the speed and efficiency of the electronic devices. The Debye temperature is a function of the aggregate elastic properties (polycrystalline bulk modulus $B_H$ and shear modulus $G_H$) [54]. The Debye temperature $\theta_D$ is related to average sound velocity $\nu_m$ in a crystal by the expression [54]

$$\theta_D = \frac{h}{k}\left[\frac{3n}{4\pi}\left(\frac{N_A\rho}{M}\right)\right]^{1/3}\nu_m \tag{17}$$

where $h$ is Planck's constant, $N_A$ is Avogadro's constant, $\rho$ is the density, $k$ is Boltzmann's constant, $M$ is the molecular mass, $n$ is the number of atoms in the molecule. Average sound velocity $\nu_m$ in a polycrystalline substance may be expressed as [54]

$$\nu_m = \left[\frac{1}{3}\left(\frac{2}{\nu_s^3} + \frac{1}{\nu_l^3}\right)\right]^{-1/3} \tag{18}$$

where $\nu_s$ and $\nu_l$ represent the average shear and longitudinal sound velocities, respectively. These velocities may be expressed in terms of density $\rho$, polycrystalline bulk modulus $B_H$ and shear modulus $G_H$ [54]:

$$\nu_s = \left[\frac{G_H}{\rho}\right]^{1/2} \tag{19}$$

$$\nu_l = \left[\frac{3B_H + 4G_H}{3\rho}\right]^{1/2} \tag{20}$$

For the alpha phase of $CdP_2$, the calculated values of mean sound velocity and Debye temperature are 2769 m s$^{-1}$ and 288.1 K respectively. The calculated values of shear sound velocity and longitudinal sound velocity are given in table 10.

## 4. Conclusions

The present study presents the first principle investigation of electronic and elastic properties of $\alpha$-$CdP_2$ by employing GGA-PBEsol functional in the CRYSTAL code. The obtained equilibrium volume of the unit cell is in quite agreement with experimental data. Our work predicts the existence of the indirect band gap of 1.76 eV in $\alpha$-$CdP_2$ crystal. The p orbitals of phosphorus atoms make the major contribution to DOS lying at the top of the valence band and the bottom of the conduction band. Broadly speaking, P(II) atom contributes more to DOS in comparison to P(I) atom. Mulliken population analysis shows that the total charge transfer of nearly 1.02 electrons takes place from one Cd atom to two P atoms in each formula unit of $\alpha$-$CdP_2$. Mulliken population analysis also indicates that Cd-P bonds have mixed ionic-covalent characters. Our investigation reveals that the $Cd_1$-$P_7$ bond has a higher level of hardness among $Cd_1$-$P_7$, $Cd_1$-$P_9$, $Cd_1$-$P_5$ and $Cd_1$-$P_{10}$ bonds.

Our present findings of anisotropic properties may contribute to better predictions for the preferred orientation of crystals for designing optoelectronic devices. In this investigation, the computed value of Ranganathan's universal elastic anisotropy index $A^U$ is 0.234. The considerable variation is observed among the computed values of directional Young's moduli $E_{100}$, $E_{010}$ and $E_{001}$. It can be inferred from the present

investigation that the alpha phase of $CdP_2$ has definite elastic anisotropy and crystal is more hard (less compressible) along *a* axis than along *b* and *c* axes. Among *ab*, *ac* and *bc* planes, the anisotropy is high in *bc* plane for Young's modulus, whereas the anisotropy is high in *ac* plane for linear compressibility. The present study indicates the malleable nature of the alpha phase of $CdP_2$. The computed value of Debye temperature of $\alpha$-$CdP_2$ is 288.1 K. The Quite adequacy of the values of Debye temperature and elastic moduli is in favor of $\alpha$-$CdP_2$ to become a promising material for device application in optoelectronics. Hence, these findings provide an outlook for experimental implications.

## Acknowledgments

The author (K Kabra) is thankful to the Department of Science and Technology (DST), New Delhi, India for financial support under the WOS-A scheme via project no. SR/WOS-A/PM-032/2017, dated 04-01-2018.

## ORCID iDs

S Rajpurohit https://orcid.org/0000-0003-0021-3789

## References

[1] Rud' V Y, Rud' Y V and Bodnar' I V 2010 *Tech. Phys.* **55** 517–20
[2] Fekeshgazi I V, Sidenko T S, Czitrovszky A, Veresh M, Trukhan V M and Shoukavaya T V 2015 *J. Appl. Spectrosc.* **82** 367–73
[3] Beril S I, Stamov I G, Syrbu N N and Zalamai V V 2013 *Physica* B **422** 12–9
[4] Trukhan V M, Sheleg A U and Fekeshgazi I F 2004 *Photoelectron.* **13** 15–7
[5] Dmitruk N L, Zuev V A and Stepanova M A 1991 *Sov. Phys. J.* **34** 642–4
[6] Islam M, Feng J Y, Berkovich A, Abshire P, Barrows G and Choa F-S 2016 *Proc. SPIE* **9819** 98190G
[7] Eckstein N, Krüger I, Bachhuber F, Weihrich R, Barquera-Lozada J E, Van Wüllen L and Nilges T 2015 *J. Mater. Chem.* A **3** 6484–91
[8] Goodyear J and Steigmann G A 1969 *Acta Crystallogr.* B **25** 2371–4
[9] Olofsson O and Gullman J 1970 *Acta Crystallogr.* B **26** 1883–4
[10] Persson K 2014 Materials Data on CdP2 (SG:33) by Materials Project (United States) (https://doi.org/10.17188/1207767) (https://materialsproject.org/materials/mp-402/)
[11] Jain A *et al* 2013 *APL Mater.* **1** 011002
[12] de Jong M, Chen W, Geerlings H, Asta M and Persson K A 2015 *Sci. Data* **2** 150053
[13] Feng S Q and Cheng X L 2011 *Comput. Theor. Chem.* **966** 149–53
[14] Shportko K V 2016 *Semicond. Phys. Quantum Electron. Optoelectron.* **19** 377–83
[15] Feng S Q, Wang L L, Jiang X X, Li H N, Cheng X L and Su L 2017 *Chin. Phys.* B **26** 046301
[16] Shportko K V and Venger E F 2019 *Appl. Nanosci.* **9** 1127–31
[17] Mulliken R S 1955 *J. Chem. Phys.* **23** 1833–40
[18] Dovesi R *et al* 2014 *Int. J. Quantum Chem.* **114** 1287–317
[19] Dovesi R *et al* 2014 *CRYSTAL14 User's Manual* (Torino: University of Torino)
[20] Perdew J P, Ruzsinszky A, Csonka G I, Vydrov O A, Scuseria G E, Constantin L A, Zhou X and Burke K 2008 *Phys. Rev. Lett.* **100** 136406
[21] https://crystal.unito.it/Basis_Sets/cadmium.html
[22] https://crystal.unito.it/Basis_Sets/phosphorus.html
[23] Monkhorst H J and Pack J D 1976 *Phys. Rev.* B **13** 5188–92
[24] Broyden C G 1965 *Math. Comput.* **19** 577–93
[25] Johnson D D 1988 *Phys. Rev.* B **38** 12807–13
[26] Perger W F, Criswell J, Civalleri B and Dovesi R 2009 *Comput. Phys. Commun.* **180** 1753–9
[27] Erba A, Mahmoud A, Orlando R and Dovesi R 2014 *Phys. Chem. Minerals* **41** 151–60
[28] Searle B G 2001 *Comput. Phys. Commun.* **137** 25–32
[29] Beata G, Perego G and Civalleri B 2019 *J. Comput. Chem.* **40** 2329–38
[30] Vinet P, Smith J R, Ferrante J and Rose J H 1987 *Phys. Rev.* B **35** 1945–53
[31] Poirier J-P and Tarantola A 1998 *Phys. Earth Planet. Inter.* **109** 1–8
[32] Birch F 1947 *Phys. Rev.* **71** 809–24
[33] Hofmeister A M 1991 *J. Geophys. Res.* **96** 21893–907
[34] Pisani C (ed) 1996 *Lecture Notes in Chemistry vol 67 Quantum-Mechanical Ab-initio Calculation of the Properties of Crystalline Materials* (Berlin Heidelberg: Springer) (https://doi.org/10.1007/978-3-642-61478-1)
[35] Segall M D, Shah R, Pickard C J and Payne M C 1996 *Phys. Rev.* B **54** 16317
[36] Gao F 2006 *Phys. Rev.* B **73** 132104
[37] Nye J F 1985 *Physical Properties of Crystals: Their Representation by Tensors and Matrices* (New York: Oxford University Press) chapter VIII (Elasticity. Fourth-Rank Tensors)
[38] Mouhat F and Coudert F-X 2014 *Phys. Rev.* B **90** 224104
[39] Voigt W 1928 *Lehrbuch der Kristallphysik* (Leipzig: B G Teubner)
[40] Reuss A and Angew Z 1929 *Math. Mech.* **9** 49–58
[41] Hill R 1952 *Proc. Phys. Soc.* A **65** 349–54
[42] Martienssen W and Warlimont H 2005 *Handbook of Condensed Matter and Materials Data* (Berlin: Heidelberg-Springer)
[43] Kikegawa T and Iwasaki H 1983 *Acta Crystallogr.* B **39** 158–64
[44] Hall J J 1967 *Phys. Rev.* **161** 756–61
[45] Muhlstein C L, Howe R T and Ritchie R O 2004 *Mech. Mater.* **36** 13–33

[46] Gaillac R, Pullumbi P and Coudert F-X 2016 *J. Phys.: Condens. Matter* **28** 275201
[47] http://progs.coudert.name/elate
[48] Love A E H 1944 *A Treatise on the Mathematical Theory of Elasticity* (New York: Dover)
[49] Pugh S F 1954 *Phil. Mag.* **45** 823–43
[50] Surucu G 2018 *Mater. Chem. Phys.* **203** 106–17
[51] Chung D H and Buessem W R 1967 *J. Appl. Phys.* **38** 2010–2
[52] Chung D H and Buessem W R 1968 *Anisotropy in Single-Crystal Refractory Compounds* vol 2 ed F W Vahldiek and S A Mersol (New York: Plenum Press) pp 217–48
[53] Ranganathan S I and Ostoja-Starzewski M 2008 *Phys. Rev. Lett.* **101** 055504
[54] Anderson O L 1963 *J. Phys. Chem. Solids* **24** 909–17
[55] Slack G A 1973 *J. Phys. Chem. Solids* **34** 321–35

# Ab-initio Investigation of Elastic Properties of Monoclinic $ZnAs_2$ Crystal

S. Rajpurohit[1] and G. Sharma[2]

[1]*School of Science and Technology, Vardhman Mahaveer Open University, Kota 324010, India*

[2]*Department of Pure and Applied Physics, University of Kota, Kota 324005, India*

**Abstract**

Elastic properties of monoclinic $ZnAs_2$ crystal are studied under the PBEsol scheme using the CRYSTAL Program. Independent elastic stiffness coefficients have been computed. Various elastic properties, such as shear modulus, bulk modulus, Young's modulus and Poisson's ratio have been analyzed. The directional dependence of the computed Young's modulus and linear compressibility is studied using ELATE software. Our investigation reveals the finite elastic anisotropy of the monoclinic $ZnAs_2$ crystal.

**Keywords**: $ZnAs_2$, *Ab-initio*, Elastic properties, Elastic anisotropy.

*** Address of correspondence**
S. Rajpurohit
School of Science and Technology, Vardhman Mahaveer Open University, Kota 324010, India

Email: sushilrajpurohit21@gmail.com

**How to cite this article**
S. Rajpurohit and G. Sharma, Ab-initio Investigation of Elastic Properties of Monoclinic $ZnAs_2$ Crystal, J. Cond. Matt. 2023; 01 (02): 56-60

Available from:
https://doi.org/10.61343/jcm.v1i02.34

## Introduction

Monoclinic $ZnAs_2$ is a semiconducting compound of the II-V group [1]. $ZnAs_2$ has a monoclinic crystal structure with space group $P2_1/c$ ($C_{2h}^5$) [2-3]. Its unit cell has eight formula units [2]. The energy band gap is nearly 1eV [4-5]. There is tetrahedral coordination of atoms with a slight distortion of the tetrahedral structure [6]. $ZnAs_2$ crystals are useful for optoelectronic applications, such as light modulators, optical filters, lenses, etc. [7]. Anisotropy in the thermoelectric power of these crystals is useful for nonselective radiation detectors [8]. Soshnikov *et al* studied the elastic properties of $ZnAs_2$ crystals with ultrasound measurements [9]. These crystals may be utilized for the fabrication of polarization-controlled switches due to their polarization photosensitivity [10]. Photosensitive Schottky barriers may be formed on monoclinic $ZnAs_2$ crystals [10]. The variation of index of refraction of $ZnAs_2$ crystal may be utilized in fabricating infrared polarizers [11-12]. Our interpretation of the elastic properties of $ZnAs_2$ may have considerable practical utility in device design for future research. For optimum performance of the device, knowledge of the direction-dependent elastic anisotropy of $ZnAs_2$ crystals provides advantages in determining the preferred orientation of the crystals.

## Computational details

*Ab-initio* investigation of monoclinic $ZnAs_2$ is performed with CRYSTAL Code [13-14]. In the present study, the DFT exchange-correlation functional GGA is employed. The basis sets for Zn and As atoms have been utilized from the CRYSTAL-Basis Set Library [13-14]. Using initial geometry [3], optimization is performed and optimized lattice parameters and fractional coordinates are obtained. In this computation, the PBEsol [15] technique is implemented. The SCF convergence TOLDEE is set to 8. The calculations are performed using an $8 \times 8 \times 8$ Monkhorst-Pack **k**-point mesh [16]. This **k**-point mesh corresponds to 125 **k**-points in the irreducible Brillouin zone. The BROYDEN parameter [13-14, 17-18] is also implemented to obtain convergence. The elastic properties [19-20] are studied at the equilibrium volume with a strain step of 0.01. The ELASTCON keyword is used for the computation of the elastic properties of monoclinic $ZnAs_2$ crystals. ELATE software [21-22] is used for the analysis of elastic quantities.

## Results and Discussion

### Elastic Properties

The analysis of elastic anisotropy is useful for understanding the direction-dependent elastic stretchability of crystals. This analysis is useful for engineering device design. The monoclinic crystal system has thirteen

independent elastic stiffness constants [23]. Using the initial geometry [3] with lattice parameters $a = 9.287$ Å, $b = 7.691$ Å, $c = 8.010$ Å, optimized lattice parameters have been obtained by CRYSTAL Code [13-14]. Using the optimized lattice parameters and fractional coordinates, the elastic stiffness constants of the monoclinic $ZnAs_2$ crystal are obtained, which are shown in table 1.

**Table 1:** Elastic stiffness constants (in GPa) of $ZnAs_2$ at zero pressure.

| | Scheme | $C_{11}$ | $C_{12}$ | $C_{13}$ | $C_{15}$ | $C_{22}$ | $C_{23}$ | $C_{25}$ | $C_{33}$ | $C_{35}$ | $C_{44}$ | $C_{46}$ | $C_{55}$ | $C_{66}$ |
|---|---|---|---|---|---|---|---|---|---|---|---|---|---|---|
| Present Work | PBEsol | 126.72 | 63.47 | 59.95 | – 4.41 | 136.81 | 38.35 | 6.07 | 145.84 | 1.75 | 26.73 | 4.23 | 44.58 | 44.18 |
| Other Work[a] | | 95.63 | 31.47 | | | 102.5 | | | 112.6 | | 20.76 | | | 40.45 |

[a] *Ref. [9, 24].*

**Table 2.** Computed values[b] of shear modulus $G$ (in GPa), bulk modulus $B$ (in GPa), Young's modulus $E$ (in GPa) and Poisson's ratio $\nu$ (unitless) of $ZnAs_2$.

| | $B_V$ | $B_R$ | $B_H$ | $G_V$ | $G_R$ | $G_H$ | $E_V$ | $E_R$ | $E_H$ | $\nu_V$ | $\nu_R$ | $\nu_H$ |
|---|---|---|---|---|---|---|---|---|---|---|---|---|
| Present Work[b] | 81.44 | 81.28 | 81.36 | 39.60 | 36.67 | 38.14 | 102.24 | 95.63 | 98.95 | 0.291 | 0.304 | 0.297 |

[b] *Values of B, G, E and $\nu$ have been computed with the help of ELATE software [21, 22]*

**Table 3.** Variations[c] of Young's modulus $E$ (in GPa), shear modulus $G$ (in GPa), Poisson's ratio $\nu$ (unitless) and linear compressibility $\beta$ [in $(\mathrm{TPa})^{-1}$] of $ZnAs_2$.

| | $G_{min}$ | $G_{max}$ | $E_{min}$ | $E_{max}$ | $\beta_{min}$ | $\beta_{max}$ | $\nu_{min}$ | $\nu_{max}$ |
|---|---|---|---|---|---|---|---|---|
| Present Work | 25.76 | 51.76 | 70.92 | 121.47 | 3.60 | 4.45 | 0.051 | 0.491 |

[c] *These values of G, E, $\beta$ and $\nu$ have been computed through ELATE software.*

Table 1 shows that the elastic constant $C_{33}$ is greater than other elastic constants. It is obvious from table 1 that the value of $C_{22}$ is greater than $C_{11}$ at zero pressure. Elastic stiffness constants $C_{44}$ and $C_{66}$ are significantly smaller than the other elastic stiffness constant $C_{11}$.

Voigt bulk modulus ($B_V$) and Reuss bulk modulus ($B_R$) may be represented as a function of elastic stiffness constants $C_{ij}$ and elastic compliance constants $S_{ij}$ [25, 26]

$$B_V = \frac{1}{9}[C_{11} + C_{22} + C_{33} + 2C_{12} + 2C_{13} + 2C_{23}] \quad (1)$$

$$B_R = [S_{11} + S_{22} + S_{33} + 2S_{12} + 2S_{13} + 2S_{23}]^{-1} \quad (2)$$

Reuss shear modulus ($G_R$) and Voigt shear modulus ($G_V$) are represented by [25, 26]

$$G_R = 15[4(S_{11} + S_{22} + S_{33}) + 3(S_{44} + S_{55} + S_{66}) - 4(S_{12} + S_{13} + S_{23})]^{-1} \quad (3)$$

$$G_V = \frac{1}{15}[C_{11} + C_{22} + C_{33} - C_{12} - C_{13} - C_{23}] + \frac{1}{5}[C_{44} + C_{55} + C_{66}] \quad (4)$$

The Voigt-Reuss-Hill approximation provides the estimated polycrystalline shear ($G_H$) and bulk moduli ($B_H$) [25-27]

$$G_H = \frac{1}{2}[G_R + G_V] \quad (5)$$

$$B_H = \frac{1}{2}[B_R + B_V] \quad (6)$$

Also, macroscopic polycrystalline Poisson's ratio $\nu_H$ and Young's modulus $E_H$ may be represented as follows [25-27]:

$$E_H = \frac{9B_H G_H}{3B_H + G_H} \quad (7)$$

$$\nu_H = \frac{3B_H - 2G_H}{2(3B_H + G_H)} \quad (8)$$

The computed elastic moduli from elastic constants are shown in table 2.

The malleable property of a polycrystalline substance is expected to have a ratio of bulk modulus to shear modulus greater than about 1.75 [28]. The obtained value of Young's modulus shows sufficient stiffness of $ZnAs_2$. The value of

81.36 GPa of bulk modulus shows the ample material strength of $ZnAs_2$ crystals under deformation. The computed value of 0.297 of Poisson's ratio is within the theoretical limits [29] for materials. Maximum and minimum values of Young's modulus, shear modulus, Poisson's ratio and linear compressibility of $ZnAs_2$ are shown in table 3.

The elastic anisotropy of a crystal may be expressed as [30, 31]

$$A_B = \frac{B_V - B_R}{B_V + B_R} \quad (9)$$

$$A_G = \frac{G_V - G_R}{G_V + G_R} \quad (10)$$

The calculated values of anisotropy parameters $A_B$ and $A_G$ are 0.00098 and 0.0384 respectively.

Ranganathan *et al* [32] expressed the universal elastic anisotropy index in the following manner:

$$A^U = \frac{B_V}{B_R} + 5\frac{G_V}{G_R} - 6 \quad (11)$$

The obtained value of Ranganathan's universal elastic anisotropy index for $ZnAs_2$ is 0.402. All these finite values of anisotropy parameters indicate the presence of finite anisotropy in $ZnAs_2$ crystals. For isotropic materials, the value of each of the anisotropy parameters $A_B$, $A_G$ and $A^U$ is zero. With the help of ELATE software [21-22], the directional dependence of Young's modulus $E$ and linear compressibility $\beta$ is plotted in figures 1, 2 and 3. It is evident from figures 1 and 2 that directional Young's modulus has anisotropy. Similarly, figures 3 and 4 show the sufficient anisotropy of linear compressibility in $ZnAs_2$ crystal.

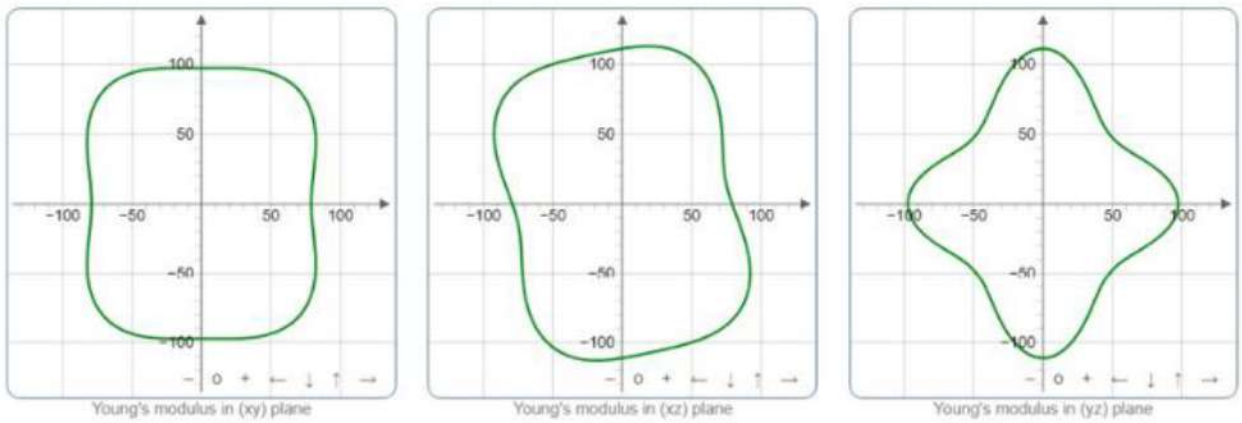


**Figure 1.** Directional dependence of the Young's modulus $E$ (in GPa) of $ZnAs_2$

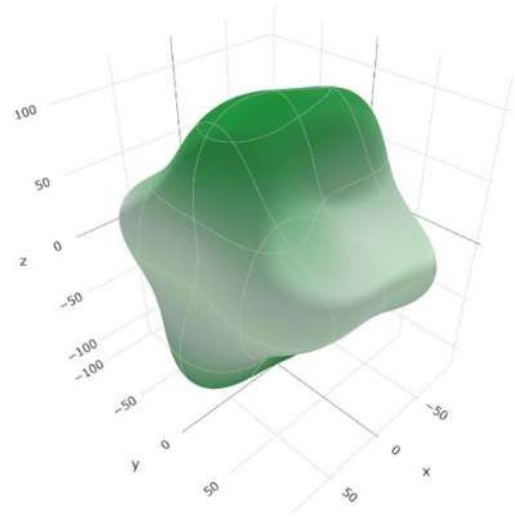

**Figure 2.** 3D View of the directional Young's modulus $E$ (in GPa) of $ZnAs_2$

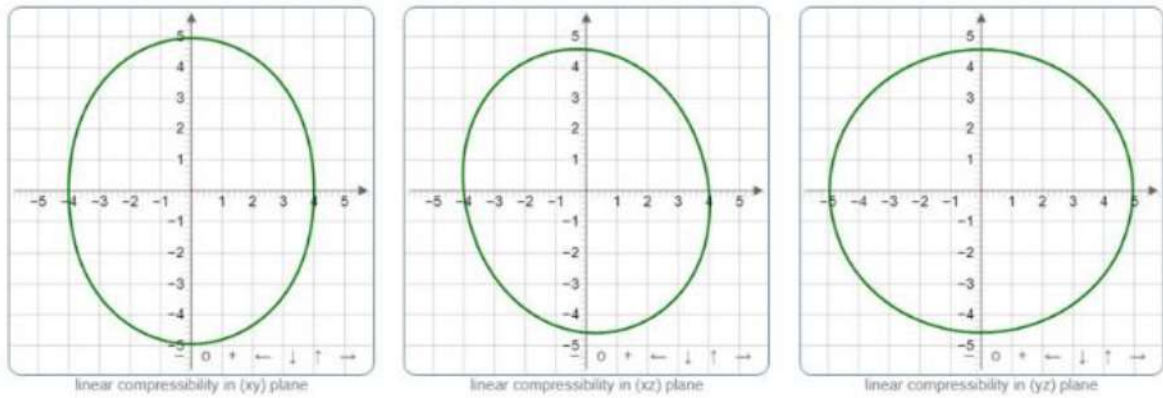


**Figure 3.** Directional dependence of the computed linear compressibility $\beta$ [in $(\mathrm{TPa})^{-1}$ ] of $ZnAs_2$

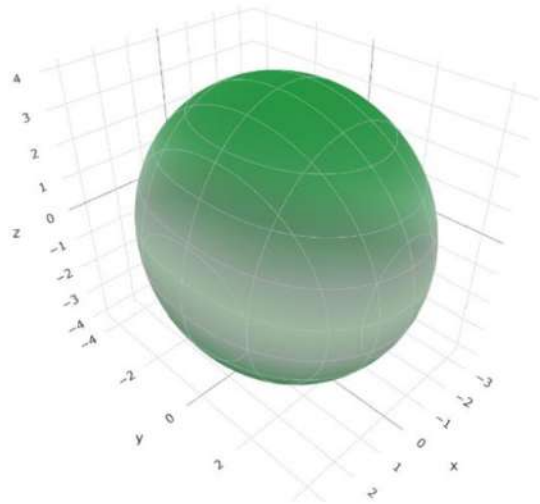

**Figure 4.** 3D View of the directional linear compressibility $\beta$ [in $(\mathrm{TPa})^{-1}$ ] of $ZnAs_2$

## Conclusion

The investigation reveals the various elastic properties of $ZnAs_2$ by using the GGA-PBEsol functional in the CRYSTAL program. Our investigation predicts the malleable nature of $ZnAs_2$. In the present findings, the obtained value of Ranganathan's universal elastic anisotropy index for $ZnAs_2$ is 0.402. It can be concluded from the study that $ZnAs_2$ has definite elastic anisotropy. Our present findings show that variation in the value of Young's modulus from its minimum value to its maximum value is 50.55 GPa. For the shear modulus, the variation in the value from minimum to maximum is 26 GPa. Our investigation of the anisotropic properties of $ZnAs_2$ may shed light on the preferred orientation of crystals for designing engineering devices using $ZnAs_2$ crystals.

## References

1. Weszka J, Mazurak Z and Pishchikov D I 1992 phys. stat. sol. (b) 170 89-92. https://doi.org/10.1002/pssb.2221700110
2. Senko M E, Dunn H M, Weidenborner J and Cole H 1959 Acta Crystallogr. 12 76 https://doi.org/10.1107/S0365110X59000214
3. Fleet M E 1974 Acta Crystallogr. B 30 122-6. https://doi.org/10.1107/S0567740874002329
4. Turner W J, Fischler A S and Reese W E 1961 Phys. Rev. 121 759-67 https://doi.org/10.1103/PhysRev.121.759
5. Madelung O 2004 Semiconductors: Data Handbook Springer-Verlag Berlin Heidelberg
6. Weszka J, Balkanski M, Jouanne M, Pishchikov D I and Marenkin S F 1992 phys. stat. sol. (b) 171 275-81 https://doi.org/10.1002/pssb.2221710130
7. Matveeva L A and Matiyuk I M 2001 Proc. SPIE Eighth International Conference on Nonlinear Optics of Liquid and Photorefractive Crystals 4418 44180X https://doi.org/10.1117/12.428319
8. Morozova V A, Marenkin S F and Koshelev O G 2002 Inorg. Mater. 38 325-30. https://doi.org/10.1023/A:1015137301787
9. Soshnikov L E, Trukhan V M, Haliakevich T V

and Soshnikava H L 2005 Mold. J. Phys. Sci. 4 201–10
10. Nikolaev Y A, Rud' V Y, Rud' Y V and Terukov E I 2009 Tech. Phys. 54 1597-601 https://doi.org/10.1134/S1063784209110073
11. Morozova V A, Marenkin S F and Koshelev O G 1999 Inorg. Mater. 35 661-3.
12. Marenkin S F, Morozova V A and Koshelev O G 2010 Inorg. Mater. 46 1001-6 https://doi.org/10.1134/S0020168510090153
13. Dovesi R, Erba A, Orlando R, Zicovich-Wilson C M, Civalleri B, Maschio L, Rérat M, Casassa S, Baima J, Salustro S and Kirtman B 2018 WIREs Comput. Mol. Sci. 8 e1360 https://doi.org/10.1002/wcms.1360
14. Dovesi R, Saunders V R, Roetti C, Orlando R, Zicovich-Wilson C M, Pascale F, Civalleri B, Doll K, Harrison N M, Bush I J, D'Arco P, Llunell M, Causà M, Noël Y, Maschio L, Erba A, Rérat M and Casassa S 2017 CRYSTAL17 User's Manual (University of Torino).
15. Perdew J P, Ruzsinszky A, Csonka G I, Vydrov O A, Scuseria G E, Constantin L A, Zhou X and Burke K 2008 Phys. Rev. Lett. 100 136406 https://doi.org/10.1103/PhysRevLett.100.136406
16. Monkhorst H J and Pack J D 1976 Phys. Rev. B 13 5188-92 https://doi.org/10.1103/PhysRevB.13.5188
17. Broyden C G 1965 Math. Comput., 19 577-93 https://doi.org/10.2307/2003941
18. Johnson D D 1988 Phys. Rev. B 38 12807-13 https://doi.org/10.1103/PhysRevB.38.12807
19. Perger W F, Criswell J, Civalleri B and Dovesi R 2009 Comput. Phys. Commun. 180 1753-9 https://doi.org/10.1016/j.cpc.2009.04.022
20. Erba A, Mahmoud A, Orlando R and Dovesi R 2014 Phys. Chem. Minerals 41 151-60 https://doi.org/10.1007/s00269-013-0630-4
21. Gaillac R, Pullumbi P and Coudert F X 2016 J. Phys.: Condens. Matter, 28 275201 https://doi.org/10.1088/0953-8984/28/27/275201
22. http://progs.coudert.name/elate
23. Nye J F 1985 Physical Properties of Crystals: Their Representation by Tensors and Matrices (New York: Oxford University Press) chapter VIII (Elasticity. Fourth-Rank Tensors)
24. Balazuk V N, Bogachev G U, Kuryachii V Y, Marenkin S F, Mihalchenko V P, Pishikov D I and Rarenko A I 1982 Solid State Phys. (in Russian) 33 2777
25. Voigt W 1928 Lehrbuch der Kristallphysik (Leipzig: B G Teubner)
26. Reuss A and Angew Z 1929 Math. Mech. 9 49–58
27. Hill R 1952 Proc. Phys. Soc. A 65 349–54 https://doi.org/10.1088/0370-1298/65/5/307
28. Pugh S F 1954 Phil. Mag. 45 823–43 https://doi.org/10.1080/14786440808520496
29. Love A E H 1944 A Treatise on the Mathematical Theory of Elasticity (New York: Dover)
30. Chung D H and Buessem W R 1967 J. Appl. Phys. 38 2010–2 https://doi.org/10.1063/1.1709819
31. Chung D H and Buessem W R 1968 Anisotropy in Single-Crystal Refractory Compounds vol 2, ed F W Vahldiek and S A Mersol (New York: Plenum Press) p 217–48
32. Ranganathan S I and Ostoja-Starzewski M 2008 Phys. Rev. Lett. 101 055504 https://doi.org/10.1103/PhysRevLett.101.055504

NCRAST 2023

NATIONAL CONFERENCE
ON
**RECENT ADVANCES IN SCIENCE AND TECHNOLOGY**
(06-07, OCT 2023)
ORGANIZED BY

राजकीय महाविद्यालय कोटा
Government College Kota
॥ सा विद्या या विमुक्तये ॥

# DEPARTMENT OF CHEMISTRY
## GOVERNMENT COLLEGE KOTA
**(NAAC 'A' ACCREDITED INSTITUTE)**

# CERTIFICATE

This is to certify that Prof / Dr. / Mr. / Ms. S. Rajpurohit from V. M. Open University, Kota has participated / presented a paper / poster entitled DFT investigation ..... of monoclinic ZnAs2 in the two day National Conference, organised by Department of Chemistry, Government College Kota(Raj) on 6th & 7th October 2023.

**Prof. MONIKA DAKSHENE**
CONVENOR
*HEAD, DEPARTMENT OF CHEMISTRY*

**Prof. RENUKA JAIN**
ORGANISING SECRETARY
*DEPARTMENT OF CHEMISTRY*

**Prof. ARUN KUMAR**
PAT RON & PRINCIPAL
*GOVERNMENT COLLEGE KOTA*

ICC2023

# 4TH INTERNATIONAL CONFERENCE ON CONDENSED MATTER & APPLIED PHYSICS

Paper ID : B1-0039

## Certificate

This is to certify that

**Mr. Sushil Rajpurohit**

of

Vardhman Mahaveer Open University, Kota (Research Scholar at University of Kota, Kota)

has participated in 4th International Conference on Condensed Matter & Applied Physics (ICC 2023) organized by Govt. Engineering College, Bikaner in joint auspices of Condensed Matter Research Society (CMRS) during Oct. 09-10, 2023 and presented a paper entitled

Ab-initio Investigation of Elastic Properties of Monoclinic ZnAs2 Crystal

Dr. Ravindra Mangal
President,
Condensed Matter Research Society

Dr. Manoj S. Shekhawat
Convener, ICC 2023
Govt. Engineering College, Bikaner

www.iccindia.in

09-10 Oct, 2023

# INDIAN COUNCIL OF CHEMISTS

## 42nd Annual National Conference

**20th - 22nd December, 2023**

**Department of Pure & Applied Chemistry**
**University of Kota**
**Kota - 324 005 (Rajasthan)**

# *Certificate*

***This is to certify that Dr. / Shri / Ms. / Mrs.*** Sushil Rajpurohit

***of*** School of Science and Tech. VMOU, Kota.

***has participated in 42nd Annual National Conference of Indian Council of Chemists held at Department of Pure & Applied Chemistry, University of Kota, Kota - 324 005 (Rajasthan) on 20th - 22nd December, 2023.***

***He / She has presented his / her paper (Oral / Poster) in Inorganic / Organic / Physical / Analytical and Environmental Chemistry / Symposium Section.***

**(Prof. Rajesh Dhakarey)**
**Secretary, ICC**
**Ex. Vice Chancellor**
**Maharaja Surajmal Brij University, Bharatpur (Raj.)**

**Kota, 22nd December, 2023**
www.chemicc.com

**Sectional President**

# A
# WORKSHOP
## ON
# ACADEMIC ETHICS AND INTEGRITY
## (JULY 27, 2017)

**Internal Quality Assurance Cell**
**University of Kota**
**Kota, Rajasthan**

## *CERTIFICATE*

This is to certify that Dr. / Mr. /Ms....Sushil....Rajpurohit.....
from.Research.Scholar..course...work.....has participated / presented a paper/ delivered invited talk entitled.....–.....in the WORKSHOP ON *ACADEMIC ETHICS AND INTEGRITY* organized by the Internal Quality Assurance Cell, University of Kota on July 27, 2017.

**Member Secretary, IQAC**

**Director, IQAC**